Etude du comportement mécanique de sédiments argileux contenant des hydrates de gaz à partir de mesures in situ

Farah Taleb

To cite this version:

Farah Taleb. Etude du comportement mécanique de sédiments argileux contenant des hydrates de gaz à partir de mesures in situ. Sciences de la Terre. Université de Bretagne occidentale - Brest, 2019. Français. NNT : 2019BRES0114 . tel-02612639

HAL Id: tel-02612639
https://theses.hal.science/tel-02612639

Submitted on 19 May 2020

UNIVERSITE SCIENCES
BRETAGNE DE LA MER
LOIRE ET DU LITTORAL

UBO
Université de Bretagne Occidentale

THESE DE DOCTORAT DE

L'UNIVERSITE
DE BRETAGNE OCCIDENTALE
COMUE UNIVERSITE BRETAGNE LOIRE

ECOLE DOCTORALE N° 598
Sciences de la Mer et du littoral

POUR OBTENIR LE TITRE DE
DOCTEUR DE L'UNIVERSITÉ DE BRETAGNE OCCIDENTALE
Spécialité : *Géosciences Marines*

Par

Farah TALEB

« Etude du comportement mécanique de sédiments argileux contenant des hydrates de gaz à partir de mesures in-situ »

Thèse présentée et soutenue à Brest, le 04 Décembre 2019
Préparée à IFREMER, Unité Géosciences Marines, Laboratoire Aléas géologiques et Dynamique sédimentaire

Rapporteurs avant soutenance :

Jean-Michel PEREIRA	Professeur, École des ponts Paris Tech
Umberta TINIVELLA	Professeur, Istituto Nazionale di Oceanografia e di Geofisica Sperimentale

Ifremer

AGENCE NATIONALE DE LA RECHERCHE
ANR

Hydre

Composition du jury:

Jean-Michel PEREIRA
Professeur, École des ponts Paris Tech / *Rapporteur*

Umberta TINIVELLA
Professeur, Istituto Nazionale di Oceanografia e di Geofisica Sperimentale / *Rapporteur*

Anh Minh TANG
Directeur de Recherche, École des ponts Paris Tech / *Examinateur*

Marc-André GUTSCHER
Directeur de Recherche, Institut Universitaire et Européen de la Mer / *Président du jury*

Nabil SULTAN
Chercheur, Ifremer / *Directeur de thèse*

Sébastien GARZIGLIA
Chercheur, Ifremer / *Encadrant scientifique*

Titre : Etude du comportement mécanique de sédiments argileux contenant des hydrates de gaz à partir de mesures in-situ

Mots clés : Hydrate de gaz, propriétés mécaniques, milieu argileux, mesures in-situ, Golf de Guinée

Résumé : Les hydrates de gaz (GH) sont composés de molécules de gaz, souvent du méthane, piégées dans des cages d'eau. Ils se trouvent principalement dans les sédiments des marges continentales et du pergélisol, où les conditions de stabilité (haute pression et basse température) nécessaires à leur présence sont réunies. Les GH sont considérés comme une source d'énergie mais aussi un facteur aggravant des aléas sous-marins et une source de gaz à effet de serre. Il est indispensable de comprendre les conséquences de la présence de ces composés métastables sur les propriétés géo-mécaniques des sédiments qui les contiennent (GHBS). Ifremer a mené plusieurs campagnes océanographiques visant à évaluer ce type d'aléas géologique dans le Golfe de Guinée, où un système à flux de gaz élevé avait pu être observé. La base de données est composée d'un ensemble de mesures in-situ acoustiques, géotechniques et de mesures de dissipation de pression interstitielle, ainsi que de carottes sédimentaires et de profils sismiques. Dans le but de comprendre l'effet de la saturation en GH et de leur morphologie et distribution sur les propriétés mécaniques des GHBS, ce travail de thèse a exploité l'ensemble de ces données. Cette étude a révélé que les GHBS argileux ont un comportement contractant lors du cisaillement qui s'oppose au comportement dilatant des sédiments sableux. En outre, différentes morphologies des GH ont été associées aux différents traits de comportement mécanique des GHBS. Pour des saturations en GH élevées (>10%), la diffusivité hydraulique des GHBS a tendance à augmenter avec l'accroissement de la concentration de ces hydrates. Ce phénomène est lié à la présence de fractures ou à la diminution de la compressibilité du sédiment. Un nouveau modèle constitutif basé sur le principe d' « indices des vides equivalents » a été utilisé pour simuler le comportement mécanique des GHBS. Les résultats ont montré qu'un seul paramètre lié à la présence et la morphologie des GH est nécessaire au modèle pour reproduire correctement le comportement mécanique des GHBS.

Title: Study of the mechanical behaviour of hydrate-bearing clayey sediments based on in situ measurements

Keywords : Gas hydrates, mechanical properties, clayey sediments, in-situ measurements, Gulf of Guinea

Abstract: Gas hydrates (GH) are composed of gas molecules, often methane, trapped in a lattice of hydrogen-bonded water molecule. They are found in sediments of continental margins and permafrost, lakes and inland seas, where their stability conditions (high pressure and low temperature) are met. GH are considered as a potential energy resource but furthermore as a potential submarine geohazard and source of greenhouse gases. It is essential to understand the consequences of the presence of these metastable components on the geo-mechanical properties of their host sediment (GHBS). Ifremer has conducted several oceanographic campaigns aiming to assess such geohazard in an area of the deep-water Niger Delta, characterised by hydrates which formed in high gas flux environments in clayey sediment. The database is composed of in-situ acoustic, geotechnical, pore-pressure dissipation measurements, as well as cores and seismic profiles. The PhD work exploited the dataset with the aim of understanding the effect of GH content, morphology and distrubution on the mechanical and hydraulic properties of the GHBS. This rare field study revealed that marine GH-bearing clays have a contractive behaviour upon shearing, which contrasts with the dilative behaviour of sandy GHBS often discussed in litterature. Alternatively, different morphologies of GH have been linked with different features of the mechanical behaviour of GHBS. For high GH saturtion (> 10%), the hydraulic diffusivity of the GHBS was observed to increase with increasing GH content, which was linked to fractures or decrease in compressibility. A new simple constitutive model based on "equivalent skeleton void ratio" was used in order to simulate the mechanical behaviour of GHBS. Preliminary results show that only one additional parameter related to the morphology of hydrate is necessary to correctly simulate the mechanical behaviour of GHBS.

Acknowledgements

Remerciements

En premier lieu, je tiens à remercier mon directeur de thèse, Nabil Sultan, pour la confiance qu'il m'a accordée en acceptant d'encadrer ce travail de thèse et de m'avoir donné une formation de si haute qualité. Sa grande disponibilité et son dévouement vis-à-vis de mon travail ont bien facilité ma tâche et l'a rendu moins stressante.

Je voudrais remercier mon encadrant, Sébastien Garziglia, pour son soutien tout au long de cette thèse et ses nombreuses corrections qui ont sans aucun doute amélioré la qualité de ce travail.

Ce travail a été possible grâce au financement de l'Agence Nationale de la Recherche(ANR) dans le cadre du projet « *Hydre* ».

I would like to thank the members of the jury for accepting to judge my work and contributing in improving this manuscript. Thank you Umberta Tinivella, Jean Michel Pereira, Anh Minh Tang and Marc-André Gutscher.

Un remerciement spécial à Hermann. C'est grâce à lui que j'ai trouvé le courage, la motivation et la patience d'aboutir ce travail jusqu'à la fin.

خالص شكري لوالديّ. طوال دراستي، كانوا دائماً يدعمونني ويشجعونني ويساعدونني. كانوا يعرفون كيفية إعطائي كل فرصة للنجاح. قد يجدون في إنجاز هذا العمل نتيجة لجهودهم والتعبير عن امتناني

Merci à mon frère Rami qui me soutient dans mes études et ma vie malgré la distance qui nous sépare.

Merci à ma sœur Dima pour ses visites à Brest qui m'ont aidé face à l'éloignement de ma famille.

Merci à Christophe et Valérie de m'avoir accepté dans leur famille et pour leurs encouragements donnés tout au long de cette thèse.

Merci à Vincent Riboulot, chercheur à Ifremer, qui a souvent su me remonter le moral et m'a donné envie d'en faire toujours plus.

Merci à Corinne pour son dynamisme, son aide administrative et sa gentillesse qui m'ont permis de m'intégrer plus facilement dès mon arrivée en France.

Un dernier merci à mes amis pour avoir partagé ces trois années avec moi : Pierre pour nos girls night, Fatima pour nos repas de midi, Florent pour toujours être prêt à charger mon téléphone et pour être le tonton de Gaïa, Shray pour être si drôle et pour ses plats indiens délicieux, Arthur et Deborah mes collègues de bureau avec lesquels j'ai passé de bons moments, Elda et Martin pour les nombreux barbecues, Simone et Anthony pour les brunch bobo vegan.

Contents

List of figures

Chapter 1

Chapter 2

Chapter 3

Chapter 4

Chapter 5

Chapter 6

Chapter 7

List of tables

Chapter 2

Chapter 3

Chapter 4

Chapter 5

Chapter 6

Chapter 1. Objectives and structure of the PhD thesis

Chapitre 1. Objectifs et structure de la thèse

Frozen methane bubbles, Abraham lake, Canada (Smithsonian magazine, January, 2014)

1.1 General Background

Gas hydrates (GH) were discovered in 1810 by Humphry Davy (Davy, 1811) and since then they started to be the interest of scientific and engineering research studies. They are often studied as a potential energy resource (Collett, 2002); a submarine geo-hazard (Mienert et al., 2005) and a potential agent in climate change (Waite et al., 2009). According to the U.S. Geological Survey, global stocks of GH account for at least 10 times the supply of conventional natural gas deposits. If these vast sources of natural gas could be safely extracted, GH could be one of the top sources of the world's energy. However, the lack in knowledge of the mechanical properties of GH, which is substantial to the understanding of the mechanical behaviour of GH-bearing sediments (GHBS) and their response to hydrates dissociation, remains an obstacle in this matter. In order to approach all these topics, detecting and quantifying GH as well as characterising the physical and mechanical properties of their host sediment have become the interest of many academic research and industrial projects. The present work relies on a unique dataset of in-situ acoustic, piezocone, pore-pressure dissipation measurements, coring and drilling as well as seismic data profiles in a high gas flux system offshore Nigeria (Figure 1. 1). The dataset has been fully exploited in order to define methods to detect and quantify GH and highlight their morphology and distribution pattern in clayey sediments. The workload has been divided into phases, which were performed in a chronological order, as follows:

Phase 1: Establishment of a petro-physical model that integrates the density, mineralogical, geochemical and in-situ acoustic measurements in order to determine GH content within the clayey sediment of the study area.

Phase 2: Correlations of in-situ acoustic and geotechnical data as well as cores with seismic profiles in order to understand the effect of GH content, morphology and distribution on the geomorphology of the study area.

Phase 3: Correlations between in-situ acoustic, geotechnical and pore-pressure dissipation measurements in order to highlight the effect of GH content, morphology and distribution on the mechanical and hydraulic properties of the host sediment.

Phase 4: Use of a constitutive model capturing the mechanical behaviour of hydrate-bearing sediment to compare numerical results with experimental data (acquired from available research) and ultimately confirm various results observed throughout this study.

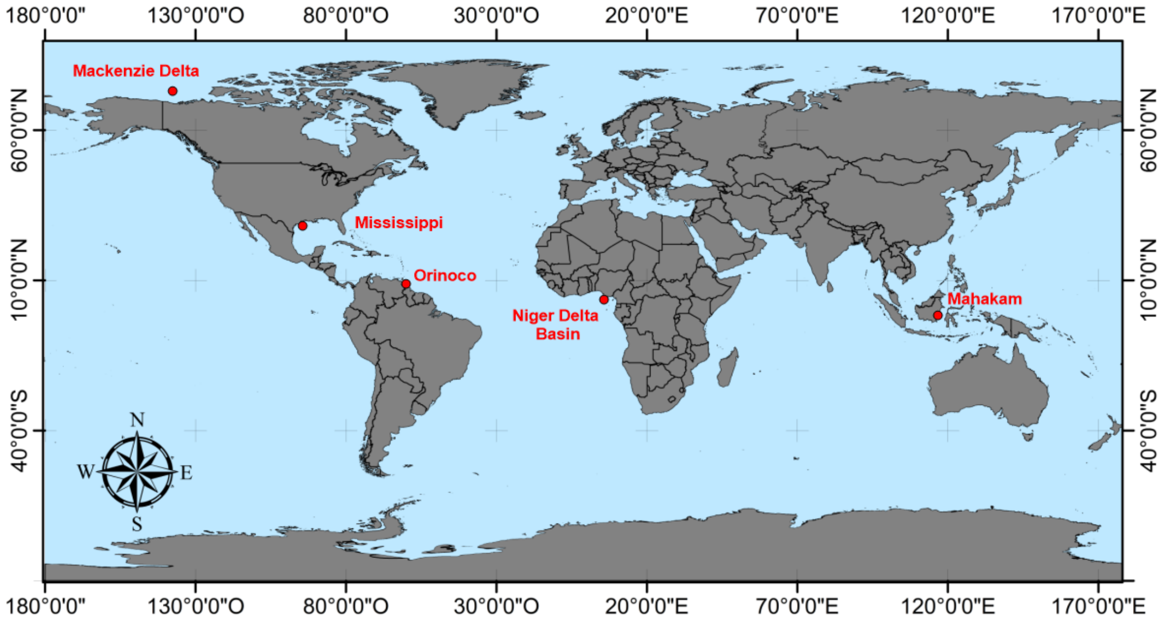

Figure 1. 1 Map showing the Niger Delta basin and other important hydrocarbon reservoirs

1.2 ANR Hydre Project

This thesis is a part of an ANR (French Research Agency) project entitled "HYDRE" (with the grant number ANR-15-CE06-0008) that aims to study the mechanical behaviour of GHBS (Figure 1. 2). The project is composed of four tasks, each with specific objectives to tackle the main subject at different scales. This allowed overcoming several scientific and technical barriers often faced when working on geomaterials containing GH.
This PhD work has been carried out as part of the fourth task of the project.

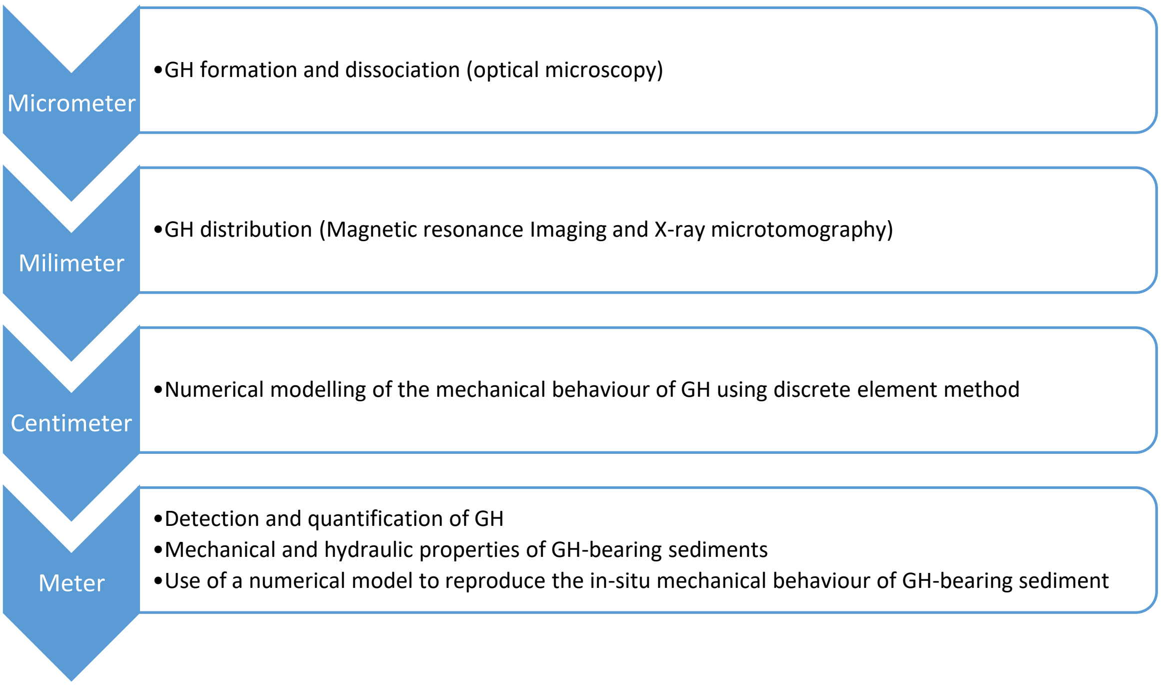

Figure 1. 2 Illustration of the multiscale approach developed through the four tasks of the ANR HYDRE project

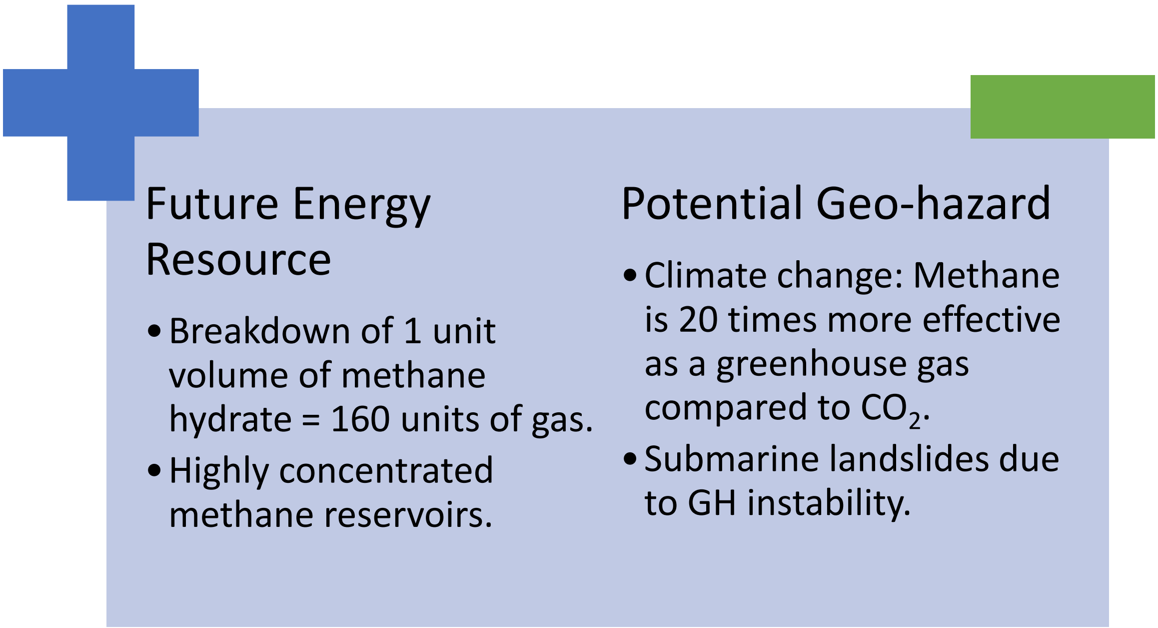

Future Energy Resource

- Breakdown of 1 unit volume of methane hydrate = 160 units of gas.
- Highly concentrated methane reservoirs.

Potential Geo-hazard

- Climate change: Methane is 20 times more effective as a greenhouse gas compared to CO_2.
- Submarine landslides due to GH instability.

Figure 1. 3 Research themes for natural GH

1.3 Scientific aims

Many questions and challenges stimulate the research of the impact of natural GH content, distribution and morphology on the mechanical behaviour of GHBS, such as:

- The ability to safely and efficiently extract and use GH as a future energy resource,
- The estimation of the impact of GH decomposition on the stability of continental slopes as well as on the climate change,

Therefore, hereafter, the main scientific questions that inspired the PhD thesis are discussed.

1.3.1 On the importance of studying gas hydrates: detection and quantification

According to Collett and Lad (2000), the main common point relating GH status as resource, geohazard and climate change agent is the need to accurately detect the presence of these hydrates as well as estimate the amount of gas they store. Figure 1. 3 shows the main research themes under which GH are often studied. While GH accumulations might present a tempting future energy resource, GH instability (decomposition) has many consequences on the host sediment as it replaces a rigid component (i.e. hydrate) with free gas and water. This results in an excess pore fluid pressure, which alters the behaviour and mechanical properties of marine sediments by significantly weakening the resistance of the sediment. This can ultimately affect the occurrence and location of submarine landslides.

Nowadays, the mechanical behaviour of natural GH-bearing sediment is poorly understood, particularly in the case of fine-grained sediments. This work aims to study the mechanical behaviour of GH-bearing clayey sediments in order to (1) solve unanswered questions concerning the effect of GH content and morphology on their host sediment and (2) limit the environmental and economic impacts that might result from their natural and anthropic destabilisation.

1.3.2 On the importance of studying different morphologies of gas hydrates

The morphology of GH and their distribution within the sediment has a significant impact on how the presence of these hydrates alters the mechanical behaviour of the host sediment.

The occurrence of GH is controlled by many factors such as the geological characteristics and physical properties of their host marine sediment. Collett et al. (2014) and You et al. (2019) identified different GH systems (Figure 1. 4) by taking into account the host lithology (sand or clay) as well as the gas supply conditions (vent or non-vent sites). For this work, the study area is characterised as a high gas flux system with dense and shallow GH accumulations; therefore, it is associated with fracture filling GH at vent sites (orange crosses in Figure 1. 4).

The effect of GH morphology and distribution on the mechanical behaviour of GH-bearing clayey sediments remains poorly understood. Therefore, this thesis aims to tackle this issue by first characterising GHBS and then comparing the results with direct observations of cores recovered in the study area.

1.3.3 On the importance of understanding the mechanical behaviour of gas hydrates-bearing sediment

It has been established that GH-rich environments are considered as a potential energy resource; thus, motivating the industry to develop methane production projects. During such projects, the temperature and pressure conditions are altered in order to modify GH stability conditions and initiate methane production. However, the mechanical behaviour of the GH-bearing sediment after GH decomposition remains poorly understood. GH decomposition may lead to various geological and geotechnical disasters such as: submarine landslides, foundation collapse and methane release in the water column and eventually in the atmosphere (ocean acidification and climate change).

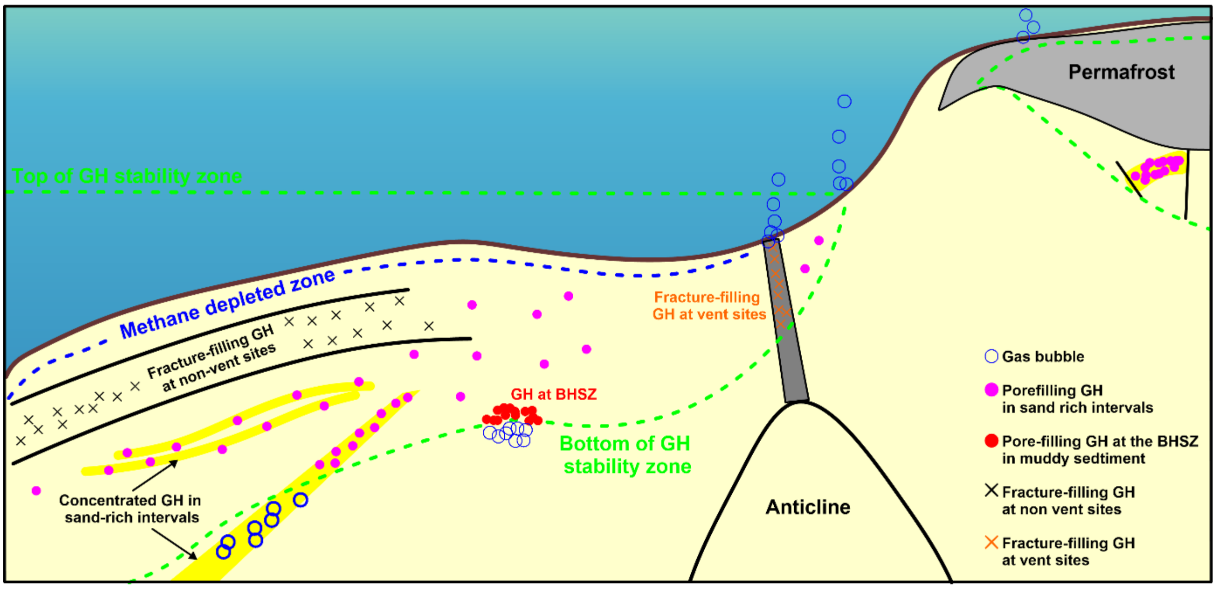

Figure 1. 4 Schematic representation of different GH occurrences and systems showing typical hydrate reservoir morphologies in geological systems (modified from Collett et al., 2014 and Yu et al., 2019)

Therefore, it is important to understand the mechanical properties and behaviour of GH-bearing sediments prior to any industrial exploitation of these resources.

Many authors have been studying the mechanical behaviour of GH-bearing sediments (Masui et al., 2008; Ning et al., 2012; Hyodo et al., 2013; Liu et al., 2013; Song et al., 2013; Winters et al., 2014; Santamarina et al., 2015; Lei et al., 2018; Li et al. 2018) by conducting laboratory triaxial tests on either natural or synthesised GH-bearing sediments. In this work, in-situ data are analysed and then plotted in normalised soil classification charts in order to characterise the behaviour of GH-bearing clayey sediments.

1.3.4 On the importance of the geomechanical modelling of gas hydrates bearing sediments

Geomechanical research aiming to simulate the mechanical behaviour of GHBS has many objectives such as:

- Simulating improvements in cohesion, friction angle, compressibility, strength and stiffness due to GH formation.
- Reproducing the strain softening behaviour that is often observed with increasing GH content during experimental studies.

These studies are generally based on models such as the Mohr-Coulomb model (Freij-Ayoub et al. 2007; Klar et al. 2010) and the critical state model (Kimoto et al. 2010; Sultan and Garziglia 2011). Such models, are often based on a significant number of parameters that mainly account for the sediments properties due to GH presence. Therefore, it is sometimes challenging to apply these models as some of the parameters are hard to determine.

Another difficulty in that matter is the fact that most models simulate the mechanical behaviour of GH-bearing sands. This is due to the lack of experimental research on fine-grained sediments containing GH.

These reasons rise the need to propose a new simple constitutive model, which requires a minimal amount of parameters, which is able to reproduce the mechanical behaviour of GHBS.

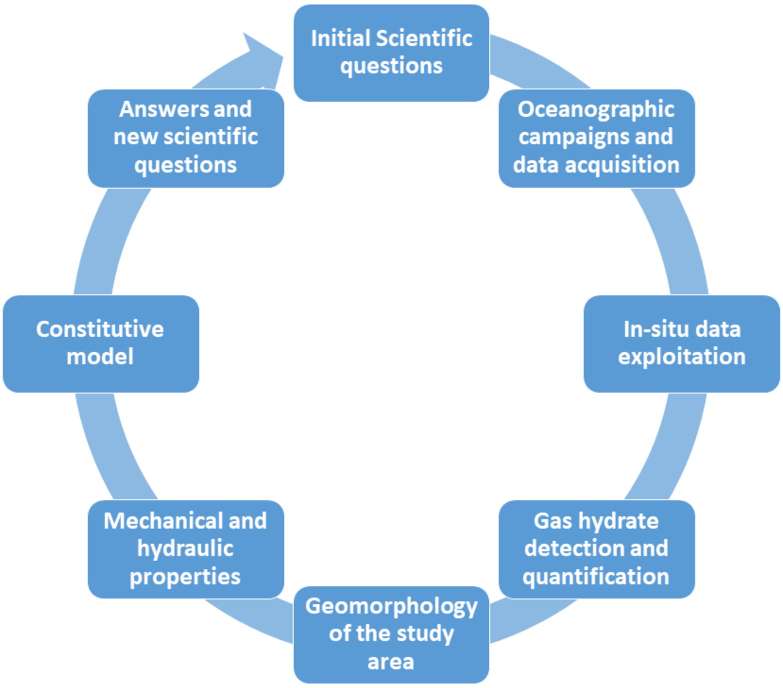

Figure 1. 5 Workflow of the thesis project

1.4 Structure and contents of the manuscript

This manuscript is composed of seven chapters including the present one. The workflow of the thesis project that was followed in order to place the chapters in the manuscript is shown in Figure 1. 5.

1.4.1 Chapter 2: Introduction to gas hydrates

In this chapter, an introduction and generalities on GH are presented. The stability conditions for GH existence as well as several factors affecting them are detailed in separate sections. Then, a review on the available literature about the mechanical properties of GH-bearing sediment is discussed. The chapter ends with a description of GH applications and research interest as (a) an energy resource and (b) a geohazard.

1.4.2 Chapter 3: Study area, tools and methods

In this chapter, the study area and its geomorphological features as well as the data collected during oceanographic campaigns and their objectives are presented. In order to avoid repetition, all tools and methods are grouped in this chapter.

The database is composed of in-situ acoustic, geotechnical, pore-pressure dissipation measurements, cores and seismic profiles. Additionally, all the methods used to detect, quantify and characterise GH are presented as well as all the equations that served to determine the hydro mechanical properties of GHBS.

1.4.3 Chapter 4: Mineralogy analysis, gas hydrates detection, quantification and correlation with seismic data

Chapter 4 focuses on establishing the petro-physical model that serves to estimate GH contents. These are then projected on seismic profiles in order to draw a link between them and the geomorphology of the study area. This eventually allowed defining a detailed GH occurrence zone, estimate its volume and its occupancy ratio in the study area.

The results of this chapter were used to write a scientific paper, which is under revision in Marine and Petroleum Geology journal.

Reference: Taleb, F et al. Seafloor depressions on the Nigerian margin: seabed morphology and sub-seabed hydrate distribution. Paper under revision. Marine and Petroleum Geology.

1.4.4 Chapter 5: Hydro-mechanical properties of gas hydrates-bearing fine sediments from in-situ testing

Chapter 5 focuses on studying the effect of GH content, distribution and morphology on the hydraulic and mechanical properties of GHBS. The work consisted of detecting, quantifying and characterising GH by correlating different in-situ and laboratory measurements. Normalised soil classification charts were used in order to outline the mechanical behaviour of GH-bearing clays. Then, different hydraulic and mechanical properties of the GHBS were determined using empirical equations.

The results of this chapter were used to write a scientific paper that makes part of a special issue entitled "Gas Hydrate in Porous Media: Linking Laboratory and Field Scale Phenomena".

Reference: Taleb, F. et al. 2018. Hydro mechanical properties of gas hydrate-bearing fine sediments from in-situ testing. Journal Of Geophysical Research - solid Earth, 123(11), 9615-9634

1.4.5 Chapter 6: Formulation of a simple constitutive model for gas hydrates-bearing sediment behaviour

In this chapter, a review of the main features of the mechanical behaviour of fine-grained and coarse-grained sediments containing GH is presented. This is followed by a review of the available numerical models in the literature that are able to reproduce the aforementioned behaviour. Then, a new simple constitutive model (Personal communication, Sultan) that requires only one additional parameter related to the GH morphology is presented. The model is validated for clean sands and clays as well as for GH-bearing sands and clays by comparing its results to available experimental results in the literature.

1.4.6 Chapter 7: Conclusion and perspectives

In this final chapter, the conclusions of all the chapters (2 to 6) are synthesised in order to determine the main achievements of this PhD work.

Perspectives and new scientific questions are proposed in order to inspire future scientific projects and research interested in tackling questions related to the geomechanics of GHBS.

1.1 Contexte général et objectifs de la thèse

Les hydrates de gaz (GH) ont été découverts en 1810 par Humphry Davy (Davy, 1811). Depuis cette découverte, les GH ont motivé de nombreuses recherches scientifiques et techniques. Les trois thématiques principales de recherche sur les GH concernent leur source potentielle d'énergie (Collett et al., 2002), les instabilités de pentes sous-marines qu'ils peuvent engendrer (Mienert et al., 2005) ainsi que leur impact sur le réchauffement climatique (Waite et al., 2009). Selon l'US Geological Survey, les réserves mondiales des GH sont au moins 10 fois plus importantes que les réserves de gaz conventionnel. S'il était possible d'extraire en toute sécurité cette source naturelle de gaz, les GH pourraient devenir l'une des principales sources d'énergie de la planète. Cependant, le manque de connaissances sur les propriétés mécaniques des GH, indispensable pour comprendre le comportement mécanique des sédiments qui contiennent ces hydrates (GHBS), reste problématique. Le présent travail s'appuie sur une base de données unique comprenant des mesures in-situ acoustiques, géotechniques, des mesures de dissipation de la pression de fluides interstitiels, des carottages et forages, ainsi que des profils de données sismiques dans un environnement caractérisé par un important flux de gaz au large du Delta du Niger (Figure 1. 1). Toutes ces données ont été analysées afin de déterminer des méthodes de détection et de quantification des GH. Ceci a permis de définir différentes morphologies/distribution des GH dans le sédiment argileux caractéristique du Golfe de Guinée. Le travail a été divisé en plusieurs phases comme suit :

Phase 1 : Établir un modèle pétro-physique intégrant des mesures de densité, de minéralogie, de géochimie et d'acoustique afin de déterminer la saturation en GH dans les sédiments argileux de la zone d'étude.

Phase 2 : Réaliser des corrélations de données in-situ acoustiques et géotechniques avec des carottes et des profils sismiques pour comprendre l'effet de la saturation en GH, de leur morphologie et distribution sur la géomorphologie de la zone d'étude.

Phase 3 : Réaliser des corrélations de données in-situ acoustiques et géotechniques avec des mesures de dissipation de la pression interstitielle pour déterminer l'influence de la saturation en GH, de leur morphologie et distribution sur les propriétés mécaniques et hydrauliques du sédiment de la zone d'étude.

Phase 4 : Utiliser un modèle constitutif capable de reproduire le comportement mécanique des sédiments contenant des GH et comparer les résultats avec des données expérimentales (issues de la littérature) pour confirmer les tendances mises en évidence tout au long de ce travail de thèse.

1.2 Projet ANR HYDRE

Cette thèse fait partie d'un projet ANR (Agence Nationale de recherche) intitulé « HYDRE » (N° ANR-15-CE06-0008) portant sur l'étude du comportement mécanique des sédiments contenant des GH (Figure 1. 2). La particularité de ce projet est qu'il est divisé en 4 tâches. Chacune a des objectifs spécifiques pour aborder le sujet à différentes échelles spatiales. Cela a permis d'éclaircir plusieurs obstacles scientifiques et techniques généralement rencontrés au cours des études des sédiments contenant des GH.

Ce présent travail de thèse s'inscrit dans le cadre de la dernière tâche du projet.

1.3 Questions Scientifiques

De nombreuses questions et défis stimulent la recherche sur l'impact de la distribution et de la morphologie des hydrates naturels sur le comportement mécanique des GHBS. On peut citer:

- La possibilité d'extraire d'une manière efficace et sure le gaz naturel des GH,
- L'impact de la décomposition des GH sur la stabilité des pentes continentales ainsi que sur le changement climatique.

1.3.1 Les enjeux de l'étude les hydrates de gaz: détection et quantification

La nécessité de détecter avec précision la présence des GH et d'estimer la quantité de gaz qu'ils stockent est selon Collett and Lad (2000) le point commun des thématiques de recherche sur ces GH (ressources énergétique ou aléa géologique). La Figure 1. 3 montre les principaux axes de recherche pour lesquels les GH sont souvent étudiés. Même si les accumulations des GH peuvent être attrayantes pour leur aspect énergétique, leur instabilité (décomposition) a de nombreuses conséquences sur les sédiments. En effet, la décomposition des GH remplace un composant rigide (hydrate) par du gaz libre et de l'eau. Ceci peut provoquer une augmentation de la pression interstitielle et altérer le comportement mécanique des GHBS en affaiblissent leur résistance. Il est proposé dans la littérature que ces processus peuvent contribuer au développement de plans de ruptures et en définitive, à la mise en place de glissements sous-marins.

Aujourd'hui, les propriétés mécaniques des GHBS sont encore trop peu quantifiées, notamment pour les sédiments argileux. Ce travail vise à étudier le comportement mécanique des GHBS afin de (1) répondre aux questions encore non résolues concernant l'effet de la saturation et morphologie des GH sur leur sédiment hôte et (2) limiter les impacts environnementaux et économiques pouvant résulter de leur déstabilisation naturelle ou anthropique.

1.3.2 Les enjeux d'étudier différentes morphologies d'hydrates de gaz

La morphologie et distribution des GH ont un impact important sur le comportement mécanique des GHBS.

La présence des GH est principalement contrôlée par les caractéristiques géologiques et les propriétés physiques du sédiment. Collett et al. (2014) et You et al. (2019) ont identifié différents systèmes de GH (Figure 1. 4) selon la lithologie du sédiment (sable ou argile) ainsi que les conditions d'alimentation en gaz (système à flux de gaz élevé ou non). Pour ce travail, la zone d'étude se caractérise par un système de flux de gaz élevé avec des accumulations d'hydrates denses et peu profondes : type « fracture-filling at vent sites » sur la Figure 1 .4.

Aujourd'hui, les études de l'effet de la morphologie et distribution des GH sur le comportement mécanique des sédiments argileux contenant des GH sont encore incomplètes. Cette thèse cherche donc à enrichir ces recherches en (1) caractérisant les GHBS puis (2) en comparant les résultats avec les données de carottage issues de la zone d'étude.

1.3.3 Les enjeux de la compréhension du comportement mécanique des sédiments contenant des hydrates de gaz

Certains environnements riches en GH sont aujourd'hui considérés comme de potentiels sites d'extraction de gaz naturels. Toutes les méthodes d'extraction pressenties impliquent de modifier les conditions de température et de pression du sédiment de manière à changer la stabilité des GH. Il ressort néanmoins que les modifications imposées et leur effet sur les propriétés mécaniques des GHBS demeurent difficiles à maitriser. La décomposition des GH peut en effet entraîner des aléas géologiques et géotechniques comme : des glissements sous-marins, des déstabilisations des fondations de plateformes maritimes et une libération du méthane dans les océans et l'atmosphère (acidification de l'océan et réchauffement climatique). C'est donc pour cette raison que la compréhension des propriétés mécaniques et du comportement des GHBS est indispensable.

De nombreux auteurs ont étudié le comportement mécanique des GHBS (Masui et al., 2008; Ning et al., 2012; Hyodo et al., 2013; Liu et al., 2013; Song et al., 2013; Winters et al., 2014; Santamarina et al., 2015; Lei et al., 2018; Li et al, 2018). La plupart de ces études se sont basées sur des essais triaxiaux en laboratoire sur des sédiments naturels ou synthétisés. Une approche complémentaire a été menée dans le cadre de cette thèse à travers l'analyse de données géotechniques in-situ.

1.3.4 Les enjeux de développer un modèle simple = capable de représenter le comportement mécanique des sédiments contenant des hydrates de gaz

Les recherches géo-mécaniques visant à simuler le comportement mécanique des GHBS ont de nombreux objectifs tels que:

- Capter l'augmentation de la cohésion, angle de frottement, compressibilité ainsi que de la résistance et de la rigidité due à la présence des GH.
- Reproduire le comportement dilatant ayant tendance à s'accroitre avec l'augmentation de la saturation en GH au cours des études expérimentales.

Ces études sont généralement basées sur des modèles tels que le modèle de Mohr-Coulomb (Freij-Ayoub et al. 2007; Klar et al. 2010) et le modèle d'état critique (Kimoto et al. 2010; Sultan and Garziglia 2011). De tels modèles sont souvent basés sur un nombre important de paramètres principalement corrélés à la présence et la morphologie des hydrates. Par conséquent, il est parfois difficile d'appliquer ces modèles en raison de la difficulté à en déterminer certain de leurs paramètres. De plus, le manque de recherche expérimentale concernant les GHBS argileux font que la majorité des modèles visent à reproduire le comportement mécanique des sédiments non pas argileux mais sableux. Pour toutes ces raisons, il est nécessaire de proposer un nouveau modèle constitutif requérant un minimum de paramètres pour simuler le comportement mécanique du GHBS dans des sédiments argileux.

1.4 Structure et contenu du manuscrit

Ce manuscrit est composé de sept chapitres (dont ce chapitre). L'articulation et la chronologie des thèmes abordés dans ces chapitres est présenté dans la Figure 1.5.

1.4.1 Chapitre 2 : Introduction aux hydrates de gaz

Le chapitre 2 aborde les notions générales relatives aux GH. Un descriptif des conditions de stabilité nécessaire à la formation des GH ainsi que les facteurs affectant cette formation sont présentés en différentes sections. Ensuite, une revue de la littérature des propriétés mécaniques des GHBS est discutée. Le chapitre se termine par une description des possibles applications industrielles des GH et de leur intérêt académique en tant que (a) ressource énergétique et (b) aléas géologique et géotechnique.

1.4.2 Chapitre 3 : Zone d'étude, outils et méthodes

Dans ce chapitre, la géologie de la zone d'étude et l'ensemble des données collectées au cours des campagnes océanographiques sont présentée. De manière à éviter les répétitions tous les outils et méthodes se trouvent dans ce chapitre.

La base de données est composée de mesures in-situ acoustiques, géotechniques, de mesure de dissipation de la pression interstitielle, de carottes sédimentaires et de profils sismiques. Toutes les méthodes utilisées pour détecter, quantifier et caractériser les GH sont présentées. Les équations ayant servi à déterminer les propriétés hydromécaniques du GHBS sont également décrites.

1.4.3 Chapitre 4 : Analyse minéralogique, détection d'hydrates de gaz, quantification et corrélation avec les données sismiques

Le chapitre 4 se concentre sur la conception du modèle pétro-physique permettant d'estimer la saturation en GH. Les résultats sont ensuite projetés sur des profils sismiques pour définir l'effet de la présence des GH sur la géomorphologie de la zone d'étude. Ces corrélations ont permis de délimiter une zone de forte présence d'hydrates et d'estimer son volume au sein de la zone d'étude.

Les résultats de ce chapitre se trouvent dans un article scientifique en cours de révision par la revue Marine and Petroleum Geology.

Reference: Taleb, F et al. Seafloor depressions on the Nigerian margin: seabed morphology and sub-seabed hydrate distribution. Paper under revision. Marine and Petroleum Geology.

1.4.4 Chapitre 5 : Propriétés hydromécaniques des sédiments argileux contenant des hydrates de gaz à partir de mesures in-situ

L'étude de l'effet de la saturation, morphologie et distribution des GH sur les propriétés mécaniques des GHBS est le sujet de ce chapitre. Cela a été possible grâce à des corrélations entre les mesures in-situ et des mesures effectuées en laboratoire. Des diagrammes normalisés de classification des sols ont été utilisés pour caractériser le comportement mécanique des GHBS argileux. Ensuite, différentes propriétés hydrauliques et mécaniques des GHBS ont été déterminées par des équations empiriques.

Les résultats de ce chapitre ont servi à rédiger un article scientifique d'un numéro spécial intitulé “Gas Hydrate in Porous Media: Linking Laboratory and Field Scale Phenomena”.

Reference: Taleb, F. et al. 2018. Hydro mechanical properties of gas hydrate-bearing fine sediments from in-situ testing. Journal Of Geophysical Research - solid Earth, 123(11), 9615-9634.

1.4.5 Chapitre 6 : Formulation d'un modèle constitutif de comportement d'un sédiment chargé en hydrates de gaz

Le chapitre 6 a pour but de passer en revue les principales caractéristiques du comportement mécanique des sédiments sableux et argileux contenant des GH. S'ensuit une analyse des modèles numériques déjà publiés pour reproduire ces traits de comportements. Un nouveau modèle constitutif simple (Personal communication, Sultan) qui ne nécessite qu'un seul paramètre lié à la présence et morphologie des GH est alors présenté. Ce modèle est ensuite validé pour les sables et argiles comportant et ne comportant pas des GH grâce à une comparaison avec des données expérimentales tirées de la littérature.

1.4.6 Chapitre 7 : Conclusions et perspectives

Dans ce dernier chapitre, les principales avancées scientifiques de ce travail sont présentées.

Afin d'inspirer de nouveaux projets visant à continuer ces recherches, des perspectives et des nouvelles questions scientifiques y sont exposées.

Chapter 2. Introduction to Gas Hydrates

Chapitre 2. Introduction aux Hydrates de Gaz

The world, (NASA, 2019)

Abstract

Gas hydrates (GH) are crystalline structures consisting of water molecules and gases. Water molecules form a cavity in which small molecules such as methane, carbon dioxide, nitrogen, hydrogen, etc. are trapped (Loveday and Nelmes, 2008; Sloan and Koh, 2008). In nature, GH are found in the sediments of continental margins and permafrost, lakes (Kvenvolden, 1988; Kvenvolden, 1995b; Matveeva et al., 2003; Kida et al., 2006, Hachikubo et al.; 2010, Khlystov et al.; 2013) and inland seas (Shipley and Didyk, 1982; Kvenvolden et al., 1993; Rastogi, 1999, Ruppel, 2018; Milkov and Sassen, 2003; Milkov, 2004). The amount of methane stored in oceanic hydrates is estimated at more than 20 billion km^3 (Kvenvolden et al., 1993, 2001; Boswell and Collett, 2011). These reservoirs are therefore a potential source of natural gas, whose exploitation is currently not economically viable due to technological constraints related to a limitation of our knowledge of these natural systems. On the other hand, the release of large amounts of methane from these hydrates can induce destabilization of the seabed and endanger offshore industrial facilities or induce tsunamis affecting coastal areas. It is therefore important to understand the dynamics of these sedimentary hydrates, and to identify the factors to which they are sensitive. In addition, since methane is a greenhouse gas, the release of methane trapped in hydrates can contribute to climate change if this gas crosses the water column and enters the atmosphere (Kvenvolden, 1993; Henriet and Mienert, 1998; Kvenvolden, 1999; de Garidel-Thoron et al., 2004; Waite et al., 2009; Boswell and Collett, 2011; Ruppel and Kessler, 2017).

Résumé

Les hydrates de gaz sont des structures cristallines constitués de molécules d’eau et de gaz. Les molécules d’eau forment une cavité dans laquelle sont piégées de petites molécules telles que le méthane, le dioxyde de carbone, l’azote, l’hydrogène, etc. (Loveday and Nelmes, 2008; Sloan and Koh, 2008). Dans la nature, on retrouve les hydrates dans les sédiments des marges continentales et le pergélisol, les lacs (Kvenvolden, 1988; Kvenvolden, 1995b; Matveeva et al., 2003; Kida et al., 2006, Hachikubo et al.; 2010, Khlystov et al.; 2013) et les mers intérieures (Shipley and Didyk, 1982; Kvenvolden et al., 1993; Rastogi, 1999, Ruppel, 2018; Milkov and Sassen, 2003; Milkov, 2004). La quantité de méthane stockée dans les hydrates océaniques est estimée à plus de 20 milliards de km^3 (Kvenvolden et al., 1993, 2001; Boswell and Collett, 2011). Ces réservoirs constituent donc une source potentielle de gaz naturel, dont l’exploitation n’est actuellement pas économiquement viable en raison de contraintes technologiques liées à une limitation de nos connaissances de ces systèmes naturels (Waite et al., 2009 ; Ning et al., 2012). D’autre part, la libération de grandes quantités de méthane de ces hydrates peut induire une déstabilisation des fonds marins, et mettre en danger les installations industrielles offshores ou provoquer des tsunamis. Il est donc important de comprendre la dynamique de ces hydrates sédimentaires, et d’identifier les facteurs physico-chimiques auxquels ils sont sensibles. De plus, le méthane étant un gaz à effet de serre, la libération du méthane piégé dans les hydrates peut contribuer à l’évolution climatique si ce gaz traverse la colonne d’eau et arrive dans l’atmosphère (Kvenvolden, 1993; Henriet and Mienert, 1998; Kvenvolden, 1999; de Garidel-Thoron et al., 2004; Waite et al., 2009; Boswell and Collett, 2011; Ruppel and Kessler, 2017).

2.1 Generalities on gas hydrates

Natural GH (Figure 2. 1) are non-stoichiometric (Helgerud et al., 1999; Sloan and Koh, 2007) ice-like solid compounds formed of gas molecules, which are trapped within a crystalline structure of water molecules (Sloan, 2003). They belong to the family of clathrate, which is clathi in Latin and means lattice bars. Natural GH accommodate hydrocarbons of low molecular mass (i.e. methane, ethane, propane and others). Being often occupied by methane in natural environments, it is also referred to as methane hydrates or the burning ice. At Standard Temperature and Pressure (STP: 0°C, 101.325kPa), 1 m^3 of GH can release 164 m^3 of methane gas and 0.87 m^3 of water.

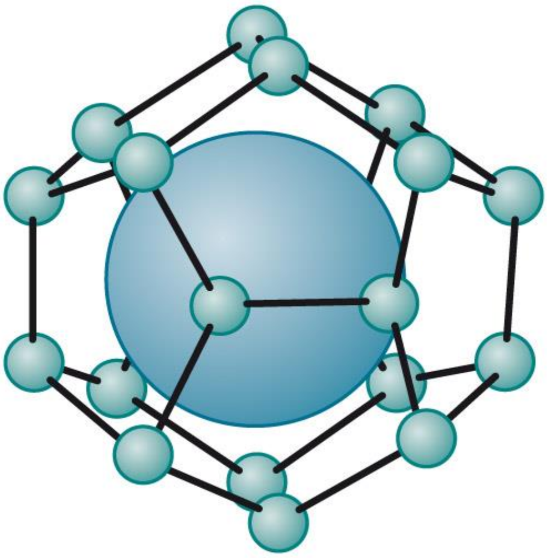

Figure 2. 1 Molecular structure of GH (world ocean review, 2010). The gas-forming molecule is trapped inside a cage formed of water molecules (clathrates).

GH are stable under high pressure and low temperature. Hence, they mainly exist in continental margins and polar permafrost layers (Kvenvolden, 1993; Buffett, 2000) where these stability conditions are well met. GH stability also requires a continuous supply of methane having a concentration that exceeds its solubility in water (Xu and Ruppel, 1999; Malinverno et al. 2008).

GH are considered as the largest untapped stock of natural gas in the world and are the main interest of many research axes focusing on the detection, formation/dissociation and quantification of these potential energy resources. However, due to their metastable nature that is highly affected by any variations in the pressure and temperature conditions of their stability zone, GH are considered as a geotechnical hazard for various offshore operations and hydrocarbon recovery projects. Their possible dissociation could contribute to current and future climate change scenarios or even lead to seafloor instabilities.

They are often studied as a potential energy resource (Collett, 2002); a submarine geo-hazard (Mienert et al., 2005) and a potential contributor in climate change (Waite et al., 2009). According to the U.S. Geological Survey, global stocks of GH would account for at least 10 times the supply of conventional natural gas deposits, with between 100,000 and 300,000,000 trillion cubic feet of gas.

Figure 2. 2 shows different locations around the world where GH can be found. It can be seen that they exist in the majority of oceans like the Arctic, the Atlantic, the Pacific and the Indian as well as in lakes such as Lake Baikal in Russia. If these vast sources of natural gas could be safely extracted, GH could be one of the top sources of the world’s energy. However, the lack in knowledge of the mechanical properties of GH, which is substantial to the understanding of the mechanical properties of GH-bearing sediments and their response to hydrates dissociation, remains an obstacle in this matter (Ning et al., 2012; Yun et al., 2007).

2.2 Gas hydrate formation and stability conditions

The formation and stability of GH is controlled by many parameters: temperature and pressure, the composition of the forming gas and its saturation, the dissolved ions in the surrounding pore water and the pore size of the host medium. These parameters will be discussed in the following sections by highlighting their effects on the formation and stability of GH.

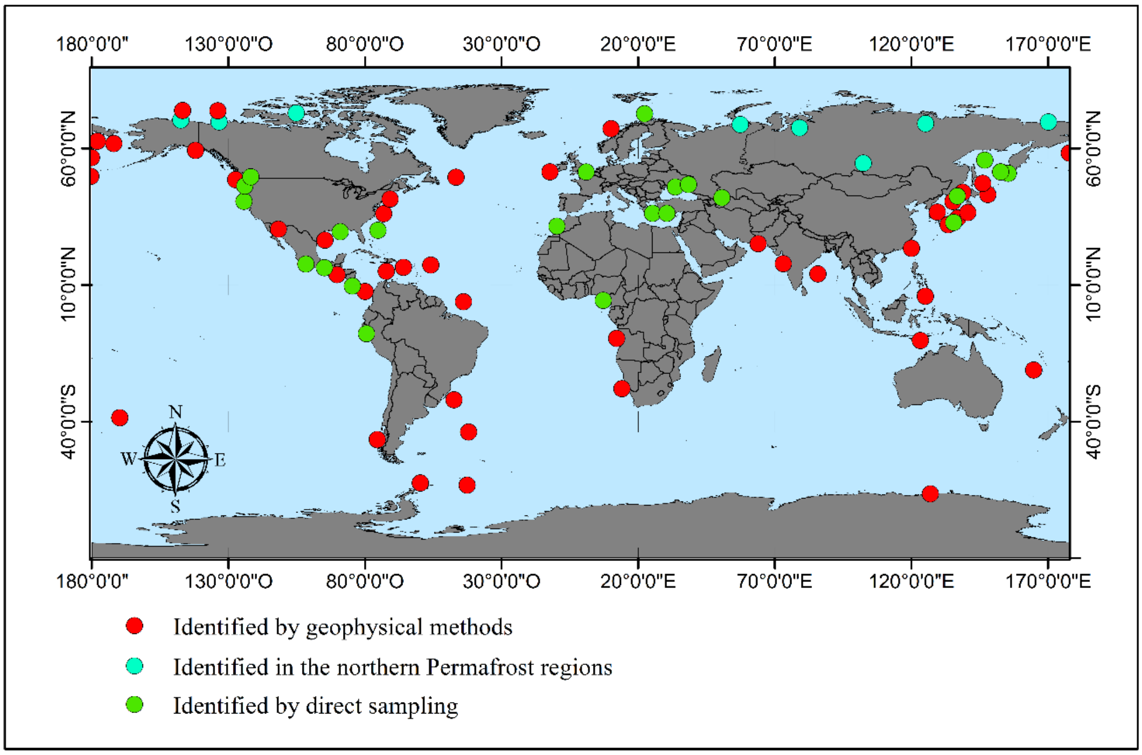

Figure 2. 2 World map showing the distribution of known recovered and inferred GH (modified after USGS)

2.2.1 Gas hydrate nucleation and growth

The nucleation is the first phase of hydrate formation. It is favoured at the water-gas interface when free gas is present and on the mineral surfaces in the absence of free gas due to the spatial distribution of the water molecules in the vicinity of the mineral surfaces (Dai et al., 2012; Chaouachi et al., 2015; Kingston et al., 2008; Priest et al., 2009). Under stable conditions of pressure and temperature, the molecules pass continuously from one phase to another, and it is necessary to achieve a minimum crystal size to generate a stable nucleus of hydrate growth.

The growth phase follows the nucleation. GH develop by forming a thin layer at the gas-liquid interface, which then propagates in the liquid phase. This phenomenon is limited by the diffusion of gas into water. Hydrate crystals may also grow in the gas phase (Youssef et al., 2009, Youssef et al., 2010). Permanent molecular transfer between the phases can gradually change the spatial distribution of hydrates by concentrating the gas molecules around the small nuclei. A concentration gradient is then created between the water surrounding the small nuclei and that surrounding the large crystals. As a result, the gas molecules diffuse to the larger crystals and further promote their growth. This phenomenon is called the Ostwald ripening (Klapp et al., 2007, Jang and Santamarina, 2012). The growth of hydrate crystals can invade neighbouring pores or displace sediment particles to enlarge pore space (Dai et al., 2012).

Chaouachi et al. (2015) investigated xenon hydrate nucleation and growth processes using 276 K X-ray tomographic microscopy in different sedimentary matrices from pure water, then water enriched with gas used after a first formation. They show that the distribution of hydrates in the pores depends on the formation scenario, and the degree of saturation in water. What does not change in all the scenarios studied is the preference of the hydrates to maintain a microlayer of water at the interface with the particles of the porous matrix.

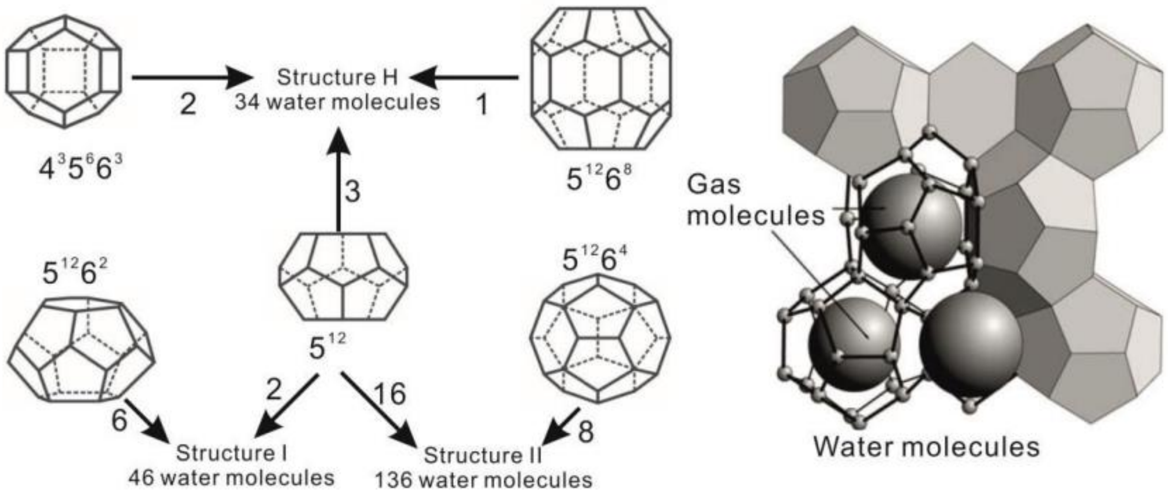

Figure 2. 3 Common GH structures (Bohrmann and Torres, 2006)

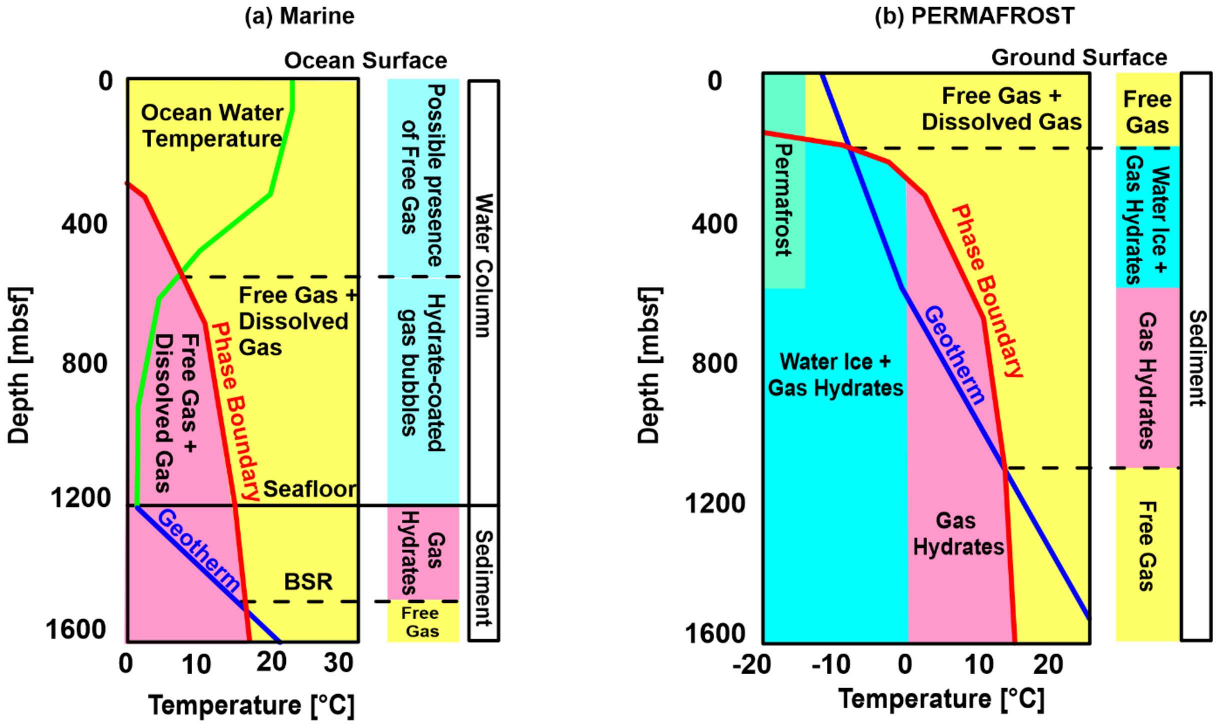

Figure 2. 4 GH stability diagrams for: (a) marine environment and (b) permafrost regions after Ruppel (2007; 2017). For the present marine environment example, GH are stable at around 500 m below sea level where the temperature is lower than that required by the stability curve (red curve). For the present permafrost regions example, GH are theoretically stable starting at around 200 m below ground surface and extending down to several hundred of meters below

2.2.2 Gas hydrate structures

GH belong to the family of clathrates, which are non-stoichiometric solid crystalline compounds with cavities formed of water molecules that are stabilized by hydrogen bonds. The interactions between the cavity and the guest molecule are of Van Der Waals type. Three main crystal structures of hydrates have been clearly identified in Figure 2. 3: cubic structures I, II, and the hexagonal structure H (Sloan Jr, 2003). They depend on the conditions of pressure, temperature and the composition of the gas. The crystalline structures of the SI and SII hydrates were first determined in the late 1940s and early 1950s by von Stackelberg and his colleagues by X-ray diffraction measurements (von Stackelberg and R. Müller, 1951; Koh, 2002; Gabitto and Tsouris, 2010). Depending on the nature of the forming gas occupying the cavities of the same mesh, two types of hydrates can be distinguished. The simple hydrates, where the cavities of the mesh are occupied by the same molecule, and the mixed hydrates, where the cavities are occupied by molecules of different nature.

It is noteworthy that SI is the most common form of GH and is often occupied by methane, ethane or carbon dioxide. Methane is known to be the most common gas found in GH and can be incorporated in structure I, II and H. Other gases, such as CO_2 and H_2S can be found in structure I in small amount. This largely affects the GH-boundary phase for stability.

2.2.3 Gas hydrate stability conditions

2.2.3.1 Temperature and pressure

Hydrate formation and stability conditions are mainly dominated by high pressure and low temperature conditions (Lerche and Bagirov, 1998). These conditions are found in the seabed and subsurface of continental margins as well as in the permafrost of Polar Regions. The most favourable areas for hydrate formation are at or below the seabed and lakes. The pressure in the water increases with the depth of about 1atm for every 10m of water column. For a water depth of 500m, the pressure of the water column will reach more than 50atm. At this depth, the water temperature of the seabed does not generally exceed 4-6 ° C (Lerche and Bagirov, 1998).

Thermobaric conditions are often presented in GH stability diagrams (Figure 2. 4), which serve as means to correlate temperature and pressure values at which GH can form and be stable. This is known as the phase boundary that is marked in red on Figure 2. 4. GH can form when local thermal conditions (geotherms) are colder than the phase boundary (Kvenvolden, 1993). The geotherm gradient slowly increases until reaching a zone where pressure and temperature stability conditions are no longer available and a BSR (Bottom simulating reflector) is formed. When free gas accumulate beneath GH the base of their stability zone can be geo-physically imaged by the so-called BSR. Accordingly, the BSR can provide clues on local P-T conditions. Therefore, the GH stability zone, which upper and bottom limits are defined based on local conditions, can be identified.

2.2.3.2 Hydrocarbon source

The gases trapped in the hydrates of marine sediments are of thermogenic or microbial origin. They generally differ in their molecular and isotopic compositions (Whiticar et al., 1986, Whiticar, 1996, 1999, Milkov et al., 2005, Etiope et al., 2009, Ruffine et al., 2017). Thermogenic gas is the natural gas formed by thermal cracking of kerogen at great depth (Berner and Faber, 1996; Pohlman et al., 2005; Kida et al., 2006; Lu et al., 2007; Bourry et al., 2009; Hachikubo et al., 2010). It is the result of chemical reactions triggered by heat and pressure rather than the presence of microorganisms. It is mainly composed of methane, but is often characterized by a large fraction of heavier hydrocarbons (C2 +) (Mazzini et al., 2004, Demirbas et al., 2016). Microbial or biogenic gas results from low temperature methanogenesis by microorganisms present in marine sediments (Whiticar et al., 1986, Ruffine et al., 2017). It is made of methane with more than 99% -mol.

2.2.3.3 Solubility of the forming gas

The composition of the forming gas, often methane, and its saturation are essential to the GH formation process. The maximum amount of methane that can occur in a methane hydrate is controlled by the clathrate geometry. Natural GH form about 90% of the cages of the clathrate, which means that 150 volumes of methane is needed per one volume of water. Additionally, the amount of methane required for GH formation should greatly exceed its solubility in water; thus limiting the regions at which GH can be found.

Figure 2. 5 shows the evolution of the solubility of methane in the sedimentary column and the water column (Waite et al., 2009). The fluid rising up the sedimentary column may not be saturated enough with methane and therefore cannot precipitate into hydrates before reaching the depth at which the solubility limit is low enough to equal the concentration of

methane in the rising fluid. In some cases, while the conditions of temperature and pressure are favourable for the formation of hydrates, there is an absence of hydrates. This can be due to a methane concentration below the saturation value (i.e. the methane concentration is less than the solubility or anaerobic oxidation of methane).

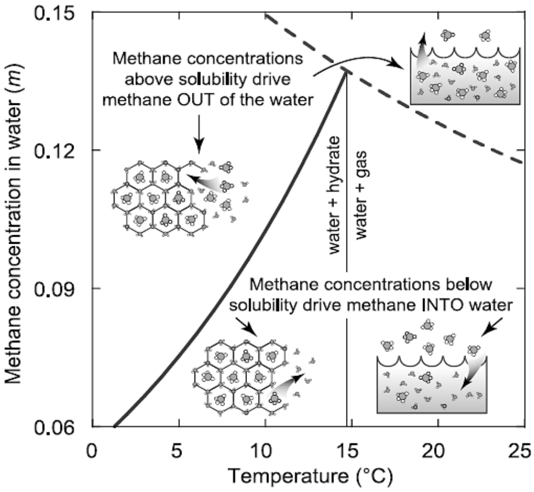

Figure 2. 5 Solubility of methane in water in the absence and presence of GH (Waite et al., 2009)

During dissolution, the hydrate dissolves in the aqueous phase, increasing the concentration of methane in the water. During precipitation, the formation of hydrates consumes methane from the aqueous phase, thus reducing its concentration in water. In the presence of hydrates, dissolution and precipitation occur at the same rate when the concentration of methane in the water reaches the solubility limit. In the absence of hydrates, the methane molecules move at equal velocities between the free gas phase and the dissolved phase when the concentration of methane in the water reaches the solubility limit. The solubility of methane in pore water is mainly controlled by the temperature and pressure and the dissolved ions in the surrounding water. All these parameters are also affected by the absence/presence of GH as seen in Table 2. 1.

Alternatively, Bai and Bai (2010) presented results regarding the effect of the gas composition on the GH stability. The formation of GH was observed to decrease with decreasing size of molecular components of the forming gas.

2.2.3.4 Dissolved ions in the surrounding water

The presence of ions in pore water can highly affect the GH stability zone. This is mainly because ions could mix up with the water molecules preventing them from being arranged into a cage structure. Thus, decreasing the chances of GH formation and stability.

Results found by Husebø et al. (2009) confirmed that the hydrate stability pressure increases with increasing salinity. It is important to know the salinity degree of the surrounding water with which hydrates will be formed in order to indicate the stability conditions of such formation.

It is noteworthy that GH formation excludes chloride ions from the process; thus, resulting in a more saline surrounding water, which could eventually prevent further GH formation Østergaard et al. (2002).

2.2.3.5 Pore size and grain distribution

Results found by Mingjun et al. (2010) suggested that the decrease in pore size increases the equilibrium pressure of GH. In other words, lower temperature and higher pressure are required for GH formation and stability.

Uchida et al. (1999; 2002) and Handa and Stupin (1992) studied the effect of different pore sizes on the dissociation of GH. However, experimental results conducted by Østergaard et al. (2002) suggests that the previously mentioned data is unreliable. Østergaard et al. (2002) discusses that in small-diameter porous media it is challenging to achieve uniform liquid concentrations though the sediment. This results in uneven and rapid hydrate formation trapping pockets of liquid within them. This suggests that these kind of hydrates drastically reduce the permeability of the medium and inhibit further fluid migrations.

Table 2. 1 Parameters controlling the solubility of methane in water in the absence and presence of GH (after Waiter et al., 2009)

Controlling parameters	Absence of GH	Presence of GH
Solubility/Temperature	When the temperature increases the kinetic energy of both water and methane molecules increases. This leads to the breakup of the intermolecular liaisons between water and methane and promote the transition to the gaseous phase. Thus, the solubility of methane decreases when the seawater temperature increases in the absence of GH.	When the temperature increases, GH will dissociate and the solubility of methane will increase.
Solubility/Pressure	The solubility of methane in water increases with increasing pressure.	High pressure implies GH formation, if temperature stability conditions are available. The solubility slightly decrease with increasing pressure as gases prefer to exist in the hydrate rather than in water
Solubility/Salinity	The addition of salt leads to the exclusion of methane in the presence and absence of gas. Methane solubility decreases when salinity increases in the surrounding water.	

2.3 Gas hydrate detection and quantification

The formation of GH in sediments alters the latter's properties and behaviour. At sufficient concentrations, GH are able to modify the sediment's properties significantly impacting therefore their acoustic signatures. Different types of evidence can be used to detect the *presence of GH in a sediment (Kvenvolden, 1998).*

2.3.1 Gas hydrate detection

Many geological hazards and seafloor deformations such as submarine slides and pockmarks have been directly related to GH' presence. Jansen et al. (1987); and Sultan et al. (2004) presented a possible connection between the Storegga slide offshore from Norway and GH occurrence. Additionally pockmarks formations in the Gulf of Guinea have been have been linked to different habits of formation, nucleation and decomposition of GH (Sultan et al., 2007; 2010; Wei et al., 2015).

2.3.1.1 Coring and sampling

The presence of GH in a sediment replaces the pore water and/or gas with a solid compound (hydrates). This reduces the effective pore space and the permeability of the sediment and increase the acoustic velocity, which can be detected using well logging tools (see chapter 3 for information about in-situ geotechnical measurements).

Additionally, GH can be recovered using classical coring systems. However, when brought to surface, the change in the pressure and temperature conditions leads to the dissociation of GH, hence releasing gas and water and changing the in-situ properties of the sediment. This results in a fluidized and mousy recovered material.

Furthermore, infrared thermal scanning of recovered cores allow the detection of GH (Wei et al., 2015). The dissociation of GH is known to be an endothermic reaction; thus, it requires the absorption of heat. Therefore, negative thermal anomalies are an indicator of the presence of GH.

Another method to detect GH is pressure coring (Santamarina et al., 215). It is the only known technique that is able to recover marine sediment to the surface while preserving the in-situ conditions (Abid et al., 2015).

2.3.1.2 Geochemistry

The formation/decomposition of GH largely affect the chemistry of the surrounding water body: during GH formation, the hydrate crystals exclude chloride ions from the process; thus, the decomposition of GH releases gas and fresh water (Malinverno et al. 2008). By combining pore water chemistry with in situ log measurements, GH profiles can be determined. Hence, the detection of GH is based on the decrease in chlorinity due to the fresh water released by hydrate dissociation during core recovery (Soga et al., 2006).

This has been observed in cores recovered from the Gulf of Guinea, where negative chloride anomalies were used as a tool for GH detection and quantification (Wei et al., 2015).

2.3.1.3 Geophysics

Data from seismic profiling and various kinds of well logging are geophysical means of detecting of GH.

Seismic reflection profiling is amongst the best techniques for remotely sensing sediments below the surface or beneath deep bodies of water (Helgerud et al., 1999), showing high-impedance seismic reflections caused by free gas at the base of the phase boundary (BSR). GH form a rigid layer with low permeability and are able to trap free gas beneath them. The BSR marks the discontinuity along the interface between higher seismic velocity zones (solid GH) and lower seismic velocity zones (free gas) (Berndt et al., 2004). This defines the base of the GH stability zone. For instance, Collett and Ladd (2000) investigated the occurrence of GH in the Blake ridge in the southeastern continental margin of North America, where BSRs have been remarkably mapped at different locations. However, as this method depends on the decrease of velocity caused by the presence of free gas, it is expected that sediments with low GH or free gas saturations will not be identified by the BSR.

2.3.2 Gas hydrate quantification

Proper knowledge of GH content is required in order to understand their effect on their host sediment and assess the geotechnical hazard they may pose.

2.3.2.1 Rock physics characterisation

Many models that allow the quantification of GH have been introduced in the last decade. The baseline of these models is to relate compressional velocity anomalies to hydrate fraction in the sediment. For instance, an empirical model has been presented by Wyllie et al. (1956). Another model developed by Kumar et al. (2007) have been used to estimate the concentration of GH at the Hydrate ridge, Oregon. Helgerud et al., (1999) developed a model based on the effective medium theory, which allows estimating GH concentration in the sediment based on the medium mineralogy and elastic properties. Validation against experimental results proved the model to yield reliable results for GH-bearing sandy sediments. Shankar et al. (2013) followed the approach of Helgerud et al. (1999) to determine the GH and free gas saturation in the Krishna-Godavari Basin, eastern Indian margin. Numerical results have shown that the effective medium models are more accurate compared with tested empirical models, since the physical properties of the sediment were taken into consideration. Ghosh at al. (2010) introduced an effective medium model of GH in clayey sediments (Krishna-Godavari basin) that takes into consideration the orientation of the fractures caused by the GH formation in fine-grained sediments.

Throughout this thesis, the effective medium model developed by Helgerud et al. (1999) has been used to quantify GH within marine sediments. The quantification of the GH content is linked to the hydrates growth habit in the sediment:

- GH are part of the pore fluid and does not affect the density or stiffness of the dry frame.

- GH are part of the dry frame, which reduces the porosity and modifies the solid phase of the sediment.

More insight on this method is provided in chapter 3.

2.3.2.2 Downhole logs and electrical resistivity

GH content can be estimated from downhole logs based on measurements of porosity and electrical resistivity, which depends on the pore water content (Malinverno et al., 2008). However, GH might act as an insulator preventing electrical conductivity throughout the sediment. Hyndman et al. (1999) and Collett and Ladd (2000) used this approach in order to quantify GH content in marine sediments based on the following equation:

$$S_h = 1 - S_w = 1 - \left(\frac{aR_w}{\phi^m R_t}\right)^{1/n} \qquad (2.1)$$

Where S_h is the GH saturation, S_w is the water saturation, R_w is the pore water resistivity, R_t is the bulk resistivity, ϕ is the sediment porosity, a is the tortuosity coefficient, m is the cementation exponent and n is the saturation exponent.

n depends on the distribution of GH within the pore space (Spangenberg, 2001) and is determined within 0.5-4 interval. Estimating values of a and m for a given marine water-saturated sediments relies on fitting of the following equation with measured porosities and resistivities:

$$R_0 = \frac{aR_w}{\phi^m} \qquad (2.2)$$

Where, R_0 is the fully water saturated resistivity.

2.3.2.3 Pore-water chloride analysis

As stated above, The formation of GH is known to exclude ions dissolved in pore water from the clathrate cage; hence, increasing the salinity of the surrounding pore water (Ussler and Paull, 2001). Therefore, the dissociation of GH upon core recovery releases fresh water, causing negative anomalies on pore-water chloride profiles (Wei et al., 2015). Malinverno et al. (2008) proposed a model that allows the quantification of GH based on negative chloride anomalies. More insight on this method is provided in chapter 3.

2.4 Gas hydrate formation in natural sediments

In general, coarse-grained soils such as sands and gravels have large pores and thus high permeability, which allows fluids to flow freely through the large and continuous void spaces. However, fine-grained soils have much smaller void spaces, which poorly connected. This leads to a low permeability preventing fluids from flowing freely. This directly affect the type of hydrate formation in the sediments. Sands are characterised by disseminated pore filling hydrates; whereas clays accommodate veined or nodule type hydrate (Lei and Santamarina, 2018). The Mallik permafrost in Canada and the Nankai Trough in Japan are characterised by their coarse-grained soil. Hence, GH are developed as pore-filling materials in these regions. On the other hand, fine-grained regions such as the Blake ridge offshore the U.S. and the Hydrate Ridge offshore western Canada, contain more GH than all coarse-grained reservoirs. However, hydrates formed in these regions are found in localised areas as nodules or veins. (Waite et al 2009, Collett et al 2014). GH are found to form more readily in coarse-grained soils. This is because, in fine-grained soils, the transport rate of gas and liquid is very slow, which can limit the accumulation of hydrates (Soga et al., 2006).

The formation of GH within sediment is mainly governed by the changing physical properties of the latter such as grain size, porosity, and permeability (Waite et al., 2009). This directly affects the morphology of the hydrate within the host sediment.

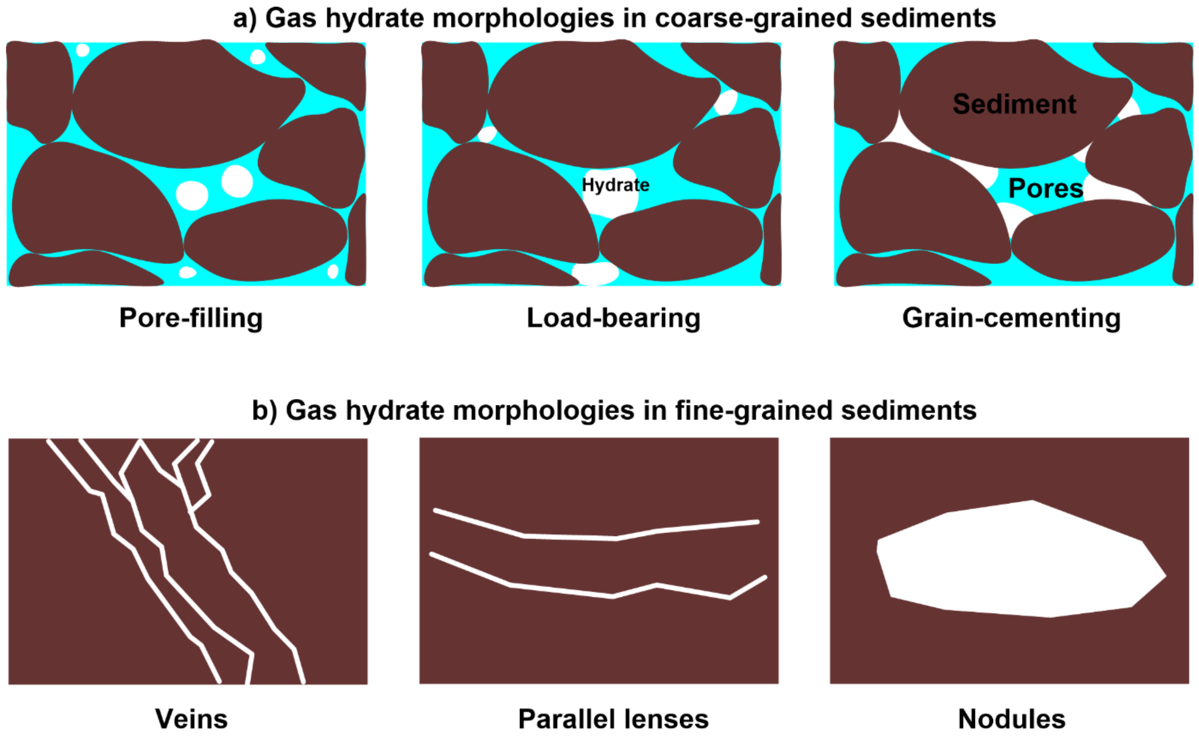

Figure 2. 6 Possible GH morphologies in: a) coarse-grained sediments and b) fine-grained sediments (Spangenberg et al., 2014)

2.4.1 Gas hydrate formation in coarse-grained sediment

The distribution of hydrates in the pores affects the properties of the host sediment. There are three main types of hydrate crystal distribution in the pores of the coarse-grained sediments as shown in Figure 2. 6.a. These distributions depend on the availability of water and gas in the pores, the size and nature of the sediment grains, and the mechanisms of hydrate nucleation and growth (Strauch et al., 2015, Waite et al. 2009).

2.4.1.1 Pore-filling

In this case, the hydrates are only part of the pore fluid. Nucleation of GH on the sediment grain boundaries takes place leading to a pore filling behaviour (growth of hydrates into pore spaces). GH occupy the pore space without bringing the grains into contact (Figure 2. 6.a) with each other at a saturation level of less than 25%. The bulk stiffness of the pore fluid and the fluid conduction properties are affected by this behaviour (Waite et al., 2009). Nankai Trough (Japan), Mallik-Mackenzie Delta (Canada), Blake Ridge (US) and Hydrate Ridge (US) are found to have a pore filling type of hydrates (Soga et al., 2006).

2.4.1.2 Load-bearing

In this case, GH act as a bridging agent between the sediment grains (Figure 2. 6.a). They contribute to the mechanical stability of the granular skeleton and act as a part of the load-bearing framework (Waite et al., 2009). This reduces the sediment porosity while the hydrates concentration increases (Soga et al., 2006). The "pore filling" formation can be transformed into "load bearing" when the hydrate saturation exceeds Sh = 25-40%.

2.4.1.3 Grain-cementing

In this case, GH are part of the dry frame Figure 2. 6.a) and act as a cementing agent between the sediment particles by bonding adjacent grains (Waite et al., 2009), even if previously discussed that a water film forms at the hydrate-sediment particle interface. This increases both the shear and bulk stiffness while decreasing the porosity (Soga et al., 2006). This type of formation has the greatest impact on the mechanical properties of the sediment for degrees of hydrate saturation as low as 13 to 22% (Waite, 2009).

2.4.2 Gas hydrate formation in fine-grained sediment

The grain-displacing morphology is mostly observed in clay-rich sediments where GH form in fractures due to capillary tension forces (Jang and Santamarina, 2016). In this case, they force the clay aggregates to move apart and hence introduce veins or cracks within the sediment. Strauch et al. (2015) discussed that for fine-grained sediments, GH accumulate in veins or fractures as seen in Figure 2. 6.b. However, Ghosh et al. (2010) suggested that in clayey sediments, GH could be present as pore filling, grain displacing, or a combination of both morphologies. Ruffine et al. (2015) observed a change in GH morphology when changing the host medium: while disseminated GH were formed in a sandy matrix, massive nodules were formed by increasing the proportion of clays in the matrix.

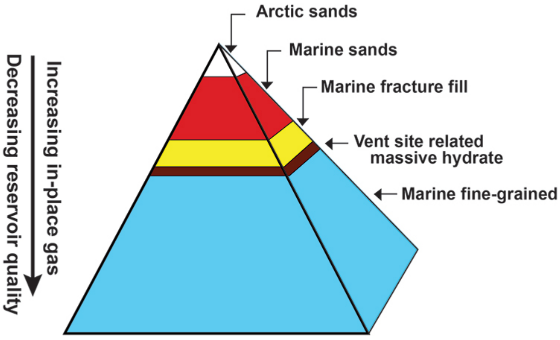

Figure 2. 7. Occurrence of GH in coarse-grained sediments compared to that in fine-grained sediments (Boswell and Collett, 2006)

Owing to their low permeability and lesser interest as a resource, the analysis of various GH morphologies in clayey sediments have rarely been the subject of laboratory investigations. However, fine-grained sediments contain over 90% of global GH accumulations, as seen in Figure 2. 7 (Boswell and Collett, 2006).

2.5 Gas hydrate formation in the laboratory

2.5.1 Gas hydrate formation in coarse-grained samples

The formation of methane hydrates in a laboratory environment remains a technical challenge due to the low solubility of this gas in aqueous media and the random nature of its reaction kinetics.

Many methods for generating GH in the laboratory result in different growth habits. For a given hydrate concentrations, different habits can have different impacts on the mechanical and physical properties of gas hydrates bearing sediments (GHBS) (Waite et al., 2009):

2.5.1.1 The dissolved gas method

The gas-saturated water circulates through a porous matrix under hydrate pressure and temperature stability conditions (Tohidi et al., 2001, Katsuki et al., 2006). At first, the water remains in the liquid state and circulates freely in the sediment. The growth rate of hydrates is here limited by the concentration of dissolved gas in water. The induction time, which defines the time between when conditions are imposed and the formation of hydrate can be relatively long (Waite et al., 2009).

Heterogeneous nucleation can occur on the surface of the particles, followed by growth in the porous space. This method leads to a degree of hydrate saturation limited to Sh = 60-70%. After 50 days of circulation, the hydrate saturation rate can reach Sh = 95% (Strauch et al., 2015, Kulenkampff et al., 2005).

2.5.1.2 The partial water saturation method

A limited and previously fixed amount of water is mixed with the sediment to only partially saturate the porous matrix with water. The system is then pressurized by gas injection, and then cooled. Depending on the degree of water saturation, the formation may take a few days. Unlike the dissolved gas method, the formation of hydrates occurs preferentially at the contacts between the grains and contributes to the rigidity of the sandy sediments.

2.5.1.3 The introduction of ice

Grains of cooled sediment are mixed with small grains of ice between 200 and 350 µm (Stern et al., 1996). The system is then pressurized in the hydrate stability field and a gradual increase in temperature is applied. In this case, the formation of hydrates is facilitated by the presence of water cages and hydrates form from the molecules of water released by the melting of the ice.

2.5.1.4 Premix of hydrates

The water is sprayed in fine droplets in a gas atmosphere under equilibrium conditions (HLV) or by melting ice particles in the presence of gas at 25-30 MPa (Hyodo et al., 2005, Stern et al., 1996). The hydrates formed are mixed with the sediment at low temperature and consolidated at a set point for a few hours. The temperature is maintained in the hydrate stability field, then a progressive increase is applied to a temperature close to equilibrium.

2.5.2 Gas hydrate formation in fine-grained samples

Since coarse-grained sediments are preferred for potential gas production (Lei and Santamarina, 2018; Yamamoto and Dallimore, 2008), laboratory studies have mainly focused on developing GH formation in sands rather than clays. GH formation in fine-grained sediments faces many challenges such as its displacive pore habit and the limitation of hydrate nucleation and that of gas supply (Clenell et al., 1999). Lei and Santamarina (2018) have proposed strategies of GH formation in fine-grained sediment that could overcome these challenges:

2.5.2.1 The TetraHydroFuran (THF) strategy

THF is a heterocyclic organic compound that is fully miscible in water, which allows the hydrate formation to take place without diffusion or advection limitations; thus, promoting rapid hydrate growth. This is ideal for laboratory studies as it tackles the issue of reducing the time of experiments.

2.5.2.2 The diatoms strategy

This strategy is the based on the ability of storing high-pressure carbon dioxide in the pore space of dry diatoms. The hydrate was allowed to form after filling the specimen with water and consumption of the already available pressured gas.

2.5.2.3 The ice-to-hydrate transformation strategy

This strategy mimics the situation, which occurs under permafrost conditions (Dai et al., 2011). It is performed by inserting premade ice lenses in cold and dry samples, which promotes the growth of hydrate lenses in predefined locations within the sediment.

2.5.2.4 The forced gas injection strategy

This strategy is equivalent to gas charging and subsequent fracturing within natural sediments. It is performed by injecting gas within water-saturated specimens in order to create gas pathways or fractures. The formation of GH within these fractures depends on the water and gas supply.

2.5.2.5 The long duration diffusion of reactants strategy

This strategy is equivalent to the process of gas transport in fully saturated fine-grained natural systems. It consists of surrounding specimens by CO_2 gas at 3MPa and 12°C for a certain maturation period, during which the CO_2 will be allowed to diffuse through the sediment. The temperature is then reduced to 2°C to promote GH formation.

2.5.3 Gas hydrates vs. ice

Although hydrates are ice-like structures, their behaviour and properties are different from that of ice. One of the major differences between the two is that ice forms as a pure component, whereas hydrates cannot form without guest molecules of proper size and type (Sloan Jr, 1998). Many tests were conducted in order to identify the differences between the two structures. It has been shown that the shear strength of pure methane hydrates is higher than that of ice under the same conditions of temperature and strain rate (Durham et al., 2003; 2005; 2008). Song et al (2013) performed tests on methane-hydrate-bearing sediments and ice-clay mixtures in order to distinguish the differences between the two materials. The deviator stress of all the ice-clay mixtures was lower than that of GHBS. This confirms the structural and chemical differences between GH and pure ice. However, remarkable similarities do exist between GH and ice:

- The formation of both solid structures (ice and GH) requires a change from the liquid phase to the solid phase.
- The decomposition of GH and that of ice is an endothermic process resulting in almost similar latent heat (Mayoufi et al., 2010).

2.6 Behaviour of gas hydrate-bearing sediment

The grain size distribution of a sediment can alter the distribution of hydrates (Soga et al., 2006). Experimental works by Uchida et al. (2002) shows that the effective pore size must exceed 3 nm for the hydrates trapped in the interstitial spaces of a medium to retain the characteristics of hydrates in a bulk medium. The work of Wang et al. (2016) shows that with the same degree of hydrate saturation, the porosity as well as the permeability of the medium increases with the size of the sediment particles while the capillary pressure decreases. Indeed, pores of small sizes lead to solid/fluid interfaces having a small radius of curvature. Under these conditions, the capillary forces are no longer negligible, and this leads to different pressures on both sides of the gas/liquid interface. Under these conditions, the properties of GH are conditioned by those of water: “The knowledge of the influence of confinement on the activity of water makes it possible to predict the conditions of hydrate stability in the pores” (Uchida et al., 2002). The presence of GH in a sediment alters its mechanical behaviour and physical properties. The instability of these hydrates may result in changes in the sediment structure, pore fluid and gas migration (Hyodo et al., 2005). Hence, it is of great importance to understand the mechanical properties of GHBS. Studies investigating the shear strength, the creep characteristics and the physical aspects of GH have been largely performed during the past years (Song et al., 2013).

In order to study the mechanical properties of GHBSG, experimental triaxial tests are conducted on retrieved samples from marine environments or on synthetic GH under highly controlled stability conditions. Most tests take into account the effect of GH content and morphology on the response of the host sediment while varying the effective confining pressure as well as the temperature values.

A short review of laboratory research performed on GHBS is presented in Table 2. 2.

2.6.1 Hydraulic properties: permeability and relative permeability

Permeability quantifies the ability of fluids to pass through a porous material. The presence of GH in a sediment reduces the pore size and the porosity, increases the capillary pressure and changes the pore shape (Kneafsey et al., 2010; Soga et al., 2006); thus, decreasing the permeability of the host sediment (Katagiri et al., 2017). The latter is a key parameter in order to evaluate the excess pore pressure generated upon GH decomposition (Taleb et al., 2018). The permeability of GHBS depends on the porosity, the shape of the pores and their connectivity as well on the GH content and distribution (Kleinberg et al., 2003; Johnson et al., 2011). Many numerical and experimental studies (Table 2. 3) have tried to determine the permeability coefficient known as "k'" by relating it to the permeability coefficient of a clean sediment matrix (k_0) and to the GH content (S_h). Several models have been developed by (Moridis, 2002; Katagiri et al., 2017) in order to draw a link between the relative permeability and the GH content and distribution. It has been observed that the relative permeability depends on the GH growth habit in the pore spaces (grain coating or pore filling). More insight about this part is provided in chapter 5.

Table 2. 2 Experimental studies conducted on natural and synthetic GHBS

Reference	Details of experiment	Observation
Winters et al. (2002)	Consolidated undrained triaxial tests on natural samples of GHBS from the Mallik permafrost, Canada	• The undrained shear strength of GHBS was found to be around five times higher than that of a reference sediment. • GHBS were found to be more dilatant than reference sediment upon shearing.
Masui et al. (2005)	Consolidated drained triaxial tests on synthetic GHBS with different GH contents and different host specimen (ice and sand or water and sand)	• The shear strength and elastic moduli increased with increasing GH content. • The formation of hydrates increases cohesion. • hydrates do not affect the friction angle.
Hyodo et al. (2005)	Consolidated drained triaxial tests on GHBS	• As the GH content occupying the pores increases, the cementing forces between the grains increase and therefore the axial deviatoric stress of the sample increases
Masui et al. (2007)	Consolidated drained triaxial tests on natural samples of GHBS from the Nankai trough, Japan with different GH contents.	• The shear strength and elastic moduli increased with increasing GH content.
Yun et al. (2007)	Consolidated drained triaxial tests on fine sands, crushed silt, precipitated silt and kaolinite containing THF hydrates.	• Hydrate formation was greater in fine sands compared to silt. • The presence of hydrates enhanced the shear strength, stiffness and dilatancy.
Hyodo et al. (2013)	Consolidated drained triaxial tests on GHBS	• The strength and stiffness of GHBS increased with increasing GH content. • The peak strength increased with increasing effective confining pressure. • Dilatancy and volumetric strain increase with increasing GH content.
Santamarina et al. (2015)	Pressure core characterisation tools were used to estimate the hydro-bio-geomechanical	• The peak shear strength and peak friction angle

	properties of natural hydrate bearing sediments retrieved from Nankai trough, Japan	were found higher for samples bearing hydrates compared to samples after hydrate dissociation.
Yoneda et al. (2015)	Consolidated drained triaxial tests on natural samples of GHBS from the Nankai trough, Japan.	• The initial stiffness and peak strength increased with increasing GH content. • While GHBS experience brittle failure, reference sediments are found to exhibit a strain hardening behaviour.
Kajiyama et al. (2017)	Consolidated drained triaxial tests on GHBS with different GH content.	• The presence of GH increased the initial stiffness, shear strength and dilatancy. • GHBS exhibited a strain softening behaviour that became greater with increasing effective confining pressure.

Table 2. 3 Numerical and experimental studies on the permeability of GHBS

Numerical studies		
Equation	**Parameters**	**Reference**
$k' = k_0\left[\frac{\eta}{\eta_0}\right]^n = k_0[1-S_h]^n$	η_0 = porosity of clean sediment matrix n = reduction factor depending on GH distribution	Dai and Seol (2014)
$k' = k_0\left[\frac{(1-S_h)^3}{(1+B\times S_h)^2}\right]$	B = constant ranging between 0.1 and 4 corresponding to lower and upper GH boundary respectively	Dai and Seol (2014)
$k' = k_0\left[\frac{(1-S_h)^3}{\left(1+\sum_i a_i\times S_h^i\right)^2}\right]$	a_i = fitting parameter depending on GH distribution	Kang et al. (2016)
Experimental studies		
Details of experiment	**Observations**	**Reference**
GH in glass beads with $S_h = 20, 25, 30, 35, 42\ and\ 49\%$	The initial water saturation (S_w) dictates the morphology of the formed GH. Cementing hydrates for $S_w < 35\%$ and pore filling hydrates for $S_w > 35\%$. The reduction factor n was found to be 4	Kumar et al. (2010)
GH at 3MPa and 0.5°C with $S_h = 10, 24, 31, 36, 42\ and\ 48\%$	The reduction factor n was found to be 8	Liang et al. (2014)
Determined the horizontal (k_h) and vertical permeability (k_v) of GHBS from offshore India	The permeability anisotropy (k_h/k_v) found to increase with increasing effective stress and S_h	Dai et al. (2018)

2.6.2 *Mechanical properties*

2.6.2.1 Shear strength and dilatancy

The strength of a sediment depends on its cohesion and friction angle, which represents its ability to withstand the sliding between soil particles (Lu et al., 2013). In order to understand the effect of GH content on the shear strength of their host sediment, the cohesion, angle of friction and angle of dilation are plotted against GH content in Figure 2. 8.

It is clear from Figure 2. 8.a that the cohesion of GHBS is increasing with increasing GH content (Masui et al., 2005, 2006). Other experimental results have confirmed the same observation (Miyazaki et al., 2011; Ghiassian and Grozic, 2013, Zhang et al., 2015). This is directly related to the fact that GH are able to bridge neighbour grains together.

Based on Figure 2. 8.b, the friction angle does not show a general trend with increasing GH content.

The dilatancy angle is experimentally known as the slope of the volumetric strain curve against the axial strain (Soga et al., 2006). It can be observed from Figure 2. 8.a that the dilatancy angle is increasing with increasing GH content; indicating that the presence of GH in coarse-grained sediment enhances the dilation. This is mainly due to the cementation resulting from GH formation (Lijith et al., 2019). Waite et al. (2009) discussed the effect of GH morphology on the dilation angle: even a small amount of cementing type GH is able to significantly increase the dilation angle value. However, GH content should exceed 30% for pore-filling type GH in order to have a noticeable effect on the dilation angle.

Many experiments were conducted in order to investigate shear strength of GHBS as seen in Figure 2. 9. Tests conducted by Masui et al (2005) and Miyazaki et al (2010, 2011) have shown that the shear strength of GH-bearing sands increases with increasing hydrate saturation and decreasing porosity. This was also confirmed by Hyodo et al. (2013) by running multiple tests on laboratory generated methane hydrate-bearing samples. Samples from the Nankai Trough were compared with laboratory synthetized GH-bearing Toyoura sand. It has been found that the initial stiffness, the peak deviatoric strength and the volumetric strain increase with increasing degrees of methane hydrate saturation. Additionally, laboratory studies performed by Winters et al. (2004) on specimens from the Mackenzie Delta showed that the strength of hydrate bearing sediments is much higher than that of sediments without hydrates. Additionally, the latter tests have shown that the strength and stiffness of the host sediment is highly affected by the hydrate distribution and growth habit. This is in line with results found by Ebinuma et al. (2005) that shows that the load-bearing hydrates have a more pronounced effect on the behaviour of the host sediment compared to the pore-filling hydrates. Therefore, the behaviour of GH-bearing coarse-grained sediments is mainly dependent on the gas hydrate saturation and morphology.

Hyodo et al. 2013 conducted triaxial compression tests on laboratory-formed GHBS in order to determine the effect of GH content on the strength of its host sediment. The results suggested that the presence of GH tends to enhance dilation by filling the pore space. Such behaviour, is confirmed by Miyazaki et al. (2011) where the tested specimens exhibited a strain-softening behaviour at an axial strain of around 3%.

On the other hand, studying the effect of GH in fine-grained sediment remains challenging and poorly understood. This is mainly due to the difficulties of recreating such samples in the laboratory.

Specimens recovered from the Krishna-Godavari Basin offshore India using a pressure controlled coring tool were the subject of a study performed by Yun et al. (2010). Results have shown significant undrained shear strength variations that correlate with the presence or absence of GH: higher strengths were recorded at depth where groups of GH veins were present. However, the shear strength of sediment intervals without

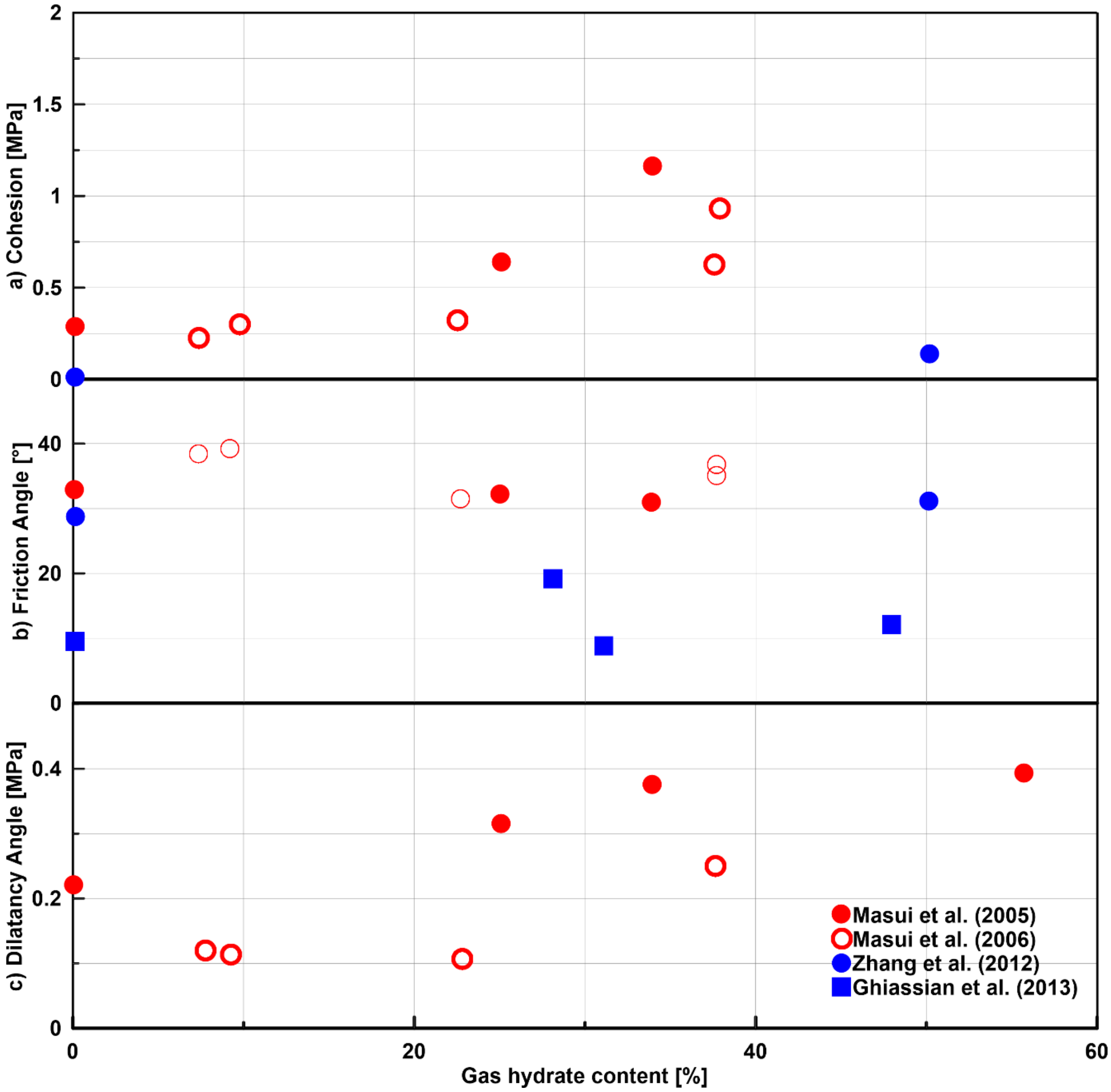

Figure 2. 8 a) cohesion, b) friction angle and c) dilatancy angle as a function of GH content (From Masui et al. 2005, 2006; Zhang et al., 2012 and Ghiassian et al., 2013)

hydrates were significantly lower than that of a normally consolidated sediment. Therefore, Priest et al. (2014) proposed that clayey sediments from the Krishna-Godavari basin are characterised by high in-situ water content as well as high shear strength due to the presence of GH veins, which have prevented the normal consolidation processes.

2.6.2.2 Compressibility

As shown in sections 2.6.2.1 and 2.6.2.3, the presence of GH increases the strength and stiffness of their host sediment. In other words, GHBS can support more overburden stress than it normally would compared to a sediment without GH. As a result, the compressibility of GHBS decreases with the presence of hydrates and eventually prevent natural consolidation processes. This causes the sediment surrounding GHBS to be under-consolidated leading to a significant reduction in the in-situ sediment strength in case of GH decomposition (Priest et al., 2014).

Kim et al. (2018) conducted experimental research with the aim of investigating the physical and geomechanical properties of sandy sediments containing GH. Results have

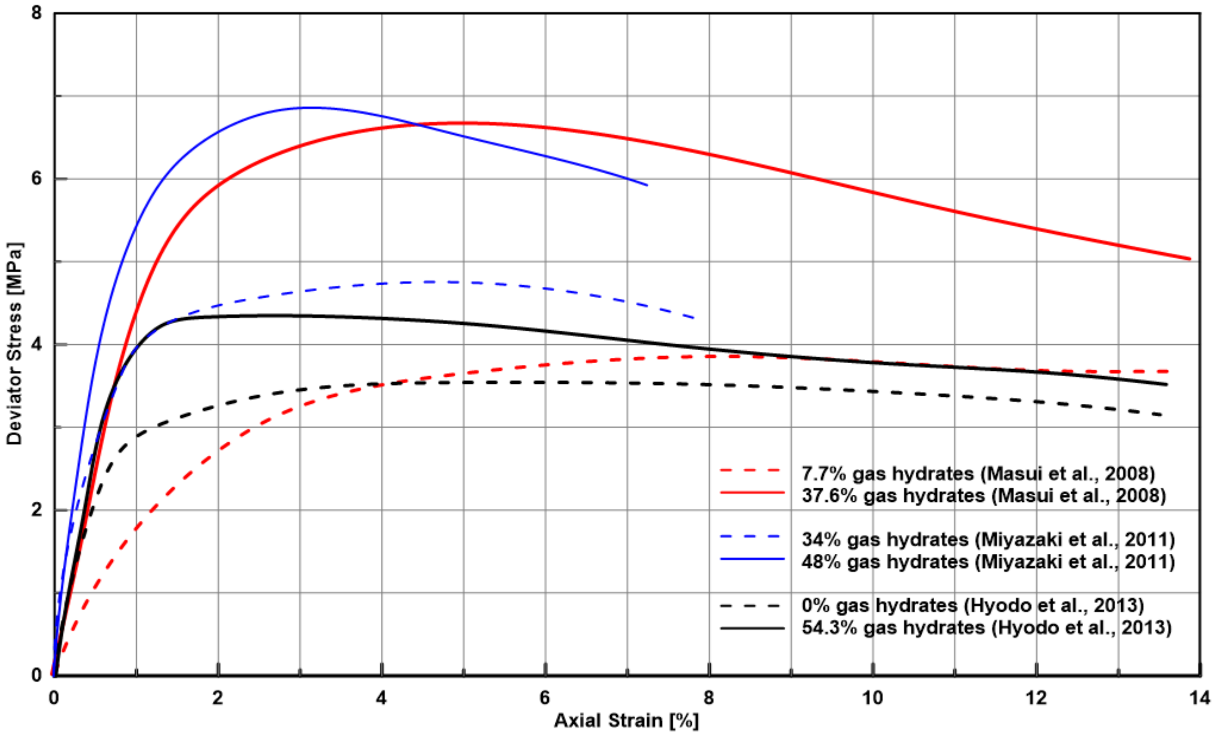

Figure 2. 9 Experimental results from Masui et al. (2008), Miyazaki et al. (2011) and Hyodo et al., (2013) showing the deviator stress as a function of the axial strain at different GH contents

shown that the compressibility of reference and GHBS decrease exponentially with increasing stress. However, for GH content exceeding 80%, the compressibility was observed to decrease by a factor of two for GHBS compared to GH free sediments.

Kim and Cho (2014) formed GH in samples recovered from the Ulleung Basin offshore Korea, which is governed by a high plasticity silty soil. The samples were tested in order to determine the volumetric strain of GHBS for different GH content values and under different vertical effective stresses. GHBS exhibited very low compression indices compared to sediment without GH. This reflects the load bearing effect of GH on their host sediment.

2.6.2.3 Methane hydrates vs. CO_2 hydrates

Liu et al. (2013) have compared the mechanical properties of CO_2 hydrates with those of CH_4 hydrates obtained by Li et al. (2011) and Zhang et al. (2011). It has been observed that the strength of both types of hydrate-bearing sediments increased with the decrease of temperature. However, under the same test conditions, the strength of the CO_2 hydrate-bearing sediments was larger than that of the CH_4 hydrate-bearing sediment.

Table 2. 4. Differences between CO_2 (Liu et al., 2013) and CH_4 (Li et al., 2011) hydrate-bearing sediments in terms of cohesion (c) and frictional strength (ϕ)

	CH_4		**CO_2**	
Porosity (%)	**c (MPa)**	**ϕ (°)**	**c (MPa)**	**ϕ (°)**
40	1.89	7.15	1.8	10.9
60	1.15	8.78	1.07	12.1

Additionally the behaviour of both hydrates was studied against porosity. The strength of both hydrates decreased as the porosity increased. Comparison between Liu et al. (2013) and Li et al. (2011), showed that the strength difference between CO_2 and CH_4 hydrate-bearing sediments arise from a difference in frictional strength (ϕ) rather than cohesive strength (c), as tabulated below (Table 2. 4).

2.6.3 Effect of GH decomposition on sediment properties

As the presence of GH enhances the strength and the stiffness of the bearing sediment, the decomposition of hydrates could contribute to a loss in stiffness and strength. Such a loss is also related to the reduction in effective stress caused by the increase in pore pressure induced by the free gas release upon hydrate decomposition (Kwon et al., 2008). Understanding the impact of the GH decomposition and its nature is of prime importance in order to assess the potential for sediment deformation and failure.

2.6.3.1 Gas hydrate decomposition: dissociation vs dissolution and generated pore pressure

While GH dissociation is the result of variations in the temperature and pressure stability conditions, dissolution can be caused by either a decrease of temperature, which leads to an increase in the gas solubility, or a decrease in the gas flow concentration (Sultan et al., 2007). The dissociation process results in water and free gas; however, the dissolution process results in water and dissolved methane. In both cases, the host sediment is subject to significant alteration of its physical properties and mechanical behaviour. This is due to the generated excess pore pressure resulting from the released gas and the decrease in the mass density. While many research neglect the generation of excess pore pressure in the case of hydrate dissolution (Xu and Germanovich, 2006), it has been shown that the excess pore pressure generated by dissolution is of the same magnitude as that generated by dissociation (Sultan et al. 2004; Sultan et al., 2007).

The excess pore pressure generated by dissociation and dissolution depends on several parameters such as the GH content, the temperature, the ratio of thermal diffusivity to hydraulic diffusivity, the gas solubility and the medium compressibility. Understanding the consequences of GH dissociation and dissolution on their host sediment is key in order to estimate the potential geohazard they pose and prevent sediment deformation and slope instabilities.

2.6.3.2 Elastic parameters: Young's modulus E_0 and secant Young's modulus E_{50}

It has been confirmed by Song et al (2013) that GH dissociation has little effect on the initial Young's modulus E_0 of the host clayey sediments. E_0 increased by 9.28%, 9.34% and 5.86% at the confining pressures 0.5 MPa, 1 MPa and 2 MPa, respectively.

The stiffness of sediments without hydrates is controlled by the applied confining pressure. An increase in the confining pressure leads to an increase in the frictional resistance, which leads to an increase in the stiffness (Yun et. al, 2007). The secant modulus E_{50} was largely affected by the dissociation process and dropped by 42.6% at a confining pressure of 1 MPa.

2.6.3.3 Compressibility

The evolution of the compressibility along with the loss of GH (due to decomposition) has significant implications on the deformation of marine sediments; particularly when subjected to environmental or man-induced changes. Therefore, it is important to understand such phenomena in order to evaluate the mechanical behaviour of GHBS during hydrate decomposition.

Lee et al. (2010) studied the volume change that accompanies GH formation and dissociation under laboratory conditions. Results have shown that GH dissociation caused sediment contraction for all effective stress values and GH contents. Additionally, results by Santamarina et al. (2015) from natural GH bearing samples showed that the coefficient of compressibility decreased from 0.06 to 0.005 after GH dissociation.

2.6.3.4 Shear strength

Sultan et al. (2004) described the effect of GH decomposition on their host sediment as similar to the destruction and softening of natural clays, which can lead to localised shear strains, the creation of shear discontinuities and the initiation of slope failures and instabilities.

Song et al (2013) studied the effect of hydrate dissociation on the shear strength of GHBS under different confining pressures. It was observed that the shear strength of GHBS decreased with the increase of the dissociation time. The strength of the sediment was decreased by the dissociation process, which transformed the solid hydrate to gas and water. The existence of free gas in the pore spaces leads to an increase in the pore pressure, which directly affects the sediment strength (Sultan et al., 2004). Similarly, Hyodo et al. (2013) and Miyazaki et al. (2011) have observed that the shear strength of dissociated GHBS is less than that of sediments without hydrate.

2.7 Gas hydrate application and research interest

2.7.1 Gas hydrate as an energy resource and production methods

The worldwide amounts of carbon bound in GH is estimated to total twice the amount of carbon to be found in all known fossil fuels on Earth (Chong et al. 2016). Hence, GH are considered by some countries and research institutes as an important energy resource (Figure 2. 10). GH formation can take place in a wide range of depositional environment such as the Nankai Trough, the Mackenzie River Delta and the Blake Ridge (Soga et al., 2006).

Gas molecules in the hydrate structure are trapped within water cages by van der Waals forces (Bonnefoy et al., 2005). Hence, techniques to recover methane from GH involve creating conduits for gas flow and dissociating the natural GH (Chong et al. 2016). Most commonly proposed techniques to dissociate GH are depressurization, thermal injection, inhibitor injection and CH_4/CO_2 exchange (Yin et al., 2015). Depressurization and thermal injection technique allow the dissociation of GH by altering the pressure-temperature conditions. Whereas, inhibitor injection works by altering the chemical properties of the hydrate.

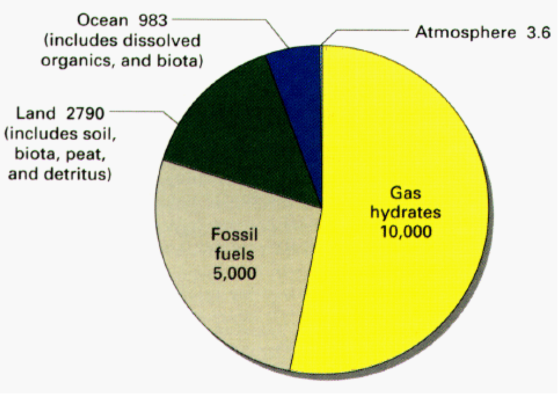

Figure 2. 10 The worldwide amounts of carbon bound in GH is estimated to total twice the amount of carbon to be found in all known fossil fuels on Earth

The specific temperature and pressure stability conditions required for GH formation have restricted their presence to only two regions: permafrost and deep oceanic regions where cold bottom water is available. For last decade, GH have been considered as a potential energy resource due to their wide geographical distribution and to the staggering amount of sequestered methane at relatively shallow water depth. It is known that the energy found in methane hydrates is 10 times higher than that found in other conventional sources of gas such as coal beds and tight sands and 2-5 times higher than that found in conventional natural gas sources.

2.7.1.1 Thermal injection or thermal recovery method

This method involves producing methane from hydrates by increasing the temperature of GHBS above that needed for stability at a specific pressure (Hyodo et al., 2013; Tang et al., 2005). This leads to the hydrates dissociation, which allows the gas release from the water cages.

2.7.1.2 Depressurisation

This method involves producing methane from hydrates by decreasing the pressure of GHBS below that needed for stability at a specific temperature (Hyodo et al., 2013; Kono et al., 2002). This method is considered as the most promising one compared with the others.

2.7.1.3 Trials for methane production

The first trial to extract methane gas from hydrates took place in the Mallik Mackenzie Delta in 2002. It was then followed by a trial at Mount Elbert on the North Slope of Alaska in 2007 (Collett et al., 2009). In March 2013, a trial based on the depressurization method took place in Japan (Collett et al., 2009). However, the region surrounding the GH was liquefied, which lead the sand to behave as a liquid. This resulted in sand production rather than hydrates and the experience was stopped after 7 days. The same scenario happened again in 2017, which motivated the Japanese scientists to develop new approaches and strategies for GH extraction. More recently, at the end of April (2019), the china Geological Survey, announced a three day mission to explore GH in the northern part of the South China Sea. This mission is probably motivated by the fact that in 2015, active GH deposit was discovered in the area (Megan Geuss, 2017).

However, while ignoring the environmental impact of extracting and producing gas from GHBS, China and Japan (as well as other countries) aim to commercialize hydrate-derived methane by 2030 (Mayuko Yatsu, 2018).

2.7.2 Gas hydrates as geo-hazards

A geo-hazard is defined as a geophysical and geological hazard that leads to uncontrolled damages. GH are often considered as geo-hazards due to the possible connection between their decomposition and submarine landslides (IEAGHG, 2009). The decomposition of GH may be triggered by natural changes in water temperature and/or pressure conditions or by human activities related to petroleum exploration projects. Other factors such as changes in gas composition or pore water salinity may contribute to the decomposition of GH (Riboulot et al., 2018). Figure 2. 11 shows different hazardous mechanisms triggered by the decomposition of GH.

While in the solid phase, GH may act as a cementing agent by gluing all the grains together and filling the voids. This prevents the normal compaction process of the sediment in the hydrate stability zone. Hence, any decomposition or instability of the hydrates may result in an under-consolidated soil. The decomposition of GH converts the solid hydrate into gas and water, which will significantly weaken the sediment and increase the pore water pressure (Ning et al., 2012).

The released gas, which was highly concentrated in the solid phase (164m^3 of gas for 1m^3 of hydrate at standard pressure and temperature conditions), can largely alter the mechanical properties of the sediment. The latter is mainly pushed apart due to the volume expansion of the released gas, which leads to a loss of compactness, formation of larger pore spaces and potentially triggering the occurrence and location of submarine landslides (global ccs institute). Submarine sediment failures or landslides involve transport of sub-seafloor material from one place to another (Hampton et al., 1996). They have a direct impact on oil and gas industry engineering structures i.e. pipelines, sea bottom installations (Kvenvolden, 2000). GH decomposition is believed to have contributed to the failure of the Storegga Slide, one of the biggest underwater slides (Sultan et al., 2004).

Additionally, the release of methane gas into the atmosphere after GH dissociation should not be neglected. Methane is 25 times more effective as a greenhouse gas compared with carbon dioxide (Collett et al., 2014) and can be at the origin of many climate change problems. This is mainly known as the clathrate gun hypothesis that suggests that continuous increase in seawater temperature can trigger the release of methane gas from GH compounds, which in turn further increase the temperature and lead to further GH decomposition. On the other hand, Ruppel and Kessler (2017) studied the interaction between climate change and methane hydrate while focusing on the link between climate warming and GH decomposition. The study showed that there is no direct proof that methane derived from GH can reach the atmosphere.

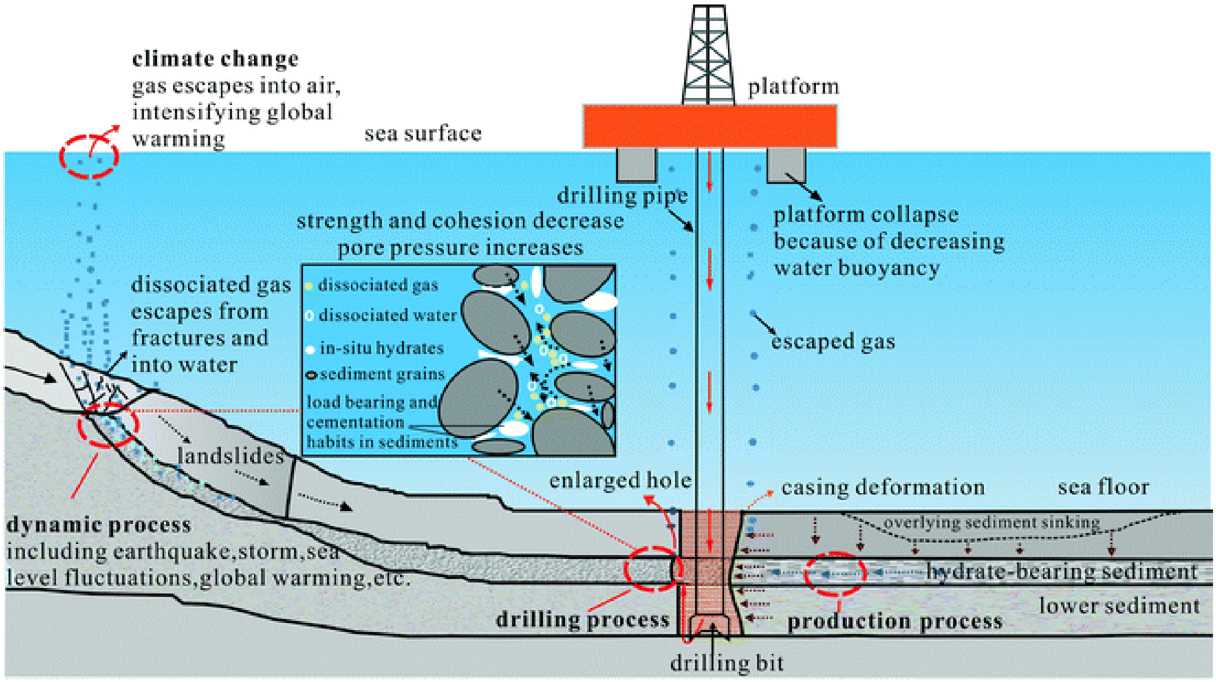

Figure 2. 11 Illustration showing different processes related to the consequences of the dissociation of GH in their natural medium (Ning et al., 2012)

2.8 Conclusion

The main objective of this chapter was to discuss generalities on GH throughout a review of available scientific research. The main addressed points took into account (1) GH formation and stability conditions, (2) GH detection and quantification, (3) characterisation of the mechanical properties of GHBS and (4) GH application and research interest.

GH are ice-like solid compounds that require low-temperature and high-pressure conditions in order to form and stay stable. GH are considered as the largest untapped stock of natural gas in the world (Boswell and Collett, 2011) and are characterised by their wide spread occurrence mainly in permafrost regions and continental margins (Kvenvolden, 1993). Their estimated staggering amounts as well as their potential as a geotechnical hazard for various offshore operations and hydrocarbon recovery projects have stimulated international academic and industrial interest. Therefore, it is of prime importance to detect their presence (section 2.3.1), estimate their content within the host sediment (section 2.3.2) as well as characterise the mechanical behaviour and response of their host sediment (section 2.6).

In the following chapter, the study area as well as the tools and methods will be detailed.

Chapter 3. Study area, materials and methods

Chapitre 3. Zone d'étude, outils et méthode

French R/V 'Pourquoi pas ?'

Abstract

The study zone is located in the Gulf of Guinea, south of Nigeria and off the modern Niger Delta. This zone is characterized by the presence of numerous circular to sub-circular features of different shapes and sizes ranging from a small ring depression surrounding an irregular floor to more typical pockmarks with deep depression. Research studies based on geophysical and geological data have shown that some of these depressions are associated to the distribution and morphology of gas hydrates and are related to different stages of formation / decomposition of gas hydrates.

The study of the mechanical behaviour of gas hydrate bearing sediments requires both the detection and quantification of gas hydrate in the study area. However, due to their metastable nature, gas hydrates are difficult to maintain within their stability field (P, T) upon recovery. For this purpose, a large in-situ data set has been acquired, which is composed of: in-situ acoustic and geotechnical measurement, coring and drilling, pore pressure dissipation data, bathymetric mapping and seismic surveys. All these data have been analysed and correlated in order to detect and quantify gas hydrates. All the methods and approaches adopted to realise this work are presented in this chapter.

Résumé

La zone d'étude est située dans le golfe de Guinée, au sud du Nigéria et au large du delta moderne du Niger. Cette zone est caractérisée par la présence de nombreuses dépressions circulaires à semi-circulaires de formes et de tailles différentes. Des recherches récentes basées sur des données géophysiques et géologiques, acquises dans la zone d'étude, ont montré que certaines de ces dépressions sont associées à la distribution et à la morphologie des hydrates de gaz et sont le résultat des processus de formation / décomposition des hydrates de gaz.

L'étude du comportement mécanique des sédiments contenant des hydrates de gaz nécessite à la fois la détection et la quantification de ces hydrates. Cependant, en raison de leur nature métastable, les hydrates de gaz sont difficiles à maintenir dans leur champ de stabilité (P, T) lors de la récupération. Afin de surmonter cet obstacle, ces travaux s'appuient sur une base de données unique comportant des mesures acoustiques et géotechniques in situ, des carottes sédimentaires, ainsi que des données bathymétriques et sismiques. Toutes ces données ont été analysées et corrélées afin de détecter et de quantifier les hydrates de gaz. Toutes les méthodes et approches adoptées pour réaliser ce travail sont présentées dans ce chapitre.

3.1 Study area

The study area is located in the Gulf of Guinea, South of Nigeria and off the modern Niger Delta, which is considered one of the major worldwide hydrocarbon bearing sites (Damuth, 1994; Reijers et al. 1997; Wiener et al., 2010).

The Niger delta is an Eocene–Holocene siliciclastic, 12km thick, sedimentary wedge (Reijers et al. 1997; Doust and Omatsola, 1999; Wiener et al., 2010; Marsset et al. 2018). According to Marsset et al. (2018), the Niger delta "has prograded over 300 km since the late Eocene over a marine shale-rich formation in response to the evolving drainage area, basement subsidence and sea-level changes". Weiner et al. (2010) studied the characteristics and structures of the mobile shale in the Niger Delta. The latter study described the Niger Delta as a classic example of "a linked extensional-contractional system developed on a passive margin driven by gravity and sediment loading». Additionally, the substrate was described as over-pressured and characterised by low seismic velocity (Marsset et al., 2018), low density and a ductile deformation style. The over-pressured nature of the area along with low permeability indeed favours high fluid pressures (Wiener et al., 2010).

Due to its distinctive regional structural styles, Damuth (1994) divided the Nigerian continental margin into three zones:

- Upper extensional zone beneath the outer shelf characterised by extensive listric growth faulting,
- Intermediate translational zone beneath the continental slope characterised by shale diapirs,
- Lower compressional zone beneath the lower continental slope and uppermost rise characterised by thrust structures.

Numerous studies have reported that the Nigerian continental slope accommodate a wide range of different fluid flow features (Sultan et al., 2007; Heggland, 2003; Hovland et al., 1997; Cohen and McClay, 1996) such as pockmarks, gas chimney and mud volcanoes. The latter have been linked to the fact that the area is an active fluid flow region where the presence of accumulations of shallow GH have been already proved by many authors (Sultan et al., 2007, 2010 2017, 2011, 2014; Riboulot et al., 2016; Wei et al., 2015). This makes the Niger Delta a focus of interest for many academic and industrial researches aiming to study GH dynamics and its impact on seafloor deformation.

In this work, the focus is given to a specific area (Figure 3. 1) where a large database of different in-situ acoustic and geotechnical measurement, coring and drilling, pore pressure data, bathymetric mapping and seismic surveys have been acquired. The investigated area in this work lies in the translational zone as defined by Damuth (1994), which is characterised by shale diapirs and ridges (Damuth, 1994). The latter is governed by the presence of several quasi-circular deformations identified as pockmarks (Wei et al., 2015). The pockmark field, which lies at a water depths ranging from 1100m to 1250m, includes three sets of pockmarks: A, B and C. The evolution and morphologies of these pockmarks have been directly linked to different stages of evolution of gas hydrates (Sultan et al., 2007; 2010). Sultan et al. (2014) presented a scheme, which can be referred to as "the plumbing system", describing the multiple steps of the formation and evolution of the pockmarks in the study area. The study allowed improving initial proposed scheme by Sultan et al. (2010) by taking into account (1) rapid GH growth, (2) GH dissolution and (3) free gas venting into the water column.

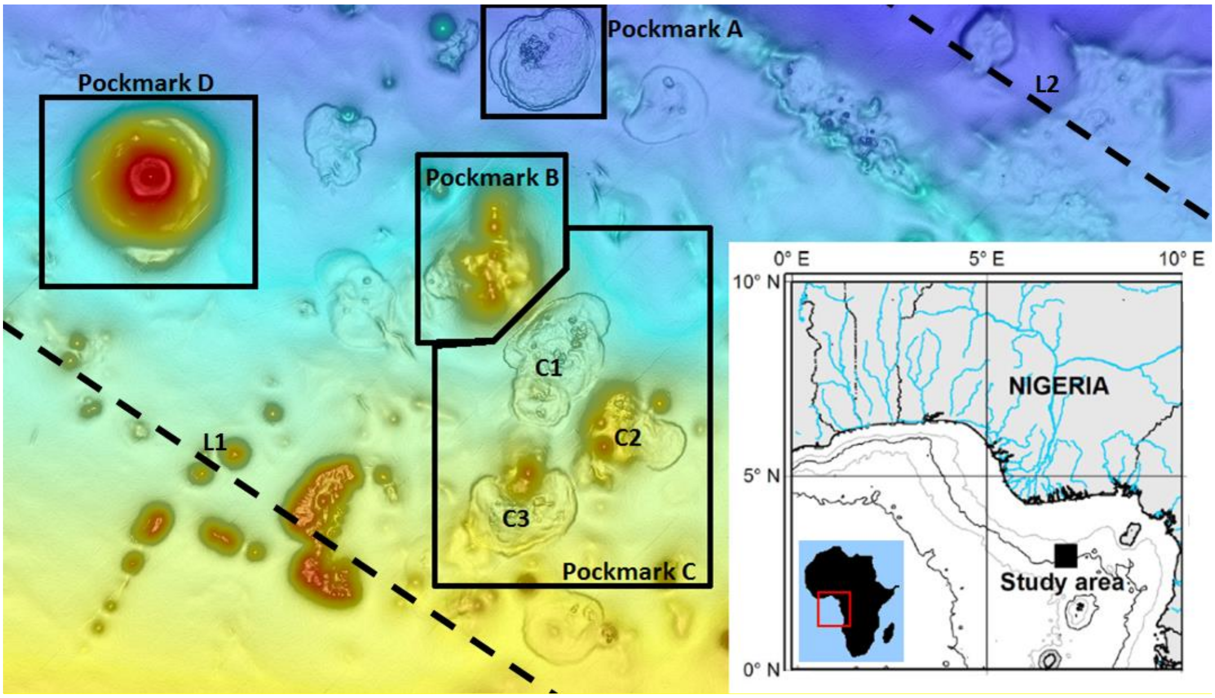

Figure 3. 1 AUV bathymetric map in the region of the deep water Niger Delta showing different pockmarks, which are bounded by two deep normal faults (L1 and L2), modified from Sultan et al. (2010)

Figure 3. 2 Gas hydrate recovered from core GMGC12 during Guineco MeBo campaign (2011): left) Spongy porous gas hydrate and right) gas hydrate nodules

3.1.1 Gas hydrates in the study area

The Gulf of Guinea is one area where the presence of dense accumulations of shallow gas hydrate have been reported by several authors (Hovland et al., 1997; Cunningham and Lindholm 2000; Sultan et al., 2010; Wei et al., 2015). Visual observations (Figure 3. 2) within the study area have revealed the presence of different gas hydrate morphologies varying from groups of thin veins to massive nodules in clay sediments (Sultan et al. 2007, 2010). In certain cases, solid gas hydrate and free gas were thought to coexist due to the presence of voids within hydrate nodules (Figure 3. 2); hence, resulting in a material with a spongy texture (Sultan et al., 2014; 2007). Wei et al., (2015) have defined GH occurrence zones based on pore water chloride analyses and infrared thermal imaging.

3.1.2 Brief description of the sediment physical and mechanical properties from the study area

In the Gulf of Guinea late Quaternary sediments consist mostly in normally consolidated structured clay (De Gennaro et al., 2005; Hattab and Favre, 2010), with a complex mechanical behaviour. It is known that sediments in this wide region appear to share similarities in terms of geotechnical properties.

Figure 3. 3 Image of the R/V 'pourquoi pas?

Using X-ray diffraction analysis, Thomas et al. (2005) showed that sediment recovered from the Gulf of Guinea is composed of 40-60% clay, 50% Kaolinite and 15-25% smectite. Sultan et al. (2012) described the behaviour of the Gulf of Guinea clay as peculiar and uncommon. For instance, it is characterised by very high water contents (150 – 250% at seabed), very low submerged unit weights (2.5 – 3 kN/m^3) and very high plasticity index (up to 120). It is noteworthy that the clay of the Gulf of Guinea is structured and prone to a strain softening behaviour(Colliat et al., 2011; Puech et al., 2005), which is captured by sensitivity values ranging between 6 and 8 with occasional peaks of high sensitivity (around 19) at certain depths of the tested samples Hattab and Favre (2010). Hattab et al., (2014) have performed mechanical tests, including triaxial shearing, on a 17m long core taken at a depth of 700m in the Gulf of Guinea. The tested samples consisted a very plastic and dark grey clay with many visible shell fragments. This allowed identifying two different types of mechanical behaviour: (1) a consolidation stress region where the loading had not yet damaged the sediment structure and (2) high consolidation stress region where the loading damages the sediment structure. Further microstructural studies have allowed to confirm that the microstructure of the clayey sediment from the Gulf of Guinea is an association of aggregates bonded by 'glue'. This is in line with other research performed by Delage (2010) and Yin et al. (2010) in order to understand the behaviour of sensitive clays, which proved that the damage of a clayey sediment structure is associated with the decrease of bounding between the grains.

3.2 Data, materials and tools

3.2.1 Oceanographic campaigns

The data used in this work were acquired within the framework of different oceanographic campaigns listed below:

The Guineco MeBo Oceanographic Campaign (2011), in partnership between Ifremer and the University of Bremen (MARUM), took place off the coast of Nigeria on the research vessel (R/V) *'Pourquoi pas?'* (Figure 3. 3), as a part of the project *'Risques Géologiques'* carried out by Ifremer. This campaign had two main objectives: (1) determining the distribution of gas hydrates and (2) understanding the link between gas hydrates and the mechanisms of the formation and evolution of pockmarks in the study area. This allowed providing a huge database of geotechnical, geochemical and geological measurements. Various techniques and measurements were implemented on board consisting of more than 300m of drilling, 430m of coring and more than a thousand meters of in-situ measurements. This allowed the determination of the physical and mechanical properties of the sediment.

The ERIG3D campaign (2008), was carried out as a part of a scientific cooperation between Ifremer and Total in the framework of Ifremer's project *'Risques Naturels'* on the R/V *'Pourquoi pas?'*. The project aimed to study the gravitational instabilities and underlying factors.

The NERIS2 campaign (2004), was carried out on the R/V *'l'Atalante'* as a part of the NERIS project. Its main objective was to study the stability of sedimentary bodies in the deep water Niger Delta.

3.2.2 In-situ measurements

Compared to classical coring and drilling measurements, In-situ measurements allow identifying the physical and mechanical properties of the penetrated sediment as well as study gas hydrates in their natural conditions. This technique proved cost effective and efficient to collect large amounts of data (Lunne et al., 1997; Sultan et al. 2007, 2010, 2014; Taleb et al., 2018; Robertson 2009).

3.2.2.1 Penfeld Soundings

In-situ acoustic and geotechnical measurements were carried out using the Penfeld seabed rig developed by Ifremer (Figure 3. 4). It is provided with a rod that can push two types of probes down to 30 m below seabed with a thrust of 40 kN at a standard rate of 2cm/s (Sultan et al., 2007).

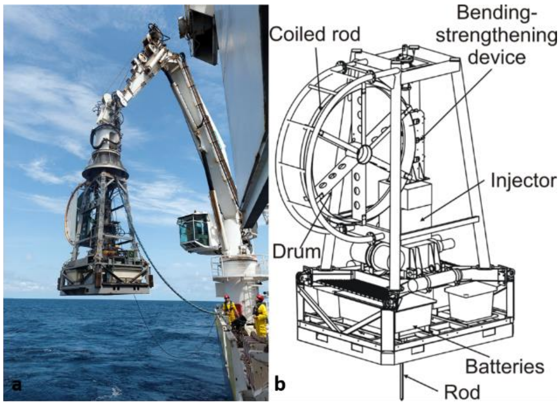

Figure 3. 4 a) Penfeld deployment in order to perform in-situ measurement and b) illustration of the tool showing its different components

The piezocone probe (Figure 3. 5) can be used to carry out Cone Penetration Testing with pore pressure measurement (CPTu); thus, providing continuous vertical readings of cone tip resistance (q_t), sleeve friction (f_s) and penetration pore pressure (Δu_2). The latter is measured with a differential pore pressure sensor located immediately behind the cone (u_2 position). The piezocone is equipped with pressure compensated sensors to provide accurate measurements irrespective of the water depth.

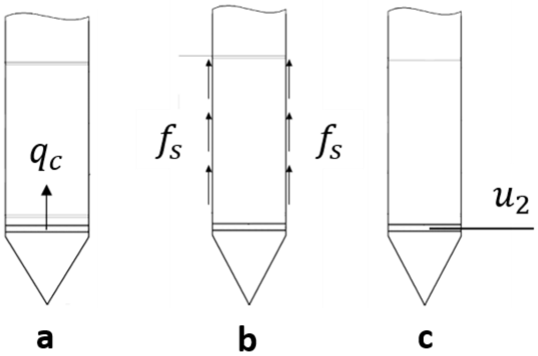

Figure 3. 5 Illustration showing the three different measurements that can be performed by the piezocone probe: a) cone tip resistance, b) sleeve friction and c) pore-water pressure

The ultrasonic fork (Figure 3. 6) can alternatively be used to measure every 2 cm the velocity of compressional waves (Vp) up to 2200 m/s. Acoustic measurements are carried out by producing a 1MHz compressional wave from on branch of the fork and recording its travel time to the opposite branch located 7cm apart. The amplitude ratio between the input and received signals provides attenuation. As an additional parameter recorded during acoustic measurements, the so-called 'applied load' corresponds to the force required to push the ultrasonic fork in the sediment.

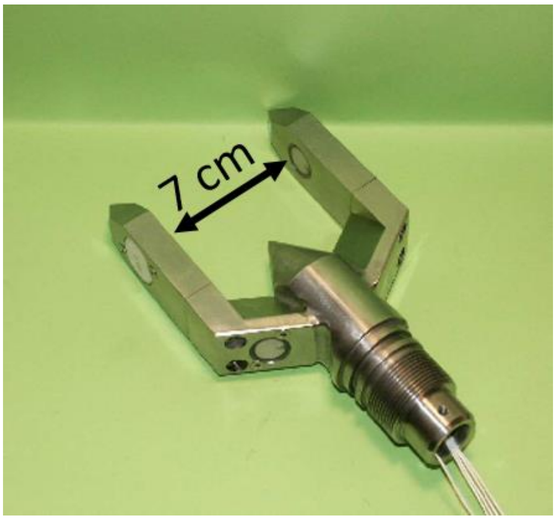

Figure 3. 6 Photo of the ultrasonic fork used to perform in-situ acoustic measurements. The branches of the fork are 7 cm apart

A synthesis of the all the acoustic and geotechnical soundings is presented in Figure 3. 7, Table 3. 1 and Table 3. 2.

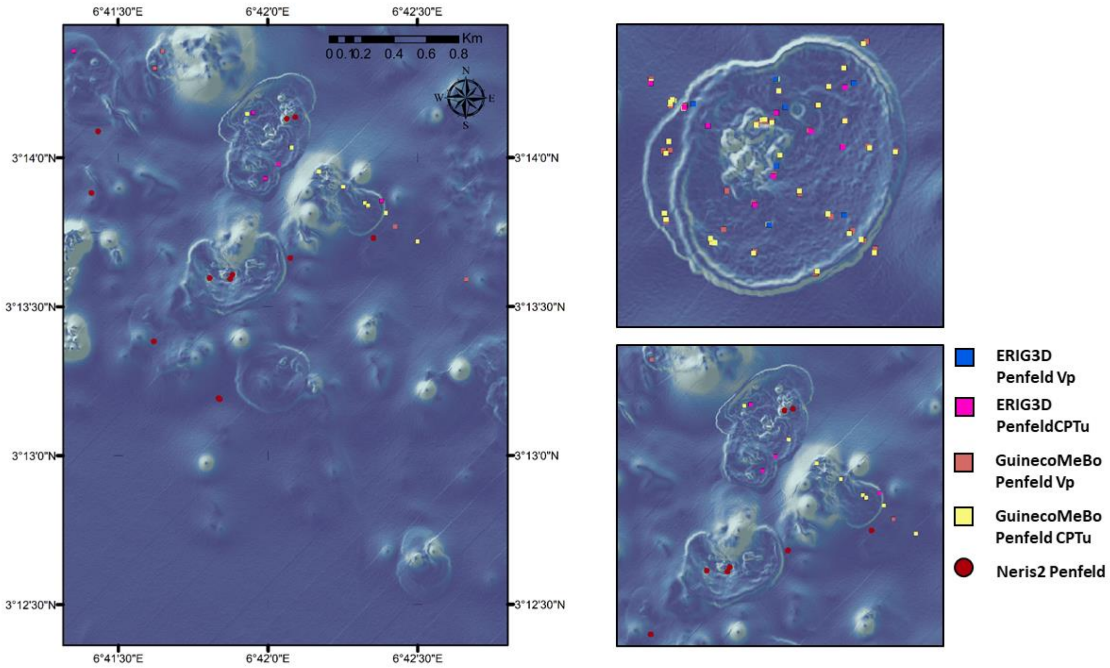

Figure 3. 7 Bathymetry of the study area showing Penfeld Vp and Penfeld CPTu measuring sites during Guineco MeBo, ERIG3D and NERIS2 campaigns

Table 3. 1 Penfeld Vp and Penfeld CPTu measuring sites during ERIG3D and NERIS2 campaigns

ERIG3D Penfeld VP			**Neris2 Penfeld Vp**		
Site	**Depth (m)**	**Penetration (m)**	**Site**	**Depth (m)**	**Penetration (m)**
VP03S01	1140	30	Pv36A	1712	15.18
VP03S02	1140	30	Pv36B	1726	07.18
VP03S03	1143	13	Pv39A	1180	15.01
VP03S04	1142	30	Pv39B	1210	17.04
VP03S05	1143	11	Pv40A	1200	04.64
VP03S06	1148	13	Pv40B	1210	15.01
VP03S07	1146	9.14			
VP03S08	1147	8.42			
ERIG3D Penfeld CPTu			**Neris2 Penfeld CPTu**		
CPT01S01	1152	14.05	Pm07A	1683	27.21
CPT01S02	1154	18.20	Pm16A	1180	30.00
CPT02S01	1179	30	Pm16B	1192	29.82
CPT02S02	1181	30	Pm22A	1190	17.08
CPT02S03	1180	13.56	Pm22B	1232	14.58
CPT02S04	1181	6.24	Pm22C	1237	12.27
CPT02S05	1180	4.16	Pm23A	1226	17.57
CPT02S06	1139	17.54	Pm23B	1206	10.77
CPT02S07	1178	8.10	Pm23Bbis	1206	12.27
CPT02S08	1177	30	Pm27A	1182	04.90
CPT02S09	1179	6.28	Pm29A	1211	30.00
CPT04S01	1168	16.5	Pm33A	1196	28.68
CPT04S02	1182	7.90	Pm33B	1204	06.87

CPT04S03	1186	15.32	Pm33C	1202	09.62
CPT04S04	1185	15	Pm33D	1216	30.00
CPT04S05	1190	30	Pm33E	1173	30.00
			Pm33F	1171	30.00
			Pm33G	1164	18.84
			Pm35A	1694	30.00
			Pm35B	1712	30.00
			Pm35C	1720	30.00
			Pm35D	1726	30.00

Table 3. 2 Penfeld Vp and Penfeld CPTu measuring sites during Guineco MeBo campaign

Guineco MeBo Penfeld Vp			**Guineco MeBo Penfeld Vp**		
Site	**Depth (m)**	**Penetration (m)**	**Site**	**Depth (m)**	**Penetration (m)**
GMPFV_02-S1	1143	30	GMPFM_01-S1	1143	23.7
GMPFV_02-S2	1144	30	GMPFM_01-S2	1144	30
GMPFV_02-S3	1144	30	GMPFM_01-S3	1144	4.54
GMPFV_02-S4	1143	10.36	GMPFM_01-S4	1151	2.2
GMPFV_02-S5	1144	12.3	GMPFM_01-S5	1111	4.84
GMPFV_02-S6	1147	6.5	GMPFM_01-S6	1145	3.26
GMPFV_02-S7	1148	30	GMPFM_01-S7	1146	14.32
GMPFV_02-S8	1146	16	GMPFM_01-S8	1144	17.16
GMPFV_03-S1	1136	30	GMPFM_04-S1	1136	30
GMPFV_03-S2	1140	30	GMPFM_04-S2	1140	1.02
GMPFV_03-S3	1142	10.3	GMPFM_04-S3	1140	6.98
GMPFV_03-S4	1140	5.7	GMPFM_04-S4	1140	2.16
GMPFV_03-S5	1145	8.52	GMPFM_04-S5	1147	2.42
GMPFV_03-S6	1147	30	GMPFM_04-S6	1147	4.12
GMPFV_03-S7	1145	30	GMPFM_04-S7	1145	30
GMPFV_03-S8	1145	30	GMPFM_04-S8	1147	1.78
GMPFV_07-S1	1140	30	GMPFM_ 05-S1	1190	30
GMPFV_07-S2	1146	11.82	GMPFM_ 05-S2	1190	28.1
GMPFV_07-S3	1152	30	GMPFM_ 05-S3	1190	26.74
GMPFV_07-S4	1148	13.78	GMPFM_ 05-S4	1195	30
GMPFV_07-S5	1146	8.5	GMPFM_ 05-S5	1205	10.22
GMPFV_07-S6	1144	4	GMPFM_ 05-S6	1180	29.64
GMPFV_07-S7	11145	7	GMPFM_ 05-S7	1180	14.4
GMPFV_07-S8	1145	7.22	GMPFM_ 06-S1	1140	30
GMPFV_07-S9	1143	10.82	GMPFM_ 06-S2	1144	6.58
GMPFV_07-S10	1145	30	GMPFM_ 06-S3	1145	30
GMPFV_09-S1	1141	1.82	GMPFM_ 06-S4	1140	6.68
GMPFV_09-S2	1141	11.74	GMPFM_ 06-S5	1145	0
GMPFV_09-S3	1141	13.52	GMPFM_ 06-S6	1152	6.68
GMPFV_09-S4	1141	4.34	GMPFM_ 06-S7	1154	30
GMPFV_10-S1	1196	30	GMPFM_ 06-S8	1147	21.44

GMPFV_10-S2	1190	30	GMPFM_ 06-S9	1143	4.74
GMPFV_10-S3	1190	24.74	GMPFM_ 06-S10	1141	6.84
GMPFV_10-S4	1195	0	GMPFM_ 06-S11	1142	11.16
GMPFV_10-S5	1178	30	GMPFM_08-S1	1141	1.44
GMPFV_10-S6	1182	30	GMPFM_08-S2	1141	1.91
GMPFV_10-S7	1221	13.1	GMPFM_08-S3	1141	2.64
			GMPFM_08-S4	1142	2.4
			GMPFM_11-S1	1196	10.78
			GMPFM_11-S2	1196	10.95
			GMPFM_11-S3	1182	12.6
			GMPFM_ 12-S1	1144	30
			GMPFM_ 12-S2	1142	10.02
			GMPFM_ 12-S3	1142	20
			GMPFM_ 12-S4	1141	4.9
			GMPFM_ 12-S5	1144	30
			GMPFM_ 13-S1	1141	30

3.2.2.2 Piezometer

The Ifremer piezometer (Figure 3. 8) is a cable-deployed device that allows pore pressure measurements. It is equipped with a 60mm diameter sediment-piercing lance whose length can be adapted to the type and the stiffness of the penetrated sediment. For example, a 12m long lance is used for soft sediments.

Table 3. 3 Specifications of the Ifremer piezometer

Differential pressure sensor	
Type	Keller PD-10LH
Measurement interval	+/- 200kPa
Precision	1 kPa
Maximum pressure	+400 kPa / -300 kPa
Temperature sensor	
Type	Thermistance CTN
Measurement interval	0°C to +50°C
Precision	0.05°C

Specifications concerning the Ifremer piezometer are shown in Table 3. 3. A synthesis of all the Piezometer measurements is presented in Figure 3. 9 and Table 3. 4.

Pore pressures are measured at up to ten ports with a minimum spacing of 70 cm using differential pressure transducers. They measure pressure relative to hydrostatic pressure with an accuracy of 0.4kPa. The lance is also equipped with temperature sensors having an accuracy of 0.05°C.

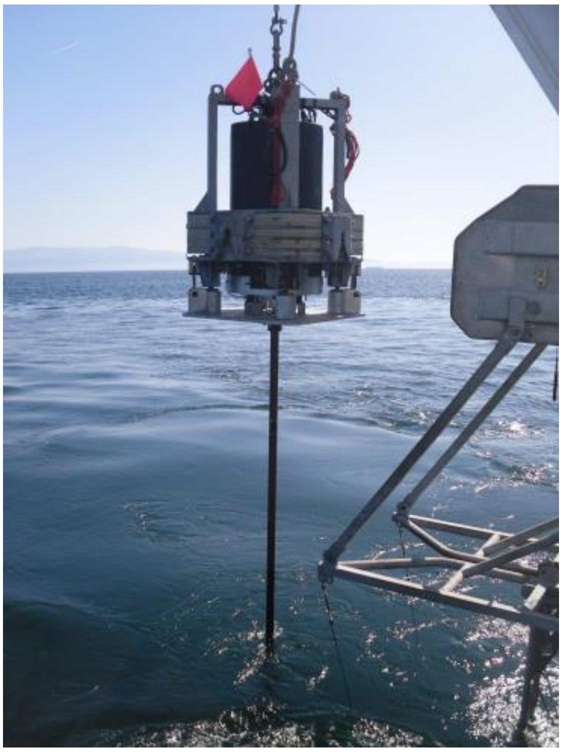

Figure 3. 8 The Ifremer piezometer being deployed during an oceanographic campaign

Table 3. 4 Piezometer measuring sites during Guineco MeBo and ERIG3D campaigns

Guineco MeBo Piezometer			**ERIG3D Piezometer**		
Site	**Depth (m)**	**Penetration (m)**	**Site**	**Depth (m)**	**Penetration (m)**
GMPZ1	1147	7.55	PZY01	1172	6.6971666
GMPZ2	1148	7.55	PZY02	1164	6.7006
GMPZ3	1144	7.55			
GMPZ4	1184	8.29			
GMPZ5	1147	11.34			
GMPZ6	1147	10.64			
GMPZ7	1183	10.64			
GMPZ8	1143	11.34			
GMPZ9	1145	10.64			
GMPZ10	1189	11.34			

The piezometer can be used in two modes: long and short-term measurements. In the former, equilibrium pore pressure can be reached after several days; whereas in the latter the equilibrium pore pressure is evaluated following the technique proposed by Sultan and Lafuerza (2013).

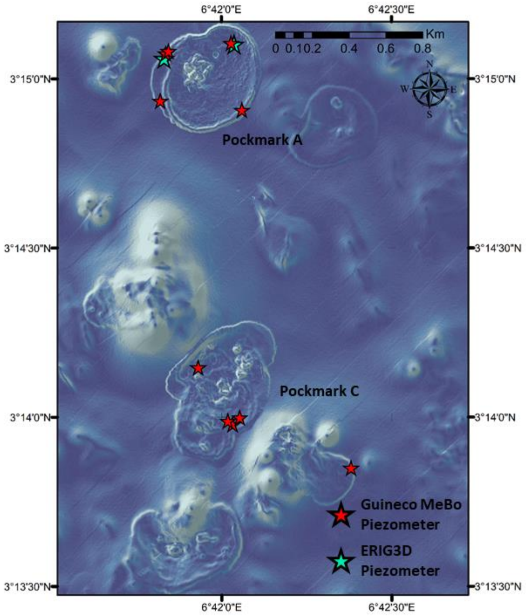

Figure 3. 9 Bathymetry of the study area showing Piezometer measuring sites during Guineco MeBo and ERIG3D campaigns

This allows achieving two types of measurements:

- Determine the hydraulic properties of the sediment based on the pore pressure dissipation generated by the penetration of the piezometer,
- Identify and quantify the hydraulic gradients in the sedimentary layers.

3.2.3 *Coring and drilling*

3.2.3.1 Coring (Calypso)

The Kullenberg calypso corer (Figure 3. 10), used in this study, is a coring system developed by Yvon Balut (IPEV) on board of the R/V *'Marion Dufresne'* and later adapted to the *'Pourquoi pas?'*.

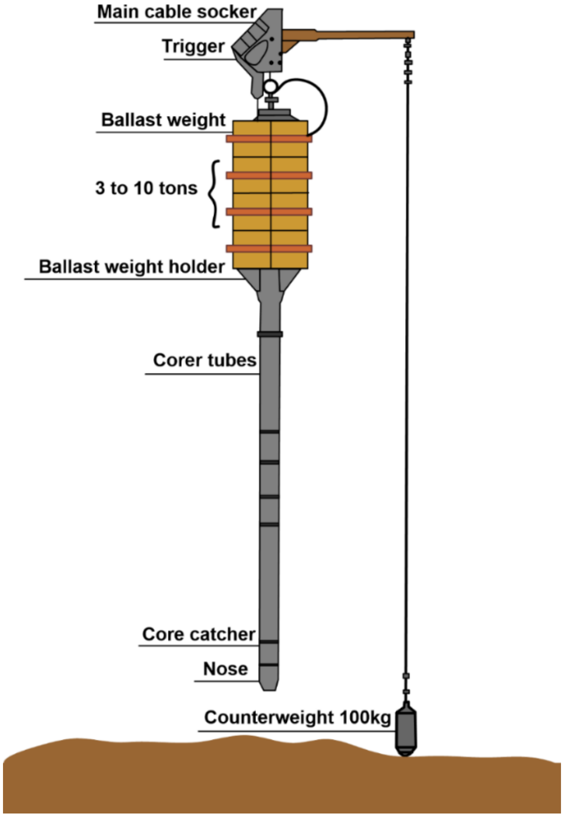

Figure 3. 10 Illustration of the Calypso corer showing its components

Table 3. 5 Calypso measuring sites during Guineco MeBo, ERIG3D and Neris2 campaigns

Guineco MeBo Calypso Corer			**ERIG3D Calypso Corer**		
Site	**Depth (m)**	**Penetration (m)**	**ER-CS01**	**1154**	**5.43**
GMCS1	1149	3.5	ER-CS02	1181	4.98
GMCS2	1149	13.305	ER-CS03	1195	16.5
GMCS3	1143	13	ER-CS04	1145	11.9
GMCS4	1147	21.6	ER-CS05	1181	16.58
GMCS5	1142	22.8	ER-CS06	1682	22
GMCS6	1186	5.3	ER-CS07	1708	28.8
GMCS7	1204	4.2	ER-CS08	1755	21.8
GMCS8	1183	4.06	ER-CS09	783	21.7
GMCS9	1183	12.83	ER-CS16	731	14
GMCS10	1192	13	ER-CS17	441	18.26
GMCS11	1196	12.85	ER-CS18	762	18
GMCS12	1187	13.51	ER-CS19	754	Vide
GMCS13	1184	21.88	ER-CS20	754	Vide
GMCS14	1185	12.86	ER-CS21	752	9.78
GMCS15	1197	13.61	ER-CS22	746	10.87
Neris2 Calypso Corer			ER-CS23	786	23.28
N1_KS21	1147	3	ER-CS24	760	25.38
N1_KSF23	1147	<2	ER-CS30	740	6.71
N1_KI27	1147	0.25	ER-CS31	752	10.67
			ER-CS36	739	10.77
			ER-CS37	217	10.95
			ER-CS38	536	6.06
			ER-CS39	735	21.13
			ER-CS40	664	4.97

Table 3. 6 Description of the recovered Calypso cores

Site	**Depth (m)**	**Pockmark**	**Description**
GMCS-01	1149	A	0cm - 14cm dark grey to black clay + strong H2S odour 0cm - 5cm abundant carbonate concretions (<5cm) 14cm - 35cm very fluid interval (GH dissociation) 53cm - 55cm platy carbonate concretions (<5cm) 68cm - 72cm large (>10cm) carbonate concretions with porous fabric 85cm - 95cm small (<1cm) semi-lithified carbonate concretions 95cm - 162cm dark grey soupy clay 160cm - 163cm nodular carbonate concretions (<5cm) 162cm - 175cm mousy to soupy sediment with small (<5cm) carbonate concretions +soupy texture of the sediment (dissociation of GH) 170cm - 173cm platy carbonate concretions (3-(cm in diameter) 175cm - 183cm soupy sediment

			183cm - 278cm mousy sediment +abundant small (<5cm) carbonate concretions 278cm - 287cm soupy sediment
GMCS-02	1149	NW A	Dark grey to black clay with shell fragments, bioturbation and burrows all along sediment
GMCS-03	1143	NE A	Dark grey to grey clay with burrows and foraminifera throughout section
GMCS-04	1147	NW A	Dark grey clay with foraminifera throughout section
GMCS-05	1142	NW A	250 cm - 60cm presence of nodules
GMCS-06	1186	C1	0m - 0,72m dark grey clay + abundant cracks and voids due to gas expansion + GH at 25cm + large void from 72cm to 100cm 0,82m - 1,72m homogeneous clay + highly fractured sediment + large void due to gas expansion with loose clumps of sediment 1,72m - 2,72m empty liner (extensive gas expansion) 2,72m - 3,72m empty liner (extensive gas expansion) 3,72m - 4,72m dark grey clay + interval with large voids and cracks due to gas expansion 4,72m - 5,3m dark grey clay + abundant cracks and voids due to gas expansion + 2 pieces of GH
GMCS-07	1204	C3	Disturbance while splitting due to presence of shell fragments Dark greyish clay + carbonate concretions
GMCS-08	1183	B	Dark greyish clay with foraminifera
GMCS-09	1183	B	Homogeneous dark grey clay with pocket of oil spots and foraminifera dispersed throughout core
GMCS-10	1192	C	Lots of burrows through section and few foraminifera Clay - change of colour from dark grey to very dark grey at 20cm and 67cm Shell fragments
GMCS-11	1196	C	Dark grey clay with few foraminifera Very soft sediment Few burrows Change of colour to very dark grey 853cm foraminifera pocket
GMCS-12	1187	B	Homogeneous dark stiff greyish clay Burrows throughout core 150cm - 280cm massive carbonate concretions 280cm - 350cm finely dispersed carbonate concretions 405cm - 410cm massive carbonate concretions 450cm - 550cm burrows throughout core 620cm - 630cm sediment fractured
GMCS-13	1184	B	0-50cm homogeneous dark grey clay + fluidized at the top + mousy sediment + burrows throughout sediment 153cm - 253cm very dark grey clay 583cm - 595cm presence of pockets of oil 1053cm - 1153cm homogeneous dark greyish clay + very stiff sediment + massive carbonate concretions + strong H2S odour

			1153cm - 1253cm homogeneous dark grey clay + oil stains + carbonate concretions finely dispersed 2053cm - 2098cm strong H_2S odour + very stiff sediment
GMCS-14	1185	C2	0cm - 96cm homogeneous dark grey clay + finely dispersed foraminifera + shell fragments and burrows 296cm - 396cm homogeneous dark greyish clay + carbonate concretions at 317cm + finely dispersed foraminifera 396cm - 496cm homogeneous dark greyish clay + burrows scattered throughout core section 496cm - 596cm homogeneous dark greyish clay + massive carbonate concretions at 510cm + burrows throughout core section 596cm - 1096cm homogeneous dark greyish clay + burrows throughout core section 11096cm - 1196cm homogeneous dark greyish clay + strong H_2s odour + burrows 1196cm - 1286cm very dark greyish clay + strong H_2S odour + abundant burrows + shell fragment at 1251cm
GMCS-15	1197	C	0cm - 60cm very dark greyish clay + abundant burrows in upper part 60cm - 160cm dark to very dark clay + shell fragment 261cm - 361cm homogeneous very dark greyish clay + abundant foraminifera

It is equipped with a 30m long corer pipe, a core catcher, a ballast weight and a ballast weight holder allowing its penetration into the sediment. This instrument allows the recovery of up to 30m of marine sediment and operates with minimal sediment perturbations due to its accelerometer system (Bourillet et al,. 2007). This is due to its piston that limits the variations of internal pressure during the coring process.

.

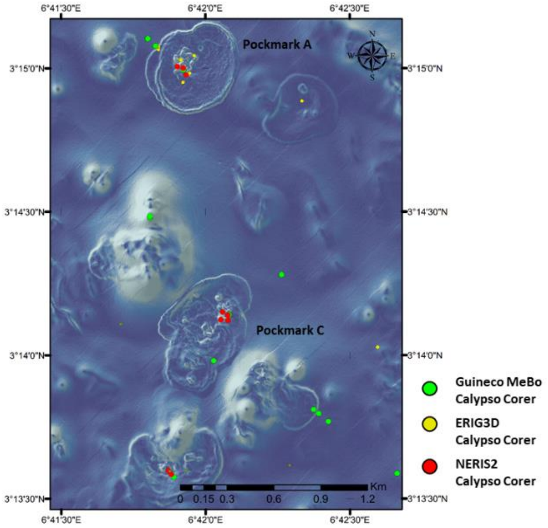

Figure 3. 11 Bathymetry of the study area showing Calypso coring sites during Guineco MeBo, ERIG3D and Neris2 campaigns

A synthesis of the all the Calypso cores recovered is presented in Figure 3. 11 and Table 3. 5 and a description of the cores is provided in Table 3. 6.

3.2.3.2 Coring (MeBo)

While standard methods of marine sediments sampling are considered reliable, they often have a limited coring depth. The seafloor drill rig MeBo (Figure 3. 12) is a mobile drilling system developed by the University of Marum.

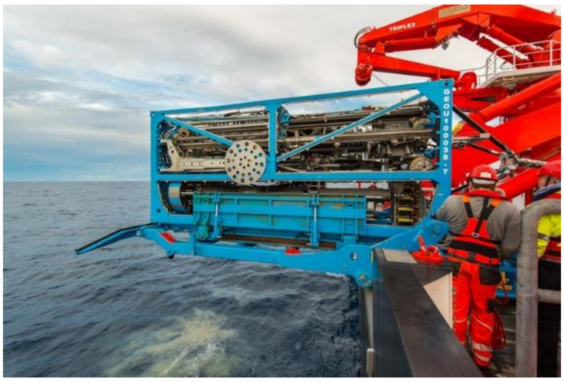

Figure 3. 12 Photo of the MeBo corer

It has a maximum operational depth of 2000m and can recover up to 75m of marine sediment (Freudenthal and Wefer, 2013; Freudenthal et al., 2015). The drilling process can be switched from simple pushing to rotary drilling, which is more effective when crossing massive hydrate layers.

A synthesis of the all the MeBo cores recovered is presented in Figure 3. 13 and Table 3. 7 and a description of the recovered cores is provided in Table 3. 8.

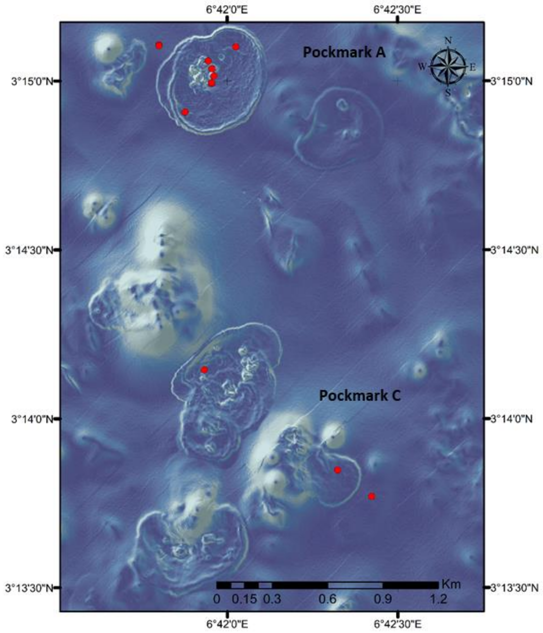

Figure 3. 13 Bathymetry of the study area showing MeBo drilling sites during Guineco MeBo campaign

Table 3. 7 MeBo measuring sites during Guineco MeBo campaign

Guineco MeBo, MeBo Corer		
Site	**Depth (m)**	**Penetration (m)**
GMMB01	1141	23.87
GMMB02	1141	53.3
GMMB03	1148	45.3
GMMB04	1189	18.61
GMMB05	1199	52.49
GMMB06	1148	6.74
GMMB07	1148	10.19
GMMB08	1142	56.84
GMMB09	1196	43.8
GMMB10	1146	23.95
GMMB11	1146	12.58
GMMB12	1144	24.75

3.2.4 Laboratory measurements

Laboratory measurements can be divided into two categories: (1) before splitting the recovered core (MSCL and pore water analysis) and (2) after splitting the recovered core into two halves (XRF and XRD).

3.2.4.1 Multi-Sensor Core Logger (MSCL)

The Multi-Sensor Core Logger (MSCL) from Geotech was used on board in order to measure the P-wave velocity, the Gamma density and the magnetic susceptibility on 1m long whole core sections. This was done at 1cm step for all cores without hydrate and at 2cm step for cores containing hydrate.

Such test provides insight on the lithology of the sediment as well as on its stress history. This allows to select which sections of the sediment are most appropriate to be used for geotechnical testing (such as oedometer test).

3.2.4.2 Pore water analysis

Pore water analysis took place on board using the Rhizon samplers (Wei et al., 2015). The latter were pushed into the recovered samples through already-drilled holes allowing to collect the pore water. In order to conduct several measurements, the extracted pore-water is then divided and stored in the refrigerator. This allowed estimating the amount of chloride within the recovered samples, which provided insight on the detection and quantification of GH.

3.2.4.3 Infra-red thermal imaging

This measurement was also carried out on-board. Recovered samples were immediately detached from the core liner and pictures taken with and Infrared (IR) camera were taken (Wei et al., 2015). The temperature measurements range from $-40°C$ to $+120°C$ with an accuracy of $\pm 2°C$. Each scan can cover around 60cm of the recovered core, which divided into sections.

Since, surface temperatures of the core liners (where GH are absent) were considered as reference temperatures, the presence of GH was possible based on negative thermal anomalies at greater depths of the recovered core. Anomalies higher than $1°C$ are interpreted as voids in the recovered sediment, while anomalies staring at $-2°C$ were considered as indicative of the presence of GH.

Table 3. 8 Description of the recovered MeBo cores

Site	Depth (m)	Pockmark	Description
GMMB-01	1141	A	0cm - 89cm Homogeneous dark clay throughout section + colour change to light grey from top to base + absence of shell
GMMB-02	1141	A	-
GMMB-03	1148	A	-
GMMB-04	1189	C1	0cm - 120cm Dark grey clay with foraminifera + few carbonate concentration
GMMB-05	1199	C2	0cm - 120cm Dark greyish heavily fractured clay + shells fragments finely dispersed throughout section + massive carbonate at 120cm
GMMB-06	1148	A	0cm - 120cm Dark greyish clay foraminifera through section (6-12, 20-25, 40-45, 55-57) cm Carbonate concentration
GMMB-07	1148	A	0cm -120cm Homogeneous dark grey clay + few carbonate concentration + liquefied sediment (0cm - 20cm) 0cm - 45cm Very abundant cracks 85cm - 110cm liquefied sediment 110cm - 120cm Very abundant cracks
GMMB-08	1142	A	0cm -120cm Dark grey mousy clay + carbonate concentration 0cm - 20cm Few cracks (20-58, 66-73, 89-92, 109-113)cm Very abundant cracks
GMMB-09	1196	C	0cm - 120cm Homogeneous dark greyish clay + fluidized sediment at the top + fractured at the base 0cm - 120cm Finely dispersed foraminifera throughout core section + strong H2S odour on entire core
GMMB-10	1146	A	0cm - 51,3cm Very dark greyish clay with abundant foraminifera 0cm - 16cm Dark brown + carbonate concentration
GMMB-11	1146	A	-
GMMB-12	1144	A	-

3.2.4.4 X-ray diffraction (XRD) and X-ray fluorescence (XRF)

The X-ray fluorescence and X-ray diffraction are non-destructive method that allows the production of high-resolution records characterizing sediment geochemistry and mineralogy. The physics lying behind this invention is the phenomenon of ionization that results in emitting electromagnetic radiations. The wavelengths of these radiations and their amplitudes are directly related to the chemical structure of the tested sediment. Each element has a specific emitted energy and the proportion in which the individual energies appear can be calculated by the instrument or by other software.

XRF data can be obtained in three forms: Quantitative, Semi-Quantitative and Qualitative data depending on the user's objective, application, the sample type and the way in which the results of the test will be used. XRF-Qualitative deals with raw data by detecting the fluorescent X-ray energies received in the XRF instrument (McCusker et al, 1998). XRF-Quantitative allows the quantification of the elements present in the sample (Rothwell and Croudace, 2015). However, in some cases, the conditions for quantitative data are not met and qualitative data is not enough to answer how much of an element is present in a sample. This test can be performed at 10KV and 30KV, which allows the detection of different chemical elements:

- Al, Si, P, S, Cl, K, Ca, Ti, MN, Fe and Rh at 10 kV
- Fe, Ni, Cu, Zn, As, Br, Rb, Sr, Y, Zr, Nb, Mo, Ru, Rh and Pb at 30kV

The XRF logging results are then interpreted in combination with other non-destructive methods such as X-ray diffraction (XRD).

While the XRF analysis, provides the content of the chemical elements in the tested samples, the XRD analysis allows to determine the mineralogical composition and quantity of different types of clay minerals present in the sample. Therefore, the concentrations of minerals in the sediment can be calculated.

3.2.4.5 Geotechnical measurements: Oedometer test

An oedometer allows performing a one-dimensional consolidation test, which consists of applying a vertical stress on a sample and then measuring the deformation caused by that stress. In order to prevent the displacement of the sample and allow water drainage, the latter is placed in a 5 cm diameter metal ring between two paper filters and two porous stone. The test serves to determine the consolidation coefficient, the compression index, the vertical yield stress and the yield stress ratio.

3.2.5 Bathymetry and Seismic data

3.2.5.1 AUV bathymetry

Sub-bottom profiles were acquired by C&C technologies with a spacing of 4 meters using an Autonomous Underwater Vehicle (AUV) in pockmark A (George and Cauquil, 2007). The AUV system produces pulses of 2-16 kHz, which are continuously narrowed in order to get a constant resolution with increasing depth. These pulses are then correlated with the recorded seismic data to enhance the vertical resolution, which is the order of 10 centimetres at the seabed while the average penetration depth reaches 70 m. The system is efficiently designed to minimize the survey time and maintain the same measuring speed (George and Cauquil, 2007); thus, resulting in an evenly dispersed data. This eventually allowed creating a 3D seismic data cube of the pockmark bathymetry and the GHOZ occupying this pockmark.

3.2.5.2 Deep towed SYSIF (SYstème SIsmique Fond de mer) seismic system

The SYSIF (SYstème SIsmique Fond de mer), shown in Figure 3. 14, is a deep-towed seismic system designed by Ifremer for High (HR: 250 – 1000 Hz) to Very High resolution (VHR: 650 – 2000 Hz) near-bottom marine seismic surveys (Marsset et al., 2010).

Figure 3. 14 Deep-towed SYSIF seismic system (Ker et al., 2010)

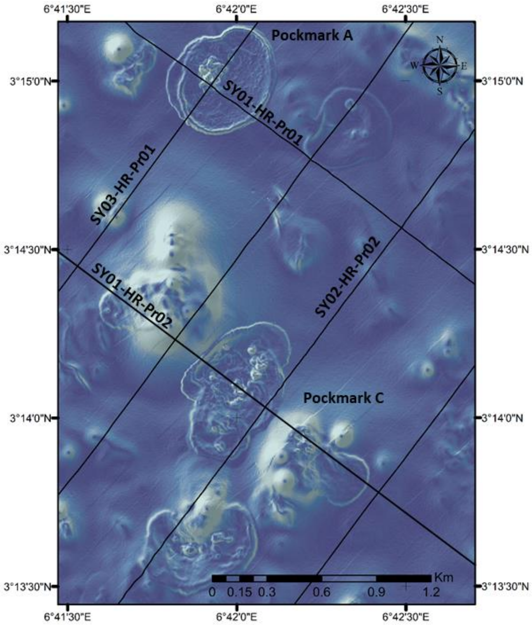

Figure 3. 15 Bathymetry of the study area showing the location of seismic profiles passing through pockmarks A and C

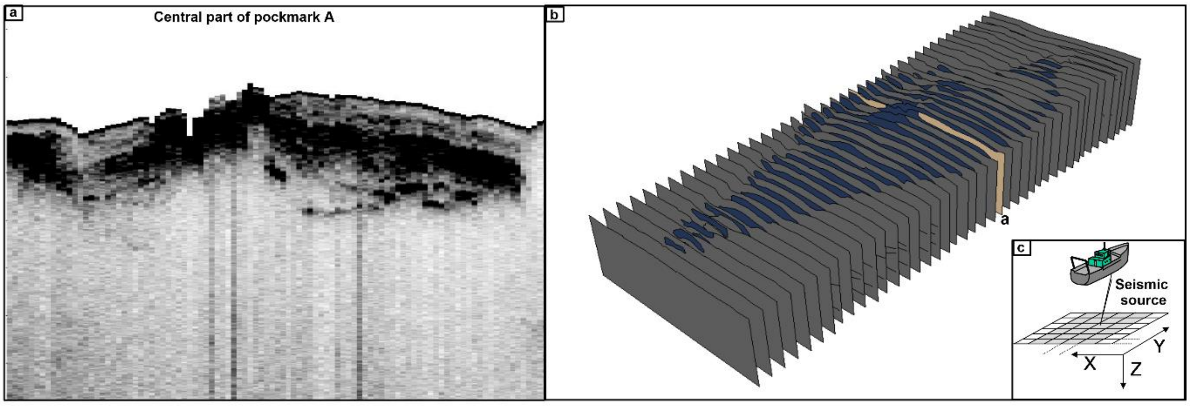

Figure 3. 16 a)Seismic profile through the central part of pockmark A showing a sharp contrast between a high-amplitude chaotic facies (black zones) and a low-amplitude to transparent facies (grey areas), b) Seismic profiles in y-axis direction interpreted in order to create a 3D seismic data cube and c) illustration showing the directions in which the seismic profiles have been made

The penetration depth below the seabed is inversely proportional to the resolution and depends on the type of the penetrated soil. Its altitude above the seabed is set at 100 m to reduce the Fresnel area where the pressure field is very irregular, which improves the lateral resolution with respect to the surface (Ker et al., 2012). The final horizontal and vertical resolutions are provided by Ker et al. (2010) to be in the order of 7m and 25m respectively. Generated seismic profiles are then analysed to identify different soil characteristics: sub-parallel facies represent undisturbed sedimentary layers while high amplitude chaotic facies are representative of dense features (Sultan et al., 2016).

A total of 103 profiles (Figure 3. 16) in the x-axis direction and 124 in the y-axis direction were aquired from the C&C AUV survey within pockmark A (George and Cauquil, 2007).

3.3 Methods

3.3.1 Derivation of geotechnical properties from piezocone results

Piezocone readings including cone tip resistance (q_t), sleeve friction (f_s) and pore pressure (Δu_2) were first used to classify sediments based on their behaviour characteristics and second to derive their geotechnical properties. The classification process relied on the method suggested by Robertson (2016) using the following equations:

The normalized friction ratio:

$$F_r = 100 \times \frac{f_s}{q_t - \sigma_{v0}} \ [\%] \qquad (3.1)$$

The normalized pore pressure:

$$U_2 = \frac{\Delta u_2}{\sigma'_{v0}} \ [-] \qquad (3.2)$$

A revised value of normalized cone resistance:

$$Q_{tn} = \left(\frac{q_t - \sigma_{v0}}{p_a}\right)\left(\frac{p_a}{\sigma'_{v0}}\right)^n \ [-] \qquad (3.3)$$

Where p_a is the atmospheric reference pressure (i.e. 100 kPa) and n a stress exponent defined as:

$$n = 0.381(I_c) + 0.05\left(\frac{\sigma'_{v0}}{p_a}\right) - 0.15 \qquad (3.4)$$

Where I_c is a soil behaviour type index defined as:

$$I_c = [(3.47 - \log\left[\frac{q_t - \sigma_{v0}}{\sigma'_{v0}}\right])^2 + (logF_r + 1.22)^2]^{0.5} \qquad (3.5)$$

For sediments without gas hydrate, the values of total and vertical effective stresses (σ_{v0} and σ'_{v0} respectively) were calculated from the unit weight profile obtained on core GMCS05. For gas hydrate-bearing sediment, the values were obtained from back calculations of gas hydrate content using the effective medium model developed by Helgerud et al., (1999).

The geotechnical properties were empirically derived from piezocone results following the unified interpretation approach presented by Robertson (2009). Since the reliability and applicability of empirical correlations vary according to precedent and local experience, the properties derived from piezocone sounding in gas hydrate-bearing sediments must be treated with caution due to the lack of statistical study on this soil type.

Compression indices were estimated from piezocone results using the following equation:

$$\lambda = \frac{[(1+e_0)\sigma'_{v0}]}{[\alpha_M(q_t-\sigma_{v0})]} \quad (3.6)$$

Where α_M is the constrained modulus cone factor. Based on correlations between piezocone data and results of oedometer tests reported by Sultan et al. (2007) a site-specific value of $\alpha_M = 1$ and a value of void ratio, $e_0 = 6.15$ (at $\sigma'_{v0} = 1$ kPa) were used to calculate compression indices for both hydrate free and hydrate-bearing sediments.

Values of shear modulus at small strain (G_0) were estimated using:

$$G_0 = 0.0188[10^{(0.55I_c+1.68)}(q_t - \sigma_{v0})] \quad (3.7)$$

Where I_c is the soil behaviour type index previously defined (equation 8). Following Krage et al., (2014) values of G_0 were converted into values of shear modulus at 50% mobilized strength (G_{50}) by assuming that $(G_{50}/G_0) = 0.26$ for both hydrate free and hydrate-bearing sediments.

Values of peak undrained shear strength (Su) were derived from:

$$Su = \frac{(q_t-\sigma_{v0})}{N_{kt}} \quad (3.8)$$

Where N_{kt} is a cone factor typically varying from 10 to 20. Following the works of Low et al. (2010) on soft clays, a N_{kt} value of 13.6 was used to calculate Su in hydrate free sediments. A lower bound estimate of the Su of gas hydrate-bearing sediments was calculated using a similar N_{kt}. Calculations were additionally performed using a N_{kt} value of 10 to provide an upper bound estimate.

Based on the assumption that values of sleeve friction (f_s) correspond to the remoulded shear strength of the sediment, values of sensitivity were estimated using:

$$St = \frac{Su}{f_s} \quad (3.9)$$

3.3.2 Derivation of hydraulic properties from piezometer results

Pore pressure measurements were carried out at several selected locations and depths where the presence of gas hydrate was suspected/proved(GMPZ2, 4, 6, 7 and 10 and ERPZY02) as well as at two reference sites (GMPZ3 and 5) using the Ifremer piezometer.

The measured pore water pressure (u) corresponds to an excess pore pressure (Δu) generated by the rod insertion and an in-situ equilibrium pore pressure (u_{eq}), which is assumed constant during the dissipation of the measured maximum excess pore pressure($u = \Delta u + u_{eq}$). The time for 50% dissipation of the measured maximum excess pore pressure (t_{50}) was determined using a graphical method (see Figure 3. 17) in which u_{eq} was either reached from the dissipation test or calculated using the Sultan and Lafuerza (2013) numerical algorithm and after determining Δu_{100}, Δu_0 and Δu_{50} (see ASTM standard D2435 – 1996). It was then possible to derive the hydraulic diffusivity C_h (or the horizontal coefficient of consolidation) of the medium normalized by the square root of the rigidity index (I_r) using the following equation (Teh and Houlsby, 1991):

$$\frac{C_h}{\sqrt{I_r}} = \frac{C_p \cdot r^2}{t_{50}} \quad (3.10)$$

Where C_p is a factor related to the location of the sensor and r is the radius of the rod.

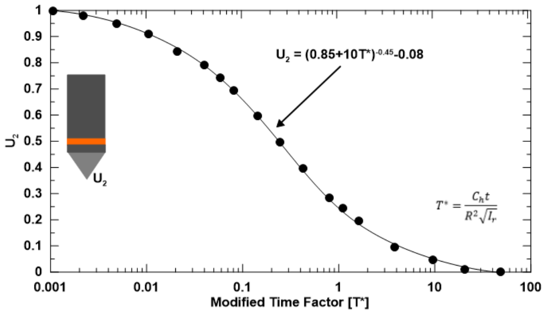

Figure 3. 17 Relationship between the normalized pore pressure and the time factor allowing to determine the time for 50% dissipation of the measured maximum excess pore pressure (t_{50})

3.3.3 Gas hydrate quantification

3.3.3.1 From pore water chloride analysis

The formation of gas hydrate is known to exclude ions dissolved in pore water from the clathrate cage; hence, increasing the salinity of the surrounding pore water (Ussler and Paull, 2001). Therefore, the dissociation of gas hydrate upon core recovery releases fresh water, causing negative anomalies on pore-water chloride profiles (Wei et al., 2015).

As reported by Wei et al., (2015), pore water were extracted using Rhizon samplers on 12 MeBo cores collected in the study area. Chloride concentrations were subsequently determined using ion chromatography (Wei et al., 2015). This led Wei et al., (2015) to determine a baseline pore water chlorinity in the absence of gas hydrate of 550mM. This was done by measuring chloride concentrations in bottom waters and in reference sediments

This value served as an input parameter in the estimation of the gas hydrate content S_h from chloride anomalies following the method presented by Malinverno et al. (2008):

$$S_h = \frac{\beta(C_{cb} - C_c)}{C_c + \beta(C_{cb} - C_c)} \qquad (3.11)$$

Where β is a coefficient that accounts for the density change from gas hydrate to water and equals 1.257, C_{cb} is the baseline pore water chlorinity prior to dissociation and C_c is the chlorinity measured in the core after dissociation.

3.3.3.2 From in-situ Vp measurements and rock physics characterisation

The effective medium model developed by Helgerud et al. (1999) was used to estimate gas hydrate content within the marine sediment from in-situ Vp measurements. The principle of this model is to relate the stiffness of the dry frame to porosity, mineralogy and effective stress. As key input parameters to the model, the sediment mineralogy, porosity and its evolution with effective stress were determined from analyses of core GMCS05 taken as representative of the study area. The elastic properties and densities used in the calculation were similar to those used by Helgerud et al. (1999) as shown in Table 3. 9.

Differences between calculated and measured P-wave velocities (Figure 3. 18) were used to obtain an upper and lower bound estimate of gas hydrate content within the sediment by assuming that:

- GH alter only the pore fluid elastic properties (S_{hmax})
- GH contribute stiffness to the sediment by becoming part of the load-bearing framework (S_{hmin}).

It is noteworthy that considering one case or the other has implications on the derivation of the lithostatic stress as explained by Helgerud et al. (1999). However, when calculating the effective stress as the difference between the lithostatic stress and the pore fluid pressure, hydrostatic conditions were always assumed for the latter.

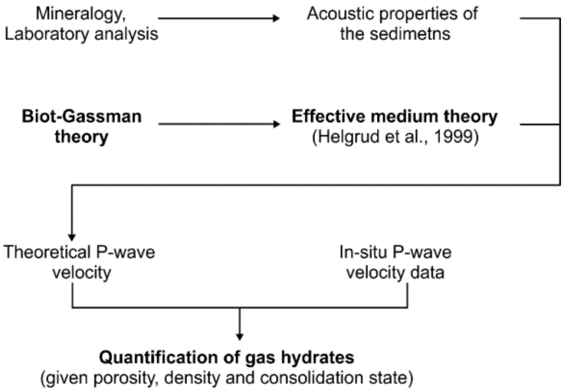

Figure 3. 18 Adopted method to apply the effective medium theory (Helgerud et al., 1999)

Table 3. 9 Elastic and density properties of selected sediment components (after Helgerud et al. 1999). K is the bulk modulus, G the shear modulus and ρ the density

Constituentm	K (GPa)	G (GPa)	ρ (g/cm^3)
Clay	20.9	6.85	2.58
Calcite	76.8	32	2.71
Quartz	36.6	45	2.65
Gas Hydrate	7.9	3.3	0.90
Water	2.4-2.6	0	1.032
Methane Gas	0.10-0.12	0	0.23

A model that can estimate gas hydrates content within the marine sediment has been developed using Fortran 90 platform (Figure 3. 19 and Table 3. 10). The code mainly works by inserting the mineralogy data of the sediment along with the measured compressional velocity values. It is able to perform iterations allowing the calculation of each constituent of the sediment (clay, calcite and quartz) at the depth values at which the velocity was measured.

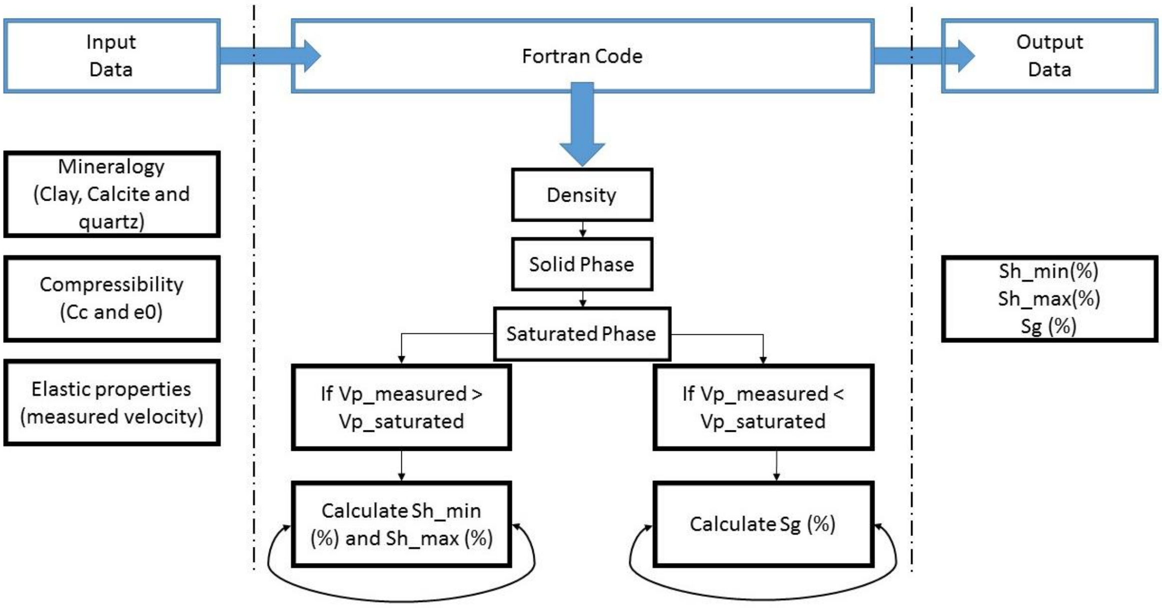

Figure 3. 19 FORTRAN Code Scheme

Table 3. 10 Sample output of the Fortran Code showing the number of iteration (j), the depth (D_Vpm) the measured velocity (Vpm) the calculated velocity (Vp_sat), the lower boundary (Sh_min) and the upper boundary GH content

j	D_vpm	Vpm	Vp_sat	Sh_min	Sh_max
456	10,795	1487,5	1470,588	0,0081	0,0336
457	10,8163	1490,9	1470,602	0,0096	0,0402
458	10,8376	1482,2	1470,616	0,0056	0,0232
459	10,8696	1474,9	1470,695	0,0023	0,0085
460	10,8803	1473,8	1470,585	0,0018	0,0065
461	10,9016	1470,2	1470,342	0	0
462	10,9229	1470,4	1470,355	0,0004	0,0001
463	10,9443	1471,1	1470,369	0,0007	0,0015

3.3.4 Constitutive modelling

A new simple constitutive model, with a limited number of parameters, which is able to reproduce the mechanical behaviour of GHBS has been developed within the framework of the PhD (personal communication with Sultan). I only used the model and did not participate in developing it. A special attention has been devoted to the contractancy/dilatancy upon shearing of the GHBS and considered through a modified expression of the steady state line and by proposing a new “equivalent skeleton void ratio” for gas hydrate. This part is largely explained in chapter 6.

3.4 Conclusion

In this chapter, the study area as well as the tools and methods used to explore it are presented. The Gulf of Guinea is one area where dense and shallow accumulations of GH have been confirmed, which makes it the centre of interest of many industrial and academic research projects. Several oceanographic campaigns took place in the study area and provided a rare and unique database of in-situ acoustic, geotechnical, pore pressure dissipation measurements as well as cores and seismic profiles. The analysis and exploitation of the data allowed detecting and quantifying GH. Correlations between different types of data provided insight on the mechanical and hydraulic properties of GHBS. The chapter ends by a detailed presentation of the methods and empirical equations used to analyse the data.

Chapter 4. Mineralogy analysis, gas hydrate detection, quantification and correlation with seismic data

Chapitre 4. Analyse minéralogique, détection d'hydrates de gaz, quantification et corrélation avec les données sismiques

Reference: Taleb, F et al. Seafloor depressions on the Nigerian margin: seabed morphology and sub-seabed hydrate distribution. Paper under revision. Marine and Petroleum Geology.

Hydrate recovered from site GMGC20 during Guineco MeBo campaign (2011)

Abstract

Proper knowledge of the physical properties, content and morphology of gas hydrate is required in order to understand their effect on their host sediment. Gas hydrate are known to be metastable, which makes them difficult to maintain within their stability field upon recovery. Thus, this work relies on a unique database of in-situ acoustic and geotechnical measurements as well as seismic surveys in a high gas flux pockmark system in the Gulf of Guinea. Gas hydrate were detected and quantified based on acoustic measurements of compressional wave velocity, and after estimation of the mineralogical proportions using a petro-physical model. Projections of the in-situ acoustic and geotechnical measurements on the seismic profiles have shown that the study area not only accommodates zones of shallow and dense gas hydrate; but also zones where solid hydrate and free gas coexist as well as pockets of free gas. Further analysis of several seismic profiles has allowed illustrating the detailed gas hydrate occurrence zone (GHOZ) within the study area, estimate its volume and its occupancy ratio of the pockmark. Correlations between gas hydrate content and 3D bathymetry sections have allowed to draw a link between different gas hydrate contents and the morphology of the pockmark, which also shares similarities with the morphology of the GHOZ it accommodates.

Résumé

Une bonne connaissance des propriétés physiques, de la saturation et de la morphologie des hydrates de gaz est nécessaire pour comprendre leur composants sur les sédiments hôtes. Les hydrates de gaz sont thermodynamiquement métastables, ce qui rend difficile de les maintenir dans leur champ de stabilité (P, T) une fois récupérés du milieu naturel. Ainsi, ces travaux s'appuient sur une base de données unique comportant des mesures acoustiques et géotechniques in situ ainsi que des données sismiques recueillies au large de Nigéria dans un système sédimentaire naturel caractérisé par la présence d'un champ de pockmarks riche en hydrates de gaz et associé à un flux de gaz élevé. Les hydrates de gaz ont été détectés et quantifiés en se basant sur une approche couplée utilisant les mesures de vitesse de compression, la minéralogie du sédiment et un modèle pétro physique. La corrélation des mesures acoustiques et géotechniques in situ avec les profils sismiques a montré que la zone d'étude n'abrite pas seulement des zones peu profondes riches en hydrate de gaz ; mais aussi des zones de coexistence d'hydrate solide et de gaz libre ainsi que des poches de gaz libre. Une analyse plus fine réalisée sur plusieurs profils sismiques a permis de déterminer la géométrie détaillée de la zone d'occurrence des hydrates de gaz (GHOZ) et d'estimer le volume et le taux d'occupation des hydrates dans le pockmark. La comparaison entre le contenu en hydrate de gaz et les sections de bathymétrie 3D a permis de définir une corrélation entre la saturation en hydrates de gaz et la morphologie du pockmark, qui partage également des similitudes avec la morphologie de la GHOZ
.

4.1 Introduction

Gas hydrate (GH) are ice-like solid mixtures of gas molecules, mainly methane, trapped within a crystalline structure of water molecules (Sloan, 1998). These geo-compounds are stable under high pressure and low temperature within a depth range known as the GH stability zone. Their presence also requires continuous supply of gas with a concentration exceeding the solubility limit in water and sufficient amount of water (Sultan et al., 2010). They have been mainly inferred and recovered along continental margins and polar permafrost layers (Kvenvolden, 1993). GH represent the largest stock of natural gas in the world (Shankar et al., 2013), but also a geotechnical hazard threatening offshore operations as well as potential agent of climate change. This made them a target for many scientific and industrial interests. Understanding the effect of GH on their host sediment behaviour requires knowledge of their physical characteristics, properties, concentration and morphology. Holland et al. (2008) showed that the morphology of GH is a means of describing the relation between GH and their bearing sediment as well as defining the physical properties of the sediment-hydrate matrix.

GH are known to be metastable; thus, their identification and characterisation through actual recovery of core samples have been proved challenging (Dai et al., 2012). Therefore, as previously shown by Sultan et al. (2014; 2010; 2007) and Taleb et al. (2018), in this work the detection of GH has been inferred via in-situ measurements. These measurements are eventually interpreted using an effective medium model. The latter, establishes a relation between the compressional wave velocity anomalies, the mineralogy of the host sediment and the hydrate morphology and fraction (Helgerud et al., 1999).

The presence of GH in the marine environment dramatically alters the physical properties of the host sediment by replacing the pore water /or gas with a solid compound. The compressional wave velocity of gas hydrates-bearing sediments (GHBS) is much higher than that of sediments without hydrate. On the contrary, free-gas bearing sediments tend to show negative compressional velocity anomalies.

(Shankar et al., 2013) used the effective medium model to determine GH and free gas saturation in the Krishna-Godavari Basin, eastern Indian margin. The basin is dominated by clayey sediments and it was reported that GH occurred in fractures as veins or nodules. Numerical results have shown that the effective medium models are more accurate compared with tested empirical models, since the physical properties of the sediment were taken into consideration. Ghosh et al. (2010) compared different GH estimation geophysical methods, such as the grain displacing model and the Helgerud effective medium model to the pressure core method, which is the most direct and reliable one. Those different approaches are often based on a well-known mineralogy of the host sediment column (by coring or drilling) and on the difference between a reference sonic velocity profile with respect to the one altered by the presence of free gas and GH. However, the use of in-situ acoustic measurements to quantify GH as proposed by Sultan et al. (2007) is restricted by the requirement to characterise the in situ mineralogy of the host sediment.

Therefore, one of the aims of the present paper is to detect and quantify GH based on in-situ acoustic measurements even for sediments where accurate mineralogical characterisation is not available. This was carried out by performing correlations between different in-situ data and comparing the similarities and the differences between reference sites without GH and GH-bearing sites.

Numerous oceanographic campaigns, aiming to study GH distribution, have been carried out along the Gulf of Guinea, which is known to accommodate dense accumulations of shallow GH (Cunningham and Lindholm, 2000; Sultan et al., 2010; Wei et al., 2015). The study area is also characterised by the presence of different

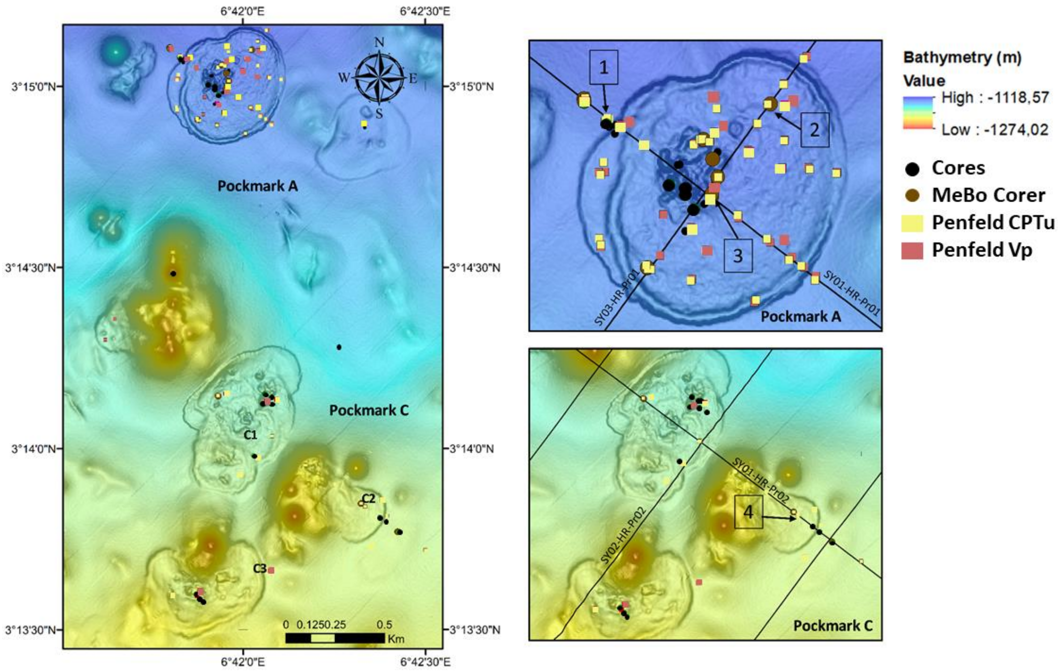

Figure 4. 1 Bathymetry of the study area showing seismic profiles through pockmarks and the investigated sites: 1: GMPFV07S05, GMMB01 and GMCS05, 2: GMPFV03S03 and GMMB12, 3:GMPFV07S05, GMMB06 and ERCS02 and 4: GMPFV10S04 and GMMB05

Table 4. 1 Investigated sites within the study area: site 1 cluster characterises reference sediment without GH nor free gas while clusters 2, 3 and 4 represent sediment where the presence of GH was suspected or proved

Penfeld Vp site	Depth (m)	Length (m)	Nearby Calypso or MeBo cores	Site	Location
GMPFV07S01	1140	30	GMMB01 GMCS05	1	NE - Outside of pockmark A
GMPFV03S03	1142	101.3	GMMB12	2	NW pockmark A
GMPFV07S05	1146	8.5	GMMB06 ERCS02	3	Centre of pockmark A
GMPFV10S04	1195	26	GMMB05	4	Eastern part of pockmark C2

seabed deformations known as pockmarks. However, little has been discussed concerning the distribution of GH below the seabed and its impact on the shapes and sizes of these pockmarks. As a step towards identifying links between GH and free gas and the geometrical features of different pockmarks, the second aim of this paper is to correlate seismic data profiles and seabed morphologies with GH content.

4.2 Study area

The study area is located in the gulf of guinea, in the southern part of Nigeria and along the

Niger Delta. Numerous studies have shown that this area is characterised by various sedimentary features such as pockmarks (Sultan et al., 2014; 2010; 2007 and Taleb et al. 2018), which were directly linked to the formation and dissolution of GH (Sultan et al., 2014).

This paper focuses on two specific pockmarks that Sultan et al. (2010) referred to as A and C. Pockmark A is situated in the northern part of the study area at depths lying between 1100 and 1200m (Figure 4. 1). It is 600 meters in diameter with 6 meters deep peripheral depression. Pockmark C is composed of a cluster of three sub-pockmarks revealing irregular seabed morphologies: C1, C2 and C3 (Figure 4. 1) located at water depths ranging from 1170 m and 1210 m. All four pockmarks are characterised by numerous moats and bumps on their surface. While the area is classified as a high gas flux system, GH have been only identified within the pockmarks.

The study area has been investigated by many authors. For instance, Wei et al. (2015) have defined GH occurrence zones (GHOZ) based on pore water chloride analyses and infrared thermal imaging. Sultan et al. (2007) have shown that the study area accommodates shallow GH formation and identified zones where solid GH and free gas coexist.

4.3 Tools and methods

Several cruises have been conducted in order to characterise the presence of GH in the study area. The Guineco-MeBo (2011) and ERIG3D (2008) oceanographic campaigns took place on the French R/V *'Pourquoi pas?'* and the NERIS2 (2004) on the R/V *'Atalante'*. All campaigns aimed to determine the distribution of GH in the study area in order to understand the link between GH and the mechanisms/formation and evolution of pockmarks as well as study the stability of sedimentary bodies.

In this chapter:

- Four Penfeld Vp were investigated as shown in Figure 4. 1 and in Table 4. 1: site 1: GMPFV07S01 (outside pockmark A), site 2: GMPFV03S03 (NW sector of pockmark A), site 3: GMPFV07S05 (centre of pockmark A) and site 4: GMPFV10S04 (eastern part of pockmark C
- Four MeBo cores (site1: GMMB01, site2: GMMB05, site 3: GMMB06 and site 4: GMMB12) and two Calypso cores (site 1: GMCS05 and site 3: ERCS02) allowed the investigation of the study area (Figure 4. 1 and Table 4. 1). These sites were particularly chosen because they are the closest to the Vp sites presented above; and therefore, the most comparable ones.
- Perpendicular SYSIF profiles have been acquired through pockmark A and C, which were used to correlate the acoustic/geotechnical data and the geomorphology of the pockmarks. This allowed understanding the distribution of GH and free gas within the pockmarks.
- Sub-bottom profiles were acquired every 4 meters using an Autonomous Underwater Vehicle (AUV) in pockmark A with an average penetration depth of around 70 meters. The AUV system produces pulses of 2-16 kHz, which are continuously narrowed in order to get a constant resolution with increasing depth. These pulses are then correlated with the recorded seismic data allowing enhancing the vertical resolution. The system is efficiently designed to minimize the survey time and maintain the same measuring speed (George and Cauquil, 2007); thus, resulting in an evenly dispersed data. This eventually allowed creating a 3D seismic data cube of the pockmark bathymetry and the GHOZ occupying this pockmark

More details about the used tools and methods are shown in chapter 3.

4.4 Results

4.4.1 Mineralogy analysis and density profile

In order to apply the effective medium theory and quantify the concentration of hydrates in sediments, the mineralogy profile characterising the sediment in question must be defined.

The mineralogical composition of the reference sediment from site GMCS05 is presented in Figure 4. 2, where it can be observed that the profile is dominated by clay, calcite and quartz fractions. While the clay fraction varies between 0.5 and 0.93, the calcite fraction varies between 0.01 and 0.42 and the quartz fraction is observed to have a quasi-constant value of around 0.06 with depth. These XRD results were compared to those acquired with the XRF method in an attempt to obtain mineralogy profiles with a spacing of 2cm along cores.

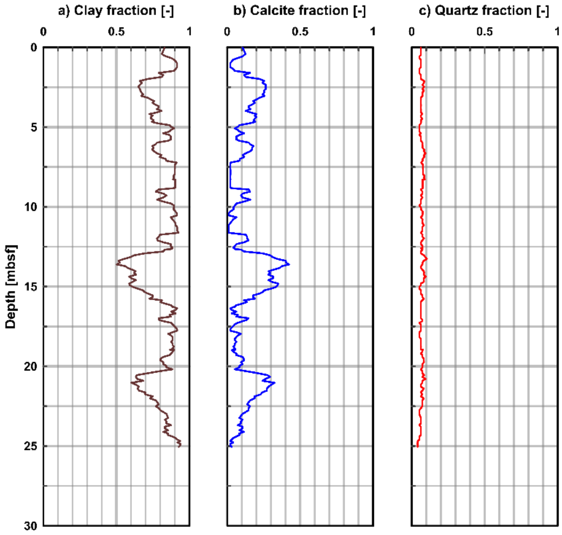

Figure 4. 2 Mineralogy profile for reference site GMCS05 (site 1 in Figure 4. 1): a) clay fraction, b) calcite fraction and c) quartz fraction

4.4.1.1 Mineralogy derived from XRF and XRD tests

Correlations between XRD and XRF for reference core GMCS05 (site 1 in Figure 4. 1) showed that the concentration of calcite (CaCo₃) can be linearly related to that of calcium oxide (CaO) (Figure 4. 3). Therefore, the following equation was proposed to determine the proportions of calcite based on the calcium oxide content in cases where the former is not available:

$$CaCO_3\ (\%) = A \times CaO\ (\%) \qquad (4.1)$$

Where A is the slope of the fitting line and is equal to 0.7 (red line in Figure 4. 3)

To further discuss the results at this stage, correlations between the mineralogical composition and acoustic data (Vp and attenuation) have been made (Figure 4. 4).

Due to the high resemblance between the attenuation profile and calcium oxide/calcite content at reference site GMCS05 (site 1 in Figure 4. 1), both profiles have been plotted against each other (Figure 4. 5). With a regression coefficient R^2 of around 0.9, values of attenuation and calcium oxide/calcite follow a linear trend. This observation is important as it allowed determining calcite profiles at sites where XRF/XRD tests could have not been performed, mainly due to high disturbance of recovered cores in question.

However, in cases where the tested core was not disturbed, calcite profiles were determined either directly from XRD results or indirectly from XRF results using equation 2. For the quartz profile, values were considered constant and equal to the average quartz content (around 6%) in sediments from core GMCS05 (site 1 in Figure 4. 1). The clay fraction is then calculated using the following equation:

$$f_{clay} = 1 - f_{calcite} - f_{quartz} \qquad (4.2)$$

This allowed estimating the concentration of GH at all sites where Vp profiles were available.

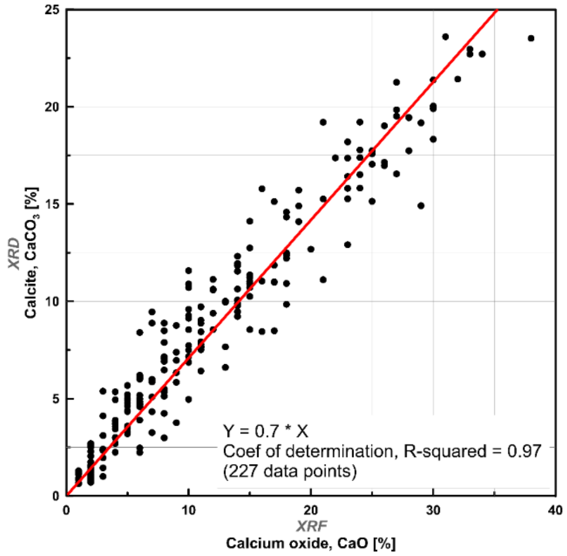

Figure 4. 3 Correlation of calcite fraction with calcium oxide fraction for core GMCS05

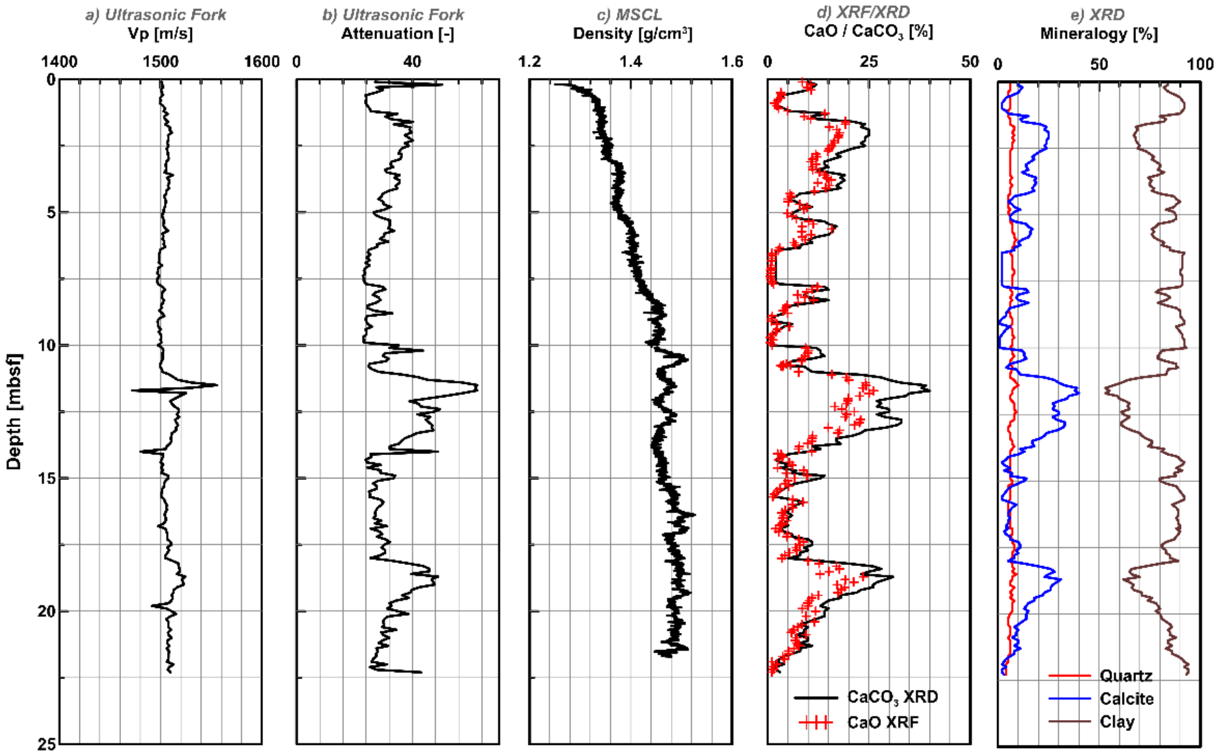

Figure 4. 4 Correlation between acoustic measurements: a) compressional wave velocity and b) attenuation and mineralogical composition: c) density, d) calcite (continuous black line) / calcium oxide (red crosses) and e) mineralogy fractions (modified from Taleb et al. 2018)

4.4.1.2 Mineralogy derived from in-situ acoustic measurements

For some sites, XRF and XRD tests could not be carried out because of the absence of cores or the disturbance of the sediment due to coring/drilling processes or GH dissociation upon core recovery.

The first step was to correlate all significant peaks and patterns of the in-situ compressional wave velocity, the attenuation and the applied load profiles of the GH bearing site in question (Figure 4. 6).

Based on earlier observations, the attenuation profile correlates best with that of calcite. Then, the attenuation profile of the investigated site can be compared and correlated with that of a reference site without GH, where XRF/XRD tests have been performed and the mineralogy profile determined. To improve correlation between profiles, data have been first adimensionalised (Figure 4. 7) using the following equation:

$$x = \frac{\bar{x}-x}{\sigma_x} \qquad (4.3)$$

Where, x is the value that will be made dimensionless (i.e. attenuation, mineralogy profile), $\bar{x}$ and σ_x are the mean and standard deviation values for x.

As represented in Figure 4. 7.a and b (using red crosses), correlations were made by relating depths of similar patterns in the attenuation profile of the reference and GH bearing sites.

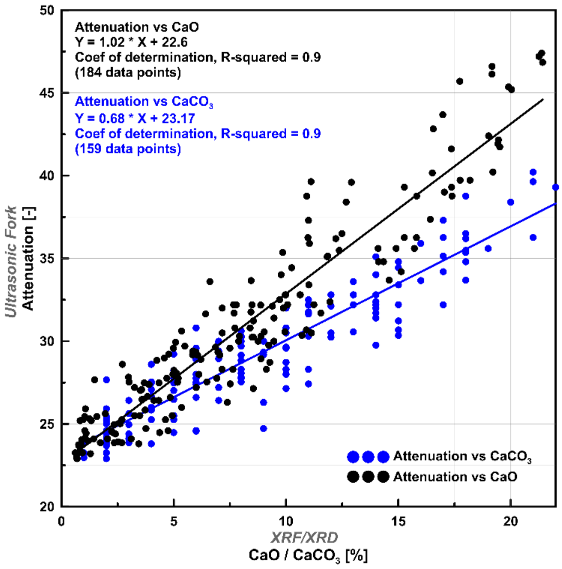

Figure 4. 5 Figure 1. Correlation of attenuation with calcium oxide and calcite fractions for core GMCS05

Then the adjusted attenuation profile of the reference site (blue line in Figure 4. 7.c) was superimposed on that of the investigated site (black line in Figure 4. 7.c). Eventually, the calcite profile was depth-adjusted with that of the updated attenuation profile following the same process (Figure 4. 7.d).

For the quartz profile, values were set to a constant that is equal to the average quartz content in the sediment (around 6%).The clay fraction is then calculated using equation 3.

Examples of other depth-adjusted attenuation profiles are provided in Figure 4. 8. The latter shows correlations between attenuation profiles from GH bearing sediments (blue profiles) and those from reference sites (red profiles). Depth corrections between both profiles have allowed determining new depth-adjusted attenuation profiles for GH bearing sediment; and, eventually use this profile to define the mineral proportions needed in order to estimat GH content (see section 4.4.1: Mineralogy analysis).

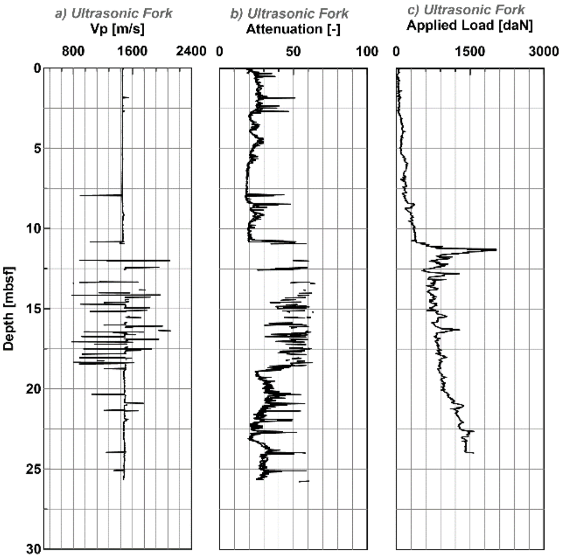

Figure 4. 6 GH bearing site GMPFV10S04 (site 4 in Figure 4. 1) acquired by the ultrasonic fork: a) compressional wave velocity, b) signal attenuation and c) applied load to penetrate the sediment

4.4.1.3 Density profile

The density profile is a substantial parameter in the process of the Vp inversion to estimate GH content (Figure 4. 4.c). It allows calculating the vertical effective stress and porosity, which in turn are key parameters for the mathematical and physical equations used to calculate the content of GH in the sediment. The density profile of core GMCS05 (Figure 4. 4.c) was used to define the reference compression index (C_c) and the initial void ratio (e_0) needed to determine the evolution of the void ratio (or porosity) with effective stress using the following equation:

$$e = e_0 - C_c . log \frac{\sigma'_v}{\sigma'_{v0}} \qquad (4.4)$$

Where σ'_v is the vertical effective stress at a given level below the seabed and σ'_{v0} is a reference vertical effective stress taken equal to 1 kPa

From the density profile of GMCS05, values of 2.5 and 9.8 were estimated for C_c and e_0 respectively. They were considered as representative only for the first 30mbsf of sediment. These values were used to calculate the porosity and hence the bulk density for each site. The sediment bulk density (ρ_b) in this model is calculated as follows:

$$\rho_b = \phi\rho_w + (1 - \phi)\rho_s \qquad (4.5)$$

where, ρ_w is the water density

ρ_s is the solid phase density: $\rho_s = \sum_{i=1}^{m} f_i \rho_i$ (4.6)

f_i and ρ_i are the clay, calcite and quartz fractions and solid densities respectively.

4.4.1.4 Parametric study: Residual error

Assumptions and correlations were carried out throughout this work in order to apply the effective medium theory. This is mainly due to sediment disturbance caused by the penetration of the in-situ tools, which will eventually promote the dissociation of GH. Therefore, in some cases, available data is insufficient to characterise the sediment in question.

The following critical parametric study aims to quantify the error resulting from this process; thus, two uncertainties are discussed: a) the assumed constant value of the quartz profile and b) the assumed values of C_c and e_0 values. The residual error is calculated using the following equation:

$$Residual\ error = \ln \frac{x_{assumed}}{x_{actual}} \qquad (4.7)$$

Figure 4. 9 shows the residual error resulting from assuming the compression index (Cc) and the void ratio (e_0) to be 2.502 and 12.302, respectively. The effective vertical pressure (σ'_{v0}) was calculated using the real density values obtained from the GMCS04 (blue) and the estimated Cc and e_0 (red). It can be observed that the two pressure curves correlate well along the depth core depth. To further test the accuracy of the numerical model, a comparative study was held between the measured velocity and the velocity calculated by the model using the actual density values, as well as between the measured velocity and the velocity calculated by the model using the assumed parameters $(Cc$ and $e_0)$. Same steps were followed to assess the residual error due to setting the quartz (Figure 4. 10) proportion as a constant along the core depth. This allowed quantifying the residual error between $(-0.006;\ +0.006)$, which is almost negligible.

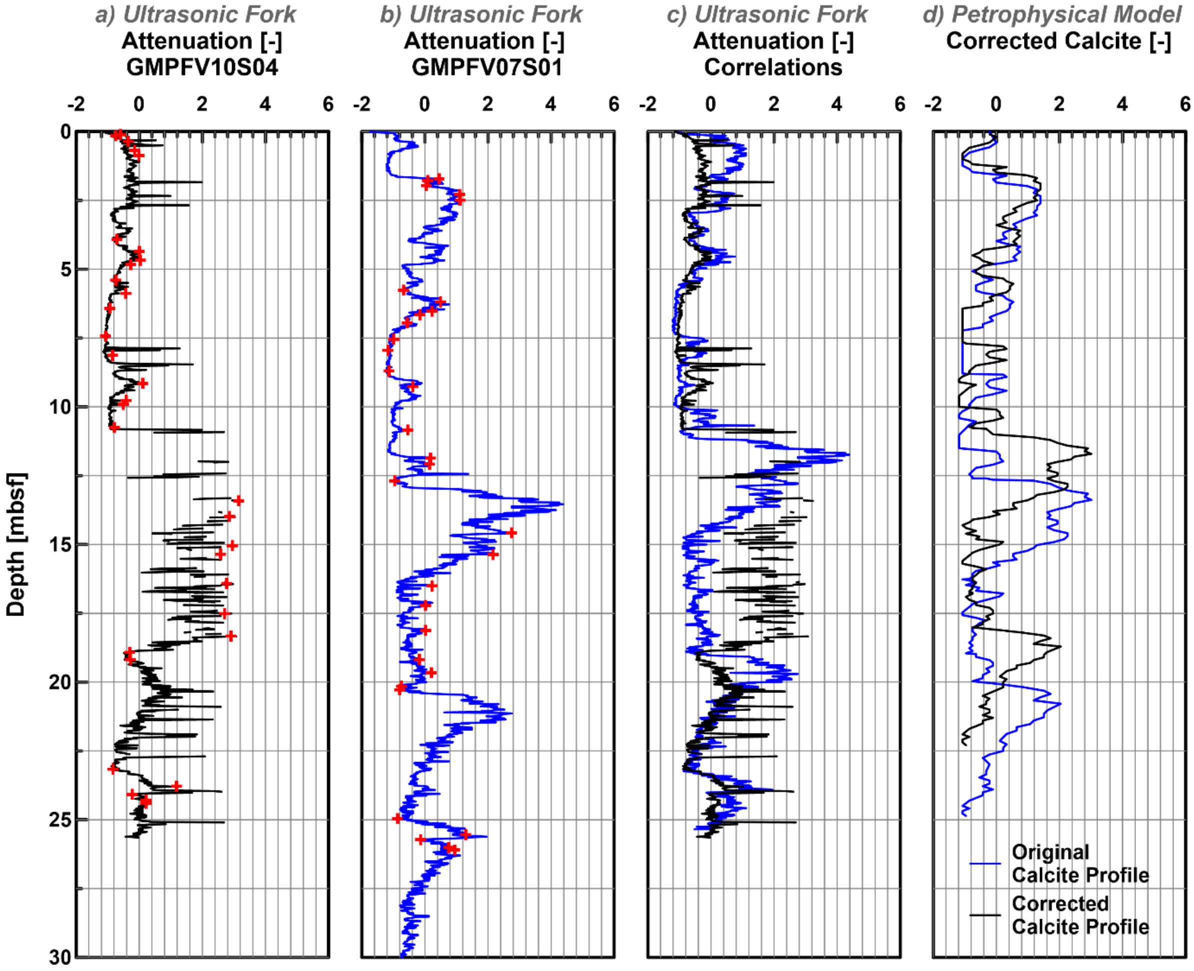

Figure 4. 7 Correlations between adimensionalised attenuation profiles of: a) GH bearing site GMPFV10S04, b) attenuation profile of reference site GMPFV07S01, c) depth to depth correlation in terms of attenuation and d) adimensionalised original calcite profile (blue continuous line) against adimensionalised depth-adjusted calcite profile (black continuous line) that allow determining the mineralogy profile of GH bearing sediment at site GMPFV10S04 (blue curve in d)

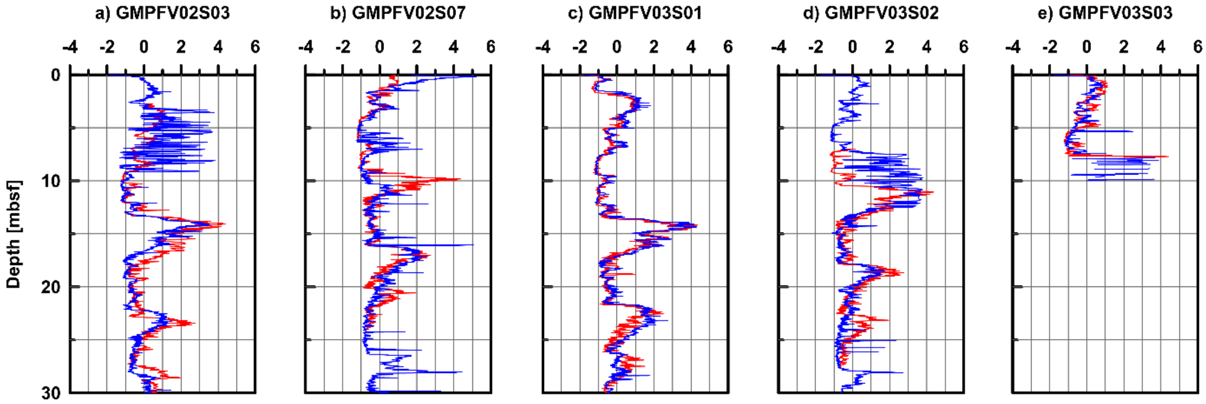

Figure 4. 8 Correlations between attenuations of reference site (red profiles) and GH bearing sites (blue profiles): a) GMPFV02S03, b) GMPFV02S07, c) GMPFV03S01, d) GMPFV03S02 and e) GMPFV03S03

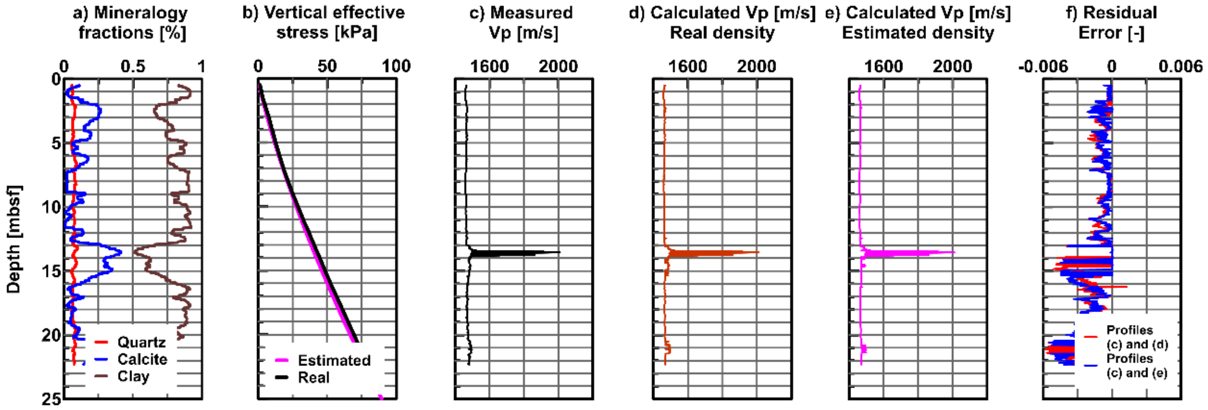

Figure 4. 9 Parametric study accounting for the constant quartz assumption: a) real and estimated quartz profiles from core GMCS05, b) vertical effective stress profile using the real and assumed quartz value, c) Measured P-wave velocity at reference site GMPFV02S02, d) Calculated P-wave velocity using real quartz value, e) Calculated P-wave velocity using estimated quartz value, f) residual error between measured and calculated P-wave velocity using real quartz value and between measured and calculated P-wave velocity using assumed quartz value

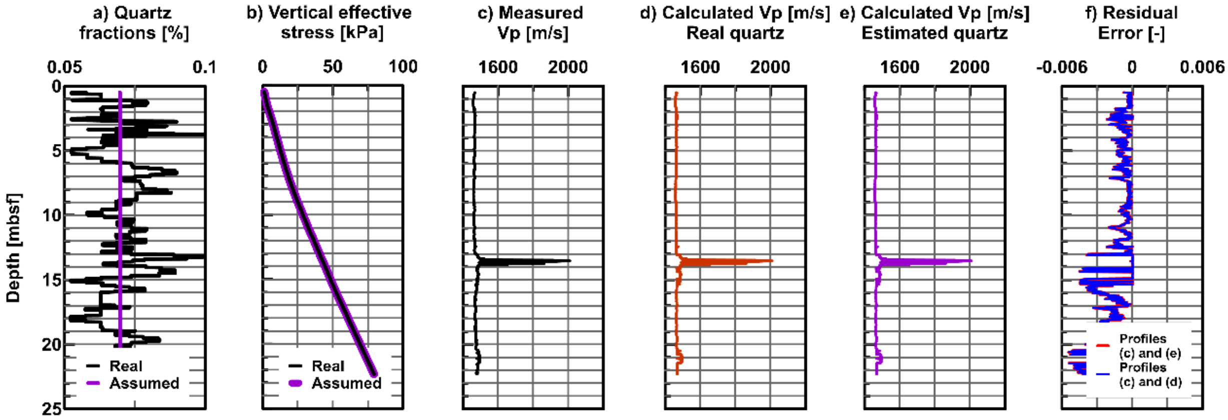

Figure 4. 10 Parametric study accounting for assumed C_c and e_0 values: a) Mineralogy fractions from core GMCS05, b) vertical effective stress profile using real and assumed C_c and e_0 values, c) Measured P-wave velocity at reference site GMPFV02S02, d) Calculated P-wave velocity using real C_c and e_0 values, e) Calculated P-wave velocity using estimated C_c and e_0 values, f) residual error between measured and calculated P-wave velocity using real C_c and e_0 values and between measured and calculated P-wave velocity using assumed C_c and e_0 values

4.4.2 Back-calculation for gas hydrate content

4.4.2.1 For sediment without gas hydrates (reference sediment)

The GMPFV07S01 is a Penfeld Vp reference site at which neither GH nor free gas were detected.

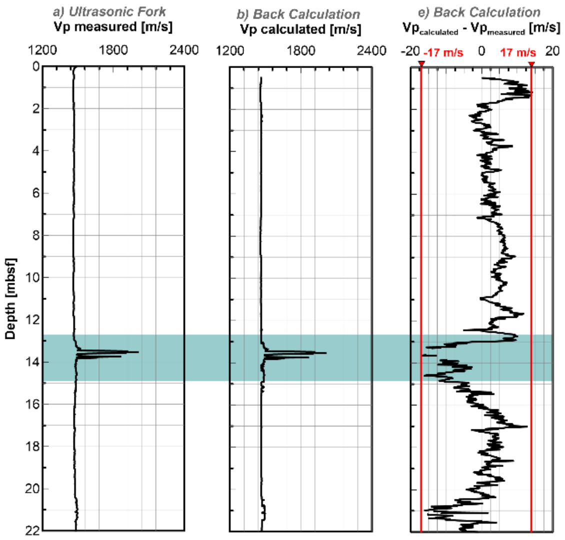

Figure 4. 11 Reference site GMPFV07S01 (site 1 in Figure 4. 1): a) Vp measured using in-situ tool, b) Vp calculated using effective medium model and c) difference between calculated velocity and measured velocity (Modified from Taleb et al. 2018)

Based on Figure 4. 11, reference sites are characterised by Vp oscillating between 1450 m/s and 1510 m/s; however, a clear peak of 2015 m/s is noticed at around 13.6 mbsf (blue rectangular zone in Figure 4. 11). Such peak was related to the presence of foraminifera in the sediment (Taleb at al. 2018). In order to confirm the reliability of the effective medium model, calculated and Vp were compared. It can be observed that both profiles yield almost the same results (Figure 4. 11). Additionally, to narrow down the calculation errors that could occur during the quantification process, the difference between the velocity calculated by the model and the measured velocity was calculated and found to oscillate in the range $\pm 17\ m/s$. Hence, GH contents will only be determined when the difference between the calculated and measured Vp is greater than $17 m/s$.

4.4.2.2 For sediment with gas hydrates

GH were quantified at all sites where Vp data were available and after definition of the mineralogy profile of the sediment in question, which was mostly done by correlating acoustic data (attenuation profile) of GH bearing sites with that of reference sites. This is because, in most cases, recovered cores from GH bearing sites are highly disturbed due to coring/drilling processes that eventually promotes GH dissociation.

Quantification results obtained from the effective medium theory were compared to pore-water chloride analysis and pictures of nearby recovered cores, which allowed carrying out a more reliable investigation of GH bearing sediments.

Figure 4. 12 presents the Vp, the signal attenuation and the applied load at site GMPFV03S03 (site 2 in Figure 4. 1). The positive and simultaneous increases of all three parameters confirms the presence of GH at this site. On the other hand, negative Vp anomalies indicate the presence of free gas within the sediment; thus, allowing determining layers where solid hydrate and free gas coexist.

At 7.5 mbsf, missing data in the Vp and signal attenuation profiles correlates with an increase of around 560 daN of the applied load, which suggests that GH were touched at this depth. This is followed by sudden increases of up to 2131 m/s in Vp and 60 in the signal attenuation at 7.8 mbsf. At the same depths, infrared thermal scanning of the nearby core GMMB12 (Wei et al., 2015) revealed temperatures as low as 16°C, which is due to the endothermic dissociation of GH. These colder temperatures, compared to reference sediments, indeed confirm the presence of GH. The GH contents estimated with the effective medium theory were averaged over depth intervals of 10 cm and then compared to those obtained from pore-water chloride analyses.

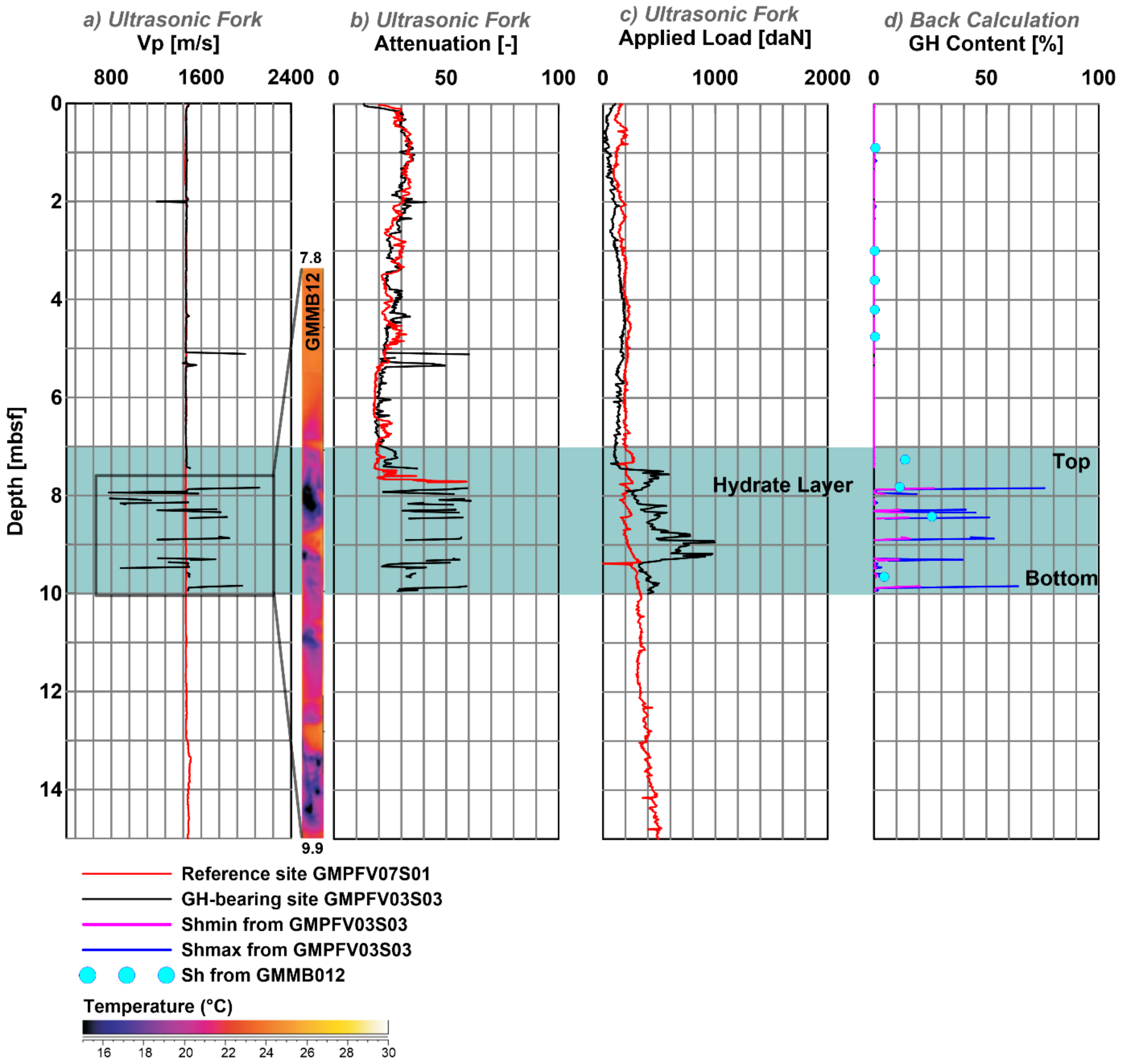

Figure 4. 12 a) P-wave velocity, b) depth-adjusted attenuation profile, c) applied load for site GMPFV03S03 (black curves) against reference site GMPFV07S01 (blue curves) and d) GH content for site GMPFV03S03 (modified from Taleb et al. 2018)

Using Vp data, maximum GH contents were estimated to occur at 7.85 mbsf with values of 27% for S_{hmin}, 76% for S_{hmax} while a lower value of 11.5% was estimated by using the pore-water chloride data For the GMPFV07S05 site shown in Figure 4. 13 (site 2 in Figure 4. 1) an abrupt increase in the applied load (1633 daN) at around 3.8 mbsf followed by a strong increase in Vp and signal attenuation (2050 m/s and 58 respectively) at 4 mbsf were observed. These values are up to 2 times higher than those obtained at the reference site at the same depths, which indicates the presence of GH. Additionally, photos of nearby Calypso core CS02 showed the presence of massive GH nodules followed by a 30 cm thick interval containing GH veins (Figure 4. 13). Using the effective medium theory, maximum GH content were estimated to occur at 4mbsf with values of 25% for S_{hmin} and 70% for S_{hmax}.

Figure 4. 14 presents the Vp, the signal attenuation and applied load profiles obtained at site GMPFV10S04 together with estimates of GH content (site 3 in Figure 4. 1). The presence of GH can be confirmed due to simultaneous increases of in-situ acoustic parameters (Figure 4. 14) and negative thermal anomalies of the nearby core GMMB12 (Wei et al., 2015)

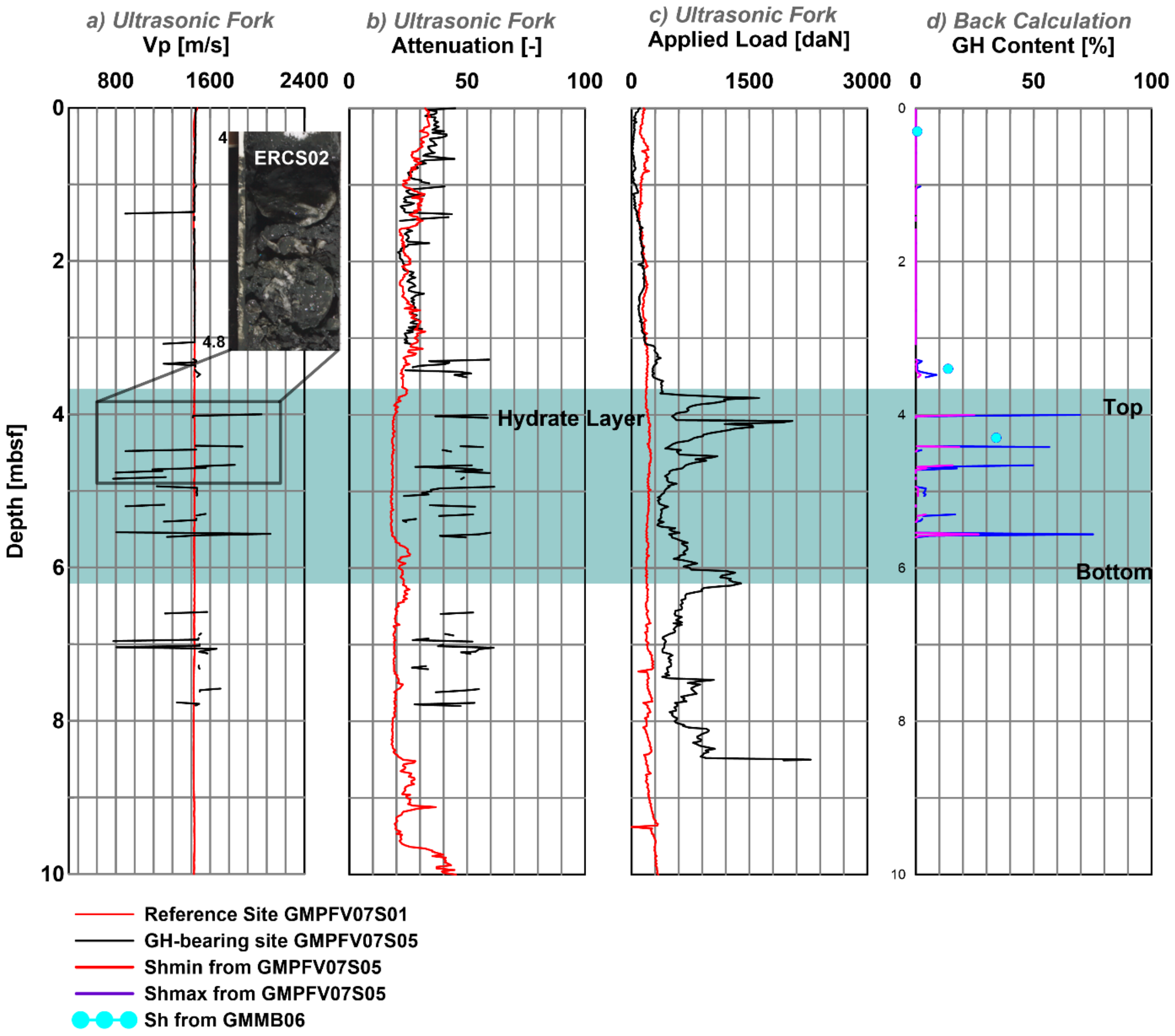

Figure 4. 13 a) P-wave velocity, b) depth-adjusted attenuation profile, c) applied load for site GMPFV07S05 (black curves) against reference site GMPFV07S01 (blue curves) and d) GH content for site GMPFV07S05

While missing data is observed in the P-wave velocity and attenuation profiles between 11 mbsf and 12 mbsf, the applied load profile suggests that GH were touched at 11 mbsf. This was confirmed by the pore-water chloride data from which GH content as high as 57.5% was estimated to occur at 11.2 mbsf. This is followed by abrupt increases of 2111.2 m/s in Vp and 60 in signal attenuation, which highlights the effect of the presence of GH within the sediment.

Maximum GH contents were found to occur at 12 mbsf with values of 20.5% for S_{hmin} and 75.6% for S_{hmax}.

Following previous work in Taleb et al. (2018), GH contents derived from the effective medium model were compared with those derived from the pore-water chloride analysis. This showed that estimates of GH contents relying on the assumption that hydrate contributes to the stiffness of the sediment by becoming part of the load-bearing framework (S_{hmin}) are closer to those obtained from the chlorinity data. Hence, in the rest of this work only S_{hmin} (referred to S_h in the following) values will be considered and discussed.

4.4.3 Correlations between estimates gas hydrates content and seismic signatures

As shown in Figure 4. 1 a number of in-situ measurements and cores can be tied to seismic profile SY03-HR-Pr01 in order to analyse the larger scale distribution and morpholgy of GH present within pockmark A and define the top and in some cases the bottom of the GHOZ.

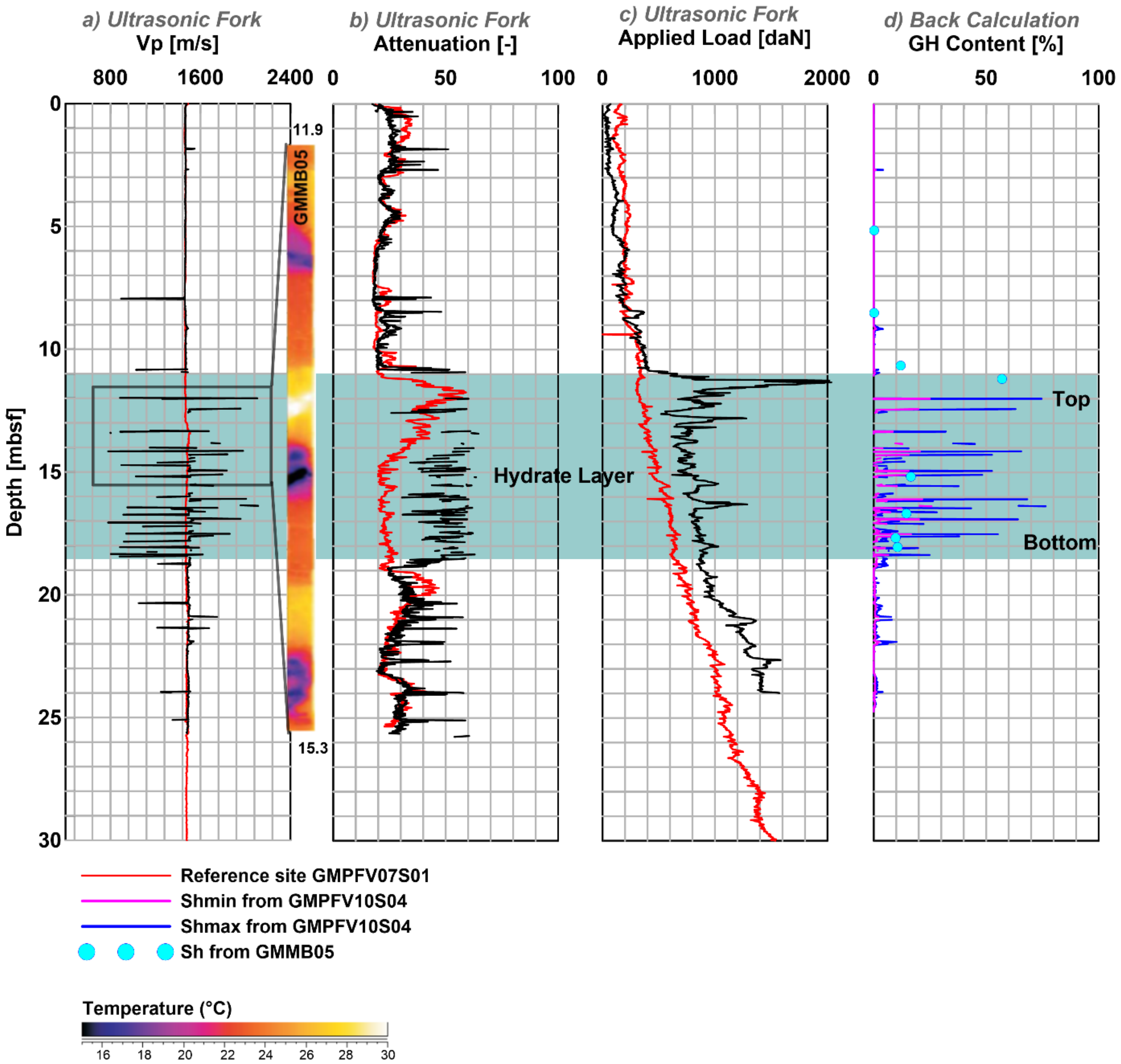

Figure 4. 14 a) P-wave velocity, b) depth-adjusted attenuation profile, c) applied load for site GMPFV010S04 (black curves) against reference site GMPFV07S01 (blue curves) and d) GH content for site GMPFV10S04

In Figure 4. 15 a significant contrast is observed between the high-amplitude chaotic facies in the central part of pockmark A and the continuous facies of low-amplitude sub parallel reflectors outside of its peripheral depression. In most zones, the top of the high-amplitudechaotic facies is observed to correlate with the top of GHOZ as infered from the analysis of in-situ and core data (yellow continuous line in Figure 4. 15). Delineating the base of GHOZ proved much more difficult since at almost all sites early refusals were met during acoustic soundings (green segments in Figure 4. 15). Early refusals suggest that the top of a second GH layer has been probably reached. The depths at which they occurred generally correlate with the presence of chaotic facies of higher energy on seismic profile SY03-HR-Pr01.These observations were found to almost correlate with the GH and free gas occurrence zones (light green zones on Figure 4. 15) proposed by Sultan et al. (2014). On both sides of the profile, disturbed zones attributed to the presence of GH were highlighted (pink zones on Figure 4. 15). They correspond to the top of a curved-shaped succession of hyperbolae interpreted as a zone of fractures/discontinuities suspected by Sultan et al. (2014).

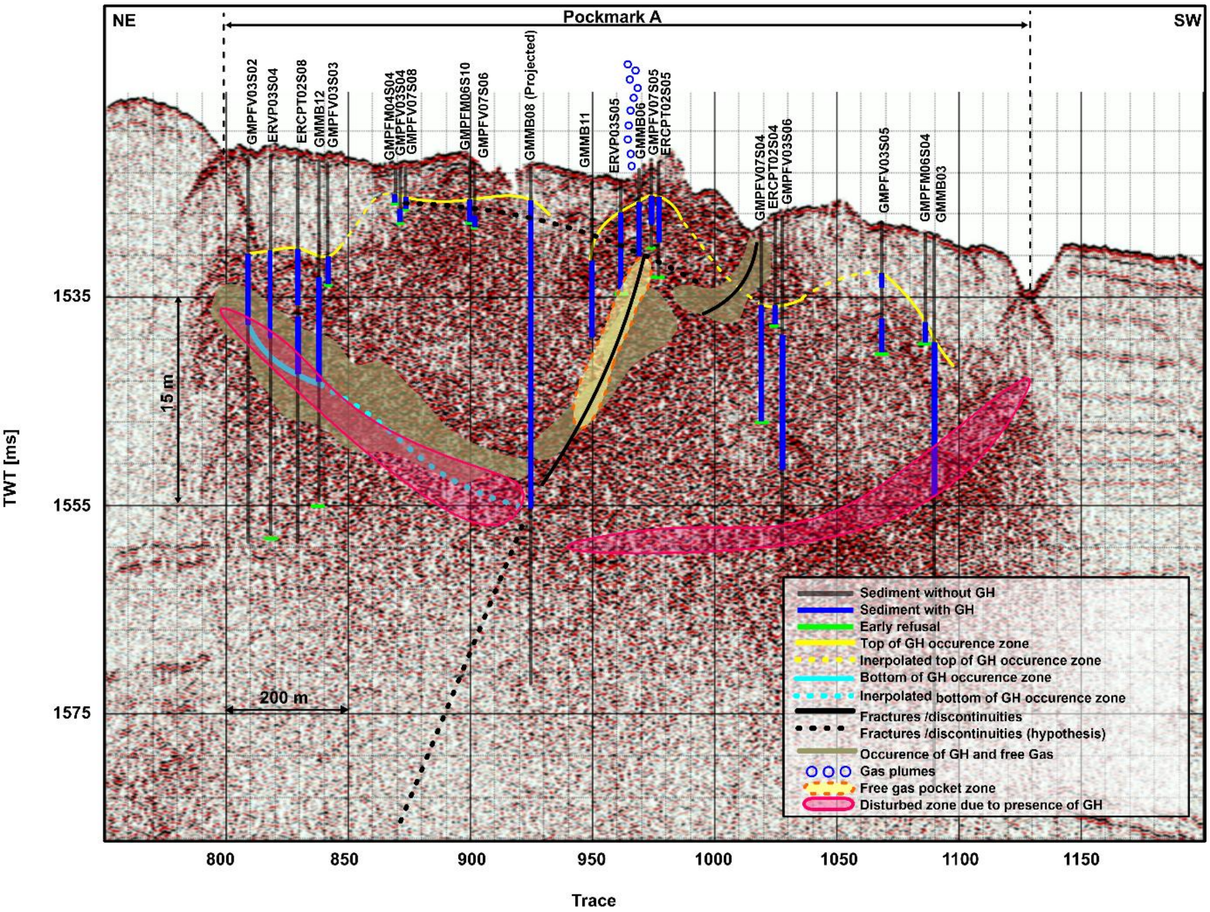

Figure 4. 15 Seismic profile SY03-HR-Pr01 showing a marked contrast between the high-amplitude chaotic facies in the central part of pockmark A and the continuous sub-parallel facies of the surrounding sediments. Blue hollow circles indicate the flow path of free gas visually observed during drilling at site GMMB06

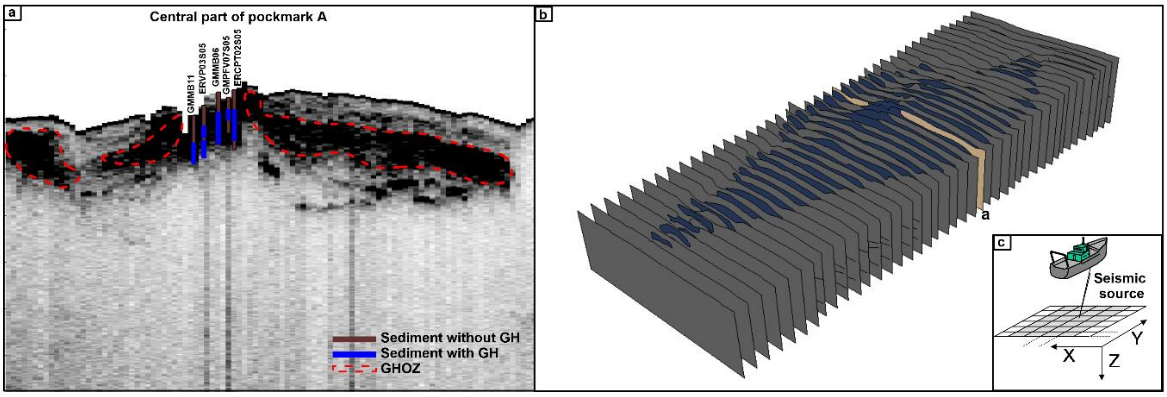

Figure 4. 16 a) Seismic profile through the central part of pockmark A showing a sharp contrast between a high-amplitude chaotic facies (black zones) and a low-amplitude to transparent facies (grey areas), b) Seismic profiles in y-axis direction interpreted in order to create a 3D seismic data cube and c) illustration showing the directions in which the seismic profiles have been made

In the central part of the NE-SW seismic profile (Figure 4. 15), it is possible to identify the presence of fractures/discontinuities (solid black lines in Figure 4. 15). These fractures are thought to be preferential paths for the free gas migration throughout the pockmark, as supported by Sultan et al. (2014). This is further confirmed by this study based on visual observation of gas plumes at the centre of the pockmark (blue bubbles on Figure 4. 15) and by the free gas pocket zone (light orange zone on Figure 4. 15), which was discovered upon drilling at core GMMB11.

Alternatively, a total of 103 sub-bottom profiles in the x-axis direction and 124 in the y-axis direction were aquired from the C&C AUV survey within pockmark A (George and Cauquil, 2007). In Figure 4. 16.a, five sites (GMMB11, ERVP0305, GMMB06, GMPFV07S05 and ERCPT02S05) were projected on a seismic profile passing through the central part of pockmark A. It can be observed that the presence of GH as infered from in-situ and laboratory measurements correlates well with the high-amplitude chaotic facies (dark zones in Figure 4. 16.a), in a way such that the surrounding low amplitude to transparent facies (grey areas on Figure 4. 16.a) is thought to be indicative of the absence of GH in sediments. All profiles were then analysed and used (Figure 4. 16.b) to create a 3D seismic data cube and identify the GHOZ throughout pockmark A.

4.5 Discussion

4.5.1 Gas hydrate detection and quantification

In this paper, GH contents have been estimated from in-situ Vp measurements as well as from pore water chloride analyses carried out on adjacent cores. The presence of GH in the marine environment significantly alters the physical properties of the host sediment by reducing the effective pore space of the sediment and increasing the P-wave velocity (Collett et al., 2014; Waite et al., 2009).

The quantification process required an accurate definition of the mineralogy profile. In some cases, the mineral proportions of sediments in question were defined using the XRD and XRF methods. However, in cases where mineralogy and density data were unknown or unavailable, due to significant disturbance of the recovered sediment, an alternative method has been followed (Figure 4. 7). This relied on the use of a petro-physical model allowing sites lacking input data to be correlated with reference sites, where background velocity profiles and mineralogy are well defined.

Velocity-derived estimates of GH were compared to those derived from pore-water chloride anomalies to evaluate the reliability of both upper and lower bound GH content. Estimates allowing a load bearing contribution of hydrate to the mineral framework (S_{hmin}) were found to match better with the results derived from the chloride concentration anomalies in pore water (Taleb et al., 2018). This is further confirmed by Ghosh et al. (2010) findings, which proved that, compared with other geophysical methods, S_{hmin} values are the closer to results from the pressure core depressurisation method. In this work, a maximum GH content of 26.5% S_{hmin} was estimated at a Vp of 2035 m/s.

The distribution of GH within the study area has been discussed by Wei et al. (2015) based on negative thermal anomalies obtained from infrared imaging results. Looking at Figure 4. 12 and Figure 4. 14, it can be seen that the GHOZ determined by Wei et al. (2015) correlates well with that derived from effective medium theory. This confirms that the presence of GH can be detected based on negative Vp anomalies.

Massive GH in the form of nodules were observed within the recovered cores between two layers of sediments. Based on laboratory analyses, one may expect the Vp to increase to values higher than 3000 m/s in the presence of such massive GH nodules (Helgerud et al., 2009). At this stage, it is important to note that the Penfeld used to perform the in-situ acoustic measurements can detect compressional wave velocities up to 2200 m/s. Therefore, this could explain the discontinuities in the Vp profiles, which could be due to the presence of massive hydrate nodules characterised by velocities higher than 3800 m/s.

4.5.2 3D model of pockmark A: seabed morphology versus hydrate/fluid distribution

Sultan et al. (2014) and Wei et al. (2015) have identified the different formation stages of the pockmarks within the study area, which is marked by a the presence of a grabben bordered by deep seated faults through which gas migrates (Marsset et al., 2018). The continuous supply of upward migrating gas will reopen sealed fractures or even create new ones (Sultan et al., 2014). This will promote GH hydrate formation that will eventually result in decreased pore space and permeability and an overpressured GH-bearing sediment; thus, causing further localised fractures/discontinuities.

In order to further investigate the effect of the presence and distribution of GH on the present geomorphology of the pockmark, AUV seismic profiles through pockmark A (George and Cauquil, 2007) were used to illustrate the detailed architecture of GHOZ inside the pockmark. This eventually allowed calculating the GHOZ volume and its occupancy ratio in pockmark A (Figure 4. 17).

In between the top and base of the GHOZ some intervals were delineated as zones where GH are absent. These so-called “GH free intervals” show three different shapes (A, B and C in Figure 4. 17). By assuming that both GHOZ and the “GH free intervals” have an ellipsoidal shape, the total volume occupied by GHBS was estimated to be on the order of $2.7 \times 10^6\ m^3$. Then, the GH volume was calculated by considering a mean hydrate fraction of 21%, which is the mean of all highest GH content at each site in pockmark A, and found equal to $0.57 \times 10^6\ m^3$. The total volume of the pockmark was estimated in order to determine the total occupancy of GH. Based on seismic data, pockmark A was assumed to extend down to 45 m below seafloor. Accordingly, GHOZ was found to occupy 17% of the total pockmark volume with a GH volume equivalent to $0.57 \times 10^6\ m^3$.

Furthermore, two sections (NE-NW and SW-SE) were extracted from the 3D bathymetry (Figure 4. 18). On both sections, seismic profiles were projected as well as GH contents from in-situ data and the GHOZ (blue zones in Figure 4. 18) as outlined in Figure 4. 17. These correlations indeed highlight the heterogeneous distribution of solid hydrate and free gas within the pockmark. Finally based on all these observations and analyses, a detailed description of the actual fluid/hydrate dynamic distribution within the pockmark can be proposed. The highest GH contents (20%-30%) are observed to be in the centre while lower contents (0%-10%) are mostly observed at the borders of the pockmark. This is in line with the actual morphology of the pockmark showing mostly bumps in the central part due to high content of GH and a slight depression on the borders where according to Sultan et al. (2010) GH might have dissolved. At this stage, it is intersting to note core GMMB08 (site11 in Figure 4. 18.a) has been projected from a distance of 86 m, which explains why it intersects GH free intervals .

It is also noteworthy that the GH and free gas occurrence zones (adapted from Sultan et al., 2014) cover all the proposed fractures/discontinuities and disturbed zones due to the presence of GH (pink zones on Figure 4. 15). Taleb et al. (2018) discussed the presence of GH having a spongy texture in the study area (light green zones in Figure 4. 18) due to free gas being trapped within the pores of GH itself. This is due to the high gas flux present in the study area, which stimulates rapid GH formation; hence, causing the coexistence of both phases. However, in other cases, GH forms on the inner walls of the fractures/discontinuities, which isolate free gas from the surrounding pore water (yellow zone in Figure 4. 18.a).

A bump can be observed at sites ERCPT02S05, GMPFV07S05 and GMMB06 (site 25, 26 and 27 in Figure 4. 18.b). This is interesting since this location accomodates shallow GH with different morphologies (Taleb et al. 2018) such as massive nodules or thin veins (direct visual observations of core ERCS02 in Figure 4. 13) as well as gas plumes at site GMMB06 (blue bubbles on Figure 4. 15). Free gas might be escaping through fractures within the sediment and contributing to further shallow GH formation. These fracture zones have preferentially near-vertical orientations (Sultan et al., 2014) and contribute to the continuous supply of free gas, which in its turn contributes to maintaining the presence of GH. Therefore, the bulge at this location might be formed to accommodate new GH formations and already existing high GH content. In other words, the shallowest GH accumulations in the pockmark are directly related to a central fracture that is supplying the water column with gas. Lateral gas migration away from the central fracture, circulating from the highest to the lowest free gas/GH contents, is thought of as the most likely factor to explain why the shallow hydrate accumulation in the central part appear to follow the same geological horizons (Figure 4. 15). All these previously described activities are possible due to the continuous high gas flux supply as it is confirmed by the gas plumes in the water column and the free gas pocket zone (yellow line in Figure 4. 18).

Thinner and deeper GH accumulations are generally observed in the peripheral depression of the pockmark (Figure 4. 15 and sites 17 and 18 in Figure 4. 18.a). This can be explained by the fact that GH in this part of the pockmark have already disappeared probably due to a dissolution process as described by Sultan et al. (2014) and lower GH content observed in Figure 4. 18. Such phenomena is not considered to be caused by dissociation because at this depth stability conditions (low temperature and high pressure) for GH formation are respected.

At this stage, a comparison between pockmarks A and other pockmarks, highlighting the similarities and differences, is interesting in order to further understand the geological features of the study area. Hovland and Svensen, (2006) and Vaular et al. (2010) have performed studies on the Nyegga pockmark in the mid-Norwegian margin, where the presence of GH has been confirmed. The authors have proposed several stages that can promote GH formation: high gas flux up to the seafloor and thermobaric conditions corresponding to the stability conditions of GH. Similarly to pockmark A, the gas flux through the seafloor of the Nyegga pockmark is heterogeneously distributed and GH forms where the flux is highest and in contact with water. After comparing pockmarks A and C with that of the Nyegga region, it can be observed that they share comparable dynamics: the morphology of the pockmark grows and collapses over time due to cycles of formation and dissociation/dissolution of GH in the shallow sub-surface sediment. On the other hand, Sahling et al. (2008) have studied three morphologically complex pockmarks (the Kouilou pockmarks) in the northern Congo Fan area, where they proved the presence of a 25-30 m thick shallow GH layer. By contrast with that of the study area, pockmarks in Kouilou did not exhibit gas venting features. This suggests that pockmarks in the Niger delta are probably more active with respect to free gas flux, compared to the Kouilou pockmarks; or that the last one is probably in an earlier phase of GH formation. Additionally, Riboulot et al. (2016) have correlated geophysical, sedimentological and geotechnical data in order to obtain insight into the inner architecture of the pockmark. The study showed that the pathway through which the free gas is migrating and feeding the GHOZ is located beneath the central part of the studied pockmark. This is in line with this work, since the highest GH contents were identified in the central part of pockmark A (at sites 14, 15 and 16 in Figure 4. 18.a and sites 25, 26 and 27 in Figure 4. 18.b). Furthermore, the GHOZ (Figure 4. 17) represents the same geometric features as the 3D bathymetry of pockmark A showing the influence of GH presence on the formation of the pockmark. All these findings confirm that GH content and distribution play an important role in the shaping and forming of their host pockmark.

Therefore, complex seafloor morphologies, such as pockmarks, can be an indicator of the presence of GH (Riboulot et al., 2016) and must be considered as a potential source of geohazard particularly for industrial seabed developments (i.e. offshore operations, pipeline installations and well drilling). The correlations between in-situ acoustic and geotechnical measurements with the seismic data have indeed allowed understanding the link between the morphology of pockmark A and that of GH. This approach can be applied to other similar pockmarks, such as the Barents Sea pockmarks (Chand et al., 2009) or in the Norwegian Sea (Hovland and Svensen, 2006), in order to define the sub-seabed distribution of GH within these pockmarks as well as different formation stages of the geological features of the study area.

For future works, it would be interesting to compare the different shapes of the GHOZ seen in Figure 4. 17 to the lithology of the surrounding sediment, which probably constitutes of alternative layers of clay and foraminifera rich muds (i.e. permeable layers). Indeed, the sediment's composition could play an essential role in the distribution of GH.

4.6 Conclusion

This paper aims to study the effect of GH content, distribution and morphology on the geomorphology and the actual state of the pockmarks present in the study area. This work mainly focused on pockmarks A and C in the Gulf of Guinea, where in-situ acoustic, coring and drilling data as well as seismic sections were acquired from different oceanographic campaigns. GH contents in the marine sediment were estimated using the effective medium model developed, which requires an accurate definition of the mineralogy profile. In cases, were the recovered cores were undisturbed, the mineral proportions were defined using the XRD and XRF techniques. In cases where the recovered cores were significantly disturbed due to GH dissociation, a petro-physical model based on the acoustic data of the site in question was developed and allowed determining the mineral proportions. The correlations and analysis of this unique database has led to the following conclusions:

- Positive Vp anomalies along with simultaneous increase of the attenuation and applied load profiles are an indicator of the presence of GH.
- A maximum GH content of 26.5% was estimated at a Vp of 2035 m/s using the effective medium model.
- Results derived from the effective medium theory and those from negative thermal and chloride anomalies were found to yield almost the same GHOZ.
- Correlations between seismic profiles and in-situ data as well as visual observations of recovered cores have shown that:
  - High amplitude chaotic facies are an indicator of the presence of GH. However, low-amplitude subparallel facies represent undisturbed sediments.
  - The study area accommodates zones where solid GH and free gas coexist as well as zones of free gas pockets.
  - Fractures/discontinuities have been identified as preferential pathways in which free gas can migrate and contribute to further GH formations.
- Extrapolation of in-situ and core measurements using seismic data indicate that with a volume of $2.7 \times 10^6\ m^3$the GHOZ occupies 17% of the total volume of pockmark A for an estimated GH volume of $0.57 \times 10^6\ m^3$.
- The seabed morphology of pockmark A is directly influenced by the distribution of underlying GH accumulations:
  - The highest GH contents (20%-30%) are observed to be in the central part of the pockmark, which is characterised by several bumps.
  - The lowest GH contents (0%-10%) are mostly observed at the borders of the pockmarkwhich are characterised by a slight depression.

The morphology of a given pockmark in the study area might be an indication that can be used to confirm the presence of GH, determine an interval of GH content and identify different GH morphologies.

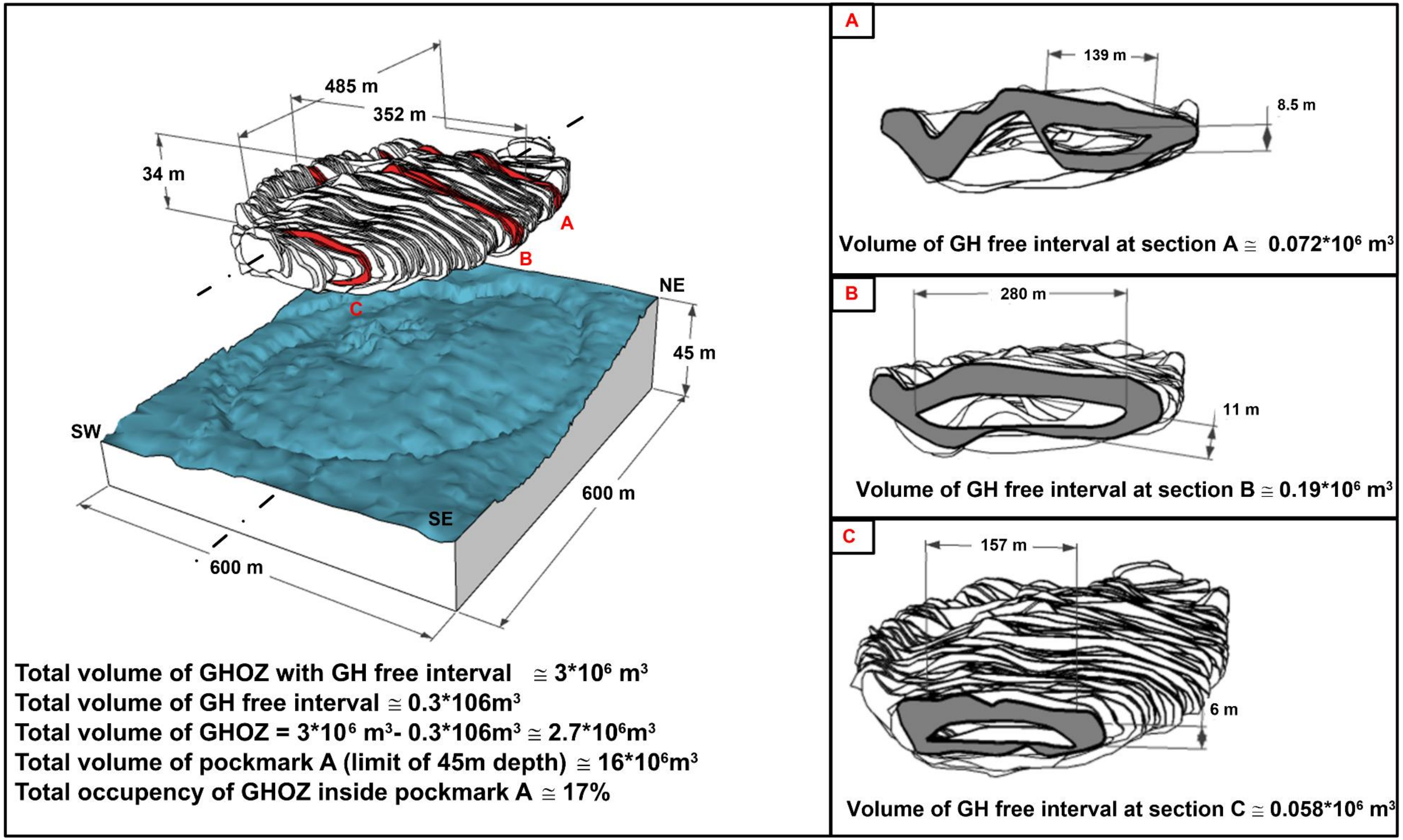

Figure 4. 17 Left: 3D bathymetry of pockmark A compared with the GHOZ as mapped from seismic data. Right: illustration of the three distinct morphologies (A, B and C) of the GHOZ as mapped from seismic data

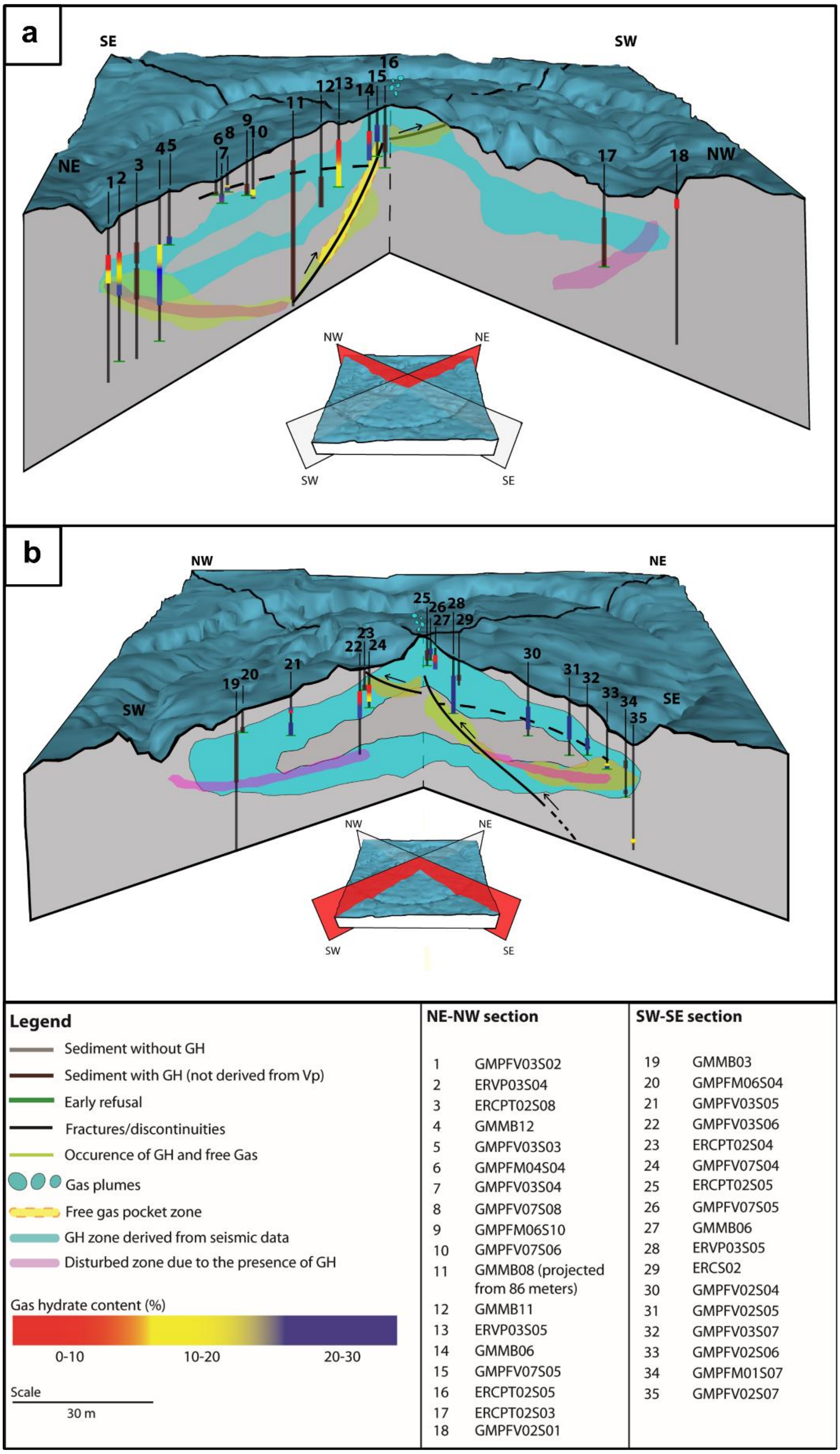

Figure 4. 18 a) Perpendicular cross section across the northern part of pockmark A and b) perpendicular cross section across the southern part of pockmark. On each cross section GH contents as estimated from in-situ measurements as well as the GHOZ and fractures/discontinuities as inferred from seismic data are projected

Chapter 5. Hydro-mechanical properties of gas hydrate-bearing fine sediments from in-situ testing

Chapitre 5. Propriétés hydromécaniques des sédiments argileux contenant des hydrates de gaz à partir de mesures in-situ

Reference: Taleb, F. et al. 2018. Hydromechanical properties of gas hydrate-bearing fine sediments from in-situ testing. Journal Of Geophysical Research - solid Earth, 123(11), 9615-9634

Hydrate recovered from site GMGC12 during Guineco MeBo campaign (2011)

Abstract

The hydro-mechanical properties of gas hydrate-bearing sediment are key in assessing offshore geo-hazards and the resource potential of gas hydrates. For sandy materials, such properties were proved highly dependent on hydrate content (S_h) as well as on their distribution and morphology. Owing to difficulties in testing gas hydrate-bearing clayey sediments (GHBC), the impact of hydrates on the behaviour of such materials remains poorly understood. Hence, to provide insight into the characterisation of GHBC, this study relies on a unique database of in-situ acoustic, piezocone and pore-pressure dissipation measurements collected in a high gas flux system offshore Nigeria. Compressional wave velocity measurements were used as means of both detecting and quantifying gas hydrate in marine sediments. The analysis of piezocone data in normalised soil classification charts suggested that, contrary to hydrate-bearing sands, the behaviour of gas hydrate-bearing clays tends to be contractive during shearing. Correlations of acoustic and geotechnical data have shown that the stiffness and strength tend to increase with increasing S_h. However, several sediment intervals sharing the same S_h have revealed different features of mechanical behaviour; suggesting that stiffness and strength of gas hydrate-bearing clays are influenced by the distribution/morphology of gas hydrate. Pore pressure dissipation data confirmed the contractive behaviour of gas hydrate-bearing clays and showed that at low hydrate content, the hydraulic diffusivity (C_h) decreases when S_h increases. However, for S_h exceeding 20%, it was shown that an increase of C_h with S_h could be linked to the presence of fractures in the hydrate-sediment system.

Résumé

Les propriétés hydromécaniques des sédiments contenant des hydrates de gaz sont des éléments clés pour l'évaluation des aléas géotechniques et l'exploitation des ressources énergétiques potentielles associées. Pour les sédiment sableux, il a été prouvé que ces propriétés sont dépendantes du contenu en hydrate (S_h) tout comme leur distribution et leur morphologies. En raison de difficultés rencontrées pour former des hydrates dans des sédiments argileux en laboratoire (GHBC), leur impact mécanique reste encore très peu connu. Ainsi, pour tenter d'approfondir la caractérisation hydromécanique des GHBC, cette étude s'appuie sur une base de données comportant des mesures acoustiques et au piézocône in-situ ainsi que des mesures de dissipation de la pression interstitielle recueillies au large du Nigéria dans un environnement caractérisé par un flux de gaz élevé. Les mesures des vitesses des ondes de compression ont été utilisées comme un moyen de détection et de quantification des hydrates de gaz dans les sédiments marins. L'analyse des données du piézocône à l'aide des diagrammes normalisés de classification des sols a suggéré que, contrairement aux sables contenant des hydrates, le comportement des GHBC est contractant lors du cisaillement. Les corrélations des données acoustiques et géotechniques ont montré que la rigidité et la résistance au cisaillement ont tendance à augmenter avec S_h. Cependant, plusieurs intervalles de sédiment avec le même S_h ont révélé des comportements mécaniques différents suggérant que la distribution et la morphologie des hydrate de gaz impactent aussi la rigidité et la résistance au cisaillement des GHBC. Les données de dissipation de pressions interstitielles ont confirmé le comportement contractant lors du cisaillement des GHBC et ont montré qu'à faible teneur en hydrates, la diffusivité hydraulique C_h diminue lorsque S_h augmente. Cependant, pour un S_h dépassant les 20%, il a été montré qu'une augmentation de C_h avec S_h pourrait être liée à la présence de fractures dans le système hydrate-sédiment

5.1 Introduction

Over the last decades, increasing world's energy demand amidst of climate change concerns have encouraged the search for alternative and cleaner energy resources. Gas hydrate (GH) are considered as the largest untapped stock of natural gas in the world (Boswell and Collett, 2011) and are characterised by their widespread occurrence mainly in permafrost regions and continental margins (Kvenvolden, 1993). Due to the estimated staggering amounts of GH and their potential as a future energy resource but furthermore as a geotechnical hazard for various offshore operations and hydrocarbon recovery projects (Kayen and Lee, 1991) and their possible contribution to current and future climate change scenarios (Yun et al., 2007), GH have stimulated international academic and industrial interest.

The formation of GH within the sediment significantly alters the physical and mechanical properties of their host sediment. Such properties are also proved dependent on the hydrate content within the sediment as well as on their morphology/distribution (Dai et al., 2012). Thus, the quantification and characterisation of GH within the marine environment have become significantly important in order to either contain their potential geotechnical threat or understand their effect on the hydro-mechanical properties of the host sediment under stability conditions (Ning et al., 2012). GH can occur in a variety of sediments such as fine-grained clays and coarse-grained sands. Due to their high permeability and high GH content, coarse-grained sediments are often preferred for potential exploitation activities. However, fine-grained sediments contain over 90% of global GH accumulations (Boswell and Collett, 2006), yet not much research have been carried out concerning the hydro-mechanical behaviour of such sediments. The formation of GH within the sediment is mainly governed by the changing physical properties of the latter such as grain size, porosity and permeability (Waite et al., 2009). This directly affects the morphology of the hydrate within the host sediment. Sands and coarse silts are characterised by disseminated pore filling hydrate (Waite et al., 2009). The grain displacing morphology is mostly observed in clay-rich sediments where GH form in fractures due to capillary tension forces (Jang and Santamarina, 2016). In this case, they force the clay aggregates to move apart and hence introduce veins or cracks within the sediment. However, Ghosh et al. (2010) suggested that in clayey sediments, GH could be present as pore-filling, grain displacing or a combination of both morphologies. This imposes a complexity when it comes to GH quantification in such sediments, since it requires knowledge of the orientation of the GH-bearing discontinuities.

The metastable nature of GH and the challenges they present in terms of identifying their presence via the recovery of natural samples have largely increased the reliance on pressure coring to prevent sediment disturbance (Santamarina at al., 2012). However, as presented by Sultan et al. (2007, 2010 and 2014) in-situ testing may be a promising alternative to costly pressure coring and testing operations. As reported in much literature, in-situ testing is an efficient and cost effective technique of collecting large amounts of data mainly in materials that are difficult to sample (Lunne et al., 1997; Robertson 2009). This is particularly efficient in the case of GH-bearing fine-grained sediments, which remain challenging to preserve or synthesise prior to laboratory testing. Hence, to provide insight into the characterisation of these geo-materials, this study relies on in-situ acoustic, piezocone and pore-pressure dissipation measurements in the Gulf of Guinea. Numerous oceanographic campaigns have been carried out along the West African margin due to the ongoing development of oil and gas projects.

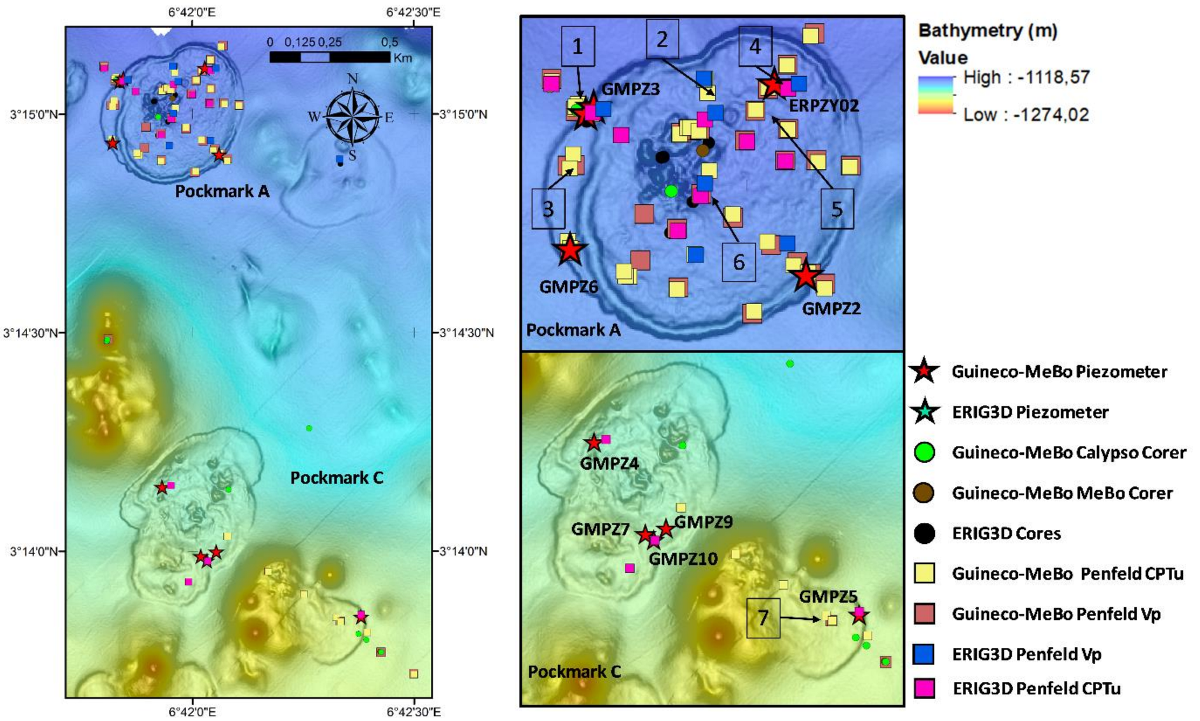

Figure 5. 1 Bathymetry of the study area showing the investigated sites: 1: GMPFV02S02, GMPFM06S01, GMPZ3, GMMB01 and GMCS05, 2: ERVP03S01 and GMPFM12S03, 3: GMPFV02S03 and GMPFM01S03, 4: GMPFV03S03, ERCPT02S08, ERPZY02 and GMMB12, 5: GMPFV03S04 and GMPFM04S04, 6: GMPFV07S05, ERCPT02S05 and GMMB06 and 7: GMPFV10S04, GMPFM05S03 and GMMB05

Table 5. 1 Investigated sites within the study area: site 1 cluster was used to characterise sediment from the reference site without GH while sites 2, 3,4,5,6 and 7 clusters represent areas where the presence of GH was suspected or proved

Investigated Sites	Depth (m)	Length (m)	Nearby CPTu	Nearby Piezocone	Nearby Calypso or MeBo core	Site
GMPFV02S02	1140	30	GMPFM06S01	GMPZ3	GMCS05	1
ERVP03S01	1140	30	GMPFM12S03	-	-	2
GMPFV02S03	1144	30	GMPFM01S03	-	-	3
GMPFV03S03	1142	10.3	ERCPT02S08	ERPZY02	GMMB12	4
GMPFV03S04	1140	5.7	GMPFM04S04	-	-	5
GMPFV07S05	1146	8.5	ERCPT02S05	-	GMMB06	6
GMPFV10S04	1195	26	GMPFM05S03	-	GMMB05	7

The Gulf of Guinea is one area where the presence of dense accumulations of shallow GH have been reported by several authors (Cunningham and Lindholm 2000; Hovland et al. 1997; Sultan et al., 2010; Wei et al., 2015). Visual observations within the study area have revealed the presence of different GH morphologies varying from groups of thin veins to massive nodules in clay sediments (Sultan et al. 2007, 2010). In certain cases, solid GH and free gas were observed to coexist due to the presence of free gas voids within hydrate nodules; hence, resulting in a material with a spongy texture (Sultan et al., 2014).

The present chapter aims to understand the effect of the concentration and distribution/morphology of GH on the hydro-mechanical properties of their host clayey sediment. This relies on the quantification and characterisation of GH using different in-situ acoustic and geotechnical methods. The investigation was carried out by correlating these parameters and comparing sites without GH with GH-bearing sites. Different soil classification charts were used to illustrate the behaviour of hydrate-bearing clays. Finally, different hydro-mechanical parameters of GH bearing fine-grained sediments were derived using empirical relations.

5.2 Study area and acquired data

The study area is located in the deep water Niger Delta at a water depth ranging from 1100m to 1250m. Numerous studies (Sultan et al., 2010, 2014) have shown that this area is characterised by several quasi-circular pockmarks (Figure 5. 1) that are ten to a few hundred meters wide. The evolution and morphologies of these pockmarks have been directly linked to different habits of formation, nucleation and dissolution of GH (Sultan et al., 2014). Wei et al., (2015) have investigated the distribution of GH in the sediment of the study area by applying infrared thermal imaging and pore water chloride analyses on MeBo cores, which allowed defining hydrate occurrence zones. These zones were shown to accommodate shallow GH accumulations (Sultan et al., 2007) as well as the coexistence of free gas and solid GH. Based on the latter findings and on seismic data showing evidence of faulting (Sultan et al., 2016), the investigated area has been identified as a high gas flux system.

The data used in this chapter were acquired during the Guineco-MeBo (2011) and ERIG3D (2008) oceanographic campaigns on the French R/V *'Pourquoi pas?'*. Both campaigns aimed to determine the distribution of GH from geophysical, geotechnical and geochemical data. Different laboratory and in-situ measurements were carried out to assess the physico-chemical properties of the sediment at a number of sites outside and within pockmarks as shown in Figure 5. 1 and Table 5. 1.

In this chapter:

- Seven Penfeld Vp (1: GMPFV02S02, 2: ERVP03S01, 3: GMPFV02S03, 4: GMPFV03S03, 5: GMPFV03S04, 6: GMPFV07S05 and 7: GMPfV10S04) and seven Penfeld CPTu (1: GMPFM06S01, 2: GMPFM12S03, 3: GMPFM01S03, 4: ERCPT02S08, 5: GMPFM04S04, 6: ERCPT02S05 and 7: GMPFM05S03) were investigated
- Ten piezometer sites will be investigated (GMPZ2, 3, 4, 5, 6, 7 and 10 and ERPZY02), with only two next to a Penfeld Vp site (1: GMPZ3 and 4: ERPZY02)
- One Calypso core (1: GMCS05) and four MeBo cores (1: GMMB01, 4: GMMB12, 6: GMMB06 and 7: GMMB05) have allowed the investigation of the study area

More details about the used tools and methods are shown in chapter 3.

5.3 Results

5.3.1 Characterisation of sediment without gas hydrate – reference site

Sites GMPFV02S02 and GMPFM06S01 (site 1 in Figure 5. 1) were considered as Penfeld Vp and CPTu reference sites respectively, since they are located outside of the pockmarks. Reference sites are characterised by compressional wave velocities varying between 1450 m/s and 1510 m/s. However at site GMPFV02S02, velocity and attenuation peaks of 2015 m/s and 59 respectively can be identified at 13.6 mbsf (Figure 5. 2.a and b). Additionally, while the quartz fraction profile is nearly constant along the core, the calcite and clay fractions vary from 0.5 to 0.9 and from 0.01 to 0.42 respectively (Figure 5. 2.c). It is noteworthy that there is great resemblance between the calcite, Vp and signal attenuation profiles. Therefore, Vp peaks were linked to the presence of calcium carbonate (mainly foraminifera) within the sediment. This is further confirmed by visual observations of core GMCS05, which do not reveal any fractures or cracks as would be expected if GH were present at this site.

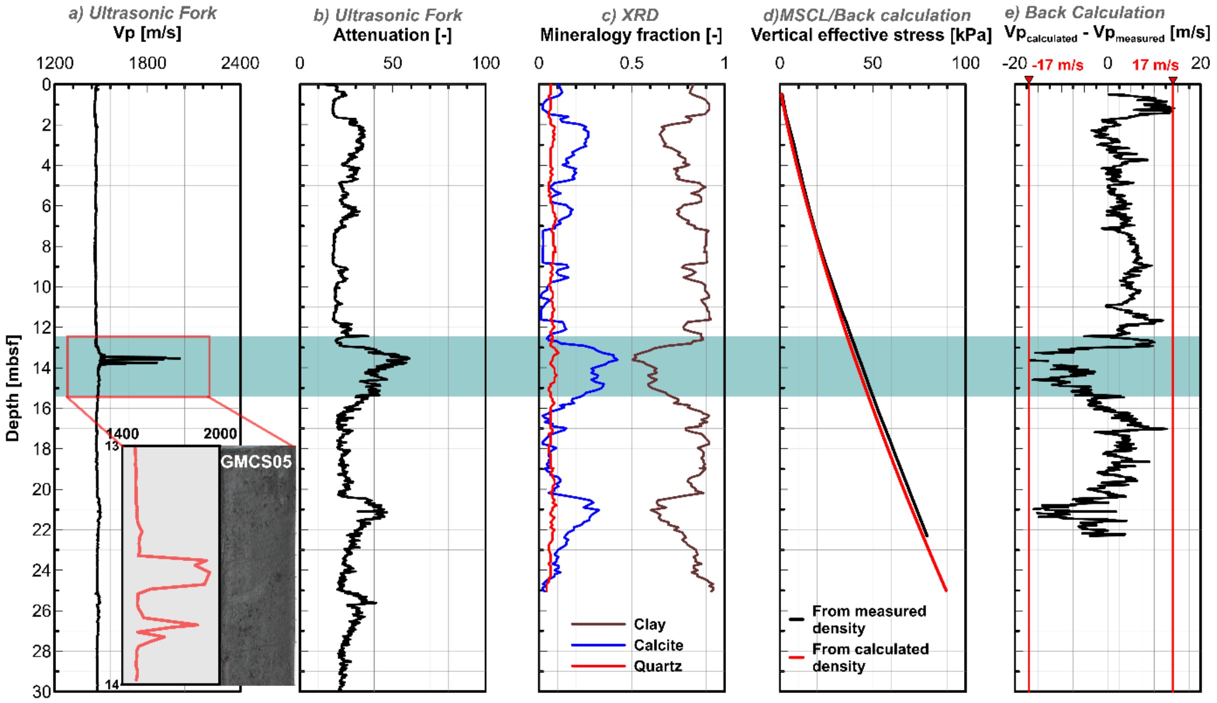

Figure 5. 2a) P-wave velocity and b) signal attenuation for site GMPFV02S02, c) Mineral fraction and d) vertical effective stress derived from MSCL density data (core GMCS05) and model calculation e) difference between calculated velocity and measured velocity

The calculated vertical effective stress (σ'_{v0}) profile (Figure 5. 2.d) was determined with the model presented in chapter 3.3.3.2 assuming hydrostatic pressure and based on laboratory pre-defined compressibility and void ratio data. It can be observed that the measured σ'_{v0} and the calculated σ'_{v0} profiles yield almost the same results, confirming the reliability of the used model. Figure 5. 2.e shows that the difference between the velocity calculated by the model and the measured velocity tend to oscillate in the range $\pm 17\ m/s$. This served to set the detection threshold of GH in sediments. That is to say that, in this study, estimates of GH contents are only provided when the difference between the calculated Vp and measured Vp is greater than 17m/s.

As shown in Figure 5. 3, piezocone data for reference site GMPFM06S01 (site 1 in Figure 5. 1) are characterised by a linear increase with depth of the corrected cone tip resistance (q_t), sleeve friction (f_s) and pore water pressure (Δu_2) up to 1000 kPa, 12 kPa and 320 kPa respectively at 30 mbsf.

By adopting the P-wave velocity inter-comparison method and considering sites GMPFV02S02 and GMPFM06S01 as a reference, the distinct features between GH-bearing sediment (GHBS) and sediments without hydrate were identified and discussed.

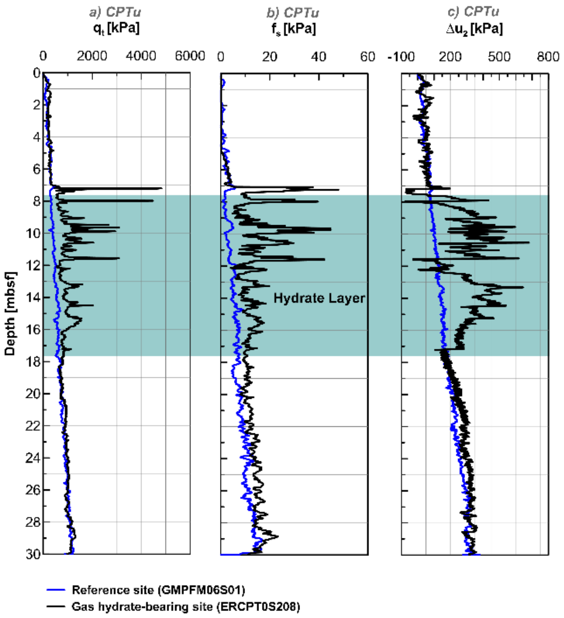

Figure 5. 3 GH-bearing site ERCPT02S08 (site 4 in Figure 5. 1): a) corrected cone tip resistance, b) sleeve friction and c) pore-water pressure. The light blue rectangle shows the GH occurrence zone identified by Wei et al., 2015 from chloride anomalies and Infrared Images

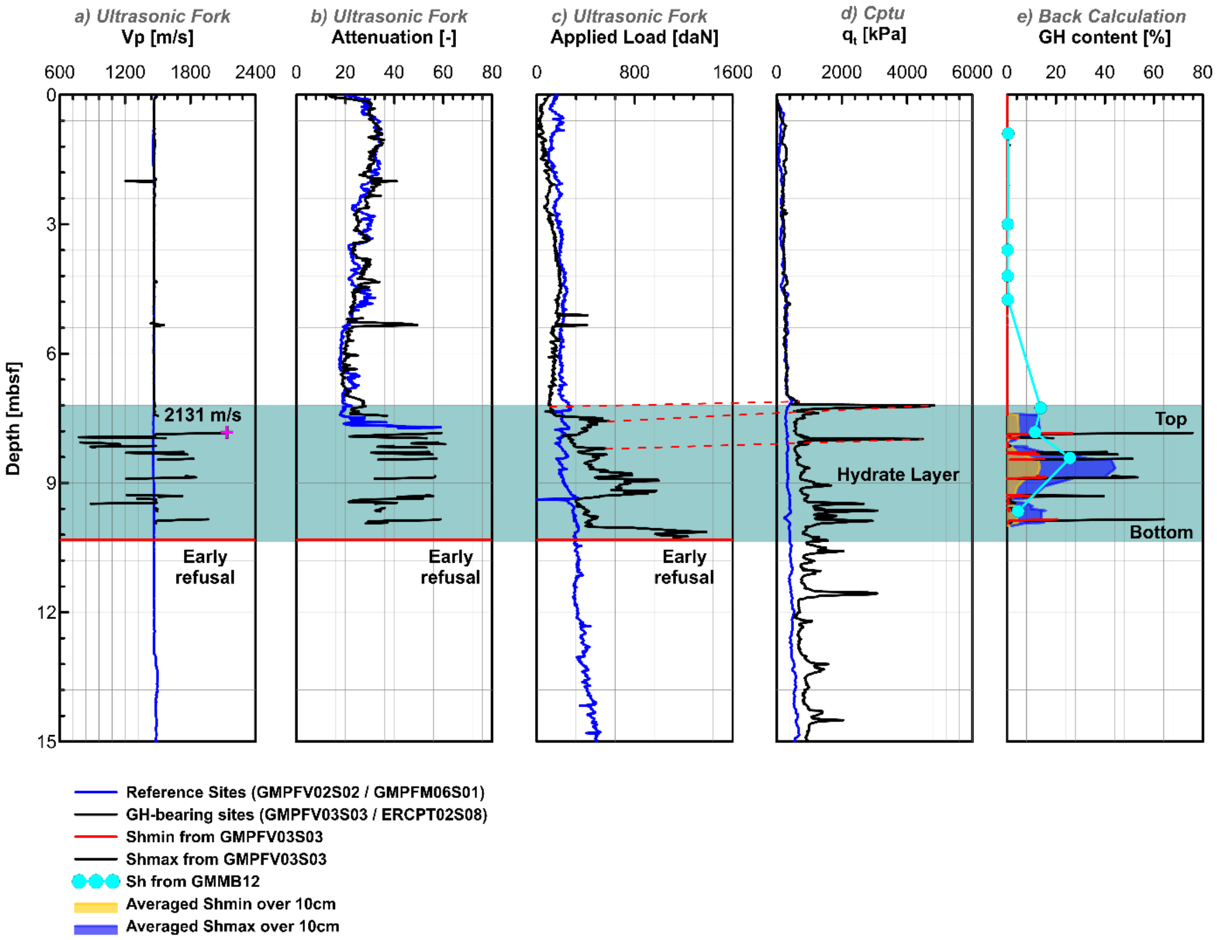

Figure 5. 4 a) P-wave velocity, b) signal attenuation, c) applied load for GH-bearing site GMPFV03S03, d) corrected cone tip resistance for GH-bearing site ERCPT02S08 and e) back calculation of GH content

5.3.2 Gas hydrate characterisation and quantification

Figure 5. 3 presents the corrected cone tip resistance (q_t), the sleeve friction (f_s) and the pore water pressure (Δu_2) from the Penfeld CPTu for site ERCPT02S08 (site 4 in Figure 5. 1). At 7.23 mbsf q_t was found to be almost 10 times higher than that of the reference site GMPFM06S01 at the same depth. Wei et al. (2015) identified the top of the GH occurrence zone atalmost the same depth (see light blue rectangle in Figure 5. 3).

The simultaneous and strong increase in these parameters $(q_t, f_s \text{ and } \Delta u_2)$confirms the presence of GH within the marine sediment. Additionally the q_t profile suggests the presence of two distinct GH layers: (1) from 7 mbsf to 11.5 mbsf with $q_t$ranging between 3153 kPa and 4913 kPa and (2) from 12.5 mbsf to 17.5 mbsf with q_t ranging between 1062 kPa and 2004 kPa. It is also noteworthy that at depths 7.23 mbsf and 8 mbsf, high f_s and q_t values correlate with negative Δu_2 values.

GH were quantified at all sites where Vp data were available and after definition of the mineralogy profile of the sediment in question. Hydrate quantification results obtained from the numerical model using the effective medium theory were compared with those obtained from chloride anomalies.

Figure 5. 4 presents the P-wave velocity (V_p), the signal attenuation and the applied load profiles obtained from the Penfeld Vp and the back calculation for GH content for the GMPFV03S03 (site 4 in Figure 5. 1) and the corrected cone tip resistance (q_t) obtained from Penfeld CPTu for the ERCPT02S08 (site 4 on Figure 5. 1). Strong and positive variations of these parameters along the depth confirm the presence of GH. However, negative anomalies in the Vp profile is an indicator for the presence of free gas within the sediment.

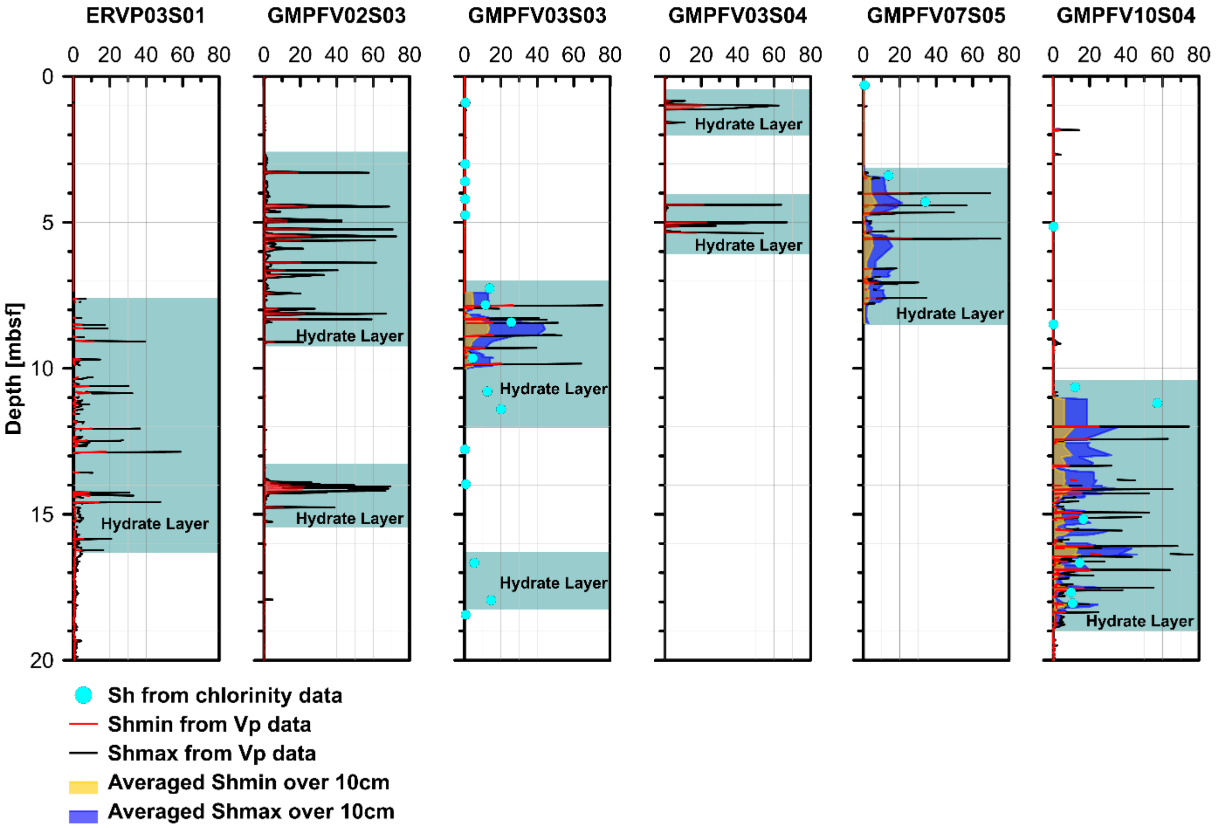

Figure 5. 5 Estimates of GH content for all the six investigated sites: ERVP03S01 (site 2 in Figure 5. 1), GMPFV02S03 (site 3 Figure 5. 1), GMPFV03S03 (site 4 in Figure 5. 1), GMPFV03S04 (site 4 in Figure 5. 1), GMPFV07S05 (site 6 in Figure 5. 1) and GMPFV10S04 (site 7 in Figure 5. 1)

Therefore, it is possible to define areas where free gas and solid GH layers form alternatively or even coexist.

While missing data is observed in the P-wave velocity and attenuation profiles between 7.45 mbsf and 7.84 mbsf for the GMPFV03S03, the applied load profile suggests that GH were reached at 7.45 mbsf (Figure 5. 4). This was confirmed by the pore-water chloride data that shows that the GH content reaches 14% at around 7.26 mbsf. This is followed by sudden increases of 2131 m/s in Vp and 60 in the signal attenuation at 7.85 mbsf, which highlights the effect of the presence of GH within the marine sediment.

Using the effective medium theory, the GH content in the sediment was estimated and then averaged over 10 cm, allowing the comparison with estimates of GH content derived from chloride anomalies. Maximum GH content were estimated to occur at 7.85 mbsf: 27% for S_{hmin}, 76% for S_{hmax}, 6% for averaged S_{hmin} and 14.5% for averaged S_{hmax}. At this same depth, a GH content of 11.5% was estimated by the pore-water chloride data, which almost equals the average value of averaged S_{hmin} and averaged S_{hmax}. Based on Vp anomalies, the top of the GH occurrence zone was assumed to start at 7.85 mbsf.

Quantification results derived from the effective medium theory and from the pore-water chloride analysis for all investigated sites are presented in Figure 5. 5. GH clearly exhibit a heterogeneous vertical distribution within the GH occurrence zones without showing any systematic pattern. By comparing both GH quantification methods for sites GMPFV03S03 (site 4 in Figure 5. 1) and GMPFV10S04 (site 7 in Figure 5. 1), it can be observed that averaged S_{hmax} and S_{hmin} values oscillate around values of S_h derived from the chlorinity data.

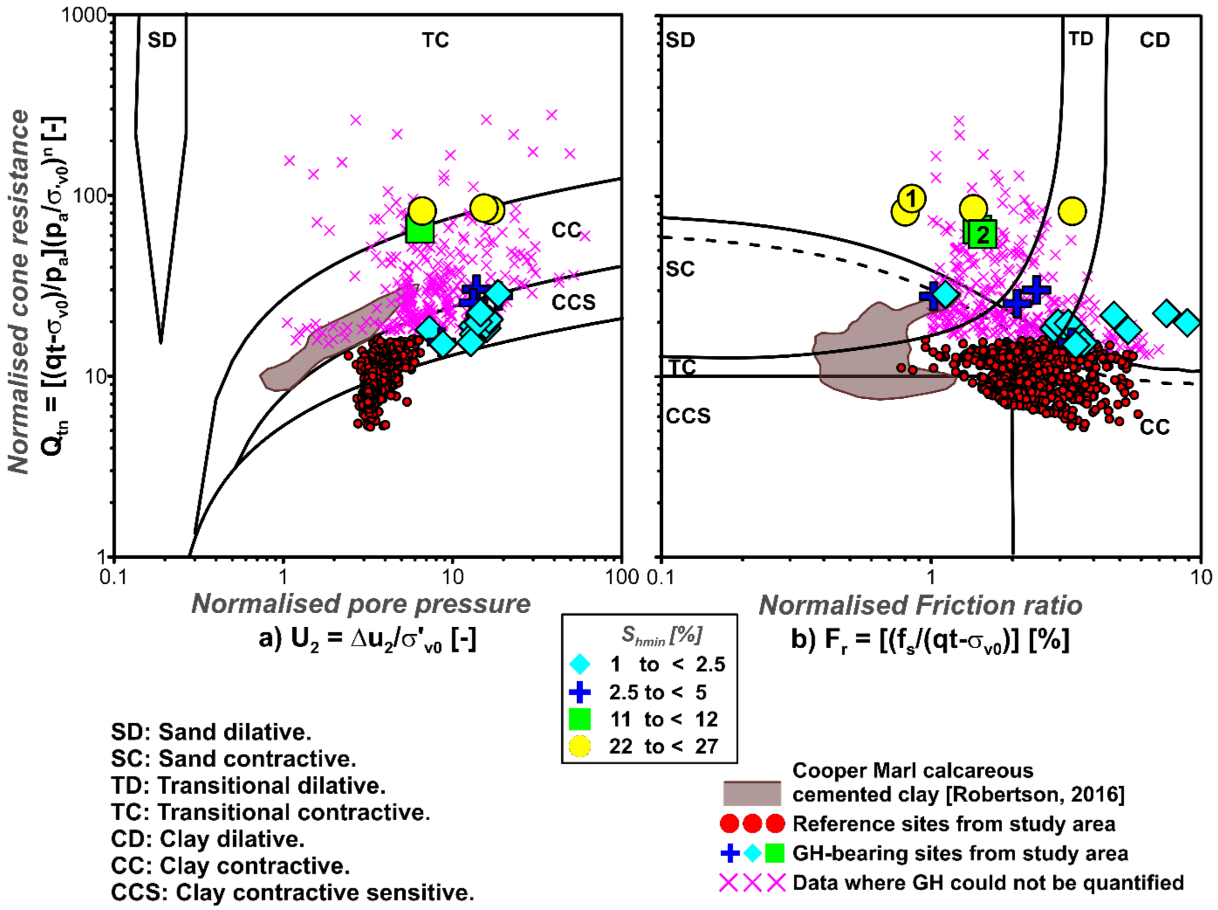

Figure 5. 6 Piezocone data from reference sites (without GH), GH-bearing sites and calcareous cemented clay (after Robertson, 2016) plotted in: a) $Q_{tn} - U_2$ chart and b) $Q_{tn} - Fr$ chart (Robertson, 2016). Data from GH-bearing sites are represented by pink crosses where the GH content could not have been estimated and by different symbols and colours referring to estimates of GH content (i.e. S_{hmin}, see legend)

On the other hand, for site GMPFV07S05 S_{hmax} values are closer to those derived from chlorinity data compared to S_{hmin} values. By contrast, non-averaged values of S_{hmax} are much higher than those estimated from chlorinity data. Additionally, studies performed by Ghosh et al. (2010), showed that for GH-bearing clayey sediments S_{hmin} yields estimates closer to that obtained from the pressure core depressurisation method compared to S_{hmax}. Hence, in the next chapters only S_{hmin} (called in the following s_h) values will be considered and discussed.

5.3.3 Soil behaviour classification charts using CPTu and Vp data

To further highlight features of GHBS, normalised CPTu data were plotted in Robertson (2016) updated classification charts. Figure 5. 6 shows the data from GH-bearing sites (GMPFM12S03, GPFM04S04, GMPFM01S03, GMPFM05S03, ERCPT02S05 and ERCPT02S08) plotted as symbols whose shape represent GH content (S_h %) within the sediment. The diagrams charts also show the piezocone data where the GH content could not have been estimated. This is mainly due to missing Vp data (values higher than 2200 m/s), which is a key parameter in the effective medium model. Correlations between in-situ acoustic and geotechnical measurements were necessary in order to highlight the mechanical behaviour of GH-bearing clayey sediment. This step was achieved by first identifying peaks and common patterns on the applied load and q_t profiles as it was thought to have the most physical meaning. As illustrated in Figure 5. 4, correlations were made by relating depths of significant peaks in both profiles.

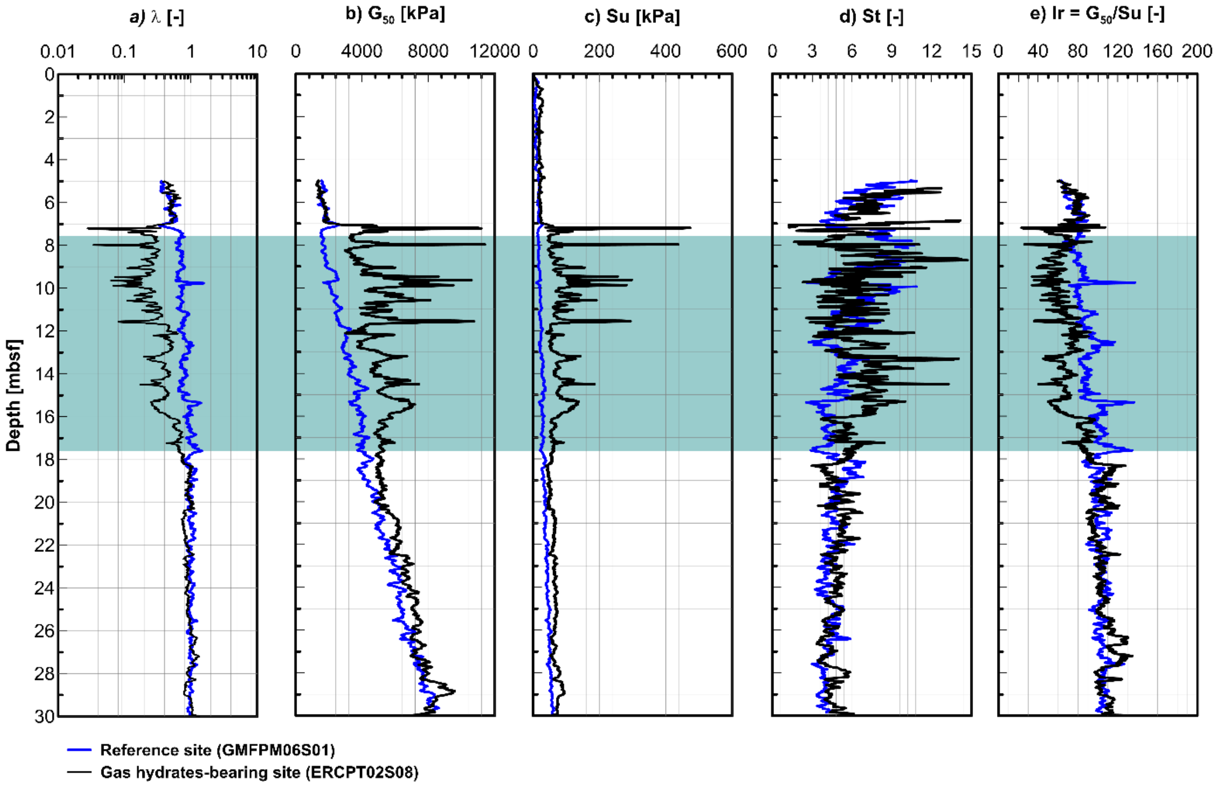

Figure 5. 7 Depth profiles of geotechnical properties derived from piezocone data from the reference site GMPFM06-01 (blue), and the GH-bearing site ERCPT02-08 (black): a. Compression index, λ; Shear modulus at 50% mobilized strength, G_{50}, Undrained shear strength, Su; Sensitivity, St; Rigidity Index, I_r. The light blue rectangle shows the GH occurrence zone identified by Wei et al., (2015) from chloride anomalies and Infrared Images

This method was adopted for all other investigated sites. Due to difficulties in constantly correlating peaks, only 25 data points were considered in this section as unambiguous.

Based on the $Q_{tn} - \mathrm{U}_2$ chart, sediment from reference sites exhibits U_2 values varying between 3 and 5.5 and Q_{tn} values not exceeding 16. Sediment containing GH is characterised by large Q_{tn} values up to 84 and correlating with U_2 values varying between 6 and 25. Most of the data from these sites plot in the contractive zone of the chart with 82% of the data in the clay contractive sensitive (CCS) region and 18% in the clay contractive (CC) region. Points having the highest GH content plot at the limit of the clay contractive (CC) region and tend towards a transitional contractive (TC) behaviour. However, points where GH could not be quantified show a more pronounced trend towards a transitional contractive (TC) behaviour with high Q_{tn} and U_2 values up to 280 and 70 respectively.

No points were detected in the sand dilative (SD) region where the pore pressure remains zero during the piezocone penetration and corresponds to the drained region on the original classification chart presented by Schneider et al. (2008). This indicates that the piezocone penetration occurred fully undrained in GHBS.

On the other hand, the $Q_{tn} - \mathrm{F_r}$ chart shows a range of $\mathrm{F_r}$ values (0.7 to 8.8) that is almost the same for GH-bearing sites and sites without hydrate. It also suggests a tendency towards a dilative behaviour for GHBS, with almost 79% of the data plotting between the sand dilative (SD), the transitional dilative (TD) and the clay dilative (CD) regions. However, some points that were classified as contractive (CC) in the $Q_{tn} - \mathrm{U}_2$ chart are also classified as contractive in the $Q_{tn} - \mathrm{F_r}$ chart. It is noteworthy that two of these points show a behaviour that correlates with the upper limit of cooper marl cemented clays on the $Q_{tn} - \mathrm{F_r}$ chart, as proposed by Robertson (2016).

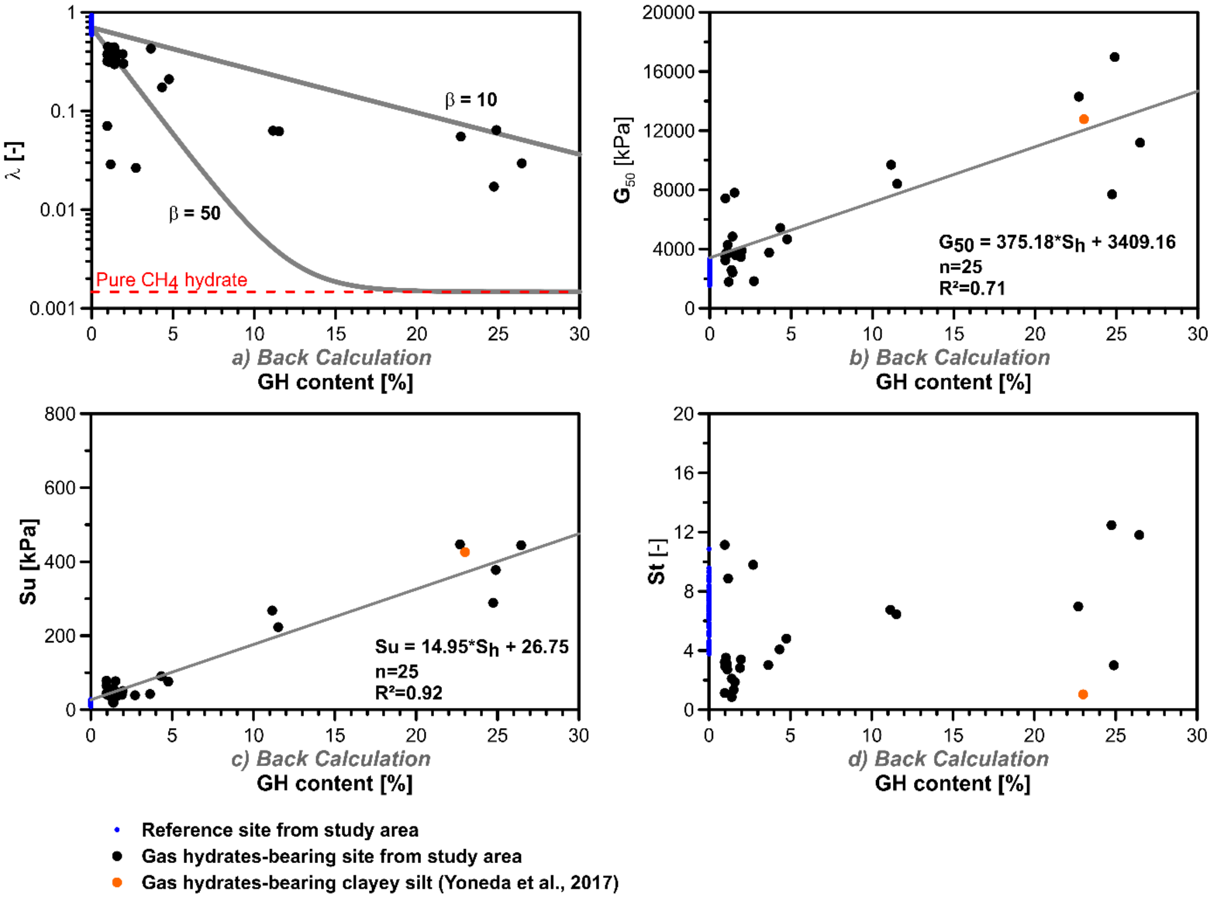

Figure 5. 8 Plots of geotechnical properties derived from piezocone data against hydrate content, S_h estimated from nearby acoustic soundings: a) Compression index, λ; b) Shear modulus at 50% mobilized strength, G_{50}; c) Undrained shear strength, Su, d)Sensitivity, St. Hydrate free sediments are plotted for reference as blue dots. The orange dots in b), c) and d) are determined from the results of triaxial compression tests on natural, never depressurized GH-bearing clayey silt samples from the eastern Nankai Trough as reported by Yoneda et al. (2017)

5.3.4 Mechanical properties of gas hydrates-bearing sediment

In line with previous observation regarding changes in corrected cone tip resistance(q_t), sleeve friction (f_s) and pore water pressure (Δu_2) in the GH occurrence zone (GHOZ) identified by Wei et al. (2015), Figure 5. 7 reveals that the presence of GH has a noticeable effect on the compressibility, stiffness and strength properties of their host clayey sediments. For instance, the compression indices (λ), the shear moduli at 50% mobilized strength (G_{50}) and the undrained shear strengths (Su) in GHBS do not follow the linear trends exhibited by the reference sediment. The compression indices (λ) are constantly lower in the GHOZ with values 20 to 40 times lower than those estimated at equivalent depths at the reference site (GMPFM06S01). Away from those spikes, λ values are about 3 to 4 times lower in GHBS.

Increases in stiffness seem less significant with G_{50} values being 1.25 to 7 times higher in GHBS compared to sediments without GH (Figure 5. 7). The increases in undrained shear strength mimic the increases in stiffness, though GHBS are up to 25 times stronger than reference sediments where spikes are observed and 2 to 3 times stronger away from the spikes (Figure 5. 7). The fact that the stiffness and strength of GHBS vary simultaneously explains why their rigidity indices ($I_r = G_{50}/S_u$) do not remarkably differ from those of sediments without hydrate (Figure 5. 7). By contrast, with the noticeable changes in compressibility, stiffness and strength, the sensitivity does not appear to be affected by the presence of hydrate (Figure 5. 7).

Plots of geotechnical properties derived from piezocone data against GH content shown in Figure 5. 8 suggest that the compressibility of GH-bearing clayey sediment follow two distinct trends. The first trend may be defined by values of compression indices decreasing from 0.47 to 0.026 for values of S_h increasing from 0.94 % to 2.76%. The second one outlines a softer decrease in compressibility with GH content with λ reaching 0.06 to 0.017 for S_h values ranging from 22.7% to 26.5%. Values of shear moduli at 50% mobilized strength (G_{50}) appear to follow a more linearly increasing trend with S_h despite some scatter at low and high S_h (Figure 5. 8). With a regression coefficient R^2 of 0.92, values of undrained shear strength follow a linear increase with increasing S_h. By contrast, no clear trend can be observed when plotting values of sensitivity against S_h. Sensitivities around 7 are indeed associated with S_h ranging from 0.94% to 22.7 %.

5.3.5 Hydraulic properties of gas hydrates-bearing sediment

Figure 5. 9 shows the initial excess pore-pressure pulse (U_{ini}) and dissipation generated by the piezometer penetration during a maximum time-period of 64 hours from different depths at sites GMPZ2, 3, 4, 6, 7 & 10 (for location see Figure 5. 1). Data in Figure 5. 9 were arbitrarily subdivided into two classes: (1) High initial excess pore-pressure pulse ($U_{ini} > 150\ kPa$) and (2) low initial excess pore-pressure pulse ($U_{ini} < 150kPa$).

Following Burns and Mayne (1999), sediments with a dilative behaviour are characterised by Δu curves increasing with time to a certain maximum and then decreasing to in-situ equilibrium pore-water pressure. In this study, Δu curves are observed to decrease in a monotonic way with time, which is indicative of a contractive behaviour as described by Burns and Mayne (1999).

Figure 5. 10 shows $\frac{C_h}{\sqrt{I_r}}$ and U_{ini} as a function of the corrected tip resistance q_t obtained from CPTu testing carried out near the piezometer sites. The clear increase of U_{ini} with q_t for the two reference sites as well as for sites with GH confirms the dependency of U_{ini} on the mechanical properties of the sediments. In effect, U_{ini} is the result of a mean normal octahedral stress (Δu_n) caused by the displacement of the sediment and fluid by the penetrating rod and the shear stress generated at the sediment-rod interface ($\Delta_{u_{shear}}$) (Burns and Mayne, 1998).

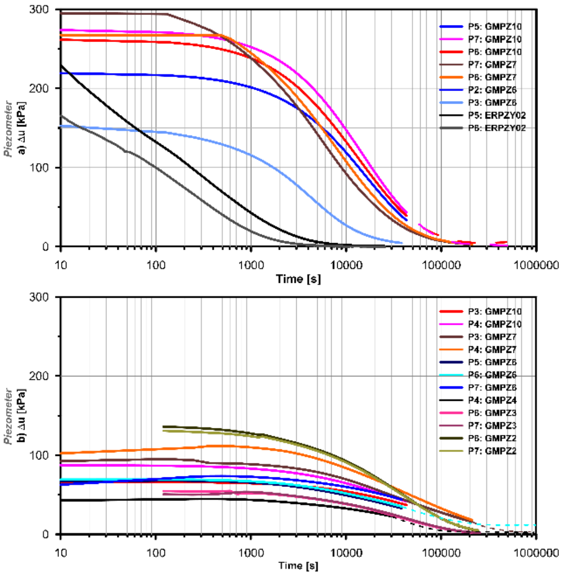

Figure 5. 9 Pore-pressure dissipation curves from different depths at different sites (GMPZ2, 3, 4, 6, 7 & 10) where the presence of GH was suspected and/or proved. (a) and (b) show data where the initial excess pore-pressure pulse (U_{ini}) values are higher and lower than 150 kPa. When the excess pore pressure was not equilibrated at the end of the deployment, the extrapolation of the excess pore pressure was carried-out using the numerical algorithm developed by Sultan and Lafuerza (2013) (dashed lines)

The $\frac{C_h}{\sqrt{I_r}}$ values obtained from the two reference sites indicate a decrease of this normalized parameter with the increase of qt (Figure 5. 10). However, $\frac{C_h}{\sqrt{I_r}}$ values for GHBS did not show any tendency to increase with q_t. Such result is unusual since the $\frac{C_h}{\sqrt{I_r}}$ values are expected to be proportional to the permeability of the medium and therefore to decrease with the increase of GH content and the increase of q_t.

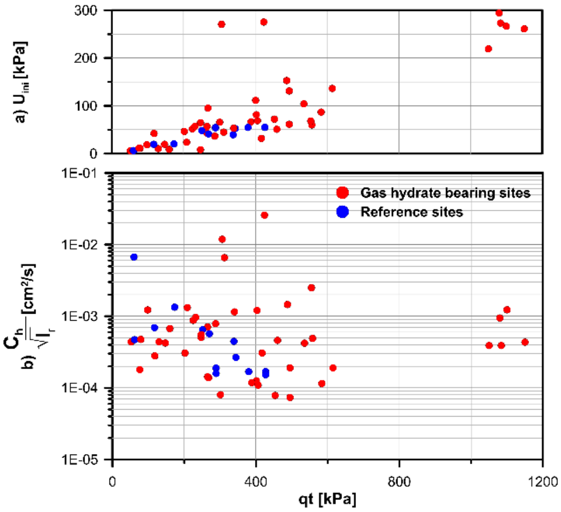

Figure 5. 10. a) U_{ini} *and b)* $\frac{C_h}{\sqrt{I_r}}$ *as a function of* q_t *showing a strong dependence of the initial excess pore pressure pulse on the corrected tip resistance.* $\frac{C_h}{\sqrt{I_r}}$ *values do not show any clear tendency*

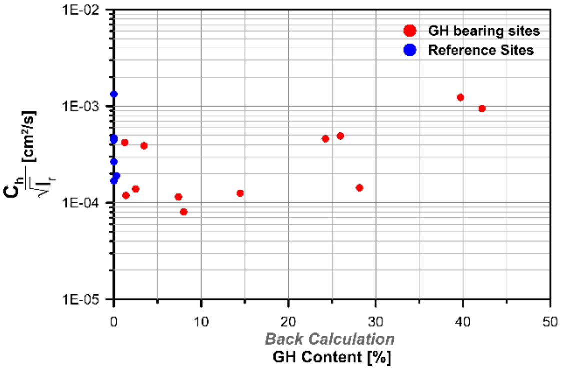

Figure 5. 11 $\frac{C_h}{\sqrt{I_r}}$ *as a function of GH content* (S_h). $\frac{C_h}{\sqrt{I_r}}$ *decreases to a minimum value for* S_h *equal 10% and then increases again*

Figure 5. 11 shows $\frac{C_h}{\sqrt{I_r}}$ as a function of GH content S_h derived from the chloride data and in situ Vp measurements. It can be observed that $\frac{C_h}{\sqrt{I_r}}$ decreases to a minimum value for S_h equal 10% and then increases again. However, considering the small change of the rigidity index I_r with S_h (Figure 5. 11), it is obvious that the tendency of hydraulic diffusivity to decrease with increasing GH content is not confirmed by the present in-situ pore pressure measurements.

5.4 Discussion

5.4.1 Quantification and characterization of gas hydrates

In this study, the presence of GH within fine-grained marine sediment have been characterised based on in-situ geotechnical and acoustic measurements. The presence of GH was linked to positive Vp anomalies that correlate with an increase in all of the CPTu parameters. However, negative Vp anomalies were indicators of the presence of free gas. The effective medium theory developed by Helgerud et al. (1999) was used to obtain an upper and lower bound estimate of GH content within the sediment based on compressional wave velocity anomalies.

Comparisons of velocity-derived estimates were made with those derived from pore-water chloride anomalies to evaluate which of the upper or lower bound GH content might be more reliable to use in the study area. It was found that S_{hmin} values are fairly close to those derived from pore-water chloride analyses. These observations are in line with studies performed by Ghosh et al. (2010), in which it was shown that S_{hmin} yields closer estimates to that of the pressure core depressurisation method compared to S_{hmax}. Hence, for this section S_{hmin} was used to carry out the investigation of the effect of GH content on the mechanical and hydraulic properties of the host sediment. In general, no systematic vertical pattern was noticed on the GH profiles (Figure 5. 5).

Wei et al. (2015) discussed GH distribution in the study area based on cold temperatures obtained from infrared imaging. Therefore, negative thermal anomalies derived from MeBo cores by Wei et al. (2015) were compared to GH occurrence zones determined using the effective medium theory. Both methods showed close results by exhibiting almost the same GH occurrence zone; therefore, confirming the relation between Vp anomalies and the presence of hydrates.

Using the effective medium theory, a maximum GH content of 26.5% (S_{hmin}) was estimated to correlate with a Vp of 2035 m/s.

Because of the limitation of the ultrasonic fork, which can only measure Vp up to 2200 m/s, higher GH content could not have been estimated.

The estimation of GH content might have been also affected by the coexistence of free gas and solid GH in the study area as reported by Sultan et al. (2007 and 2010). This phenomenon is mainly caused by the fact that the study area is characterised by a high gas flux system; hence, in some cases free gas can be isolated within the pores of GH where no water is available for the formation of solid hydrates; resulting in a GH containing voids and having a spongy texture. It is indeed thought that GH content might have been locally underestimated when the presence of free gas could have counteracted the effect of hydrates in increasing Vp.

Soil classification charts were used to define a general trend that illustrates the behaviour of GH-bearing clayey sediments by correlating in-situ acoustic data with geotechnical properties. While the highest GH content correlates with the highest U_2 and Q_{tn} values, the rest of the data does not bear a proportional relationship with hydrate content. However, GHBS are clearly characterised by slightly increasing U_2 values that correlate with large Q_{tn} values (compared to reference sites), which reflect a contractive behaviour. These observations are in contrast with results from laboratory triaxial experiments performed on GH-bearing sandy sediments, where the behaviour was found to be significantly dilative at high GH content (Hyodo et al., 2013). Interestingly, Liu et al. (2018), showed that upon shearing the dilatancy of GH-bearing sands is higher compared to that of GH-bearing silts. Moreover, data from sites where GH content could not have been estimated show a general trend of increasing Q_{tn} values towards the upper limit of the charts. This confirms that GH contribute to the increase of the stiffness and strength of their host sediment. However, the fact that no clear trend of increasing U_2 with increasing Q_{tn} can be discerned tends to suggest that the sensitivity of GHBS does not increase proportionally to their stiffness and strength. This suspicion is supported by the analysis of the $Q_{tn} - \mathrm{F_r}$ chart, which reveals that high values of Q_{tn} correlate with values of $\mathrm{F_r}$ varying over a wide range. The combination of $Q_{tn} - U_2$ and $Q_{tn} - \mathrm{F_r}$ charts also reveals that data from GH-bearing sites tend to plot in different regions.

While, the $Q_{tn} - \mathrm{F_r}$ chart suggests a dilative behaviour for most of the data, the $Q_{tn} - U_2$ chart reflects a contractive behaviour. Robertson (2016) suggested that such a difference is representative of the influence of the increasing microstructure in in-situ soils. Here, the difference between both classification charts can be explained by the increasing GH content within the sediment. By contrast, for some data points, the behaviour is classified as contractive in both charts.

These findings can be explained with reference to different GH concentrations and morphologies accommodated by clayey sediments. Visual observations of recovered cores in the study area show GH morphologies varying from groups of millimetre thick veins to massive nodules (Sultan et al. 2010). Correlations of these observations with the acoustic and geotechnical data show high GH concentrations (up to 27%) plotting in the dilative region of the $Q_{tn} - \mathrm{F_r}$ chart, which could be related to the presence of nodule type hydrate. However, low GH concentrations (1 to 5%) plotting in or at the limit of the contractive region of the $Q_{tn} - \mathrm{F_r}$ chart could be an indicator of the presence of a group of hydrate veins.

Alternatively, Ramsey (2010) discussed that the presence of massive inclusion (i.e. GH nodules in this study) within the sediment might influence piezocone response. This can eventually lead to local suctions that prevent the proper functioning of the pore pressure sensor; therefore, producing sharp drops in pore-water pressure data correlating with spikes in the f_s profile. Such a response has been observed twice during this analysis (Symbols 1 and 2 on Figure 5. 6) for GH content of 26.5% and 11.5% respectively.

During the penetration, Δu_2 did not reduce below -70kPa confirming that it did not drastically affect the reliability of the measuring method.

5.4.2 Mechanical properties of gas hydrates-bearing sediment

The derivation of geotechnical properties from piezocone data allowed estimating the extents to which the presence of GH tend to decrease the compressibility of clayey sediments while increasing their stiffness and strength (Figure 5. 7 and Figure 5. 8). Keeping in mind that empirical correlations primarily defined for "ideal soils" have been used to derive these properties as well as that there are difficulties inherent to the estimation of GH content, the trends that emerged are cautiously discussed here. A common feature to the compression index, shear modulus and undrained shear strength is to show a wide scatter with S_h ranging from 0.94% to 3%. In the lack of laboratory results to substantiate these observations, one may suspect that the morphology and orientation of grain displacing hydrate readily take over from S_h as the primary control of the compressibility, stiffness and strength. Following Ghosh et al. (2010) one may also infer that the orientation of grain displacing hydrate affects the estimation of GH content (S_h) using an effective medium theory approach.

Values of compression indices can be compared to the model proposed by Sultan et al., (2010) to capture the evolution of compressibility with S_h. According to this empirical model, compression indices of GHBS (λ_h) are expected to asymptotically decrease from a value typical of purely water-saturated sediments in the study area ($\lambda_0 = 0.7$) towards that of pure hydrate ($\lambda_1 = 0.00147$) according to the following equation:

$$\lambda_h = \lambda_0 \left[1 - \left(1 - \left(\frac{\lambda_1}{\lambda_0}\right)\right)\left(1 - \exp\left(-\beta.\frac{S_h}{100}\right)\right)\right] \qquad (5.1)$$

Where the coefficient β is expected to reflect the distribution and morphology of GH within the sediment.

As shown in Figure 5. 8, a β value of 10 appears to provide an upper limit for the compression indices of GHBS. It would predict that the compressibility of the host sediments approaches that of pure methane hydrate for S_h= 100%. A β value of 50 would provide a lower limit for the compression indices of most of GHBS. The fact that it implies that the compressibility of GHBS approaches that of pure methane hydrate for S_h = 18% can hardly be reconciled with the data showing that when S_h is in the range 25-27%, compression indices remain one order of magnitude higher than that of pure GH. This raises the possibility that a single β value cannot capture the change in compressibility with S_h as the morphology of GH is itself evolving with S_h. Thus, the identification of robust trends from laboratory testing of natural, fine-grained GHBS is required to expand upon this empirical suspicion.

Despite some scatter in the plots of Figure 5. 8.b, the overall distribution suggests that the stiffness and strength of GH-bearing clayey sediments tend to increase linearly with S_h. The fact that S_u data appear less scattered than the G_{50} data may be ascribed to the fact that the latter have been calculated using the soil behaviour type index (I_c), whose calculation may be affected by a lack of accuracy of sleeve friction measurements, f_s. An additional note of caution has to do with the fact that density was assumed to be constant when calculating G_{50}. One may however note that the unique natural GH-bearing fine-grained sediments subjected to triaxial compression by Yoneda et al. (2017) has G_{50} and S_u values falling close to the linear trends that emerged from the present study. As for compression indices, it can be expected that the stiffness and strength is influenced by the distribution and morphology of GH such that S_h alone cannot wholly capture the natural variability of these properties.

Sensitivity values are discussed separately from the previous properties as they appear to be the most scattered when plotted against S_h. Such a scatter might be attributed to a lack of accuracy of sleeve friction measurements. However, the plots in the $Q_{tn} - \mathrm{U}_2$ chart in Figure 5. 6.a, which do not rely on sleeve friction measurements, also suggest that sensitivity bears little relationship to S_h. Indeed, values of Q_{tn} ranging from 11 to 80 are observed to display similar U_2 values for S_h ranging from less than 2.5% to more than 22% while sensitive sediment are expected to display trends of increasing Q_{tn} with increasing U_2 (Robertson, 2016).

In line with previous interpretations, this tend to support the view that the distribution and morphology of GH have a strong influence on sensitivity.

5.4.3 *Hydraulic properties of gas hydrates-bearing sediment*

The water permeability of GHBS is a constraint for reservoir engineering studies but moreover a key parameter to evaluate the excess pore pressure generated by hydrate decomposition in natural environment.

The evolution of the octahedral stress (Δu) with time is a means to predict if the investigated soil is contractive or dilative. Pore-pressure dissipation curves from different piezometer sites have indeed showed a monotonic change with time. This trend is representative of a contractive behaviour as proposed by Burns and Mayne (1999)

The rare available data from literature are often obtained from laboratory experimental tests carried out on reconstructed GH-bearing sand samples. Those laboratory data show a clear tendency of the permeability to decrease with increasing GH content (see for instance Katagiri et al., 2017 and references therein). On the other hand, different authors show that the water permeability versus porosity of the hydrate-sediment system depends on the way GH accommodates the pore spaces (grain coating or pore filling). Several theoretical models were developed in the recent years in order to define the link between GH content and relative permeability (Moridis et al., 2002; Kleinberg et al., 2003; Katagiri et al., 2017 among others).

Kleinberg et al. (2003) have summarized existing expressions for the relative permeability k_{hw} in hydrate-bearing sediment. For pore filling hydrate, a simple relative permeability to water can be expressed by the following expression:

$$k_{hw} = \frac{k}{k_0} = \frac{(1-S_h)^{m+2}}{(1+\sqrt{S_h})^2} \qquad (5.2)$$

where k_0 is the reference permeability of the saturated sediment, k is the permeability of the system for a given hydrate saturation and m is the saturation exponent decreasing from 0.4 for $S_h = 10\%$ to 0.1 in a fully hydrate saturated system. For grain-coating hydrate, a simple expression of the relative permeability to water is given by:

$$k_{hw} = \frac{k}{k_0} = (1 - S_h)^{m+1} \qquad (5.3)$$

where m=1.5 for $S_h < 80\%$.

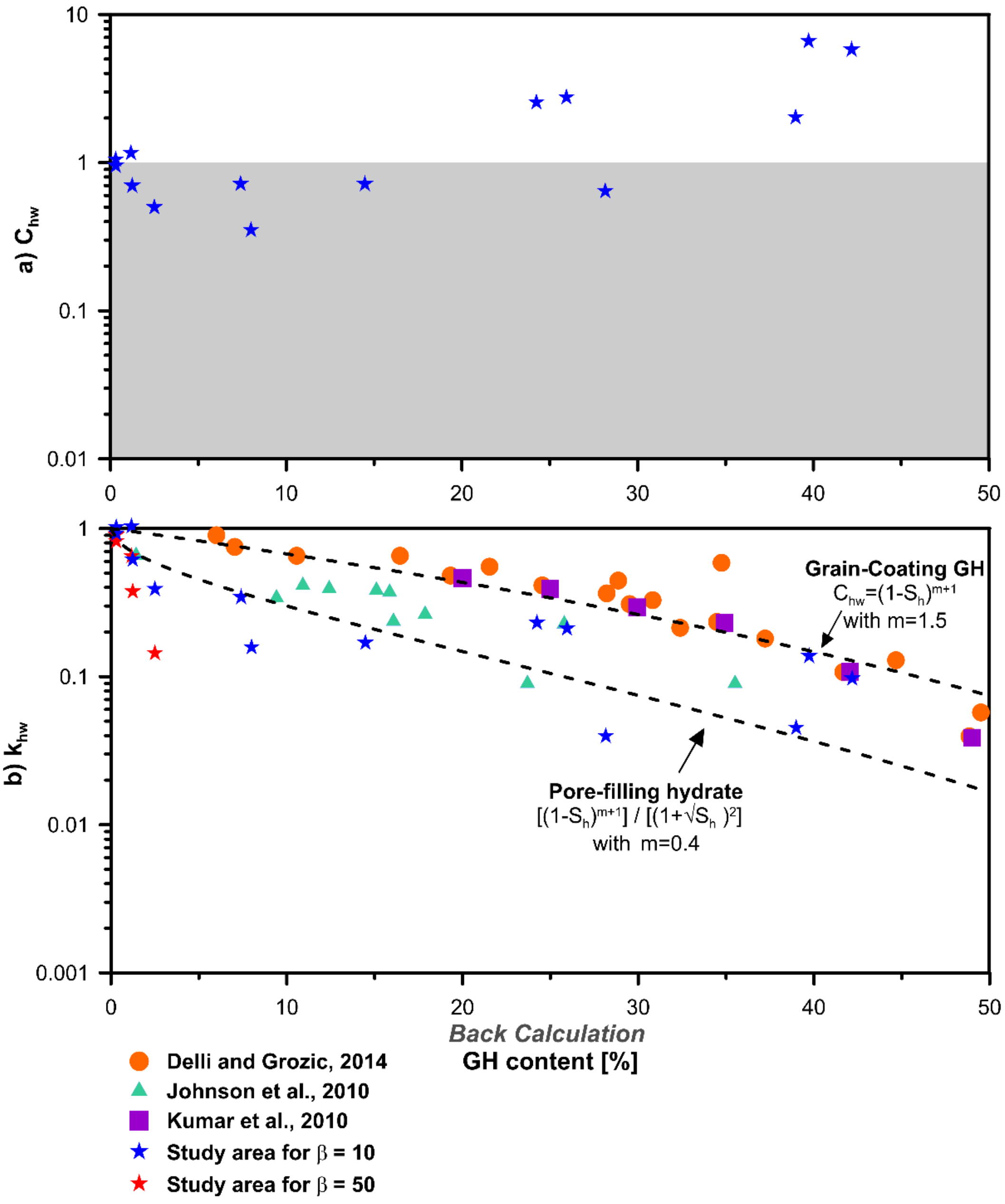

Figure 5. 12 a) Relative hydraulic diffusivity (C_{hw}) as a function of hydrate content (S_h) showing a decrease tendency with the increase of S_h to 15%. A clear increase of C_{hw} with Sh can be observed for S_h values higher than 20%.b) Relative permeability data for β values of 10 and 50

Before discussing changes in relative permeability to water, attention is paid to the changes in relative hydraulic diffusivity with GH content from in-situ measurements:

$$C_{hw} = \frac{C_h}{C_{h0}} \quad (5.4)$$

where C_h is the hydraulic diffusivity of the system for a given hydrate content and C_{h0} is the reference hydraulic diffusivity of the saturated sediment.

The C_{hw} values shown in Figure 5. 12.a are derived from piezometer data in Figure 5. 11 and the rigidity indices (I_r) obtained from CPTu data using the Robertson (2009) method (Figure 5. 7). The plots in Figure 5. 12.a confirm the decreasing trend of C_{hw} with increasing S_h up to 15%. However, a clear increase of C_{hw} with S_h can be observed for S_h values higher than 20%. Such results were unexpected and were initially considered as erroneous data, compromising the used in-situ method to determine the hydraulic properties of GHBS.

Table 5. 2 Hydraulic properties from different depths at different sites (GMPZ2, 3, 4, 6, 7 & 10) where the presence of GH was suspected and/or proved.

Site	**Depth (mbsf)**	t_{50} (s)	S_h %	C_h (m^2/s)	C_{hw}	k_{hw} $for\ \beta = 10$	k_{hw} $for\ \beta = 50$
GMPZ2	7.08	23686	0.3	2.23E-07	0.951	0.923	0.819
GMPZ2	7.11	23686	0.3	2.46E-07	1.049	1.018	0.904
GMPZ3	7.11	28347	1.16	2.72E-07	1.161	1.034	0.651
GMPZ4	6.17	31550	28.15	1.51E-07	0.642	0.040	
GMPZ4	6.97	9806	24.2375	5.99E-07	2.555	0.231	
GMPZ4	7.005	9183	25.95	6.47E-07	2.761	0.211	
GMPZ6	6.98	10715	1.24	1.64E-07	0.698	0.616	
GMPZ7	6.23	32546	2.5	1.17E-07	0.500	0.390	
GMPZ7	7.78	35944	14.475	1.68E-07	0.716	0.169	
GMPZ7	10.13	3668	39.725	1.55E-06	6.591	0.138	
GMPZ7	10.165	4766	42.175	1.36E-06	5.787	0.097	
GMPZ10	6.93	56169	8	8.22E-08	0.350	0.158	
GMPZ10	8.48	39219	7.4	1.68E-07	0.718	0.343	
GMPZ10	10.03	11574	38.9875	4.75E-07	2.025	0.045	

However, published experimental data and models often consider the sediment-hydrate medium as a continuous system without discontinuities and fractures. In natural environments, the presence of fractures at different scales may imply high hydraulic diffusivities and fluid flows paths through GH-bearing areas. The coexistence of free gas and GH as well as gas plumes in the water-column above hydrate occurrence zones is a clear evidence of the presence of these discontinuities (Torres et al., 2002, Sauter et al., 2006, Riboulot et al., 2018). The impact of those discontinuities on the evolution of the hydraulic diffusivity with the GH content seems essential to account for accurate prediction of fluid flow through hydrate-sediment systems. The use of *in-situ* pore pressure measurements and the pore-pressure decay with time to derive the hydraulic diffusivity of the medium looks, at first sight, as a reliable method to access the *in-situ* hydraulic properties of sediment-hydrate fracture mediums. Therefore, our data importantly suggest that, in the study area, fractures occurring for S_h values higher than 20% may drastically increase the hydraulic diffusivity of GHBS. Unfortunately, this strong conclusion is premature, since alternative explanation related either to the piezometer installation or to the important decrease of the compressibility could also be at the origin of the increase in C_{hw} with S_h. The free fall method used for piezometer installation with a rod diameter of 0.06 m and the stiffness of GHBS could enhance fracture propagation or even initiation. The expected consequence would be an increase in hydraulic diffusivity. Although, fractures generated by piezometer penetrations are more likely to occur at the tip of the piezometer and not all over its shaft (Santamarina et al., 2015), at this stage, it is not possible to firmly conclude about their origin. However, it is obvious that the general thought about the decrease of the hydraulic diffusivity with increasing hydrate content cannot be systematically applied in natural sediment-hydrate systems.

To further the discussion, it is important to mention that the hydraulic diffusivity is equal to the relative permeability to water divided by the storage parameter:

$$k_{hw} = \frac{k}{k_0} = \frac{C_h . St_h}{C_{h0} . St_0} = C_{hw} . \frac{\gamma_w . m_{vh}}{\gamma_w . m_{v0}} = C_{hw} . \frac{\lambda_h}{\lambda_0} = C_{hw}\left[1 - \left(1 - \left(\frac{\lambda_1}{\lambda_0}\right)\right)\left(1 - \exp\left(-\beta . \frac{S_h}{100}\right)\right)\right] \quad (5.5)$$

Where St_0 and St_h are storage factors, γ_w is the water unit weight and m_{v0} and m_{vh} are the volume compressibility coefficients of water-saturated and hydrate-bearing sediments respectively. As shown in Table 5. 2 and Figure 5. 12, values of relative permeability to water (k_{hw}) can be calculated using equation 16, assuming upper and lower β values of 10 and 50 as explained in chapter 5.2. However, since for $S_h > 5\%$ no data plot near the limit curve obtained using a $\beta = 50$ (Figure 5. 8.a), k_{hw} values were calculated using β = 50 only for values of $S_h < 5\%$.

Figure 5. 12.b shows that overall the calculated k_{hw} data decrease with increasing S_h . This trend reflects the fact that the compressibility of GH bearing sediments decreases more rapidly than the hydraulic diffusivity does with increasing S_h. The k_{hw} values obtained with β values of 10 generally plot between the two limit curves defined by equations 13 and 14 while showing a decreasing trend with increasing S_h. While these equations were developed for coarse-grained sediments, they appear here to have the potential to serve as lower and upper bounds for describing the evolution of permeability as a function of hydrate content in clayey sediments also. On the other hand, for $\beta = 50$, k_{hw} data plot completely outside of the grain-coating and pore-filling hydrate limits (equations 13 and 14) while decreasing with a slope 14 times steeper than that of the k_{hw} obtained with $\beta = 10$. This implies that the trends defined by equations 13 and 14 are clearly not adapted to represent the evolution of k_{hw} calculated with β values of 50. This highlights the need for developing new models that can account for the evolution of the morphology of GH with that of S_h.

5.5 Conclusion

The main objective of this chapter was to study the effect of GH concentration and morphology on the mechanical and hydraulic properties of their host clayey sediment. This was achieved by using a unique database containing multiple in-situ acoustic, geotechnical, coring and drilling data. This investigation allowed capturing the behaviour of clayey sediment with GH content varying between 1% and 26.5% in a high gas flux system in the Gulf of Guinea. This analysis led to the following key observations:

- Positive Vp anomalies correlating with simultaneous increase of all geotechnical parameters $(q_t, f_s \text{ and } \Delta u_2)$ are indicative of the presence of GH.
- Using the effective medium theory, a maximum GH content of 26.5% was estimated to correlate with a Vp of 2035 m/s.
- Comparisons of results derived from the effective medium theory with those derived from negative thermal anomalies yielded almost the same GH occurrence zone.
- GH-bearing clayey sediments generally show a contractive behaviour, which was confirmed by the analysis of pore pressure dissipation data recorded by piezometers. Such a behaviour contrasts sharply with the dilative behaviour of GH-bearing sandy sediments
- Results have shown that the normalised piezocone resistance (Q_{tn}) increases with the GH content. High Q_{tn} values were found to correlate with the same range of U_2 values. This suggests that the morphology and the distribution of GH has an important effect on the mechanical properties of the host sediment.
- The use of different soil behaviour classification charts, while carefully analysing all used parameters, might be a means to identify different GH morphologies based on zones in which the piezocone data plot.
- The presence of GH has a noticeable effect on the compressibility, stiffness and strength properties of their host clayey sediments. It tends to increase the stiffness G_{50} and undrained shear strength (S_u) while decreasing the compressibility. While, no clear trend was observed between the sensitivity and GH content, S_u and G_{50} appear to follow a linear increase with GH content.

- Oscillations around the linear trend are thought to reflect the superimposed influence of the distribution and morphology of GH on the stiffness and strength.
- Pore pressure dissipation data were used to derive the relative hydraulic diffusivity (C_{hw}) as a function of hydrate content (S_h). At low hydrate content, C_{hw} was observed to decrease with increasing S_h. For S_h values higher than 20, C_{hw} values rising above 1 were linked either to the presence of fractures in the hydrate-sediment system or to the important decrease of compressibility with increasing GH content. This observation leads to the conclusion that the pore pressure diffusion within GH systems could be much faster than previously thought for high hydrate content.

Further investigations supported by experimental data would be helpful in substantiating the influence of various morphologies and amount of GH on the mechanical and hydraulic properties of the clayey host sediment.

Chapter 6. Formulation of a constitutive model for gas hydrate bearing sediment behaviour

Chapitre 6. Formulation d'un modèle constitutif de comportement d'un sédiment chargé en hydrates de gaz

A drill rig at the Mallik test site in Canada's McKenzie Delta (Tim Collett, USGS)

Abstract

The mechanical behaviour and response of GH-bearing clayey sediments is challenging to reproduce using theoretical and numerical models due to the lack of data in the literature. However, most research efforts have been focused on coarse-grained sediments as they represent a medium, which is simpler to investigate and reproduce synthetically.

Throughout the chapter, a literature review of the mechanical properties of fine-grained and coarse-grained sediments containing gas hydrates is presented. The review revealed that the strength and stiffness of GH-bearing sediments increase with increasing GH content and are highly affected by GH morphology and distribution. Then, a review on the available numerical models and how they compare with existing experimental data is presented. Some of the models in the literature seem to decently reproduce the behaviour of GHBS but require a significant number of physical and empirical parameters.

This chapter aims to present a new simple constitutive model based on an “equivalent skeleton void ratio” in order to reproduce the main features of the mechanical behaviour of GHBS. Compared to other published models, the new proposed model requires introducing only one parameter related to the presence of gas hydrates.

Lastly, the proposed model performance is evaluated by comparing the numerical results with experimental results for sandy and clayey sediments without and with GH. The results were in general satisfactory if one keeps in mind the simplicity of applying the model, in terms of the number of required parameters.

Résumé

Le comportement mécanique des sédiments argileux contenant des hydrates de gaz est considéré complexe à reproduire à l'aide de modèles théoriques et numériques. Cela est dû au manque de connaissances concernant ce genre de sédiments. Jusqu’à aujourd’hui, la plupart des travaux de recherche se sont concentrés sur les hydrates dans les sédiments grossiers nettement plus facile à étudier et à reproduire artificiellement en laboratoire.

Ce chapitre présente premièrement une revue de la littérature sur les propriétés mécaniques des sédiments fins et à grossiers contenant des hydrates de gaz. La revue a révélé que la résistance et la rigidité des sédiments contenant des hydrates de gaz augmentent avec l’augmentation du contenu en GH ; et sont fortement affectées par la morphologie et la distribution des hydrates. La seconde partie se focalise, quant à elle, sur une revue des modèles numériques aujourd’hui disponibles. Certains modèles semblent bien reproduire le comportement des GHBS mais nécessitent un nombre important de paramètres.

Ce chapitre propose un nouveau modèle constitutif simple basé sur l’introduction d’un indice des vides « équivalent » pour reproduire les principales caractéristiques du comportement mécanique des sédiments contenant des hydrates de gaz. Contrairement à d'autres modèles publiés précédemment, nécessitant souvent un nombre important de paramètres physiques et empiriques pour pouvoir être appliqués, ce nouveau modèle n’a nécessité que l’introduction d’un seul paramètre associé aux hydrates de gaz.

Enfin, la performance du modèle proposé est évaluée à l’aide d’une comparaison des résultats numériques et des résultats expérimentaux pour des sédiments de type sableux et argileux avec et sans hydrate de gaz. Les résultats ont été globalement satisfaisants si l’on tient compte du fait que le modèle ne dépend que d’un seul paramètre associé aux hydrates de gaz.

6.1 Introduction

The influence of GH presence and content on the properties of their host sediment has been extensively studied in the literature (Winters et al. 2004 ; Ebinuma et al. 2005 ; Hyodo et al. 2005 ; Masui et al. 2005 ; Waite et al. 2009; Miyazaki et al. 2011a; Hyodo et al. 2013; Kajiyama et al. 2017; Yang et al. 2019; Wang et al. 2019; Chen et al. 2019). Although the actual scientific knowledge about the mechanical properties of GH bearing sediment (GHBS) is immature, laboratory experiments have allowed to better highlight the effect of GH on their host sediment. GH are known to increase the strength and stiffness of their host sediment (Li et al. 2019; Jiang et al. 2018; Kajiyama et al. 2017; Yoneda et al. 2015; Masui et al. 2007; Hyodo et al. 2005) with a magnitude that is dependent on the GH content, the formation process of GH and the nature of the host sediment (Grozic and Ghiassian 2010; Winters et al. 2007). Nowadays, there is a significant lack of practical field experience with GH systems and methods dealing with their exploitation as a potential energy resource remain poorly approached (Collett et al., 2014). Therefore, understanding the effect of GH on the mechanical behaviour of their host sediment is essential to assess any potential geohazard related to the decomposition of these hydrates or eventual exploitation of gas.

In this manuscript, the behaviour of gas hydrate bearing fine-grained sediment has been the centre of discussion of previous chapters. Therefore, this chapter aims to propose a new simple constitutive model that is able to reproduce the main mechanical properties and features of such materials. It is noteworthy that in order to validate such model an extensive database is required. However, most previous research efforts have been focused on sandy sediment since they represent a medium in which GH can form easily compared to clayey sediments; thus, not enough data is available for fine-grained materials containing gas hydrates. As a first step towards checking the performance of the new model based on "equivalent skeleton void ratio", numerical results are compared with existing experimental data on coarse-grained sediments. Then, an extension of this model aiming at capturing the behaviour of fine-grained sediments is proposed; keeping in mind that its validation remains challenging due to the lack of experimental data.

6.2 Mechanical properties of gas hydrate bearing sediments: literature review

Throughout this paragraph, a literature review of the mechanical properties of fine-grained and coarse-grained sediments containing gas hydrates is presented. Although fine grained clayey sediments contain over 90% of the global GH accumulations (Boswell and Collett, 2006), not much research have been carried out on the mechanical properties of such sediments. Indeed, significant research and industrial efforts have been placed on coarse-grained sediments containing GH. This is because of their high permeability, which is a necessary and critical parameter for gas production.

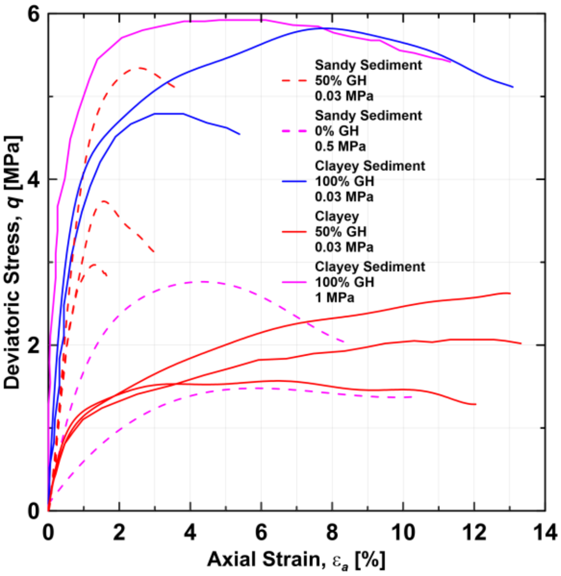

Figure 6. 1 Deviatoric stress-Axial strain curves for sandy sediments (dashed lines) and clayey sediments (solid lines) with different gas hydrate content (Yun et al. 2007)

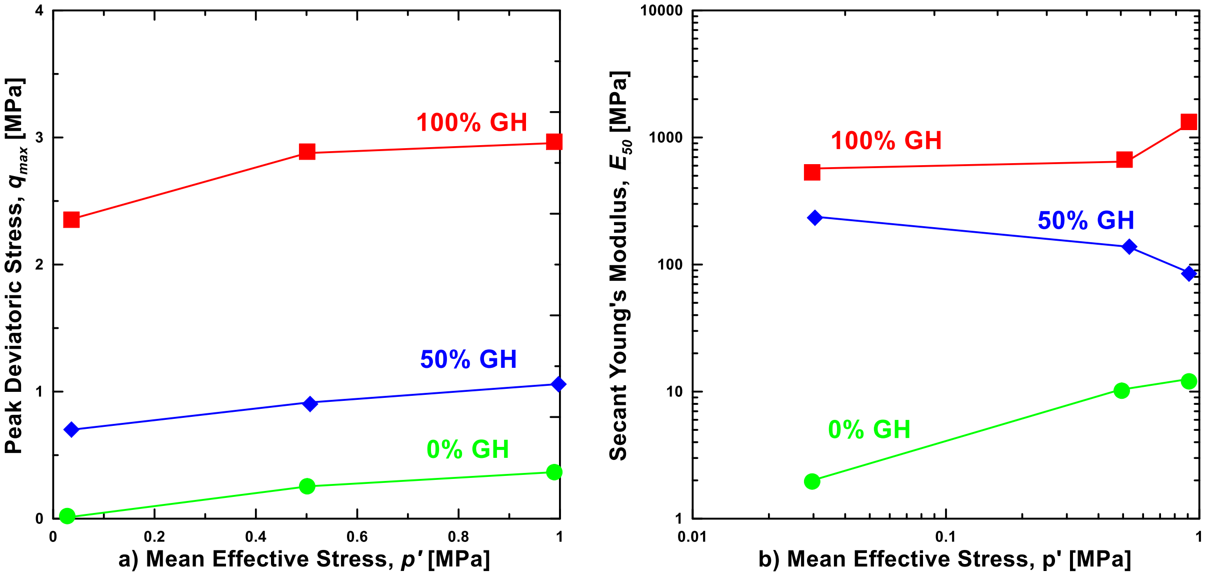

Figure 6. 2 a) Peak deviatoric stress and b) secant Young's modulus as a function of mean effective stress for fine-grained sediments (Yun et al. 2007)

6.2.1 Behaviour of gas hydrate bearing fine-grained sediments

Lei and Santamarina (2018) studied the challenges of forming gas hydrates in fine-grained sediments by accelerating the supply of guest molecules to the hydrate formation interface. It was confirmed that GH hydrate formation in fine-grained sediments is of a displacive nature and eventually compacts the host sediment as it extracts pore water. It was also observed that under low effective stress, the formed GH lenses are thicker and closer to each other. Additionally, triaxial tests on fine-grained sediments containing cylindrical GH veins were conducted by Smith (2018). The study showed that the strength and stiffness of the host sediment increase with increasing GH content and increasing diameter of the veins. Alternatively, Yun et al. (2010) studied the strength and stiffness of GH-bearing fine-grained sediments recovered from the Krishna-Godavari Basin offshore India. It was observed that variations in shear strength along the length of the recovered cores correlate with the presence of hydrate veins. That is to say that when hydrate veins are present, the shear strength was noticed to increase.

Due to significant challenges faced when trying to form gas hydrate in fine-grained sediments (Lei and Santamarina 2018), many laboratory experiments (Lee et al. 2007; Yun et al., 2007) have been performed by replacing methane gas with tetrahydrofuran (THF). Lei and Santamarina (2018) discussed different morphologies resulting from THF hydrate formation. For instance, ice lenses and pore-filling morphologies were observed in some cases. Li et al. (2011) proved that the deviatoric stress at failure of gas hydrate bearing fine-grained sediments increased with increasing effective confining stress. Additionally, Yun et al. (2007) showed that the mechanical response of the host sediment is dependent on the type of the sediment, GH content and the applied confining pressure. While sands clearly exhibit a maximum yield point at 100% GH content after which a sudden decrease in strength is noticed, clayey sediment a more developed post-peak strength behaviour (Figure 6. 1). This suggests that in fine-grained sediments the bonding between hydrates and grains is weaker compared to sandy sediments. Figure 6. 2 shows the peak deviatoric stress and stiffness as a function of mean effective stress for fine-grained sediment (Yun et al. 2007). The peak strength and stiffness are observed to increase with increasing GH content as well as with increasing mean effective stress.

Although results by Yun et al. (2007) may represent the mechanical features of gas hydrate bearing fine sediments, THF is still considered as a proxy for methane hydrates.

Li et al. (2010) performed an experimental study on the mechanical properties of gas hydrate-bearing sediments using kaolin clay by mixing ice powder with pure methane gas in a high-pressure reactor. The GH content was around 30% for the performed tests. Figure 6. 3 shows the effect of the mean effective stress as well as the kaolin volume ratio on the mechanical response of the host sediment. The stiffness of the sediment seems to be unaffected under different p’ values; however, the post peak strength behaviour seems to be hardening with increasing mean effective stress (Figure 6. 3).

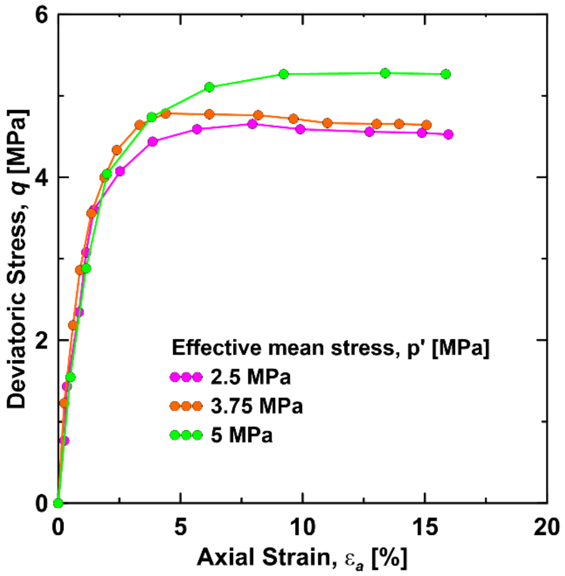

Figure 6. 3 Deviatoric stress-Axial strain curves for kaolin clay containing methane hydrates (30% GH) under different mean effective stress (from Li et al., 2010)

Additionally, Li et al. (2019) studied the mechanical behaviour of methane hydrate-bearing clayey sediments at a fixed GH content of 30%. The study took into account the effect of pressure, temperature and porosity on the mechanical response of the GHBS. As shown earlier (Figure 6. 3), results have shown that at different mean effective stress, the stiffness of the host sediment is not affected; however, strain hardening is observed to increase with increasing p’. Wang et al. (2019) also showed that the failure strength of the tested samples increases with decreasing temperature. As for the porosity, results revealed that the strength of the sediment decreases with increasing porosity; however, the stiffness remains constant. Moreover, Hyodo et al. (2017) performed triaxial compression tests on synthetic methane hydrate-bearing sediments with varying amounts of fines content. Results have shown that the peak shear strength and stiffness of the host sediment increase with increasing fines content and with decreasing void ratio. As for the dilation, it is enhanced with increasing fines content.

Santamarina et al. (2015) have used pressure-coring techniques to characterise the hydro-bio-geomechanical properties of natural GH-bearing sediments retrieved from Nankai trough, Japan. It was clearly observed that the peak shear strength was higher for samples containing GH compared to reference samples without GH. On the other hand, it has been proven that in-situ measurements are a promising means to determine the geotechnical properties of marine sediments (Sultan et al., 2007, 2010 and 2014) and thus study their mechanical behaviour. Taleb et al. (2018) have analysed a set of in-situ data in order to characterise the behaviour of marine clayey sediments in the Gulf of Guinea. The stiffness and strength of the host sediment were observed to (1) be strongly influenced by the distribution/morphology of GH as well as (2) increase with increasing GH content. Additionally, contrary to GH-bearing sands, the behaviour of GH clayey sediment was observed to be contractive. This also contrasts with experimental results conducted on clays (see for instance Yun et al., 2007). While a contractive behaviour is the natural response of clayey sediments upon shearing, the aim of the Taleb et al. (2018) study was to state that natural clayey sediments preserve their contractive behaviour in the presence of hydrates.

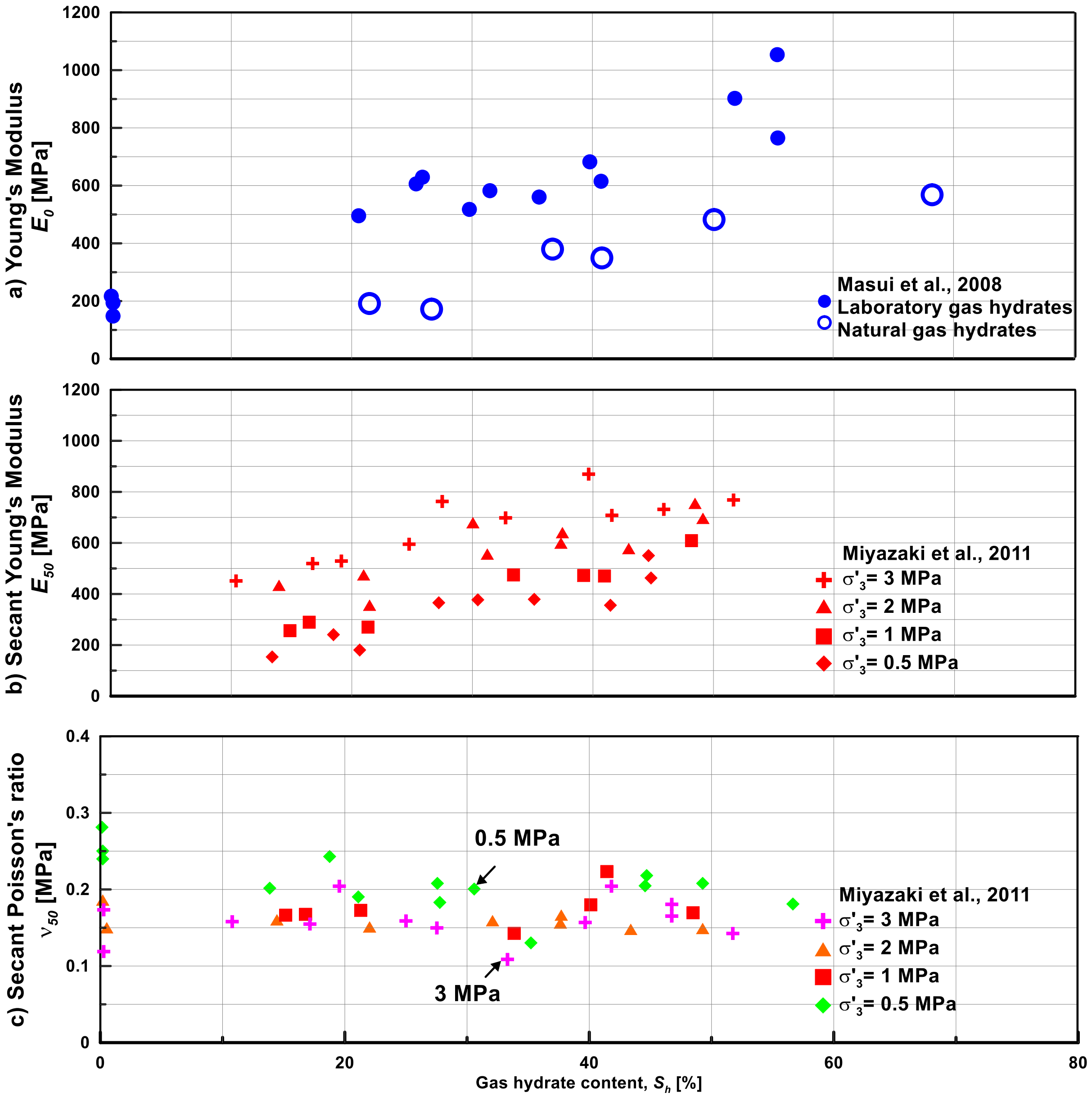

Figure 6. 4 a) Young's modulus (Masui et al. 2008), b) secant Young's modulus (Miyazaki et al., 2011) and c) secant Poisson's ration (Miyazaki et al., 2011) as a function of gas hydrate content

6.2.2 Behaviour of gas hydrate bearing coarse-grained sediments

The behaviour of GHBS has been proved highly dependent on GH content but furthermore on GH morphology and distribution within the sediment. Indeed, different morphologies of GH will lead to different mechanical consequences of the host sediment. The main GH morphologies found in sandy sediment are the (1) pore-filling GH, (2) cementing GH and (3) Load bearing GH (Waite et al. 2009; Soga et al. 2006).

Hyodo et al. (2005; 2013; 2014) studied the shear behaviour of GH-bearing sands to conclude that as the GH content occupying the pores increases, the cementing forces between the grains increase and therefore the peak deviatoric stress of the sample increases. The general trend for volumetric strain of GH bearing sands exhibited a compressive behaviour at first changing to dilative as the shearing progressed. However, this tendency seems to change with increasing confining pressure: volumetric strain shows a strictly compressive behaviour at higher confining pressure values. On the other hand, Hyodo et al. (2013) discussed that such behaviour is particular to GHBS formed using the gas-saturated method.

Xiu et al. (2019) conducted experimental studies on the mechanical properties of methane hydrate bearing sandy sediments in a way to obtain two types of gas hydrate morphology. Results have shown that the morphology of GH is changing from grain contacts to pore spaces with increasing GH content. Additionally, the shear strength, stiffness and dilation were found to increase with increasing GH content. Alternatively, Chen et al. (2019); Ebinuma et al. (2015); Masui et al. (2005) and Yun et al. (2007) proved that as the GH content increases, the host sediment becomes stiffer and stronger. Hyodo et al. (2013) and Masui et al. (2005) showed that compared to reference sediments without GH, GHBS were more dilative when subjected to shearing.

In the following chapter the elastic (Young's Modulus, secant Young's modulus and secant Poisson's ratio) and mechanical (shear strength and dilatancy) properties will be discussed

6.2.2.1 Elastic parameters: Young's Modulus E_0, secant Young's modulus E_{50} and secant Poisson's ratio v_{50}

In order to understand the mechanical properties of a given material, it is important to evaluate its elastic properties: Young's modulus and Poisson's ratio, which represents the stiffness of the material and its Poisson effect respectively.

The stiffness of material is the slope of its stress strain curve and the Poisson's ratio is the ratio of the lateral strain over the axial strain. Masui et al. (2008) and Miyazaki et al. (2011) performed studies showing the effect of GH on the elastic parameters of gas hydrate bearing sediment (Figure 6. 4). It has been clearly observed that: (1) the stiffness of the sediment increases with increasing gas hydrate content, (2) the secant Poisson's ratio decreases with increasing confined pressure and (3) the secant Poisson's ratio does not seem to be affected by the increasing GH content. This is mainly due to the cementation effect between the sediment particles.

Miyazaki et al. (2011) have also observed that while the strength of a sediment is independent of the type of material used (coarse or fine-grained sands), the stiffness seems to be changing with the type of the used sediment. For instance, the stiffness of a fine-grained sand is lower than that of a coarse-grained sand.

6.2.2.2 Deviatoric Stress: Shear Strength

The effect of gas hydrate presence on the increase of the shear strength of the gas hydrate-bearing sediment is now experimentally well recognised (Masui et al., 2008; Mizayaki et al., 2011; Hyodo et al., 2013). Figure 6. 5 shows a synthesis of recent research studying the effect of GH on the strength and stiffness of their host sediment. The tests are of a consolidated drained type (CD) and the experimental conditions are presented in Table 6. 1.

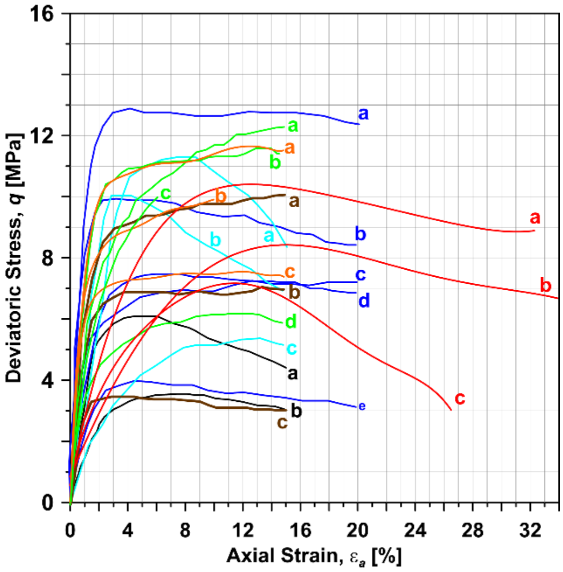

Figure 6. 5 Deviatoric stress against axial strain for GHBS (solid lines). The detailed legend for this image is presented in table 1.

It can be clearly observed that GHBS are characterised by higher deviatoric stress, and therefore higher strength, compared to GH free sediments. Winters at al. (2004) proved that this strength depends on many factors such as: GH content, cage occupancy and

Table 6. 1 Legend for Figure 1 showing the effective pressure, GH content, peak deviatoric stress, porosity and void ratio for each test CD triaxial test

Colour code	**Letter code**	**Reference**	**Effective Pressure (MPa)**	**Gas hydrate Content (%)**	**Peak Deviatoric Stress (MPa)**	**Porosity [%]**	**Void Ratio [-]**
🟥	a	Yang et al. (2019)	1.5	22	10.19	32	0.47
	b		1	22	8.07	32	0.47
	c		0.5	22	6.79	32	0.47
⬛	a	Masui et al. (2007)	6.11	37.6	6	44.2	0.79
	b		3.52	7.7	3.046	50.8	1.03
🟧	a	Hyodo et al. (2013)	5	35.1	10.35	40	0.66
	b		5	24.2	2.669	40	0.66
	c		3	53.7	6.97	40	0.66
🟦	a	Kajiyama et al. (2017)	5	41.9	12.72	39.1	0.64
	b		3	73.8	9.83	40.6	0.68
	c		3	38.9	5.4	40.5	0.68
	d		3	38.7	6.78	39.3	0.64
	e		1	54.3	3.64	39.4	0.65
🟦	a	Yoneda et al. (2015)	1.6	70	3.68	39.6	0.65
	b		1.6	79	1.03	39.4	0.65
	c		1.5	38	5.32	44.1	0.78
🟫	a	Hyodo et al. (2005)	5	21.2	9	43.25	0.76
	b		3	26.3	6.53	43.25	0.76
	c		1	23.5	3.35	43.25	0.76
🟩	a	Hyodo et al. (2014)	5	44.9	12.01	40	0.66
	b		5	35.1	10.44	40	0.66
	c		5	32.7	11.19	40	0.66
	d		2	43.1	5.94	40	0.66

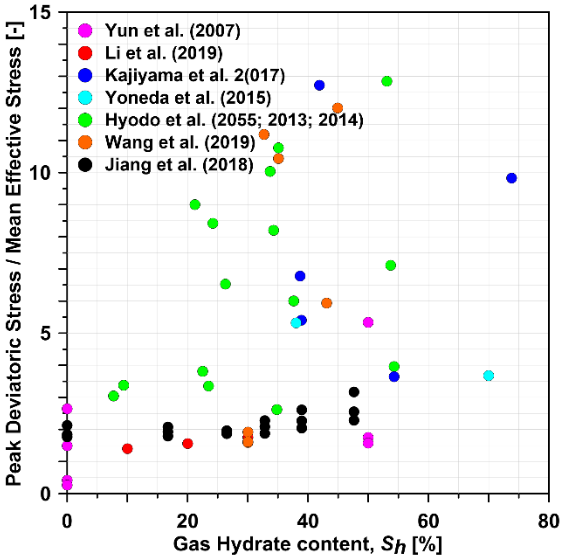

Figure 6. 6 Normalised peak deviatoric stress against GH content

effective confining pressure. Additionally, the adopted GH formation method highly influence the mechanical properties of the tested specimen (Winters et al., 2014). Indeed sediments with the same GH content but different GH morphologies can have different mechanical responses. It is important to note that the stress – strain curves are changing from strain softening to strain hardening with increasing effective confining pressure as well as with increasing GH content. For example curve (c) from Yang et al. (2019) (red curve (c) in Figure 6. 5 shows a strain-softening behaviour compared to that from Hyodo et al. (2014) (green curve (a) in Figure 6. 5), which is exhibiting a strain hardening behaviour.

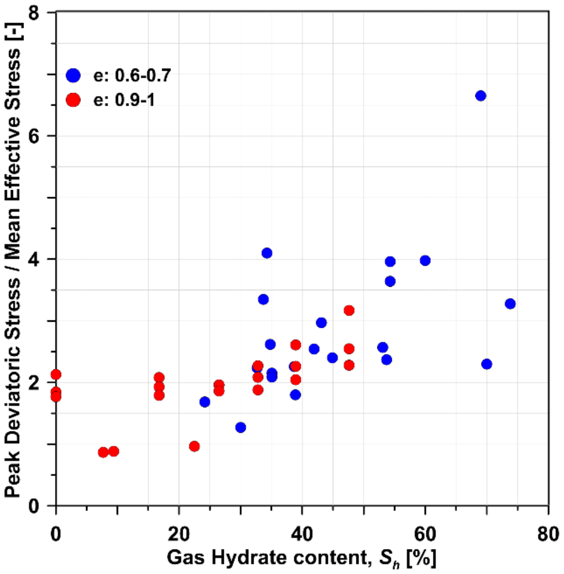

Figure 6. 7 Normalised peak deviatoric stress against gas hydrate content at different void ratio values (data from table 6.1, table 6.2 and table 6.3)

In Figure 6. 6 are presented the normalised peak deviatoric stresses against the GH content for GHBS. One might say that the strength of GHBS increase with increasing GH content. However, Figure 6. 6 shows GHBS with the same content of GH but with different normalised peak deviatoric stress values. This is mainly due to the presence of different GH morphologies resulting from different formation habits. Grozic and Ghiassian (2010) showed that GHBS with 60% GH content *(dissolved gas method)* exhibit insignificant strength increase compared to a specimen with 69% GH content *(partially saturated specimen)*. Since there is no great difference in the gas hydrate content, this was attributed to the hydrate formation mode. Indeed, Winters et al. (2014) have noticed that following the dissolved gas method results in GH filling the pore space and acting as extra particles; therefore, not greatly affecting the strength of the host sediment nor contributing to the cementation between the particles.

In the following sections, the effect of GH content, effective confining pressure and that of void ratio on the strength of the host sediment will be discussed. Figure 6. 6 shows the effect of initial void ratio on the gas hydrate bearing sediment. The general trend one may observe at first is that the peak deviatoric stress is increasing with increasing GH content. It can also be observed that for sediments with initial void ratio ranging between 0.6-0.7, the peak deviatoric stress reaches higher values compared to sediment with higher initial void ratios (0.9-1). Such observations are supported by results found by Hyodo et al. (2013).

Figure 6. 8 shows peak deviatoric stress against GH content at different confining pressure values in order to highlight the effect of the latter on the mechanical response of GHBS.

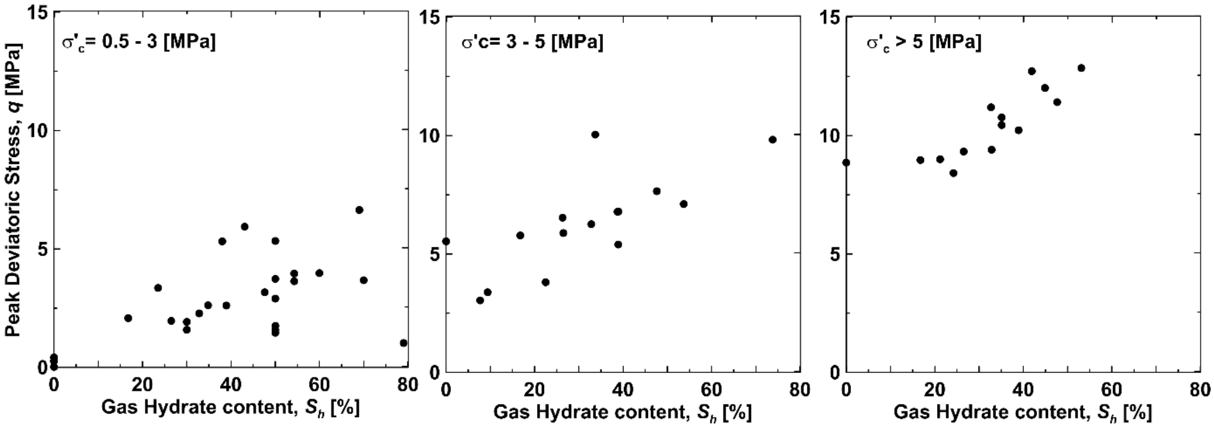

Figure 6. 8 Peak deviatoric stress against gas hydrate content at different effective mean stress values: a) 0.5-3 MPa, b) 3-5 MPa and c) higher than 5 MPa. Data used in these figures are presented in Table 6.1 and Table 6.3

All three parts Figure 6. 8 exhibit an increasing peak deviator stress with increasing GH content as well as with increasing effective confining pressure. It is also noteworthy that in all three cases the peak deviatoric stress is observed to increase with increasing the effective mean stress along the same trend. However looking at Figure 6. 5 peak deviator stress for almost all tests took place between 3% - 4% axial strain regardless of the value of the effective confining pressure. This shows that, in addition to cementation forces resulting from the presence of GH, there is a frictional contribution to the strength increase of GHBS.

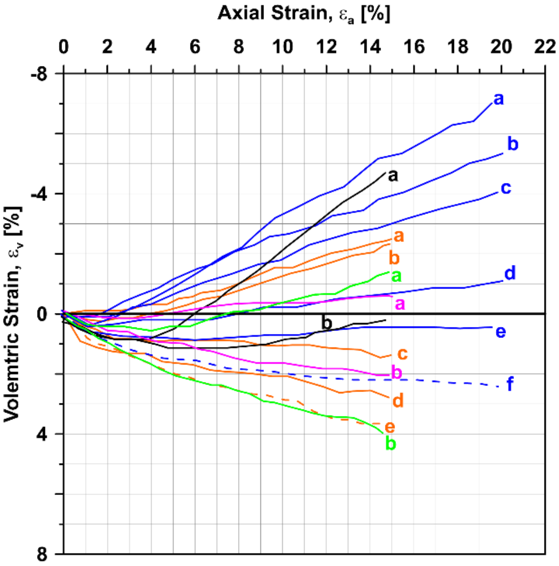

Figure 6. 9 Volumetric strain against axial strain for GHBS (solid lines) and GH free sediment (dashed lines). The detailed legend for this image is presented in table 6.2

6.2.2.3 *Volumetric Strain: Dilatancy*

Figure 6. 9 shows a literature review of recent research studying the effect of GH on the strength of their host sediment. The tests are of a consolidated drained type and the experimental conditions are presented in Table 6. 2. For almost all curves, a general trend can be observed: GHBS under an effective confining pressure inferior to 3 MPa exhibit a compressive volumetric strain, in the first stages of axial strain, which changes into dilative as the test progresses. However, under higher effective confining pressure (5 MPa), GHBS are immediately characterised by a compressive volumetric strain.

Figure 6. 10 represents the effect of effective confining pressure (left) and void ratio (right) on the volumetric strain – gas hydrate content relation at 5%, 10% and 25% axial strain.

Effect of effective confining pressure:

- *At 10% axial strain:* the volumetric strain is observed to decrease for effective confining pressure ranging between 0.5 MPa – 5 MPa. However, when the 5 MPa threshold is exceeded, the volumetric strain starts to increase. This is in line with earlier discussions, stating that at higher effective confining pressures, GHBS will continuously exhibit a compressive behaviour rather than change from a compressive to a dilative behaviour as shearing progresses.
- *At 15% axial strain:* same observations as for the 10% axial strain applies to this case. Volumetric strains at effective confining pressure less than 5 continue to decrease while the ones at 5 MPa increases.

Effect of void ratio:

For the void ratio differences, the data is more scattered. At 5%, 10% and 15% axial strain, the volumetric strain seems to be increasing with GH content for the void ratio ranging between 0.9 and 1 but decreasing for lower void ratio (0.6-1). This observation seems logical since loose sands (higher void ratio) tend to contract while dense sands (lower void ratio) tend to dilate upon shearing.Throughout this section, the effect of GH on their host sediment has been highlighted under different experimental conditions. It has been proved that the strength and dilatancy of gas hydrate bearing sands are highly affected by the GH content and morphology as well as by the applied mean effective stress and the initial void ratio.

a) At 5% ε_a

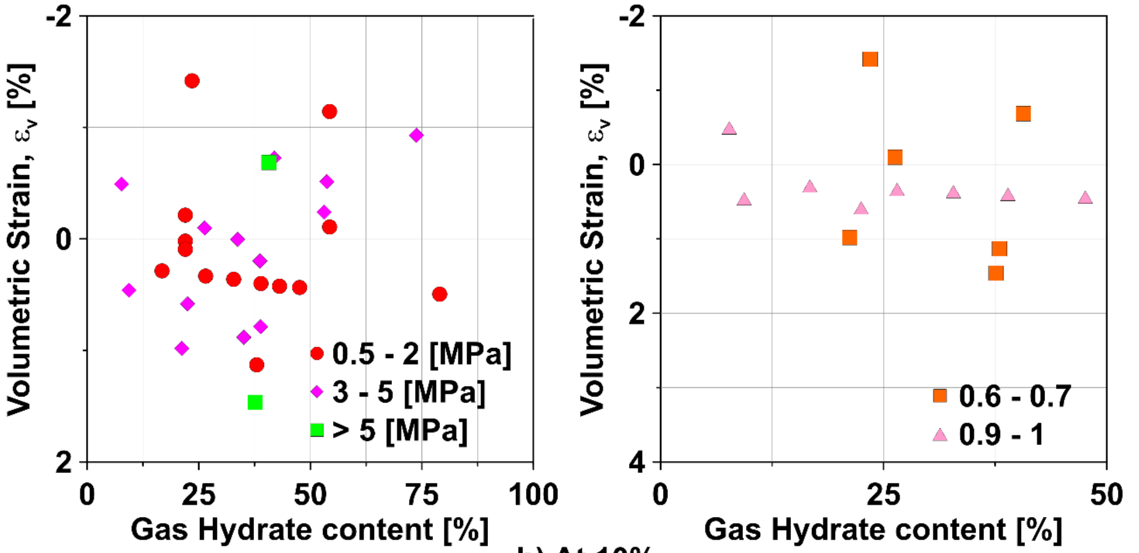

b) At 10% ε_a

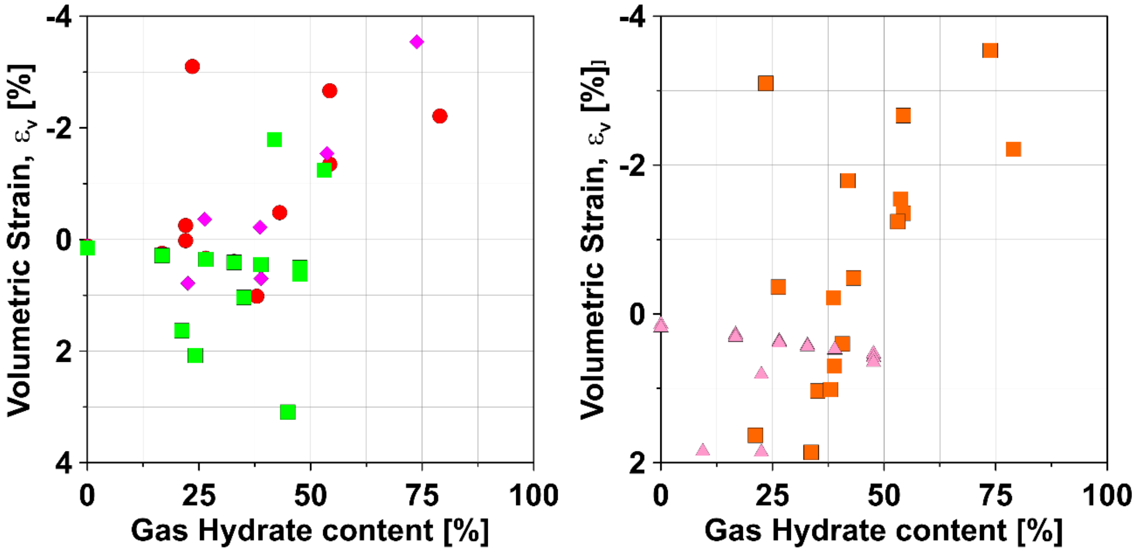

c) At 15% ε_a

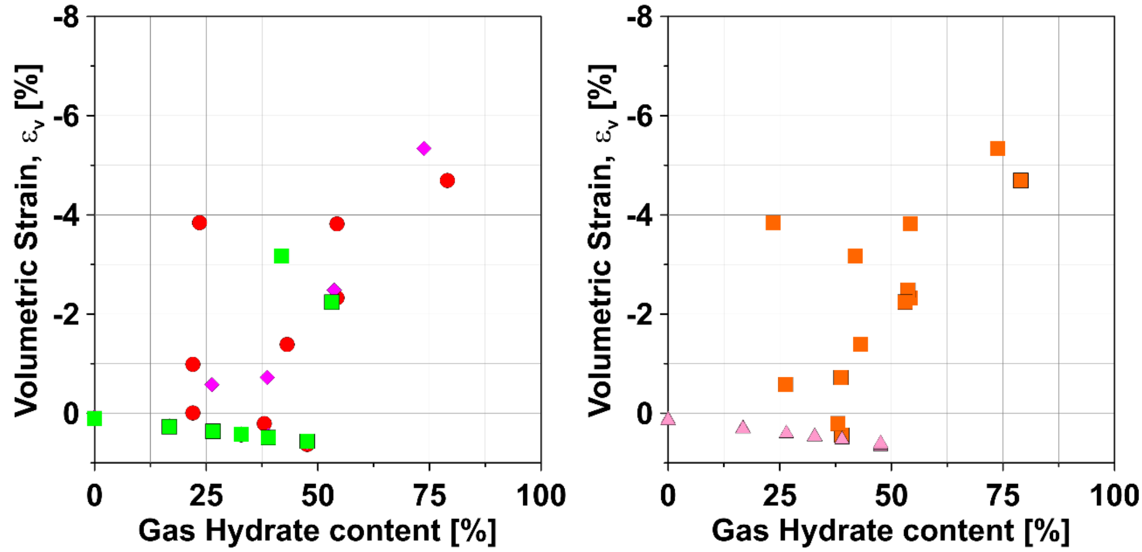

Figure 6. 10 Effect of effective confining pressure (left) and void ratio (right) on the volumetric strain as a function of gas hydrate content at: a) 5% axial strain, b) 10% axial strain and c)15% axial strain

Table 6. 2 Legend for Figure 6.8 showing the effective pressure, GH content, peak deviatoric stress, porosity and void ratio of specimens subjected to CD triaxial test

Colour code	**Letter code**	**Reference**	**Effective Pressure (MPa)**	**Gas hydrate Content (%)**	**Porosity [%]**	**Void Ratio [-]**
🟧	a	Hyodo et al. (2013)	3	53.7	40	0.66
	b		1	54.3	40	0.66
	c		5	35.1	40	0.66
	d		5	24.2	40	0.66
	e		5	0	40	0.66
🟦	a	Kajiyama et al. (2017)	3	73.8	40.6	0.68
	b		1	54.3	39.4	0.65
	c		5	41.9	39.1	0.64
	d		3	38.7	39.3	0.647
	e		3	38.9	40.5	0.68
	f		3	0		
⬛	a	Yoneda et al. (2015)	1.6	79	39.4	0.65
	b		1.5	38	44.1	0.78
🟪	a	Hyodo et al. (2005)	3	26.3	45.25	0.82
	b		5	21.2	43.25	0.76
🟩	a	Hyodo et al. (2014)	2	43.1	40	0.66
	b		5	44.9	40	0.66

Table 6. 3 Data from CD triaxial tests used in the study but not shown in Figure 6.5 and Figure 6.9

Reference	**Effective Pressure [MPa]**	**GH content [%]**	**Peak Deviatoric Stress [MPa]**	**Porosity [%]**	**Void Ratio [-]**
Li et al. (2019)	3	10	1.4		
	3	20	1.56		
	3	30	1.75		
Masui et al. (2007)	3.95	22.5	3.81	49	0.96
	3.82	9.38	3.38	49.3	0.97
Masui et al. (2005)	3	33.7	10.04	37.5	0.60
	2	34.3	8.2	37.5	0.60
	1	34.8	2.62	37.5	0.60
Hyodo et al. (2013)	1	54.3	3.96	40	0.67
Grozic and Ghiassian (2010)	1	69	6.65	37.5	0.60
	1	60	3.98	37.5	0.60
Jiang 2018	1	47.62	3.16	48.45	0.94
	1	38.94	2.61	48.45	0.94
	1	32.83	2.27	48.45	0.94
	1	26.52	1.96	48.45	0.94
	1	16.75	2.07	48.45	0.94
	1	0	2.13	48.45	0.94
	3	47.62	2.54	48.45	0.94
	3	38.94	2.26	48.45	0.94
	3	32.83	2.08	48.45	0.94

	3	26.52	1.96	48.45	0.94
	3	16.75	1.92	48.45	0.94
	3	0	1.84	48.45	0.94
	5	47.62	2.28	48.45	0.94
	5	38.94	2.04	48.45	0.94
	5	32.83	1.87	48.45	0.94
	5	26.52	1.86	48.45	0.94
	5	16.75	1.7	48.45	0.94
	5	0	1.77	48.45	0.94

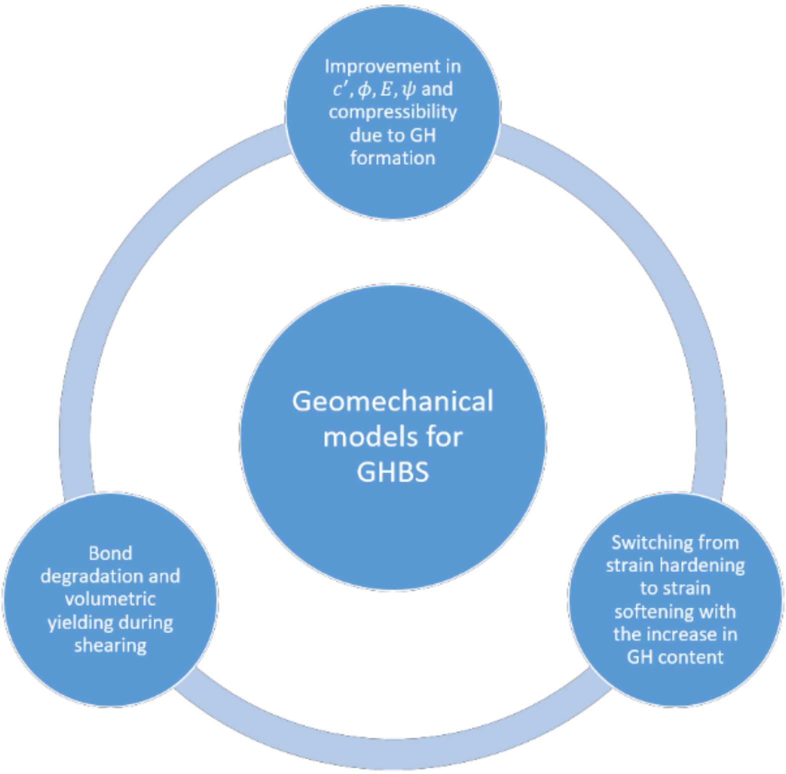

Figure 6. 11 Main objectives of developing a model able to simulate the mechanical behaviour of gas hydrate bearing sediments (modified from Lijith et al. 2019)

In general, the peak deviatoric stress was observed to increase with increasing GH content as well as with increasing mean effective pressures. Moreover, the peak deviatoric stress was observed to reach higher values with decreasing void ratio. Therefore, theoretical models need account to account for such features in order to simulate the mechanical response of coarse-grained materials in the presence of gas hydrates.

6.3 Available research on numerical models investigating the mechanical properties of GHBS

Many efforts in Geomechanics have been made in the last decades in order to simulate the mechanical response of gas hydrate bearing sediments (GHBS) using various models such as the Mohr-Coulomb model (Freij-Ayoub et al. 2007; Klar et al. 2010;; Pinkert et al. 2017) and the critical state model (Sultan and Garziglia 2011, Uchida et al. 2012; Gai and Sanchez 2017).

Table 6. 4 Parameters in the hypoplastic model proposed by Zhang et al. (2017)

Zhang et al. (2017): Hypoplastic model for gas hydrate-bearing model			
Model Type	Parameter	Physical significance	Value
Model I: Shear strength modelled by the Drucker-Prager criterion	C1 C2 C3 C4	Dimensionless material parameters	Depends on the initial tangent modulus, initial Poisson ratio, and the failure stress ratio.
Model II: Shear strength modelled by Mohr-Coulomb criterion			
Model III: Hypoplastic model for the strain softening of GHBS			

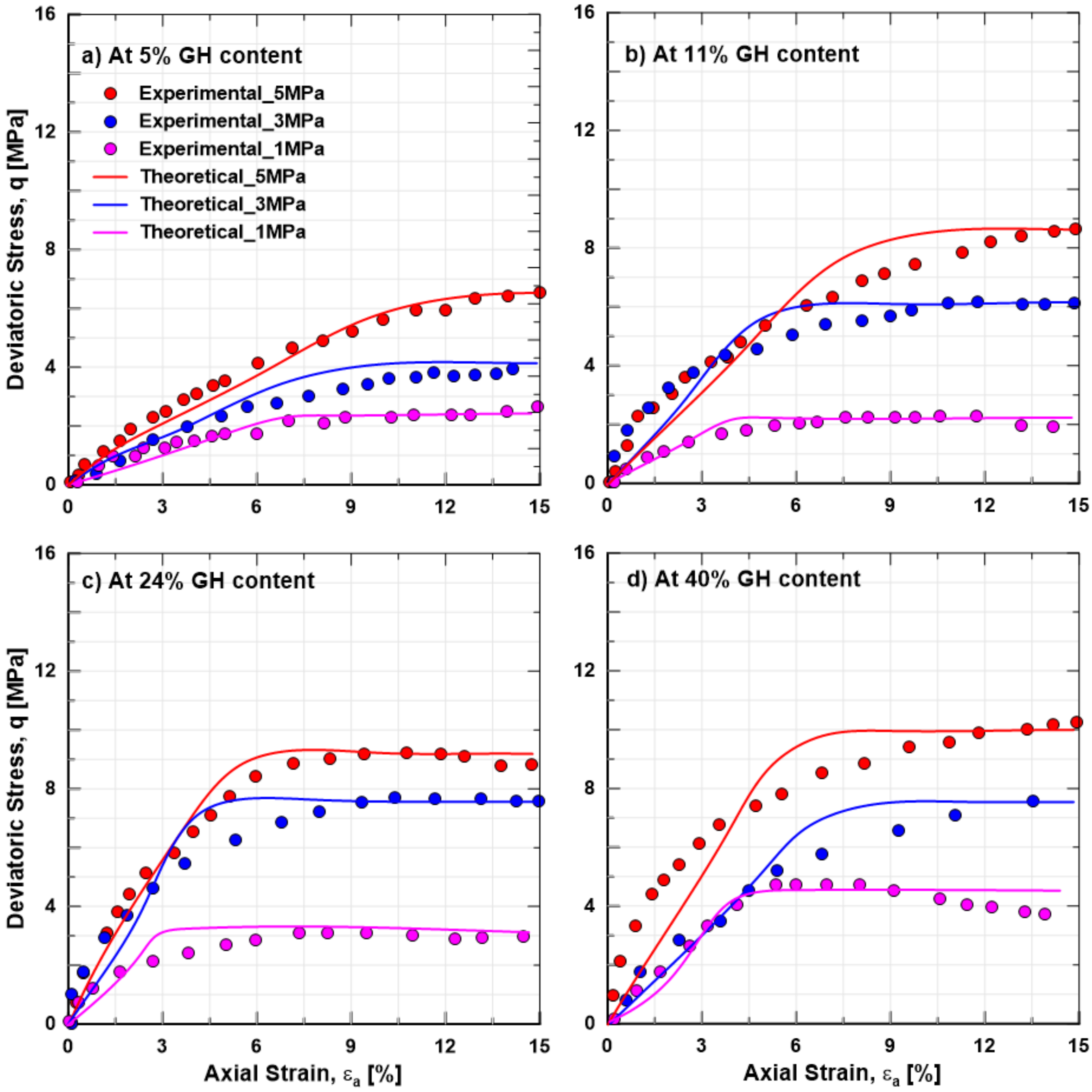

Figure 6. 12 Comparison between theoretical and experimental results of stress-strain curves accounting for the effect of different confining pressures (5MPa, 3MPa and 1 MPa) and of different GH content: a) 5%, b) 11%, c) 24% and d) 40% on the mechanical behaviour of GHBS (modified from Zhang et al. 2017)

Table 6. 5 Parameters for critical state constitutive model proposed by Uchida et al. (2012), Gai and Sanchez (2017) and Sanchez et al. (2017)

Uchida et al. (2012): Critical state constitutive model for methane hydrate soil		**Gai and Sanchez (2017): Geomechanical model for gas hydrate-bearing sediments**		**Sanchez et al. (2017): Geomechanical model for gas hydrate-bearing sediments incorporating inelastic mechanisms**	
Parameter	**Physical significance**	**Parameter**	**Physical significance**	**Parameter**	**Physical significance**
λ	Slope of normal compression line	λ	Slope of normal compression line	λ	Slope of normal compression line
κ	Slope of swelling line	κ	Slope of swelling line	κ	Slope of swelling line
p'_{cs}	Pre-consolidation stress	p_c	Pre-consolidation stress	p_c	Pre-consolidation stress
M	Slope of the critical state line	M	Slope of the critical state line	M	Slope of the critical state line
n	porosity	n	Parameters controlling the shape of yield surface	a	Parameters controlling the shape of yield surface
u	Material constant controlling plastic deformation while soil is elastic	a		n	
p'_{cd}	Hardening dilation parameter	γ		γ	
p'_{cc}	Hardening cohesion parameter	S_h	GH content	C_h	Volumetric concentration of GH
G	Shear modulus	α	Degree of GH contribution to the hardening law	α	Degree of GH contribution to the hardening law
m	Rate of mechanical degradation	β		β	
		μ	Rate of mechanical damage	r_1	Rate controlling damage
		η	Rate of sub-loading yield surface	r_0	Hydrate damage locus
				η	Rate of sub-loading yield surface
				χ_0	Strain partition evolving through loading: initial reference value
				K_h	Bulk modulus
				G_h	Shear modulus

Figure 6. 11 shows the main three objectives these models aim to accomplish. Zhang et al. (2017) conducted numerical as well as experimental studies in order to investigate the mechanical properties of GH-bearing sandy sediments. The model is based on a hypoplastic approach and requires four dimensionless material parameters (see Table 6. 4). Experimental results confirmed earlier observations for GHBS and were compared to numerical modelling ones at different confining pressure values and different GH content (Figure 6. 12). The proposed model by Zhang et al. (2017) yielded very close estimates to those derived from experimental data. Sultan and Garziglia (2011), proposed a geomechanical constitutive model in order to theoretically account for the effect of GH on the mechanical properties of their host sediment. The model is developed in the framework of a critical state model and requires 12 parameters. The model was validated by comparing its results with experimental ones performed on natural and synthetic sand samples containing GH from Masui et al. (2008, 2005). While results were rather satisfactory and the model succeeded in reproducing the main features of the mechanical behaviour of GHBS, the simulated post-peak behaviour did not capture the smooth strain softening behaviour reported in Masui et al. (2005).

Uchida et al. (2012) presented a critical state constitutive model for methane hydrate soil that considers the effect of GH on the stress-strain behaviour of the soil. The model can predict the behaviour of GHBS with GH content of up to 70%, where experimental data exists.

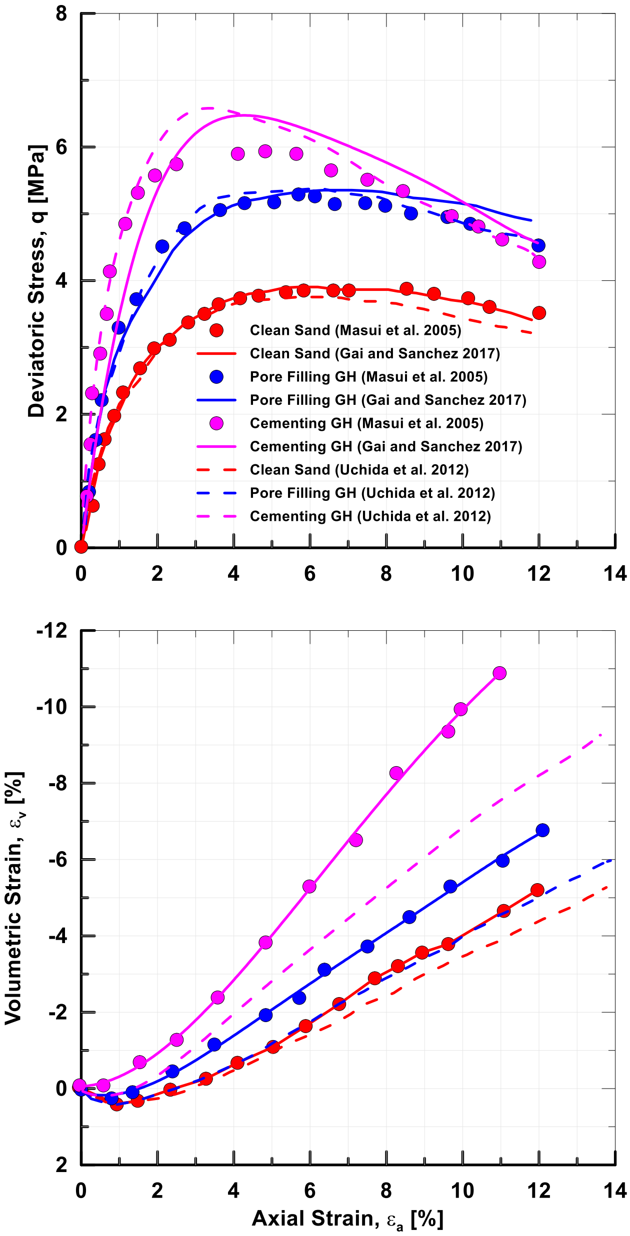

Figure 6. 13 Comparison between experimental and numerical results accounting for the effect of GH morphology on a) the stress-strain behaviour and b) the deformation behaviour of GHBS from Masui et al. (2005), Gai and Sanchez (2017) and Uchida et al. (2012)

This model is an enhanced form of the MCC model as it contains five extra parameters, which can simulate the enhancement in c', E, strain softening and volumetric behaviour of GHBS.

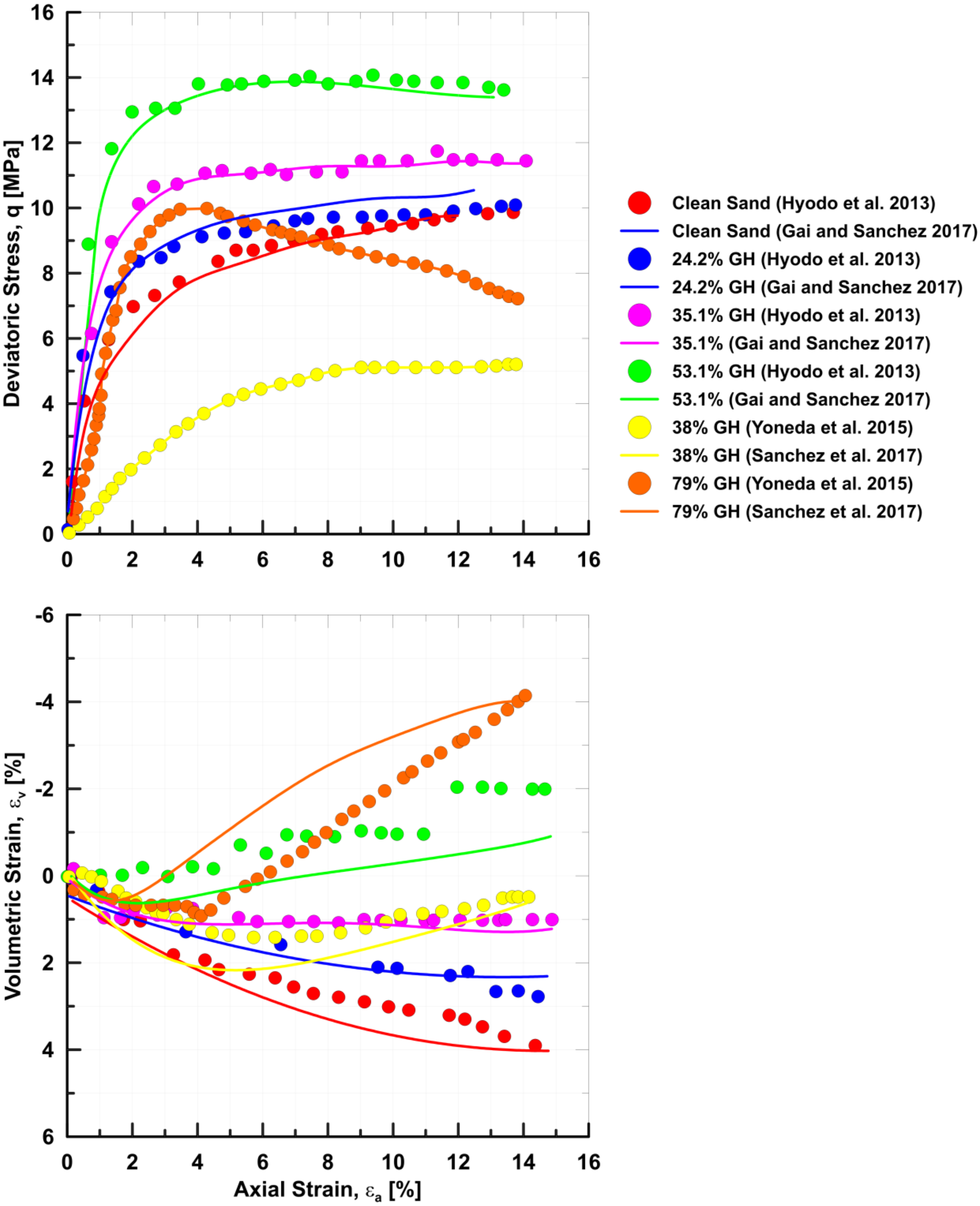

Figure 6. 14 Comparison between experimental and numerical results accounting for the effect of GH content on a) the stress-strain behaviour and b) the deformation behaviour of GHBS from Hyodo et al. (2005) and Gai and Sanchez (2017)

Details about the model's parameter are presented in Table 6. 5.

Results have shown that GH morphology (cementing and pore-filling) greatly influence the mechanical behaviour of GH bearing soil. The cementing GH contributes more to the strength and dilatancy enhancement compared to pore-filling GH. Parameters such as the slopes of the critical state line ($M = 1.07$), the slope of the normal compression line ($\lambda = 0.16$) and the slope of the swelling line ($\kappa = 0.004$) are independent of GH morphology as they are soil material properties.

Lin et al. (2015) developed a CS model that is able to show enhancement in E, ψ and strain softening with hydrate formation. Nevertheless, results have shown that the model was not able to accurately determine the volumetric behaviour of the GHBS. Following that, Gai and Sanchez (2017) proposed an elastoplastic constitutive model that considers the bonding and damage effects during shearing and requires 12 parameters (Table 6. 5). This model allows smooth transition between the elastic and plastic behaviour of GHBS and accounts for the inelastic deformation of GHBS within the yield surface. Another constitutive mechanical model for GHBS, which requires 13 parameters, has been later proposed by Sanchez et al. (2017). The model proposes the concept of dividing the mechanical loads between the hydrate and the soil and was able to show the effect of GH content and dissociation on the mechanical properties of GHBS (Table 6. 5).

A comparison between experimental (Masui et al. 2005) and model results (Uchida et al. 2012; Gai and Sanchez, 2017) accounting for the effect of GH morphology on the mechanical properties of GHBS is presented in Figure 6. 13. Experimental and modelling results, agree in revealing that cementing GH morphology exhibit a stronger, stiffer and more dilative behaviour compared to pore filling GH (Figure 6. 13). It is also clear that the presence of GH enhances the strength and the stiffness of the host sediment. Gai and Sanchez (2017) introduced a parameter (α) in their model to capture the effect of GH pore habit. Higher values of (α) were attributed to the cementing case and lower ones to the pore filling case. Alternatively, Uchida et al. (2012) adjusted their dilation (p'_{cd}) and cohesion (p'_{cc}) parameters to account for different GH morphologies. Based on Figure 6. 13, the models developed by Gai and Sanchez (2017) and Uchida et al. (2012) succeeded in reproducing the results from experimental investigations performed by Masui et al. (2005) for the cases of clean sand and pore filling GH morphology. However, an underestimation can be identified for the cementing GH morphology for both models (Figure 6. 13).

In order to highlight the effect of GH content on the mechanical properties of GHBS, a comparison between experimental (Masui et al. 2005; Yoneda et al. 2015; Hyodo et al. 2013) and model results (Gai and Sanchez, 2017; Sanchez et al. 2017) is presented in Figure 6. 14. It is clear that specimens with higher GH (from Hyodo et al., 2013) content stronger and stiffer, except for the 79% GH content specimen from Yoneda et al. (2015). This might be due to the use of different GH formation conditions as well as the presence of different GH morphologies, which have been proven to highly affect the mechanical response of the GHBS. Experimental results from Masui et al. (2005), Yoneda et al. (2015) and Hyodo et al. (2013) show that dilation increases with increasing GH content (Figure 6. 14.b). The modelling results from Gai and Sanchez (2017) and Sanchez et al. (2017) proved reliable in predicting the stress-strain response of specimens (Figure 6. 14.a). On the other hand, the modelling results were found to underestimate the dilatant behaviour presented by the experimental results (Figure 6. 14.b).

6.4 New simple constitutive model for GHBS using the critical state soil mechanics

Most of the GHBS constitutive mechanical models of Mohr-Coulomb or critical state type. Models based on the critical state theory are considered amongst the most advanced ones and some of them showed very realistic results when compared to experimental data (see for instance Figure 6. 12, Figure 6. 13 and Figure 6. 14). However, those models rely on an important number of physical and empirical parameters that need to be determined prior to reproduce the natural mechanical behaviour of GHBS.

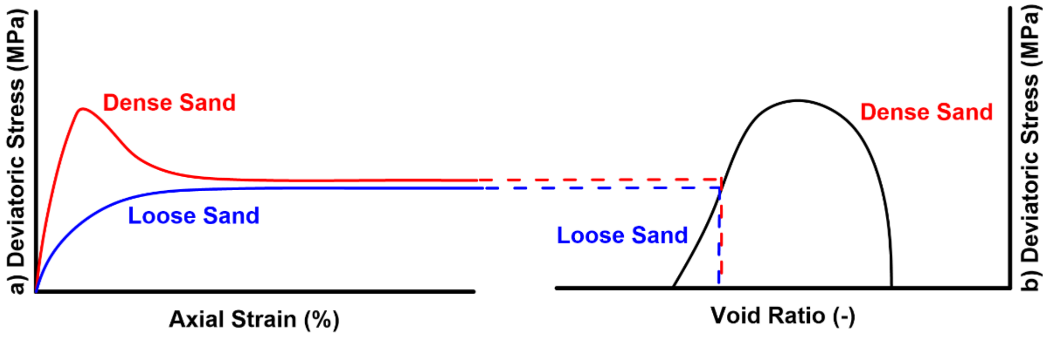

Figure 6. 15 a) stress-strain and b) stress-void ratio for loose and dense sands. While loose sands are characterised by a contractive behaviour correlating with a decrease of the void ratio, dense send exhibit a dilative behaviour and an increasing void ratio during shearing. At large strains, both specimens reach the same critical void ratio

For instance, the *Uchida et al. (2012) model needs 10 parameters, while the Gai and Sanchez (2017) need* 12 parameters. Therefore, in this section a new simple model based on the modified Cam Clay theory, which considers the hydrate impact through the "equivalent skeleton void ratio" is proposed. A new formulation of the steady state locus in e-p' space is also included in order to consider the dilative/contractive behaviour of sand during shearing through a parameter entitled β. In addition to the classical modified Cam Clay parameters, this new model requires a parameter that is equivalent to the Gai and Sanchez (2017) "α", which accounts for the effect of GH morphology. The fact that a minimum amount of parameters is required is at the same time advantageous and challenging. In other words, while the model might not be able to precisely reproduce experimental results of GHBS mechanical properties as other introduced models (Figure 6. 12 Figure 6. 13 and Figure 6. 14); it remains simpler to use, as it requires a minimum amount of parameters.

6.4.1 Steady state line and void ratio path during mechanical loading

In the Cam Clay model, the contractive/dilative behaviour during shearing cannot be reproduced for normally consolidated or slightly over-consolidated materials. However, this feature is essential in order to describe the mechanical behaviour of sand during shearing.

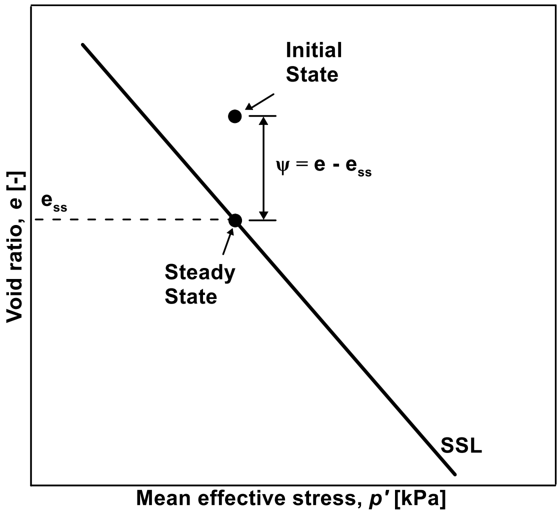

Figure 6. 16 Illustration showing the concept of the state parameter

The modern understanding of soil strength evolution is mainly based on triaxial tests conducted by Casagrande 1936 on initially loose and dense sands. It has been observed that all tested specimens eventually approached the same density when sheared (critical density). This allowed characterising the void ratio correlating with the critical density as the critical void ratio (Figure 6. 15). Thus, a critical void ratio line was introduced and used to mark boundary between contractive and dilative regions, which respectively represent loose and dense sands.

Static and cyclic triaxial tests have allowed Castro (1969) to illustrate the mechanical response of loose, dense and intermediate density sand specimens. It was observed that loose sands are characterised by a peak shear strength followed by a sudden failure (or liquefaction), dense sands started to contract and then dilate and intermediate density sands exhibited a strain softening behaviour that was followed by a dilative behaviour. This is further confirmed by studies performed by Manzari and Dafalias (1997) and Wei and Yang (2018). These findings eventually allowed to draw a relationship between the void ratio and the effective confining pressure and define the so-called steady state of deformation. This is only observed to occur under large strains after omitting the effects of stress and strain history and loading conditions.

The steady state line can, therefore, be used to assess the ability of a particular soil to undergo important deformation (or even liquefaction). Correlating these observations with the critical state mechanics of soils, implies that loose sands under very low effective confining pressure located at the same distance from the steady state line should exhibit similar behaviour (Figure 6. 15). Been and Jeffries (1985) defined this logic by presenting a state parameter (Figure 6. 16):

$$\psi = e - e_{ss} \tag{6.1}$$

Where e_{ss} is the void ratio at the steady state line at a certain effective confining pressure.

The state parameter can be an indicator of the mechanical response of a given soil specimen: a positive state parameter correlates a soil with a contractive behaviour and a negative state parameter correlates a soil with a dilative behaviour.

In the present model, a new formulation is proposed: the void ratio path during loading is not necessary parallel to the critical state line as it is considered in the Cam Clay model. Therefore, the steady state line is defined by equation (4) where the critical void ratio e_{cr} depends on the reference critical void ratio e_{cr0}, on three intrinsic parameters $(\lambda_{cr}, \kappa \; and \; M)$ and on the stress path inclination $\eta = q/p'$.

$$e_{cr} = \left[e_{cr0} - (\lambda_{cr} - \kappa).\,ln\left(\frac{M^2+\eta^2}{M^2}\right)\right] - \lambda_{cr}.\,ln\left(\frac{p'}{p'_0}\right) \tag{6.2}$$

Where λ_{cr} is the slope of the critical state line in e-p’ space

Equation 6.2 indicates that e_{cr} is equal to $e_{cr0} - (\lambda_{cr} - \kappa).\,ln\left(\frac{M^2+\eta^2}{M^2}\right)$ while the mean effective stress $(p’)$ is equal to the reference mean effective stress (p'_0).

The void ratio path during loading is expressed using the following equation:

$$e = \left[\left(e_i - \lambda_{cr}.\,ln\left(\frac{p'}{p'_i}\right)\right) - e_{cr}\right].\,e^{-\beta\frac{\eta}{M}.(p'-p'_i)} + e_{cr} \tag{6.3}$$

The proposed equation considers that the void ratio path depends on the:

- Initial void ratios (e_i, e_{cr0}),
- Initial and reference mean effective stresses $(p'_i \; and \; p'_0)$,
- Three intrinsic parameters $(M, \lambda_{cr} \; and \; \kappa)$,
- Stress path inclination η and
- Shape parameter called β, which describes the way the void ratio reaches the locus of the steady state line (SSL) during shearing.

Equation (6.3) allows for the void ratio path to reach the SSL for high p’ values. This implies a dilative behaviour for void ratios below the SSL or a contractive behaviour for void ratios above the SSL.

Then, the classical Cam Clay formulation allows determining the void ratio (e) from the following equation:

$$e = e_i - \lambda.\,ln\left(\frac{p'}{p'_i}\right) \tag{6.4}$$

The slope of the normal compression line (λ) becomes variable and is expressed as:

$$\lambda = \frac{e_i - e_{cr} - e^{-\beta\frac{\eta}{M}\left(p'-p'_i\right)}.\left[\left(e_i - \lambda_{cr}.ln\left(\frac{p'}{p'_i}\right)\right) - e_{cr}\right]}{ln\left(\frac{p'}{p'_i}\right)} \tag{6.5}$$

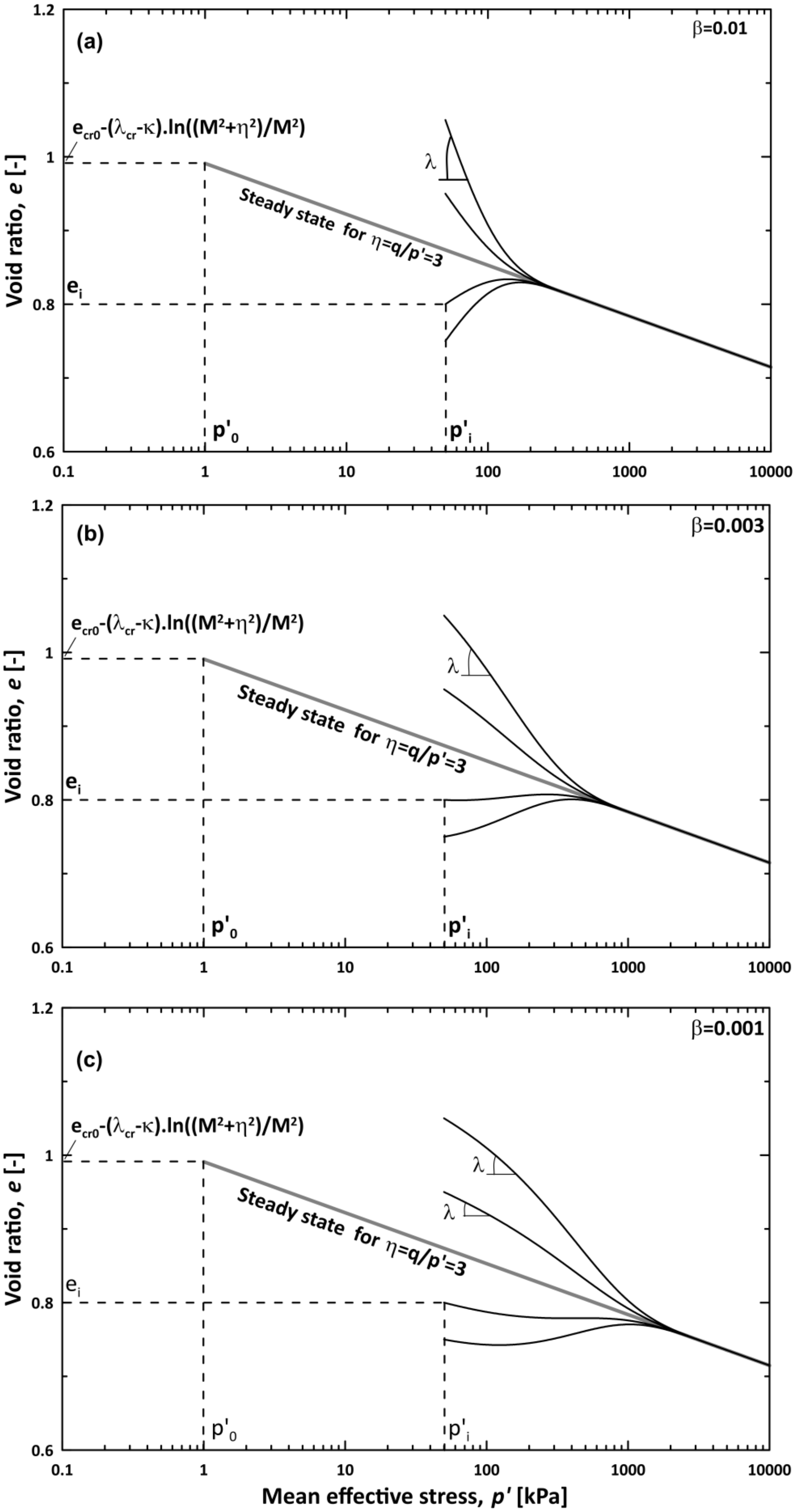

Figure 6. 17 Steady state lines for η=3 and void ratio paths during shearing for various β values. a) β=0.01, b) β =0.003 and c) β =0.001

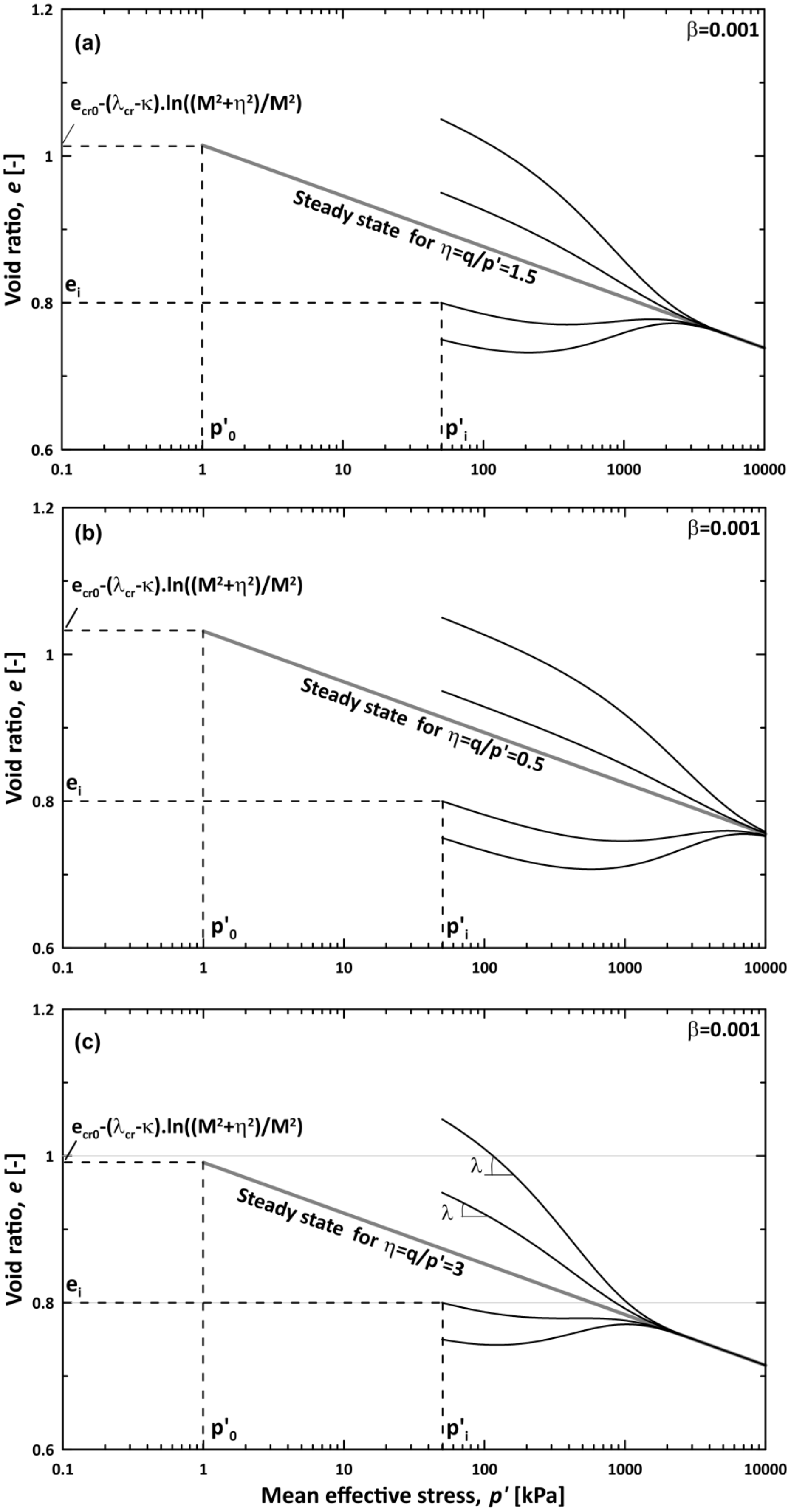

Figure 6. 18 Steady state lines for $\beta = 0.001$ and void ratio paths during shearing for various η values. a)$\eta = 0.5$, b) $\eta = 1.5$ and c)$\eta = 3$.

The impact of η and β values on the void ratio path in a $e - p'$ diagram is presented in Figure 6. 17 and Figure 6. 18. Figure 6. 17 shows the impact of β values for a constant η of 3. The void ratio – stress path reaches the SSL in $e - p'$ diagram faster for higher β values: the void ratio path reaches the SSL at a mean effective stress of 200 kPa for $\beta = 0.01$ and at 2000 kPa for $\beta = 0.001$. The main parameter controlling the dilatant or contractant behaviour during shearing is the position of the initial void ratio e_i with respect to the SSL.

Figure 6. 18 clarifies the impact of η on the void ratio for a constant β value of 0.001. The void ratio path reaches the SSL in e-p' diagram faster for higher η values: the void ratio path reaches the SSL at a mean effective stress of 2000 kPa for η =3 and at 10000 kPa for η =0.5. For low η values (Figure 6. 18.a), a tendency towards a contractive behaviour may be observed even if e_i is below the SSL. Indeed, the proposed formulation suggests that under isotropic loading, the Steady State Lines are all parallel and the void ratio decreases (indicating a contractive behaviour) during loading. This is illustrated in Figure 6. 20 and where the case of fully isotropic loading ($\eta = 0$) is considered.

For isotropic loading, equations 6.6 to 6.8 indicating the locus of the SSL in $e - p'$ diagram can be simplified as follows:

$$e_{cr} = e_{cr0} - \lambda_{cr}\, ln\left(\frac{p'}{p'_0}\right) \tag{6.6}$$

$$\lambda = \lambda_{cr} \tag{6.7}$$

$$e = e_i - \lambda\, ln\left(\frac{p'}{p'_i}\right) \tag{6.8}$$

It is also interesting to show that for $\beta = 0$ and even if η is not equal to $0, \lambda$ becomes constant and equal to λ_{cr}. In fact, $\beta = 0$ corresponds to the modified Cam Clay formulation.

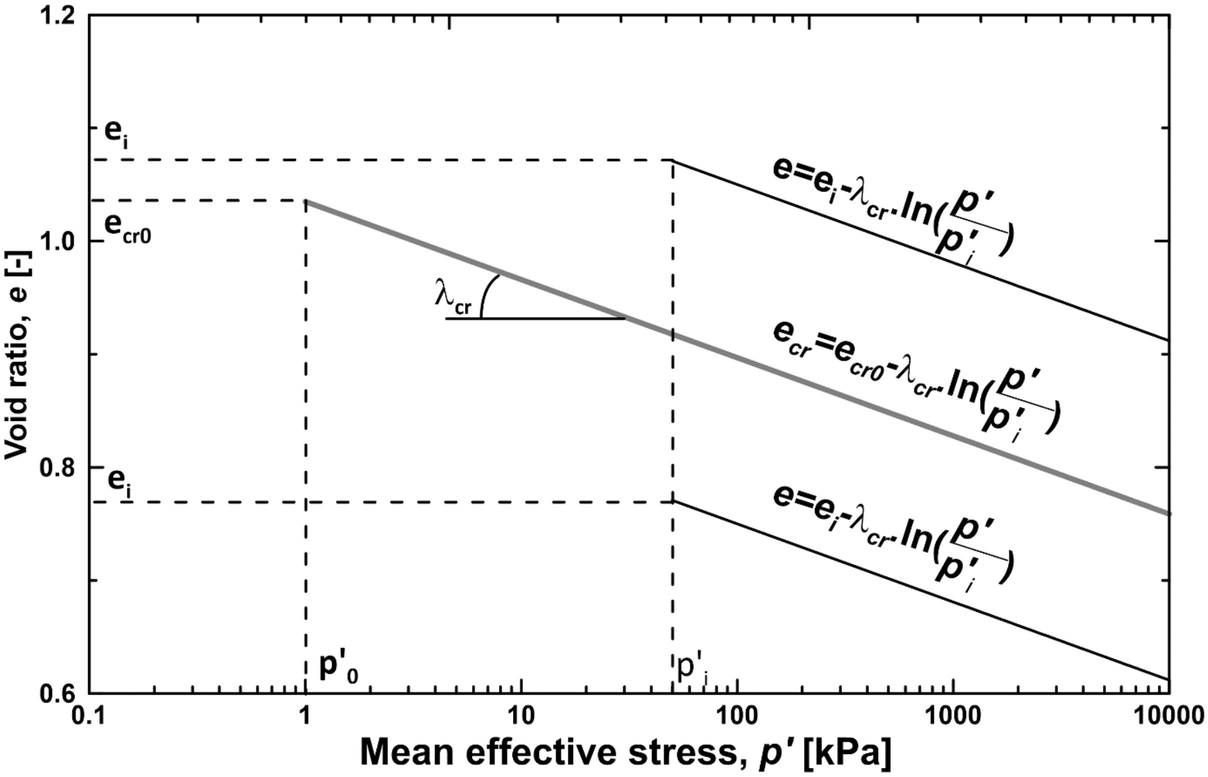

Figure 6. 19 e-p' diagram and void ratio paths for various initial void ratio.

6.4.2 Gas hydrate and void: the equivalent skeleton void ratio

We define an equivalent skeleton void ratio e_{ih}, which depends on the initial void ratio e_i at which the hydrate was formed, on the hydrate saturation S_h and on a "b" parameter corresponding to the fraction of hydrate effectively affecting the structure and the mechanical behaviour of the sample.

$$e_{i_h} = e_i.(1 - b.S_h) \qquad (6.9)$$

The situation where b equals to 0 corresponds to the case where the presence of hydrate is not impacting the mechanical behaviour of the sand while b equal to 1 corresponds to the upper bound limit where the hydrate behaviour is considered equivalent to the solid matrix. This formulation is based on previous works carried out on sand with fines and where the equivalent skeleton void approach was shown to be convenient for complex materials (Thevanayagam et al., 2002; Rahman et al., 2008).

The void ratio expression becomes (equation 6.10):

$$e = e_i.(1 - b.S_h) - \lambda.\,ln\left(\frac{p'}{p'_i}\right) \qquad (6.10)$$

The decrease of the void ratio due to the presence of gas hydrate is expected to affect the compressibility of the host sediments. Our working hypothesis is that, under isotropic loading, the void ratio of the GH bearing sediment will follow the κ line until reaching the corresponding Steady State Line (Sultan and Garziglia, 2011). This hypothesis leads to an increase of the preconsolidation pressure p'_{c0} according to the following equation (eq. 6.11):

$$p'_{c0h} = p'_{c0} e^{\frac{S_h.b.e_i}{\lambda - \kappa}} \qquad (6.11)$$

Where p'_{c0h} is the virtual preconsolidation pressure affected by the presence of gas hydrate.

Figure 6. 20 shows the evolution of the normalized preconsolidation pressure $\frac{p'_{c0h}}{p'_{c0}}$ as a function of hydrate saturation for different b values. For $b = 0$, the presence of hydrate is not affecting the preconsolidation pressure. Figure 6. 21 shows a set of calculation results for three different $S_h and\ b$ values. It can be observed how the void ratio of GHBS follows the κ line until reaching the Steady State Line.

During shearing, yielding may occur before reaching the preconsolidation pressure leading to plastic deformation and dilatancy. This is illustrated in Figure 6. 22 where the stress path A-C cross the virtual yield curve at B leading to dilatancy in order to reach the corresponding SSL. It is important to notice that the deviatoric stress path A-C without gas hydrate is expected to generate contractancy.

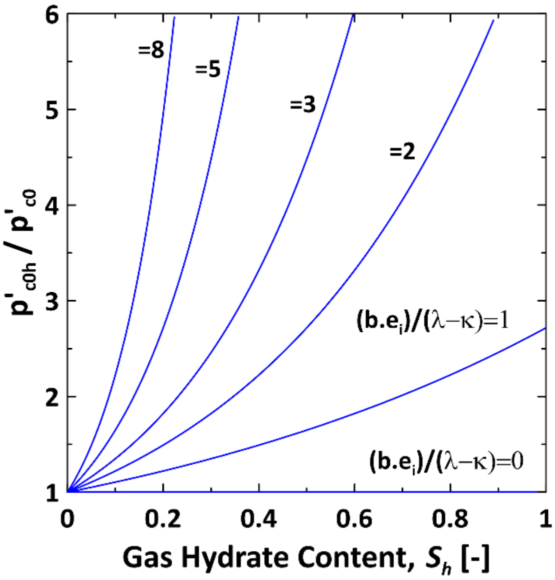

Figure 6. 20 Normalized preconsolidation pressure $\frac{p'_{c0h}}{p'_{c0}}$ as a function of hydrate saturation for different b values

For clayey materials, the compressibility may be strongly affected by the hydrate occurrence. Therefore, the λ can be modified in order to include the compressibility of the pure hydrate as it was suggested by Sultan et al. (2010). The void ratio can therefore be expressed by the following expressions (equations 6.12 and 6.13):

$$e = e_i.(1 - b.S_h) - \lambda_h.\,ln\left(\frac{p'}{p'_i}\right) \qquad (6.12)$$

With

$$\lambda_h = \lambda.\left(1 - \left(1 - \frac{\lambda_1}{\lambda}\right).(1 - e^{-\beta_h.S_h})\right) \quad (6.13)$$

Where λ_1 is the compressibility of pure hydrate (=0.00147) (Durham et al., 2003). Equation (6.16) suggests that the compression indices of the GHBS (λ_h) are expected to asymptotically decrease from a value typical of purely water-

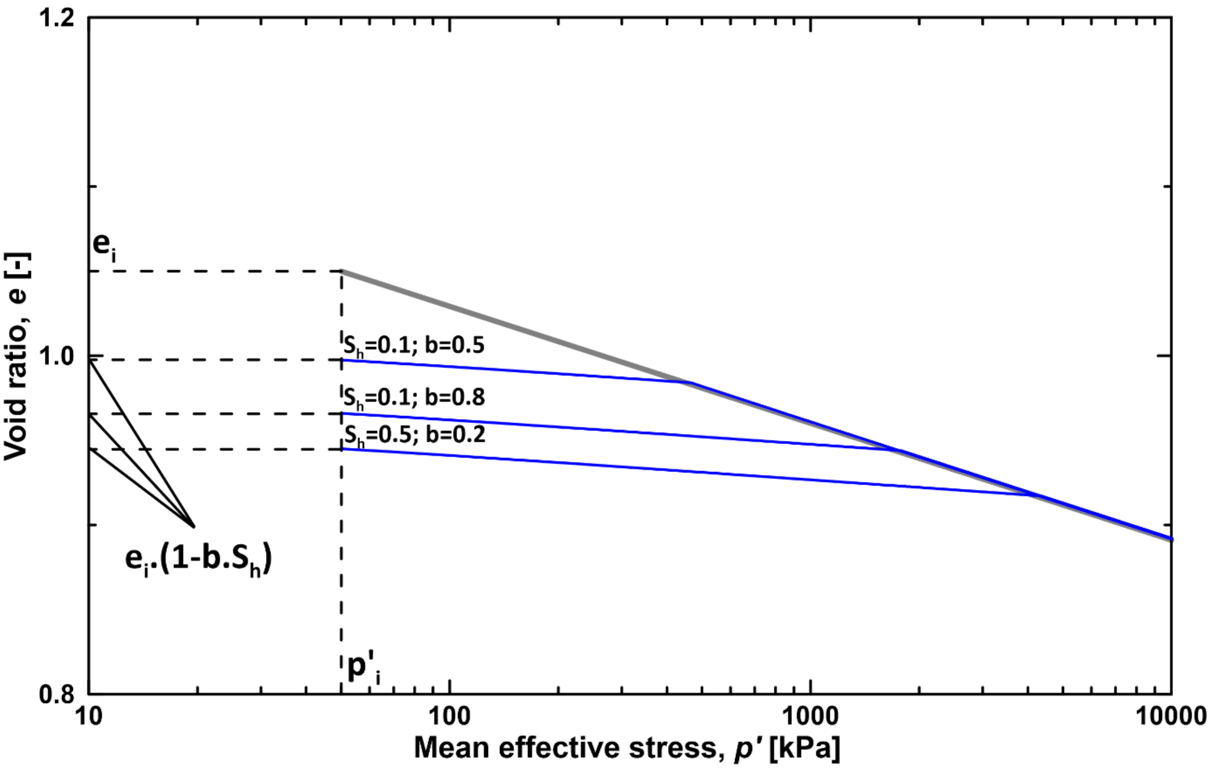

Figure 6. 21 Void ratio of the GH bearing sediment follows the κ line (blue lines) under isotropic loading until reaching the corresponding Steady State Line (grey line). Three different calculations for three different set of S_h and b parameters are shown in the figure

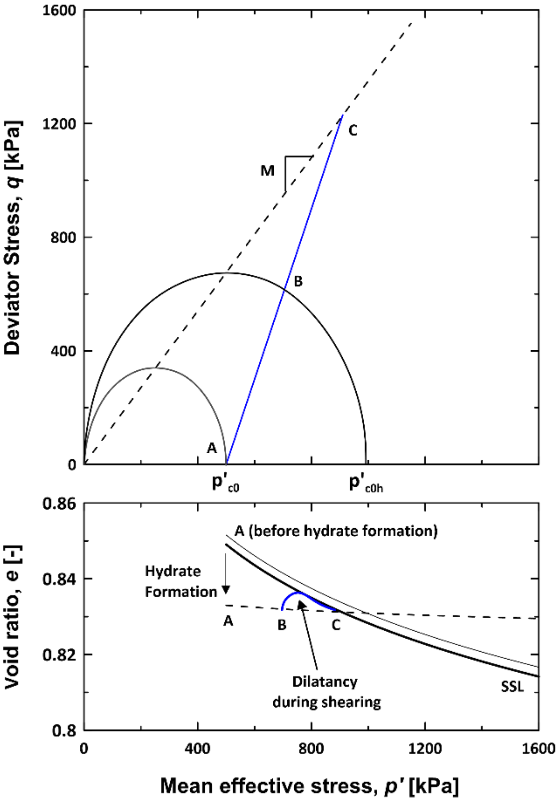

Figure 6. 22 Hydrate formation and dilatancy during shearing

saturated sediments toward that of pure hydrate λ_1. β_h is a parameter reflecting the impact of the hydrate distribution and morphology on the GHBS compressibility.

This new expression of void ratio and compression index (λ_h) lead to the following expression of the virtual effective stress p'_{c0h}, which is determined from the intersection between the slope of the swelling line (slope κ) and the slope of the normal compression line (slope λ_h) (Figure 6. 24).

$$p'_{c0h} = p'_{c0} e^{\frac{S_h.b.e_i}{\lambda_h-\kappa}} \qquad (6.14)$$

In the present work, the β_h parameter is taken equal to zero for the sandy materials considering that the SSL is not impacted by the presence of hydrate. For clayey materials, $\beta_h$was shown to be at around 10 (Taleb et al., 2018).

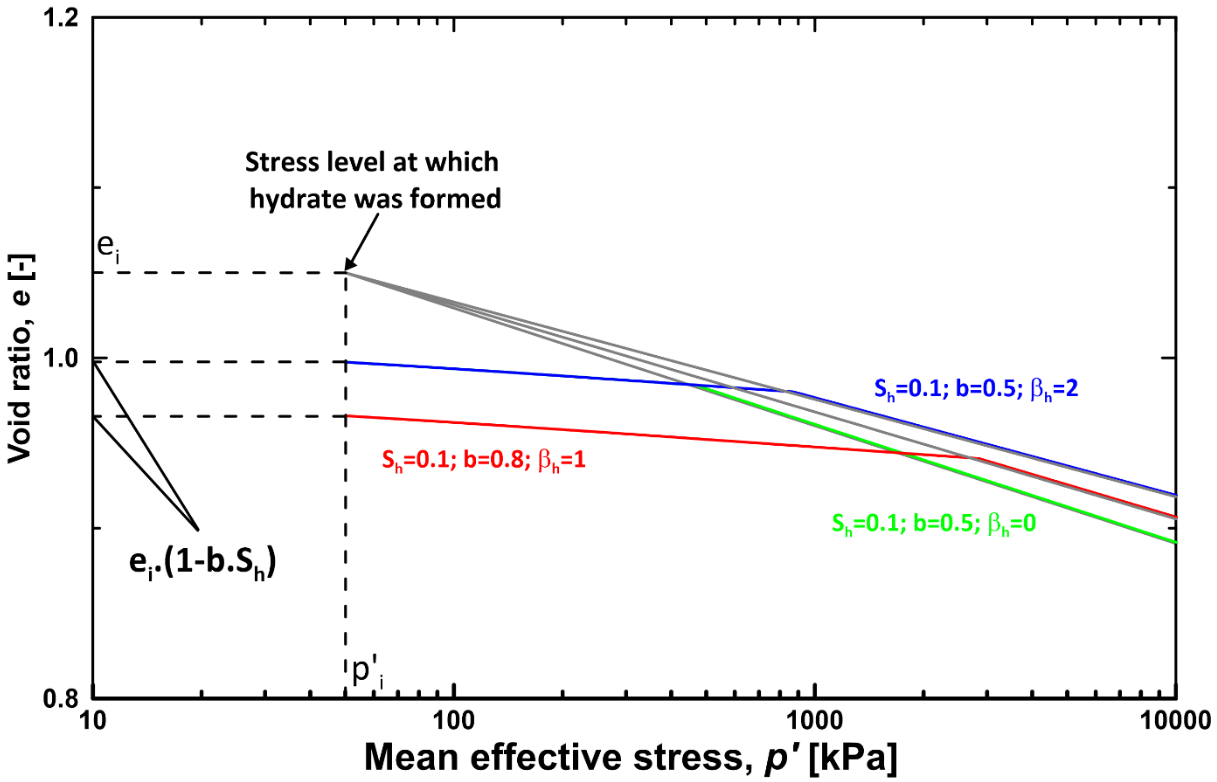

Figure 6. 23 Void ratio of the GH bearing sediment follows the κ line under isotropic loading until reaching the Steady State Line impacted by the presence of hydrate. Three different calculations for three different sets of S_h, b and β_h parameters are shown in the figure

6.4.3 Model Formulation

6.4.3.1 Elasticity

In the present work, the impact of the hydrate saturation on the slope of the swelling line (κ) and shear modulus (G) is neglected. Therefore, the elastic volumetric (ε_v^e) and deviatoric (ε_s^e) strains are determined through the following equation:

$$\begin{bmatrix} d\varepsilon_v^e \\ d\varepsilon_s^e \end{bmatrix} = \begin{bmatrix} \frac{\kappa}{(1+e0)p\prime} & 0 \\ 0 & \frac{1}{3G} \end{bmatrix} \cdot \begin{bmatrix} dp' \\ dq \end{bmatrix} \qquad (6.15)$$

6.4.3.2 Yield surface

The considered yield function defined by equation 6.16 is that of the Modified Cam-Clay model (MCC) (Roscoe and Burland (1968) passing in a $p' - q$ space, through the origin and the preconsolidation pressure at q equal to 0 (Figure 6. 24.

$$F = q^2 - M^2[p'(p'_{c0} - p')] = 0 \qquad (6.16)$$

where M is the slope of the critical state line in $q - p'$ space. The critical state line (CSL) characterises the critical state at which further shearing of the soil takes place without any changes in stress or volume. In the $p' - q$ space, the CSL is presented by a straight line passing through the origin with a slope equals to M (Figure 6. 24).

This yield curve depends on the hydrate saturation through the virtual preconsolidation pressure p'_{c0h}. The present model is developed to consider the mechanical behaviour of GHBS under a given hydrate concentration during mechanical loading (no formation or dissociation of hydrate during mechanical loading). Therefore, in the following, the hydrate concentration is considered as constant and not affecting the yield curve during mechanical loading.

6.4.3.3 Hardening law and consistency conditions

Similarly, to the modified Cam Clay model, the hardening law adopted is isotropic. It gives dp'_{c0} as a function of the volumetric plastic strain increment $d\varepsilon_v^p$.

The increment of plastic volumetric strain $d\varepsilon_v^p$ can be calculated by applying the consistency condition, defined by $dF = 0$

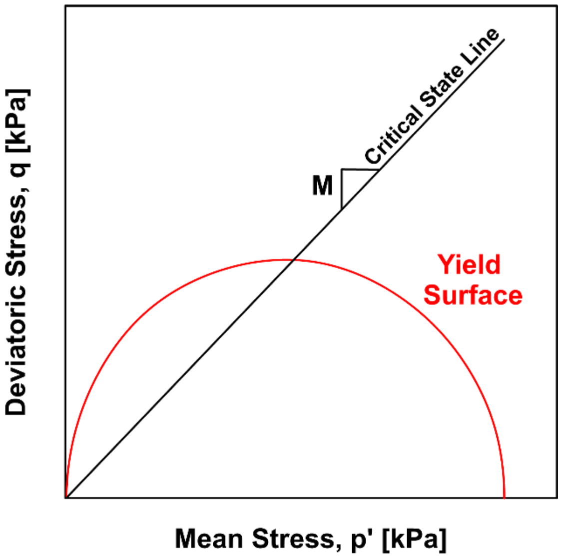

Figure 6. 24 Typical yield surface of the Modified Cam Clay model in the q-p' diagram

For a constant hydrate saturation, the consistency condition during loading (i.e.$dF = 0$) implies:

$$dF = \frac{\partial F}{\partial p'}dp' + \frac{\partial F}{\partial q}dq + \frac{\partial F}{\partial p'_c}dp'_c = 0 \quad (6.17)$$

Equation 6.17 leads to the following expression

$$d\varepsilon_v^p = \left[\frac{Mp\prime(\kappa-\lambda_{cr})(q^2-M^2p\prime^2)+A}{Mp\prime^2(1+e_i)(M^2p\prime^2+q^2)}\right]dp'_c \quad (6.18)$$

Where A is given by equation 6.19:

$$\begin{aligned}A = qe^{-\beta\frac{\left(\frac{q}{p\prime}\right)}{M}(p'-p'_i)}\Bigg[&\beta p'_i q^2(e_i - e_{cr0}) - \\ &2Mp'q(\kappa-\lambda_{cr}) - ln\left(\frac{M^2p'^2+q^2}{M^2p'^2}\right)\beta p'_i q^2(\kappa - \\ &\lambda_{cr}) + M^2\beta p'^2 p'_i(e_i - e_{cr0}) + \\ &\beta p'_i q^2\lambda_{cr}\left(ln\left(\frac{p'}{p'_0}\right) - ln\left(\frac{p'}{p'_i}\right)\right) - \\ &M^2\beta p'^2 p'_i ln\left(\frac{q^2}{M^2p'^2}+1\right)(\kappa-\lambda_{cr}) + \\ &M^2\beta p'^2 p'_i\lambda_{cr}\left(ln\left(\frac{p'}{p'_0}\right) - ln\left(\frac{p'}{p'_i}\right)\right)\Bigg]\end{aligned} \quad (6.19)$$

For $\beta = 0$, equation 6.22 becomes equivalent to that of the simplified Cam Clay equation (eq. 6.20):

$$d\varepsilon_v^p = \frac{\lambda_{cr}-\kappa}{1+e_i}dp'_c = \frac{\lambda-\kappa}{1+e_i}dp'_c \quad (6.20)$$

6.4.3.4 Flow rule

The aim of this work is to propose a simple model with few parameters able to reproduce the main features characterizing the behaviour of gas hydrate bearing sediments. Therefore, as a first approach we consider an associative flow rule where the plastic deviatoric strain $d\varepsilon_s^p$ is determined from the following equation:

$$d\varepsilon_s^p = \frac{2\eta}{{M_c}^2-\eta^2}\,d\varepsilon_v^p \quad (6.21)$$

It is important to mention that the flow rule of the Modified Cam-Clay corresponds to $M_c = M$.

By contrast with what is usually developed *(see for instance Been and Jefferies, 2011)*, in the present model M_c is not a model parameter and corresponds to η value where $d\varepsilon_v^p$ changes from positive to negative during loading.

6.4.3.5 Parameters of the model and their determination

The model is based on the MCC framework and requires only six parameters ($\lambda, \kappa, G, M, \beta and\ b$) in order to perform:

- κ, G, λ_{cr} and M are common Cam-clay parameters, which can be determined in a common fashion.
- β describes the way the void ratio reaches the locus of the steady state line (SSL) during shearing. This parameter can be determined from consolidated drained shearing tests with volume change measurement. Only one test is needed to determine such parameter but it is desirable to carry out at least two different tests with two different void ratios leading to contractancy and dilatancy during shearing.
- b is the main parameter used to consider the impact of gas hydrates on the strength of the GHBS. The "*b*" parameter characterises the fraction of hydrate effectively affecting the structure and the mechanical behaviour of the material. This parameter can only be determined through a trial-and-error manner based on shearing tests at different hydrate concentrations.

An additional optional β_h parameter is introduced. This parameter reflects the impact of the hydrate distribution and morphology on the GHBS compressibility. This parameter is taken equal to zero for sandy materials considering that the compression indices are not impacted by the presence of hydrate. For clayey materials, β_h was shown to be at around 10 (Taleb et al., 2018). At least two isotropic consolidation tests with two different hydrate saturations are needed to define this parameter.

6.4.4 Model performance

In the following section, the model performance will be discussed based on four case studies: clean sediment without GH, 10% GH, 20% GH and 50% GH. Table 6. 6and Table 6. 7 shows the parameters used in order to simulate the behaviour of sands with and without GH. Parameters like $M, \kappa \; and \; \lambda$ were unchanged throughout all study cases and were set to 1.35, 0.0064 and 0.028 respectively. While parameters $\beta \; and \; b$ varied for each case in order to highlight their effect on the performance of the model and eventually on the response of GHBS. β_h was set to 0.

6.4.4.1 Clean sand without GH (cases 1, 2, 3 and 4 in Table 6. 6)

In Figure 6. 25 presents the model's results for a sandy sediment without GH in order to evaluate the effect of β on the performance of the model. It can be observed that for a value of $\beta = 5 \times 10^{-5}$, higher values of deviatoric stress (solid lines in Figure 6. 25. a) and lower values for volumetric strain (solid lines in Figure 6. 25. b) are reached compared to those reached for $\beta = 5 \times 10^{-4}$. This implies that the deviatoric stress increases and the volumetric strain decreases with decreasing β for the same value of e. Additionally, the stress path expanded and a stiffer behaviour is observed with decreasing β (Figure 6. 25.c and Figure 6. 25.d).

In order to account for the dilatancy of the sediment, values of e (0.65 and 0.68) that are lower than the initial critical void ratio where taken (dotted line in Figure 6. 25). Thus, confirming that the model is able to capture the dilative behaviour of dense sandy soils.

Furthermore, numerical simulations were performed with cases of (1) different void ratio values and fixed mean effective stress Figure 6. 26) and (2) different mean effective stress values with a fixed void ratio (Figure 6. 27). It can be observed that the strength and stiffness of the GHBS are increasing and the dilation is enhanced with decreasing void ratio and increasing mean effective stress.

6.4.4.2 Sandy sediments with GH (cases 1, 2 and 3 in Table 6. 7)

This section focuses on the model's results for a sandy sediment containing GH in order to evaluate the effect of β and different GH contents on the performance of the model. The same value of $\beta = 5 \times 10^{-4}$ has been used for all the cases (10%, 20% and 50% GH).

For GH content of 10%, it can be observed that the deviatoric stress increases with increasing b values while showing a strain hardening behaviour for $b < 0.5$ and a strain softening behaviour for $b > 0.5$ (Figure 6. 28.a). The volumetric strain decreases and starts exhibiting a dilative behaviour with increasing b (Figure 6. 28.b). Figure 6. 28c shows the possible yield surfaces for different values of b: The stress path in the q-p' plane as well as the yield surfaces are observed to expand with increasing b. Therefore, the strength and stiffness of the sediment increases with increasing b. Figure 6. 29 shows the void ratio against the mean effective stress, where it can be seen that mainly the b value dictates the way the initial void ratio will meet the critical void ratio line. The initial void ratio is observed to decrease with increasing b.

For 20% GH content the same observations took place in terms of deviatoric stress, volumetric strain and yield surface (Figure 6. 31). The strength and stiffness of the sediment increased with increasing the b value. However, lower values of b were used as yielding was reached faster compared to the case with 10% GH content. This shows that the model is able to capture the effect of increasing GH content on the host sediment.

Table 6. 6 Parameters used to simulate the behaviour of sands without GH

Case	e_i	$e_{i_{cr}}$	e_{min}	$p'(kPa)$	β	S_h	b	β_h
1	0.831	1.045	0.61	1000	0.005	0	0	0
	0.831	1.045	0.61	1000	0.0005	0	0	0
	0.831	1.045	0.61	1000	0.00005	0	0	0
2	0.65	1.045	0.61	1000	0.005	0	0	0
	0.68	1.045	0.61	1000	0.005	0	0	0
3	0.8	1.045	0.61	0.1	0.0005	0	0	0
	0.8	1.045	0.61	0.2	0.0005	0	0	0
	0.8	1.045	0.61	0.5	0.0005	0	0	0
	0.8	1.045	0.61	1	0.0005	0	0	0
4	0.7	1.045	0.61	0.5	0.0005	0	0	0
	0.8	1.045	0.61	0.5	0.0005	0	0	0
	0.9	1.045	0.61	0.5	0.0005	0	0	0
	1	1.045	0.61	0.5	0.0005	0	0	0

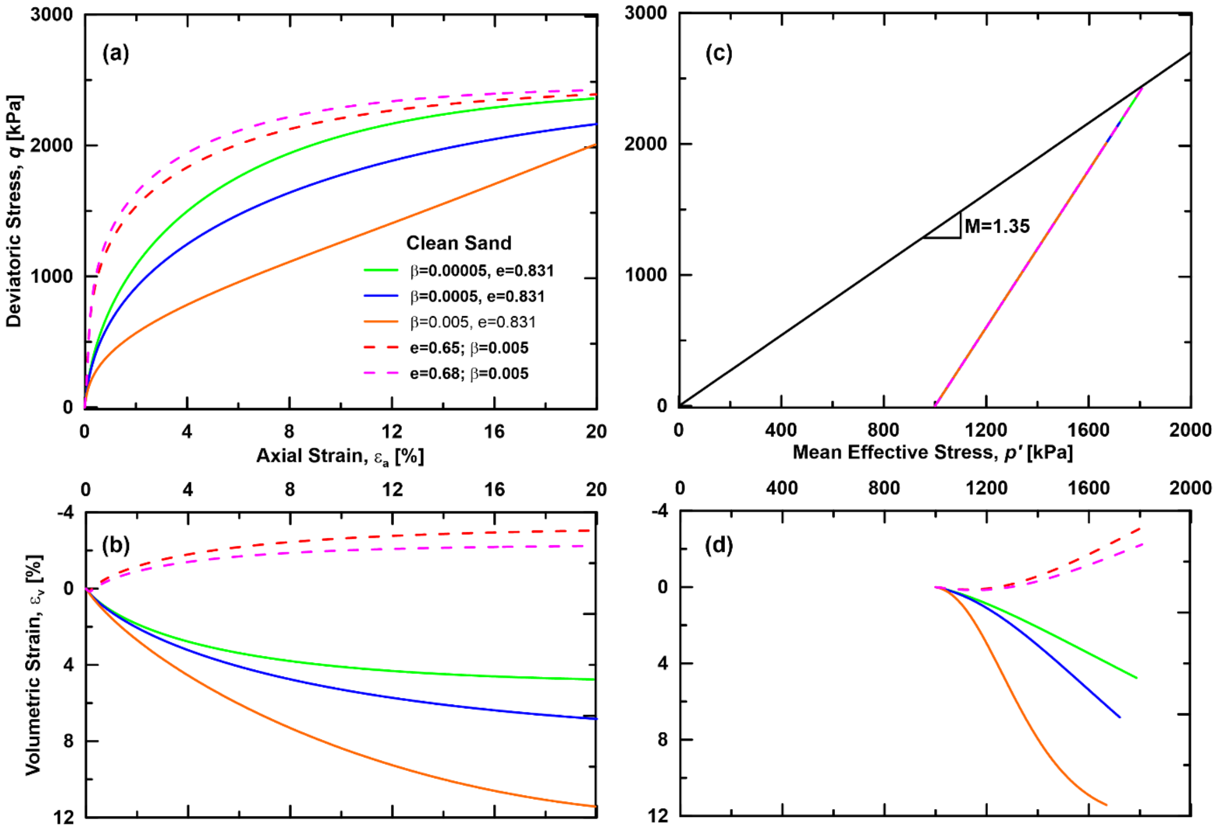

Figure 6. 25 Behaviour of clean sandy sediment without GH under drained conditions: a) Deviatoric stress against axial strain, b) Volumetric strain against axial strain, c) stress path in the p'-q plane and d) volumetric strain against mean effective stress

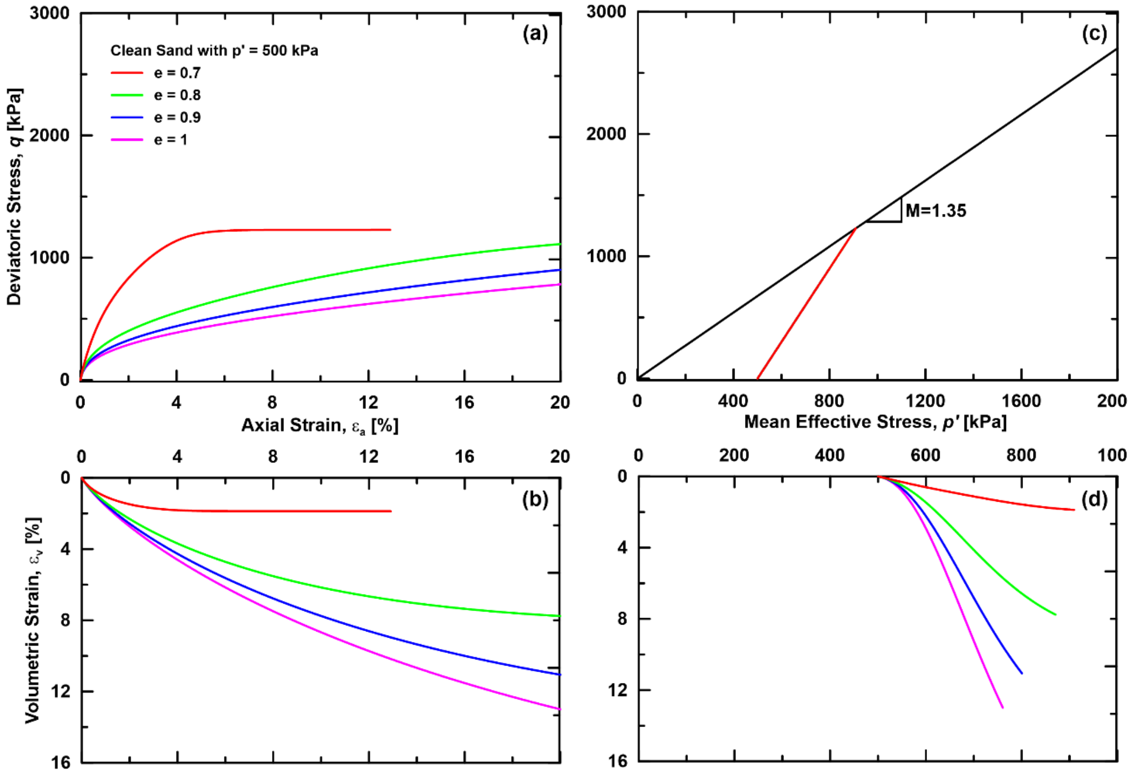

Figure 6. 26 Behaviour of clean sandy sediment without GH under drained conditions and different mean effective stress values: a) Deviatoric stress against axial strain, b) Volumetric strain against axial strain, c) stress path in the p'-q plane and d) volumetric strain against mean effective stress

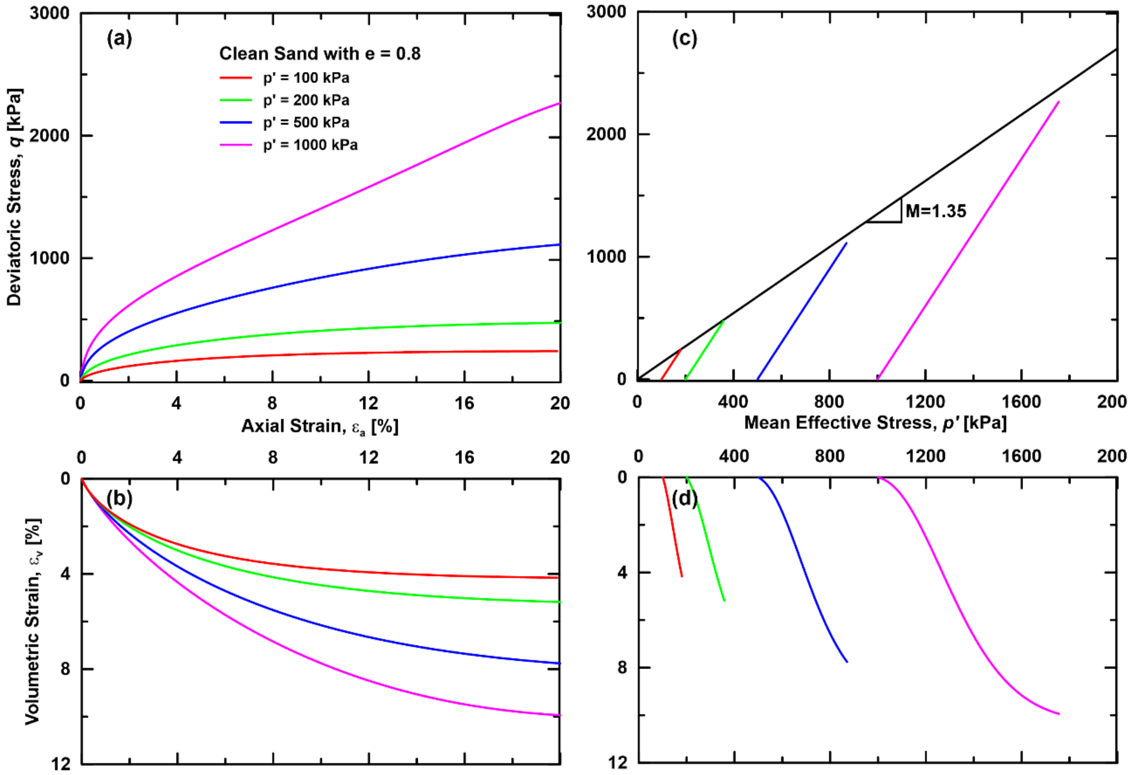

Figure 6. 27 Behaviour of clean sandy sediment without GH under drained conditions and different void ratio values: a) Deviatoric stress against axial strain, b) Volumetric strain against axial strain, c) stress path in the p'-q plane and d) volumetric strain against mean effective stress

Table 6. 7 Parameters use to simulate the behaviour of sands with GH

Case	e_i	$e_{i_{cr}}$	e_{min}	***p'(kPa)***	β	S_h	b	β_h
1	0.831	1.045	0.61	0.5	0.0005	10%	0	0
	0.831	1.045	0.61	0.5	0.0005		0.5	0
	0.831	1.045	0.61	0.5	0.0005		0.8	0
	0.831	1.045	0.61	0.5	0.0005		1	0
2	0.831	1.045	0.61	0.5	0.0005	20%	0	0
	0.831	1.045	0.61	0.5	0.0005		0.2	0
	0.831	1.045	0.61	0.5	0.0005		0.3	0
	0.831	1.045	0.61	0.5	0.0005		0.4	0
3	0.831	1.045	0.61	0.5	0.0005	50%	0	0
	0.831	1.045	0.61	0.5	0.0005		0.1	0
	0.831	1.045	0.61	0.5	0.0005		0.15	0

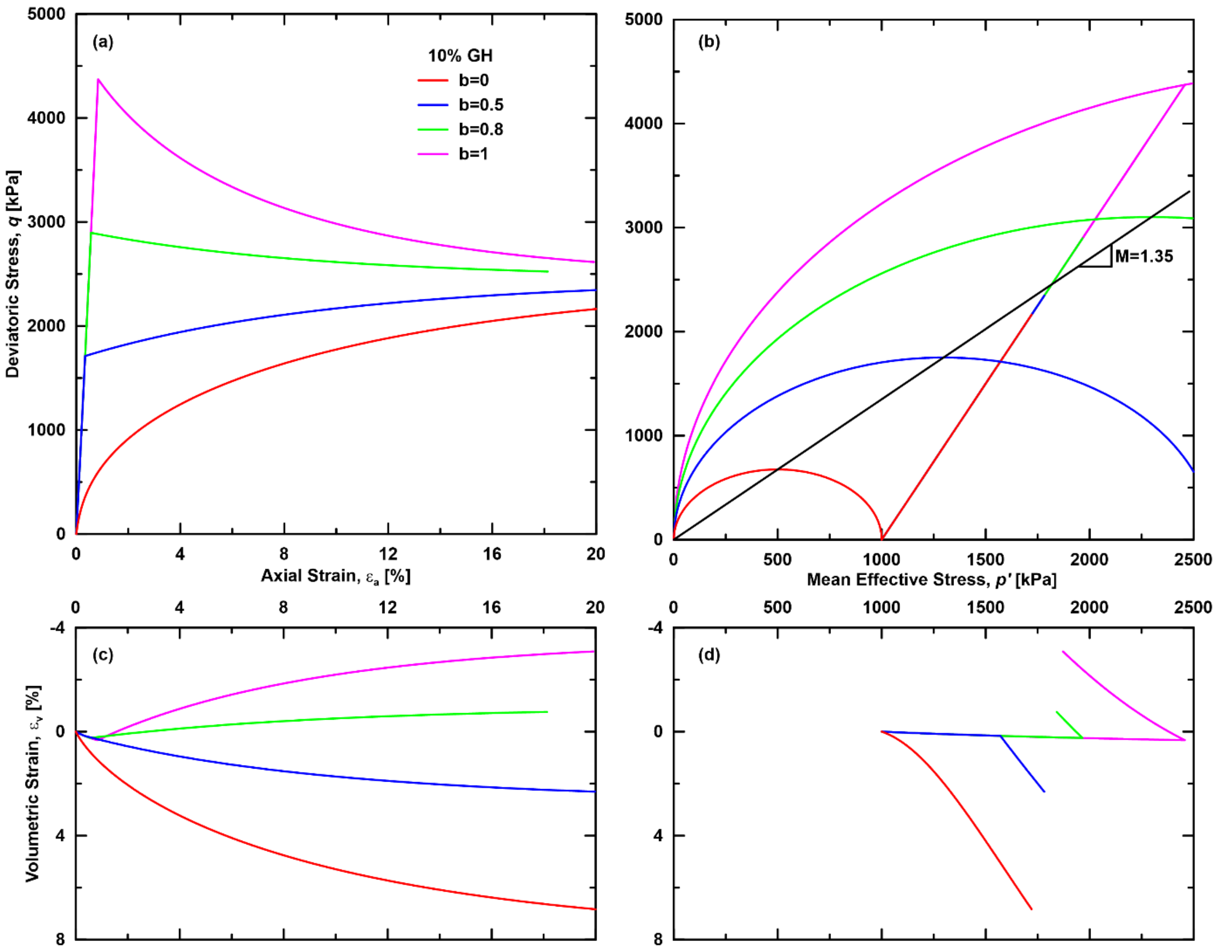

Figure 6. 28 Behaviour of GHBS under drained conditions at 10% GH content: a) Deviatoric stress against axial strain, b) stress path and yield surfaces in the p'-q plane, c) Volumetric strain against axial strain and d) volumetric strain against mean effective stress

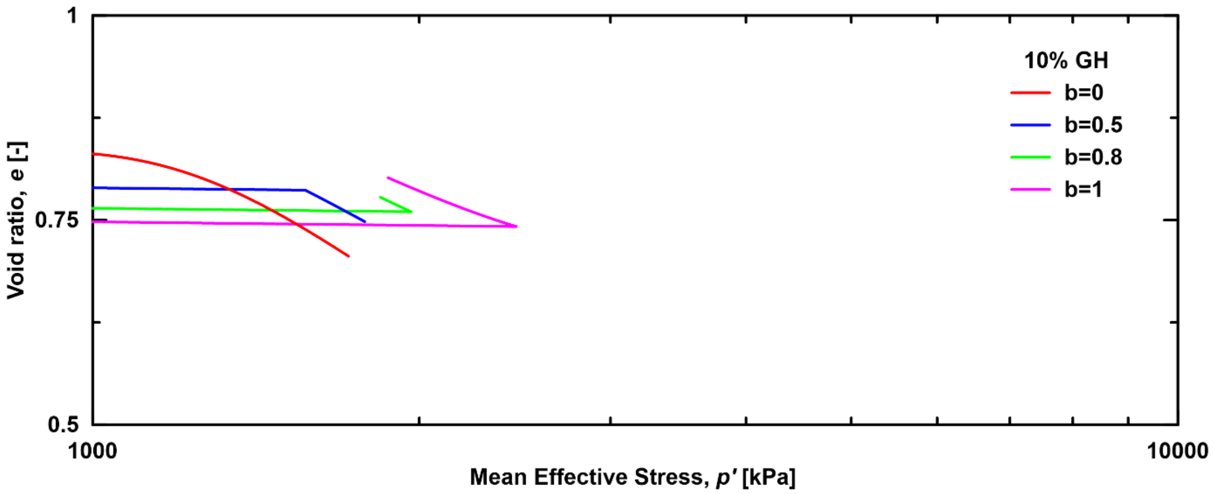

Figure 6. 29 Void ratio against mean effective stress for GHBS under drained conditions at 10% GH content

Figure 6. 34 presents the model's results for GHBS under drained conditions at 50% GH. It is also observed that the deviatoric stress increases, the volumetric strain decreases and the yield surface expands with increasing b values. However, the highest value of b was 0.15. This confirms that with increasing GH content, lower values of b are to be used as the yielding process is reached faster.

6.4.4.3 Sandy sediments with different GH contents

In the following section different values of GH content (10%, 20%, 30%, 40% and 50%) and a constant value of b (0.2) were used in order to evaluate the effect of GH content on the response of GHBS. Model's results are presented in Figure 6. 37 and Figure 6. 38.

It is noteworthy that the maximum deviatoric stress for GHBS containing 10% GH is around 643 kPa; that is almost 7 times lower compared to the maximum deviatoric stress for GHBS containing 50% GH (Figure 6. 37.a). Alternatively, for GH content of 10%, 20% and 30% GHBS showed a compressive behaviour that changed into dilative for GH content of 40% and 50% (Figure 6. 37.b). Thus, the stiffness and dilatancy of the sediment is enhanced with increasing GH content. Additionally, the yield surfaces are observed to expand with increasing GH content (Figure 6. 37.c). Therefore, the strength of the sediment increases with increasing GH content.

Generally, the model proved capable of capturing the effect of GH in terms of porosity on the strength and dilatancy enhancement of the GHBS while varying only one parameter (b): The stiffness, strength and dilatancy were observed to increase with increasing b as well as with increasing GH content.

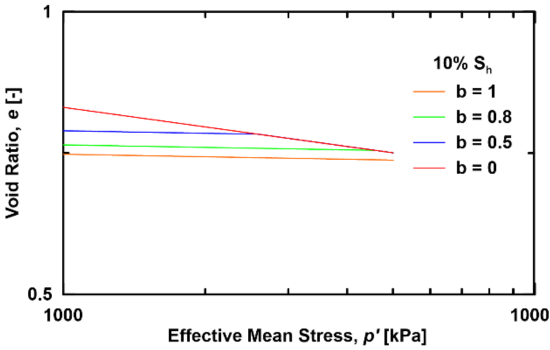

Figure 6. 30 Void ratio against mean effective stress for GHBS under isotropic conditions at 20% GH content

It can be discussed that the proposed MCC model have many drawbacks especially when dealing with coarse-grained sediments. However, the fact that only one parameter is required to do so is a great advantage compared to other models. Additionally, most available research and experimental data tackles the effects of GH content and distribution on sandy sediments, where the formation of hydrates is proven more efficient.

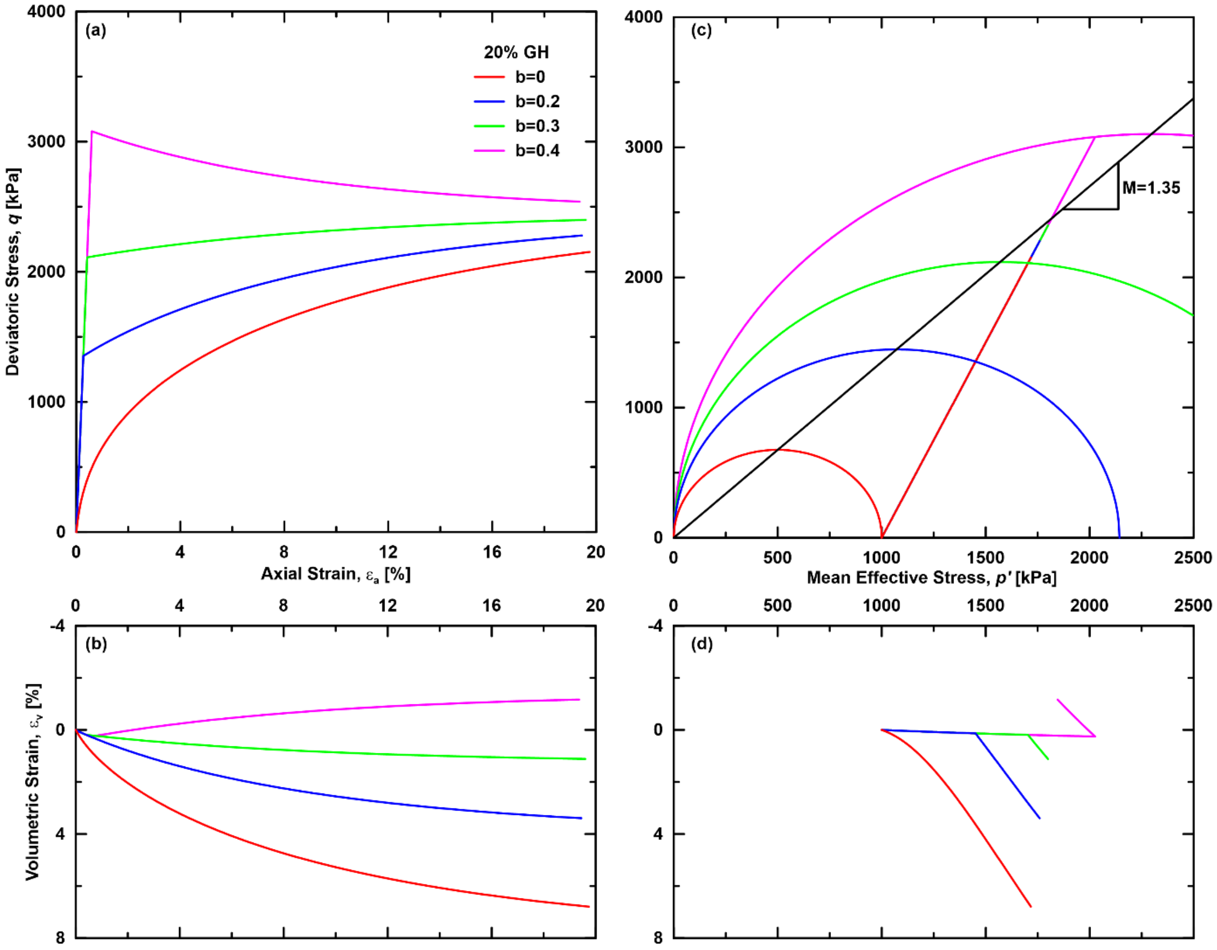

Figure 6. 31 Behaviour of GHBS under drained conditions at 20% GH content: a) Deviatoric stress against axial strain, b) Volumetric strain against axial strain, c) stress path and yield surfaces in the p'-q plane and d) volumetric strain against mean effective stress

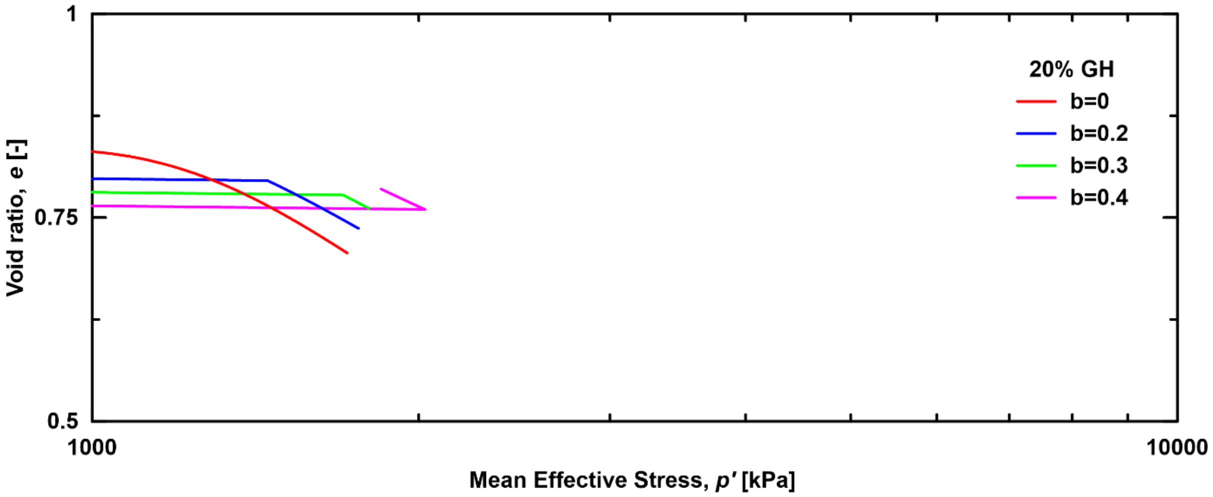

Figure 6. 32 Void ratio against mean effective stress for GHBS under drained conditions at 20% GH content

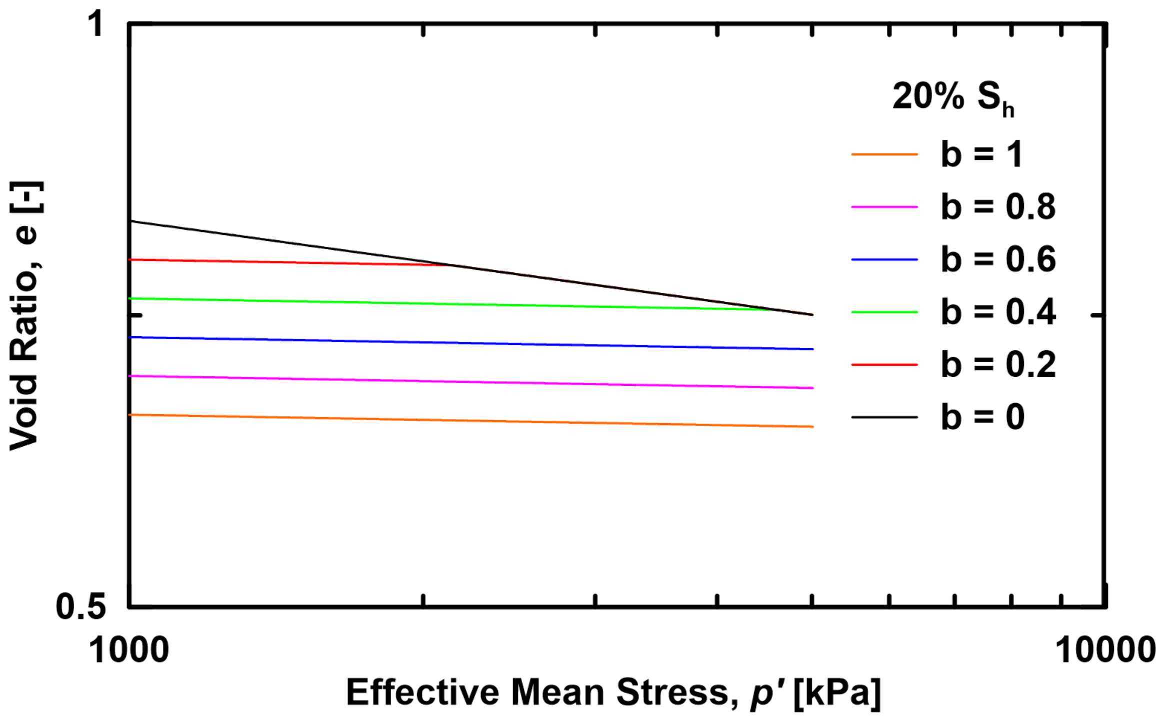

Figure 6. 33 Void ratio against mean effective stress for GHBS under isotropic conditions at 20% GH content

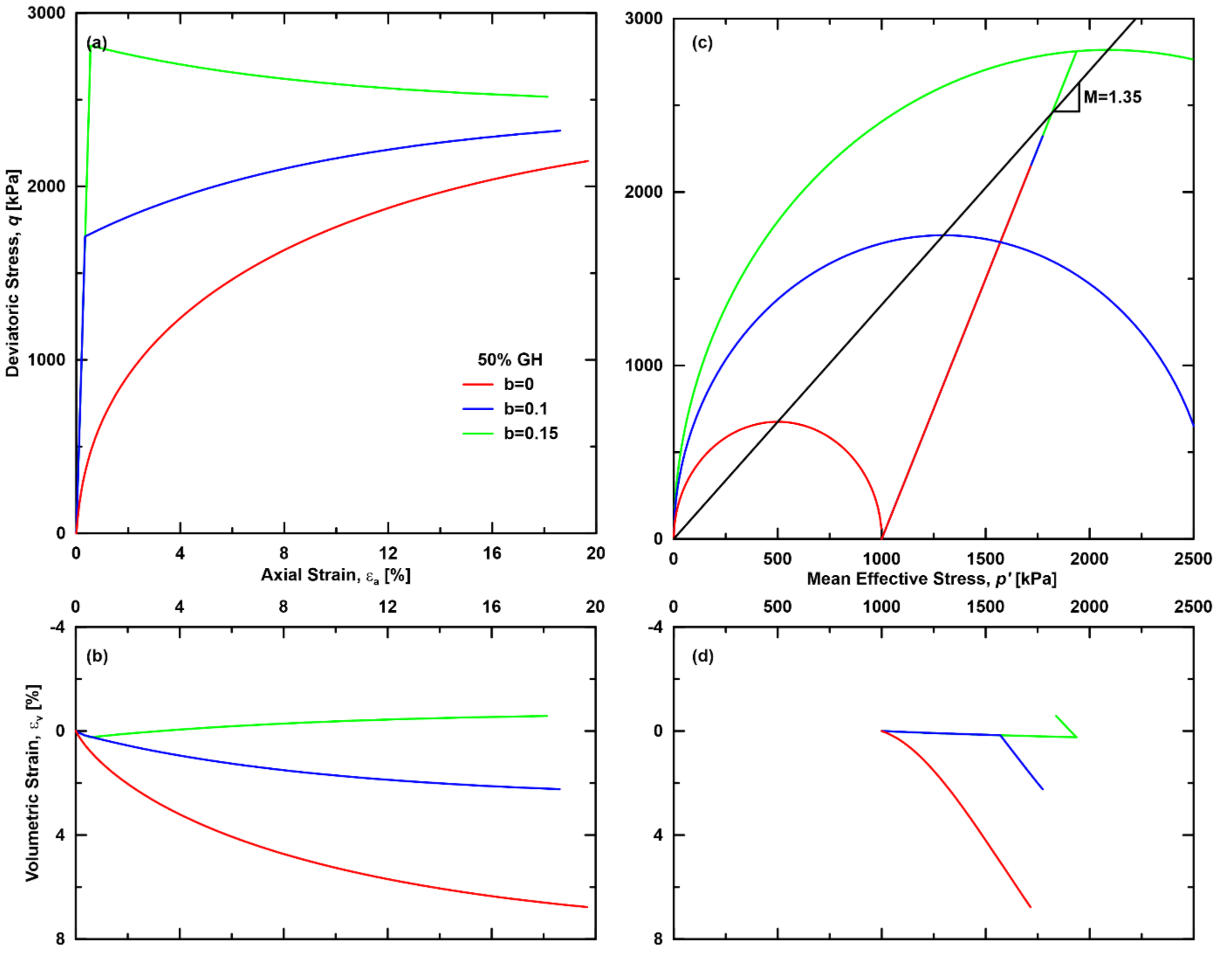

Figure 6. 34 Behaviour of GHBS under drained conditions at 50% GH content: a) Deviatoric stress against axial strain, b) stress path and yield surfaces in the p'-q plane, c) Volumetric strain against axial strain and d) volumetric strain against mean effective stress

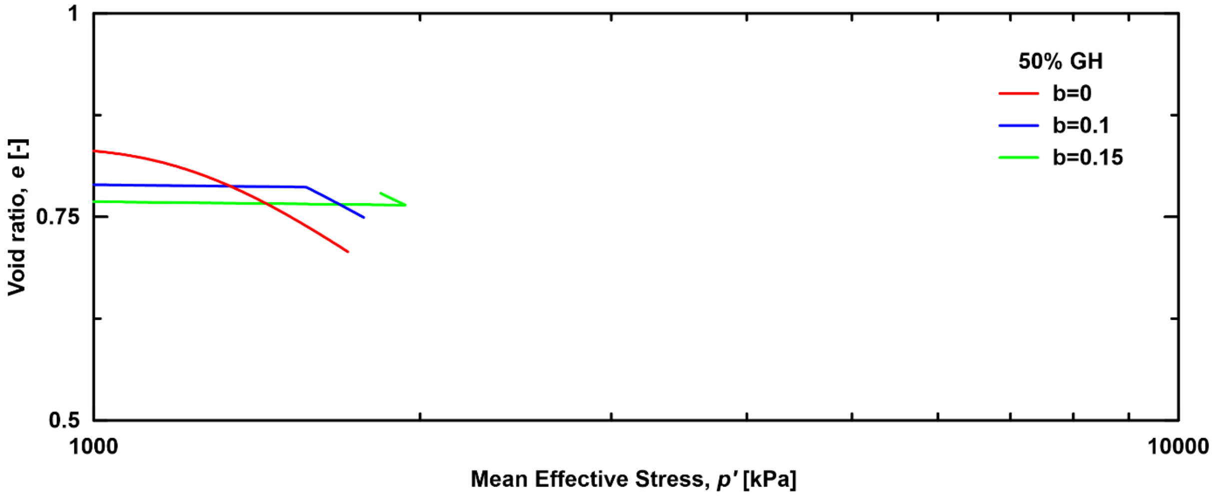

Figure 6. 35 Void ratio against mean effective stress for GHBS under drained conditions at 50% GH content

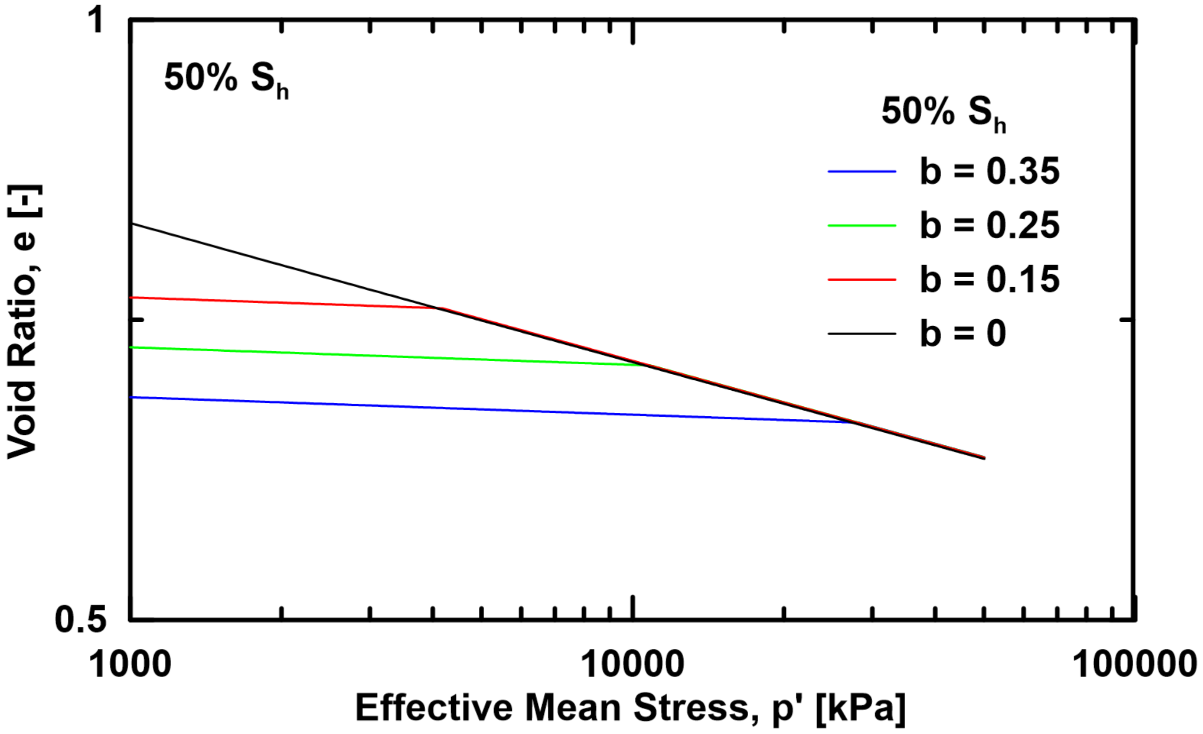

Figure 6. 36 Void ratio against mean effective stress for GHBS under isotropic conditions at 50% GH content

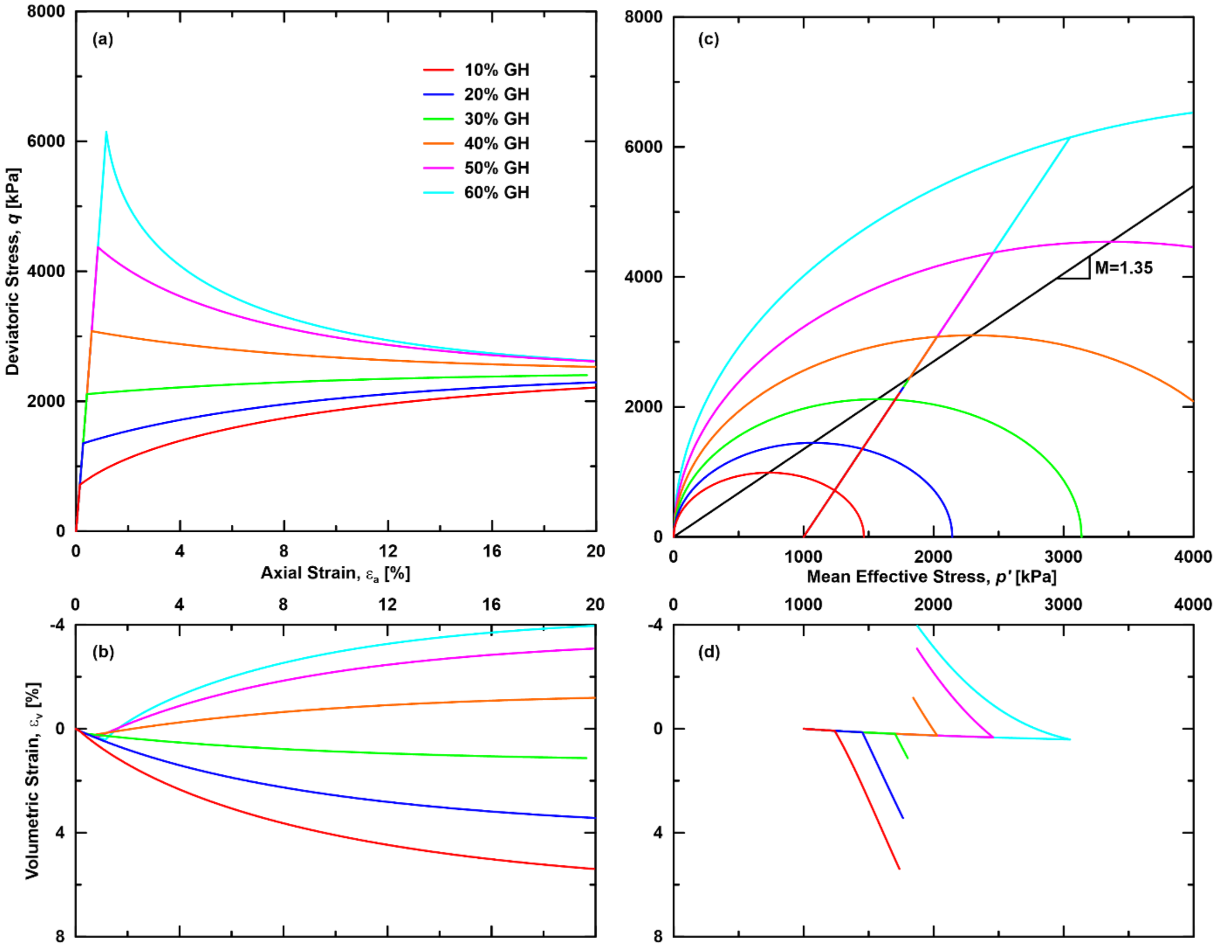

Figure 6. 37 Behaviour of GHBS under drained conditions at different GH contents: a) Deviatoric stress against axial strain, b) stress path and yield surfaces in the p'-q plane, c) Volumetric strain against axial strain and d) volumetric strain against mean effective stress

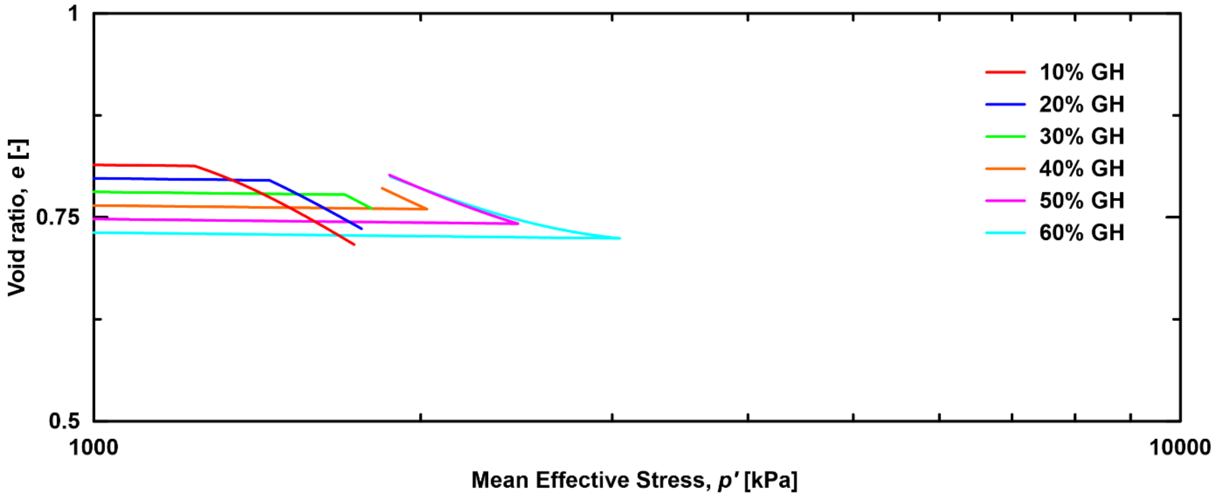

Figure 6. 38 Void ratio against mean effective stress for GHBS under drained conditions at different GH contents

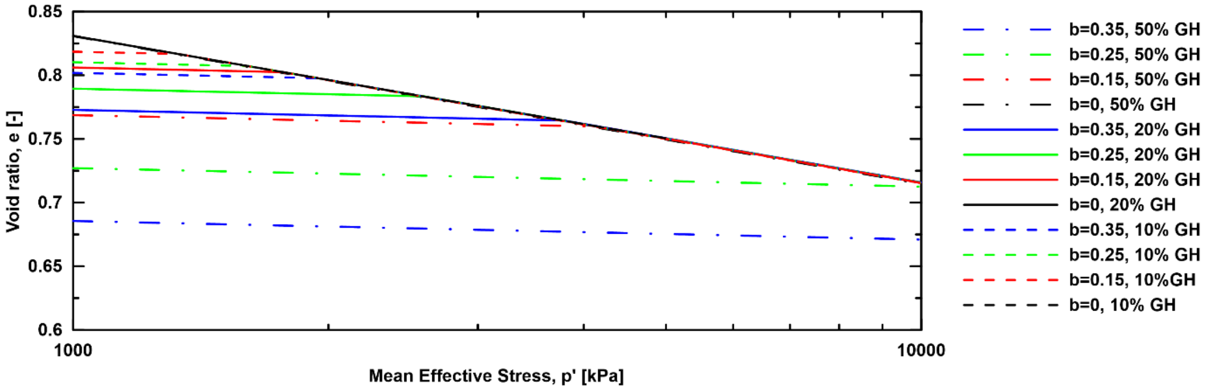

Figure 6. 39 Void ratio against mean effective stress for GHBS under isotropic conditions at different GH content

6.4.4.4 Clean clays without GH (case 1, 2 and 3 in Table 6. 8)

As a step towards adapting the b parameter to clayey soils containing GH and eventually determine their mechanical response, the β parameter is set to zero in the following section. Therefore, the model functions as a classic MCC model. Table 6. 8 shows the parameters used in order to simulate the behaviour of clays without GH. Parameters like M, κ and λ were unchanged throughout all study cases and were set to 1, 0.0494 and 0.19 respectively (as recommended by Marto et al., 2014). β, β_h and b were set to 0 for clean clays.

Table 6. 8 Parameters used to simulate the behaviour of clayey sediments without GH

Case	e_i	p'(kPa)	β	S_h	b	β_h
1	1	500	0	0	0	0
	1.5	500	0	0	0	0
	2	500	0	0	0	0
2	1	1000	0	0	0	0
	1.5	1000	0	0	0	0
	2	1000	0	0	0	0
3	1	1500	0	0	0	0
	1.5	1500	0	0	0	0
	2	1500	0	0	0	0

Results are shown in Figure 6. 40 for calculations at different void ratios and different mean effective stresses. The main observation is that the strength and stiffness of GHBS are increasing with increasing mean effective stress and decreasing void ratio values.

6.4.4.5 Clayey sediments with GH (cases 1 and 2 in Table 6. 9)

This section focusses on the model's results for a clayey sediment containing GH at 10% (Figure 6. 41 and Figure 6. 42) and 20% Figure 6. 43 and Figure 6. 44). While parameters β_h and b (Table 6. 9) varied for each case in order to explain their effect on the performance of the model and eventually on the response of GHBS, β was set to 0.

Table 6. 9 Parameters used to simulate the behaviour of clayey sediments with GH

Case	e_i	p'(kPa)	β	S_h	b	β_h
1	1	1500	0	10%	0	5
	1	1500	0		0.5	5
	1	1500	0		0.8	5
	1	1500	0		1	5
2	1	1500	0	20%	0	3
	1	1500	0		0.2	3
	1	1500	0		0.3	3
	1	1500	0		0.4	3

GH clearly increase the strength and stiffness and expands the yield surface. The effect of GH is observed to be of higher magnitude with increasing GH content. The deviatoric stress increases, the volumetric strain decreases and the yield surface expands with increasing b. Values of b and β_h were varied with varying GH content. Lower values of b and β_h had to be used with increasing GH content. The effect of b is observed to be the same as in the case of sandy sediments. Increasing β_h increases the peak strength and changes the post-peak strength behaviour from strain hardening to strain softening (Figure 6. 41.a, Figure 6. 41.b, Figure 6. 43.a and Figure 6. 43.b).

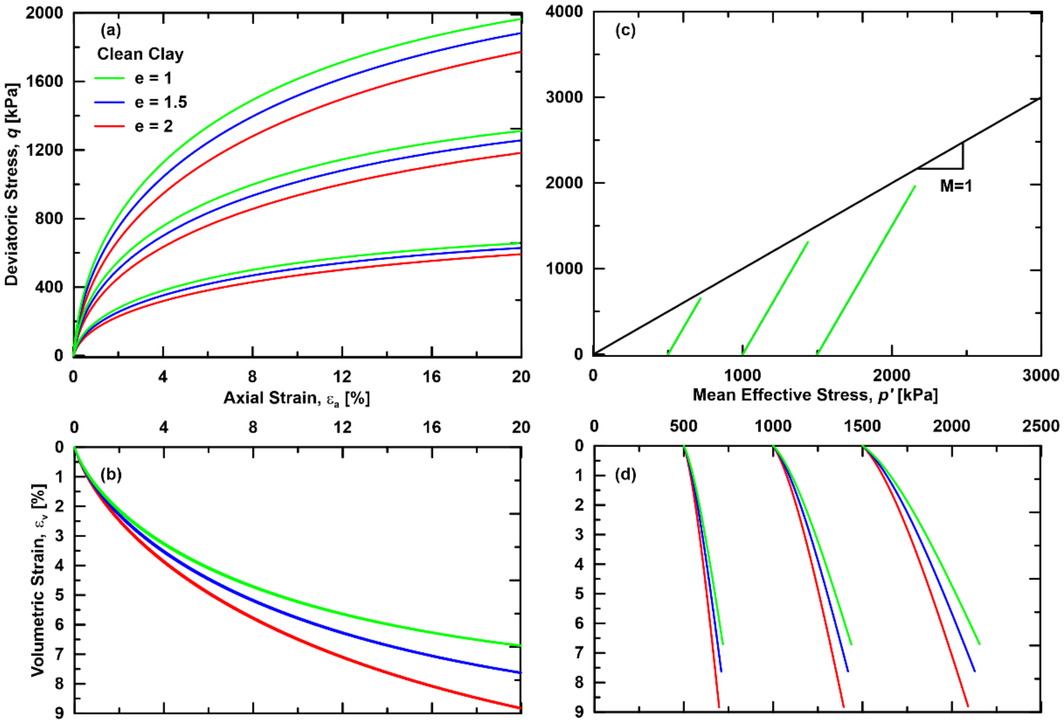

Figure 6. 40 Behaviour of clean clayey sediment under drained conditions content: a) Deviatoric stress against axial strain, b) Volumetric strain against axial strain, c) stress path and yield surfaces in the p'-q plane and d) volumetric strain against mean effective stress

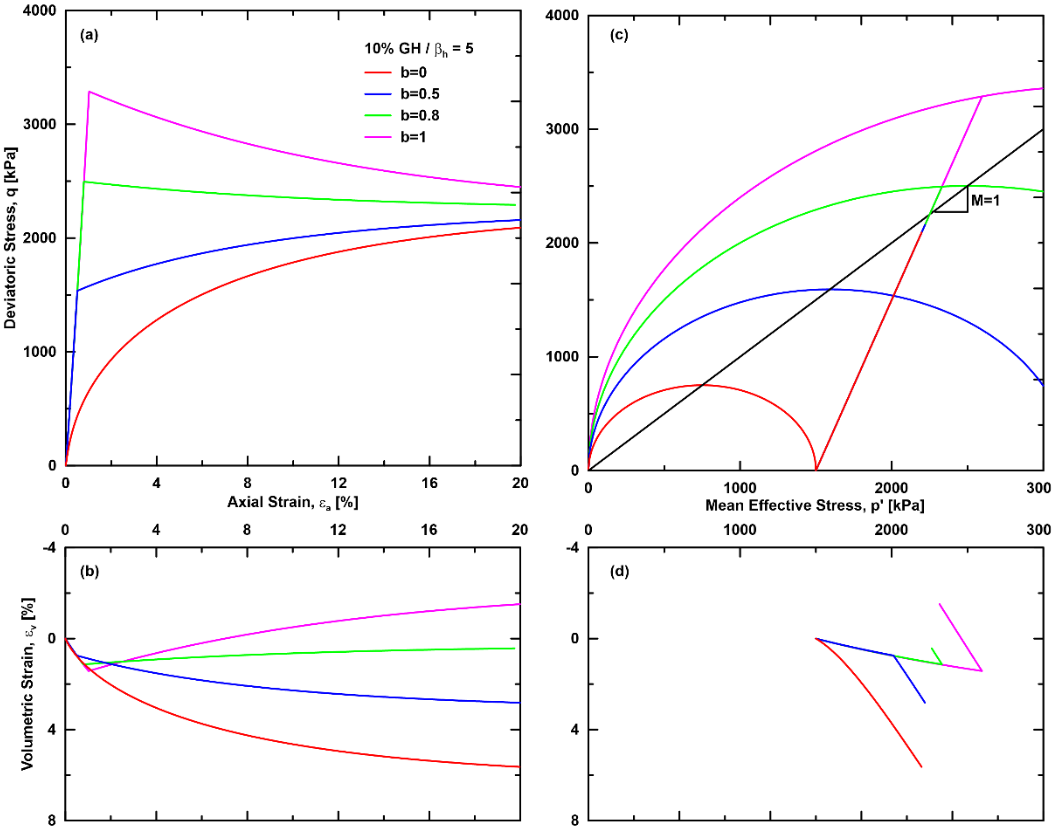

Figure 6. 41 Behaviour of GHBS under drained conditions at 10% GH content: a) Deviatoric stress against axial strain, b) stress path and yield surfaces in the p'-q plane, c) Volumetric strain against axial strain and d) volumetric strain against mean effective stress

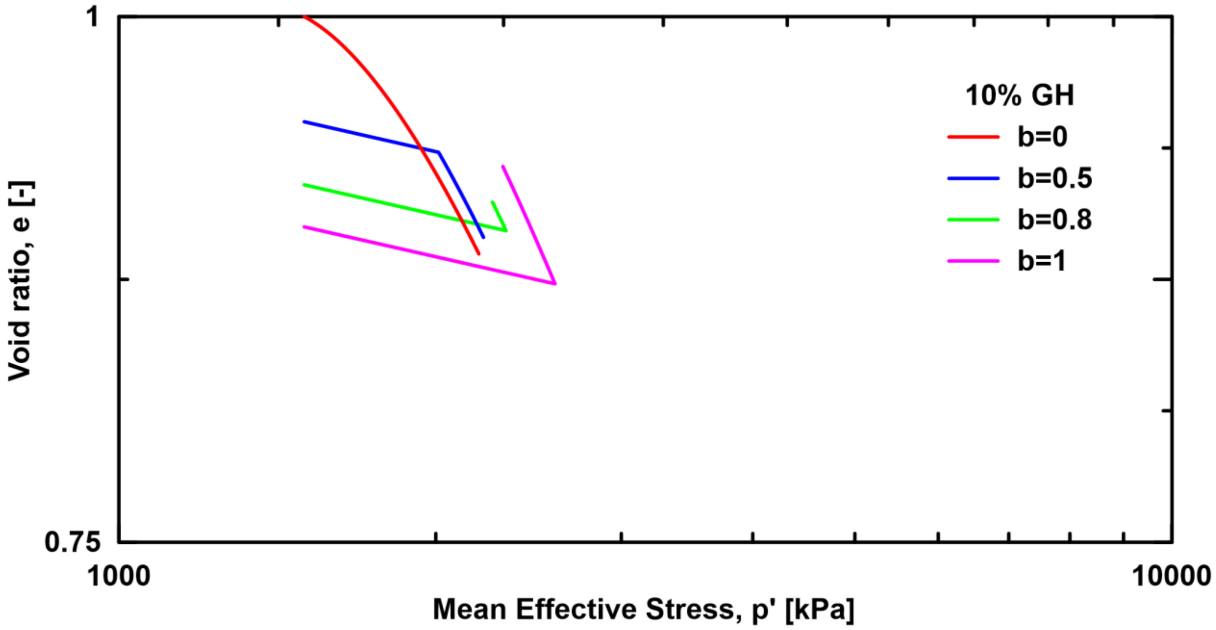

Figure 6. 42 Void ratio against mean effective stress for GHBS under drained conditions at 10% GH contents

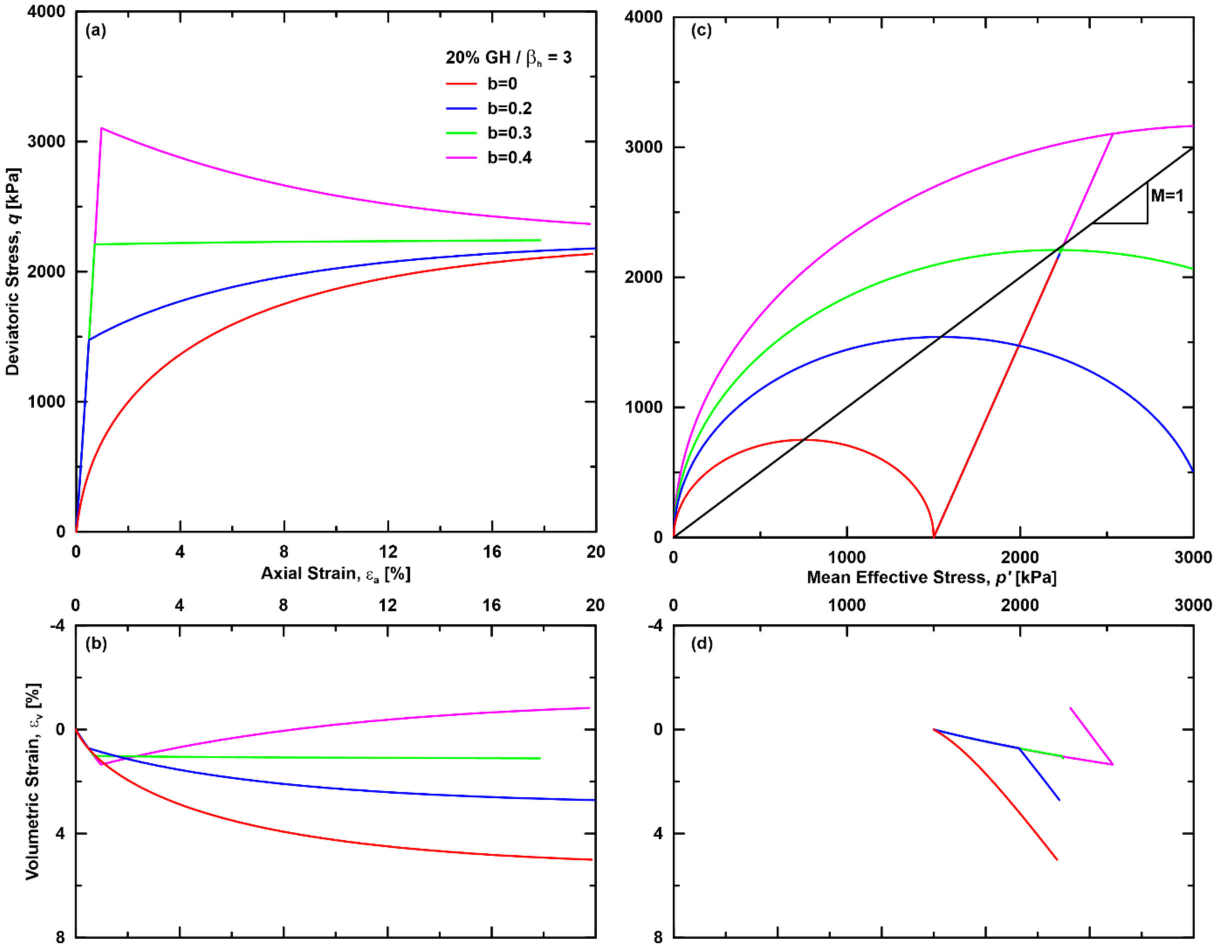

Figure 6. 43 Behaviour of GHBS under drained conditions at 20% GH content: a) Deviatoric stress against axial strain, b) stress path and yield surfaces in the p'-q plane, c) Volumetric strain against axial strain and d) volumetric strain against mean effective stress

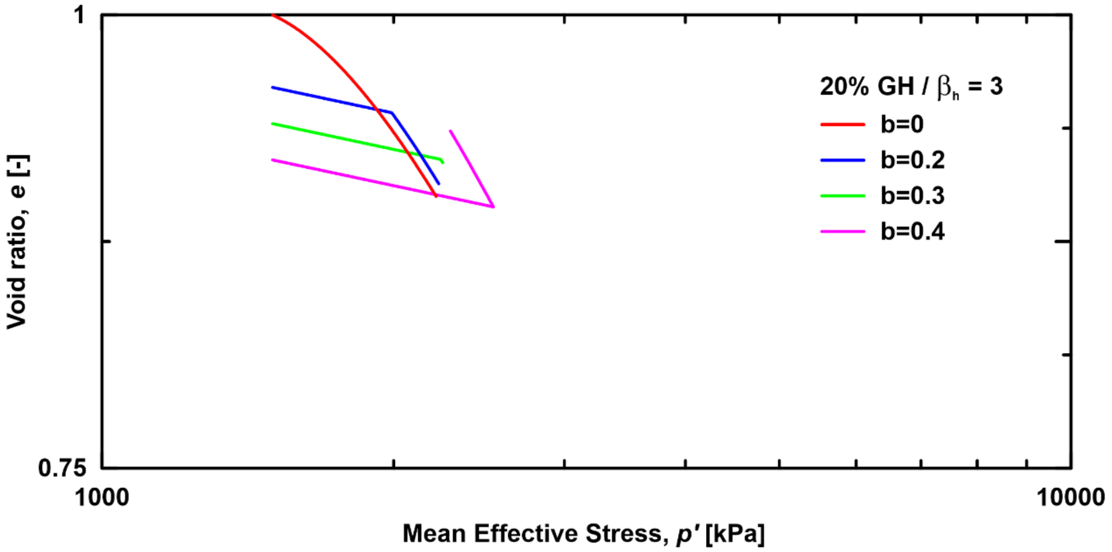

Figure 6. 44 Void ratio against mean effective stress for GHBS under drained conditions at 20% GH contents

Table 6. 10 Parameters for reproducing results by Verdugo and Ishihara (1996)

Case	e_i	$e_{i_{cr}}$	e_{min}	p'(kPa)	β	S_h	b	β_h
1	0.831	1.045	0.61	100	0.0015	0	0	0
	0.917	1.045	0.61	100	0.0015	0	0	0
	0.966	1.045	0.61	100	0.0015	0	0	0
2	0.810	1.045	0.61	500	0.005	0	0	0
	0.860	1.045	0.61	500	0.005	0	0	0
	0.960	1.045	0.61	500	0.005	0	0	0

6.4.5 Validation of the model against experimental data

In order to validate the performance of the model, modelling results are compared to experimental ones performed on sandy sediments and clayey sediments with and without gas hydrates.

6.4.5.1 Clean sands

For clean sands, the numerical results were compared with results from tests on Toyoura sand conducted by Verdugo and Ishihara (1996) at 100 kPa and 500 kPa mean effective stress (Figure 6. 45 and Figure 6. 46).

The parameters used to simulate the experimental tests are shown in Table 6. 10. Parameters like $M, \kappa \; and \; \lambda$ were set to $1.35, 0.0064 \; and \; 0.028$ respectively. While parameters such as the void ratio values and the effective mean stress are given by Verdugo and Ishihara (1996), $S_h, b \; and \; \beta_h$ were set to zero due to the absence of GH. Generally, the numerical results from the model yield estimates that are close to the results from experimental data.

The stress-strain curve plots in Figure 6. 45.a and Figure 6. 46.a show great resemblance thus, proving that the model is able to capture the mechanical behaviour of sands under different values of mean effective stress and void ratio. For the volumetric strain plots (Figure 6. 45.b and Figure 6. 46.b), results are rather satisfactory. However, the precision to reproduce experimental results seems to be decreasing with decreasing void ratio values. Lastly, numerical results for the stress path in Figure 6. 45.c and Figure 6. 46.c also show resemblance with experimental results from Verdugo and Ishihara (1996).

Therefore, the model is proved capable of simulating the mechanical behaviour of coarse-grained sandy sediments without GH. However, as for dilatancy (Figure 6. 45.b and Figure 6. 46.b), the model seems to face some troubles recreating a neat representation of the experimental results.

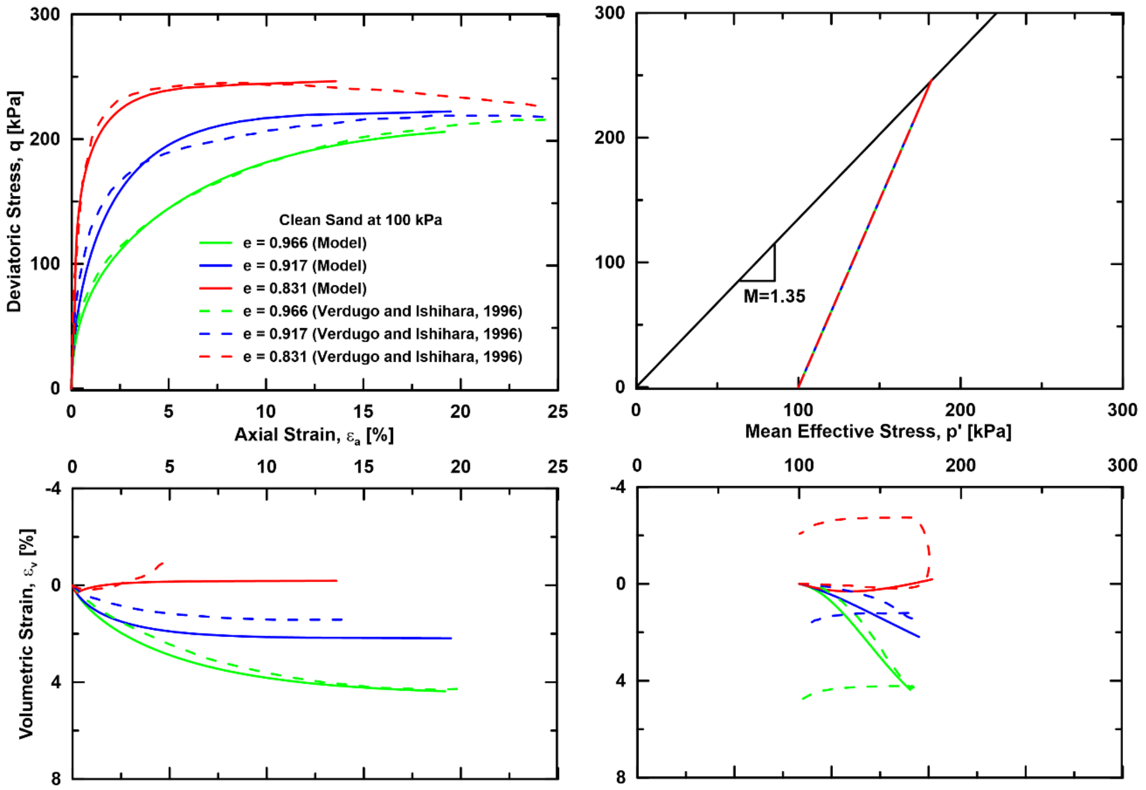

Figure 6. 45 Behaviour of clean sand under drained conditions at 100 kPa: a) Deviatoric stress against axial strain, b) stress path and yield surfaces in the p'-q plane, c) Volumetric strain against axial strain and d) volumetric strain against mean effective stress

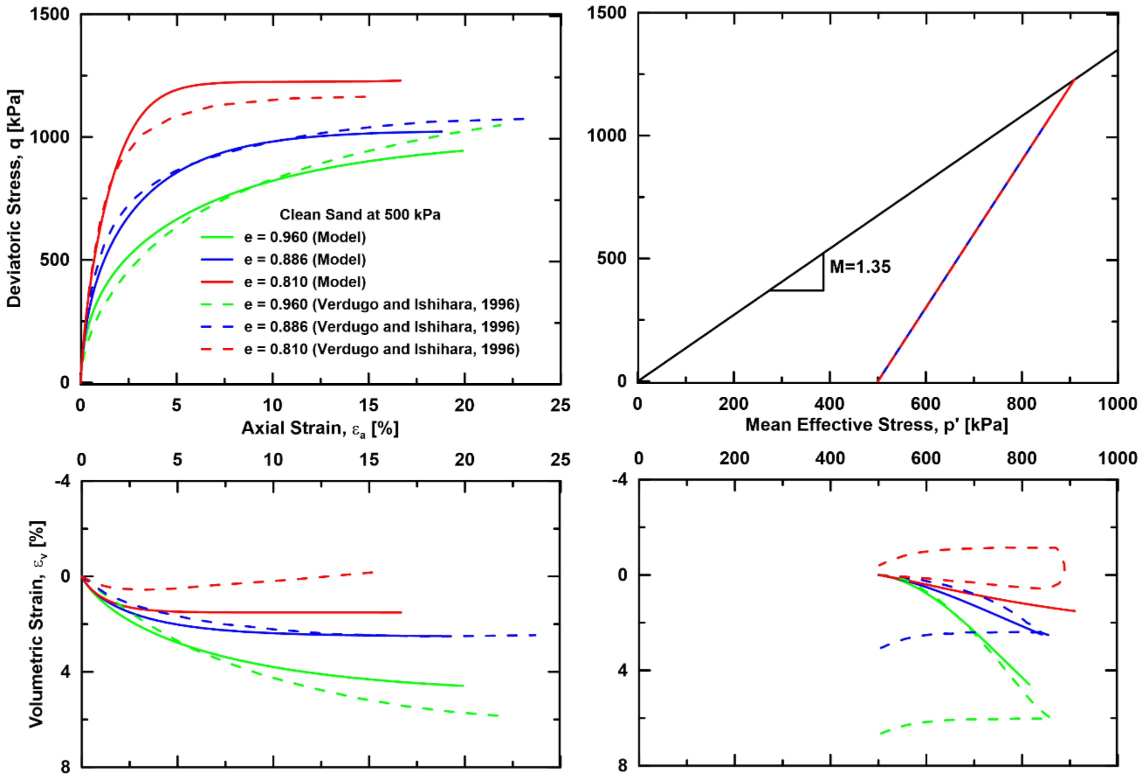

Figure 6. 46 Behaviour of clean sand under drained conditions at 500 kPa: a) Deviatoric stress against axial strain, b) stress path and yield surfaces in the p'-q plane, c) Volumetric strain against axial strain and d) volumetric strain against mean effective stress

Table 6. 11 Parameters for reproducing results by Masui et al. (2005) and Hyodo et al. (2013)

Parameter	**Value**						
	Case 1: GH morphology (Masui et al. 2005)			**Case2: GH content (Hyodo et al. 2013)**			
	Clean Sand	**Pore-filling**	**Cementing**	**Clean Sand**	**24.2%**	**35.1%**	**53.1%**
M	1.7	1.7	1.7	1.45	1.45	1.45	1.45
$\boldsymbol{\lambda}$	0.028	0.028	0.028	0.028	0.028	0.028	0.028
$\boldsymbol{\kappa}$	0.0064	0.0064	0.0064	0.0064	0.0064	0.0064	0.0064
$\boldsymbol{\beta}$	0.0002	0.0002	0.0002	0.0001	0.0001	0.0001	0.0001
$\boldsymbol{b}$	0	0.135	0.165	0	0.113	0.113	0.113
$\boldsymbol{S_h}$	0	0.4	0.4	0	0.242	0.351	0.531
$\boldsymbol{\beta_h}$	0	0	0	0	0	0	0

6.4.5.2 Sands with GH

In this part, the numerical results for sandy sediments containing gas hydrates are compared to experimental results from Masui et al. (2005) to account for GH morphology and from Hyodo et al. (2013) to account for GH content. The parameters used to simulate the experimental tests are based on the Toyoura sand critical state parameters and shown in Table 6. 11. Parameters such as λ and κ were determined for Toyoura sand as recommended by Verdugo and Ishihara (1996). β_h was set to zero since its effect was observed to counteract the b effect. S_h values for the case 1 and case 2 were set as recommended by Masui et al. (2005) and Hyodo et al. (2013). As for b, it was varied in a way that it fits best the experimental results by Masui et al. (2005) and Hyodo et al. (2013).

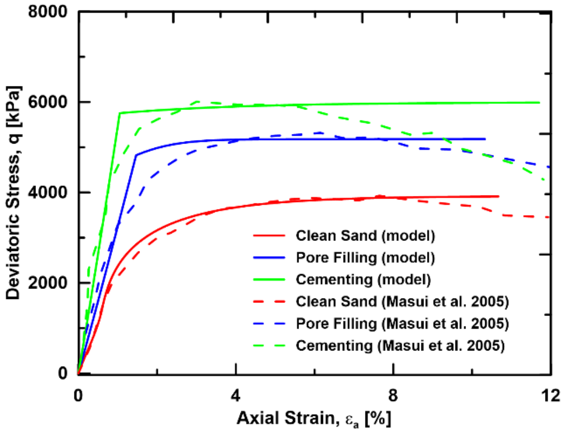

Figure 6. 47 Deviatoric stress against axial strain for GH bearing sandy sediments from numerical results and from Masui et al. 2005

Figure 6. 47 presents the numerical results from the model against the experimental results from Masui et al. (2005) for clean sand, pore filling GH and cementing GH. In this section the β parameter was set as a constant and the b parameter was varied in order to account for different morphologies of GH. It is clear that the model succeeded in recreating the mechanical response of all the three cases.

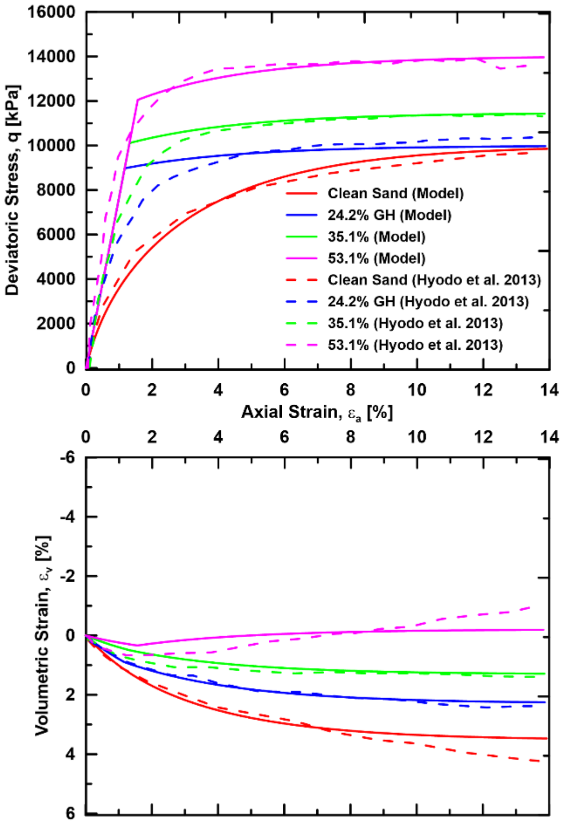

Figure 6. 48 a) Deviatoric stress against axial strain and b) volumetric strain against axial strain for GH bearing sandy sediments from numerical results and from Hyodo et al. 2013

Table 6. 12 Parameters used for reproducing results by Yun et al. (2007)

Parameter	**Value**			
	Case 1: Clean Clay	**Case 2: Clay with GH**		
M	1	1	1	1
λ	0.19	0.19	0.19	0.19
κ	0.0494	0.0494	0.0494	0.0494
$p'(kPa)$	30, 500 and 1000	500	1000	1000
β	0	0	0	0
b	0	0.05	0.05	0.05
S_h	0	0.5	0.5	1
β_h	0	0.1	0.1	0.1

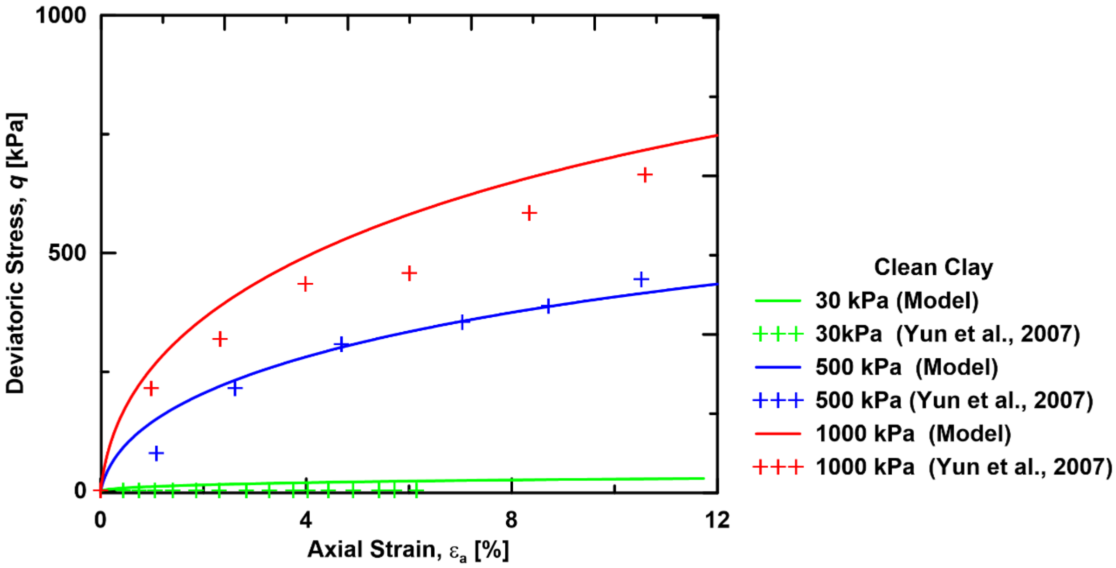

Figure 6. 49 Deviatoric stress against axial strain clean clayey sediments from numerical results and from Yun et al. (2007)

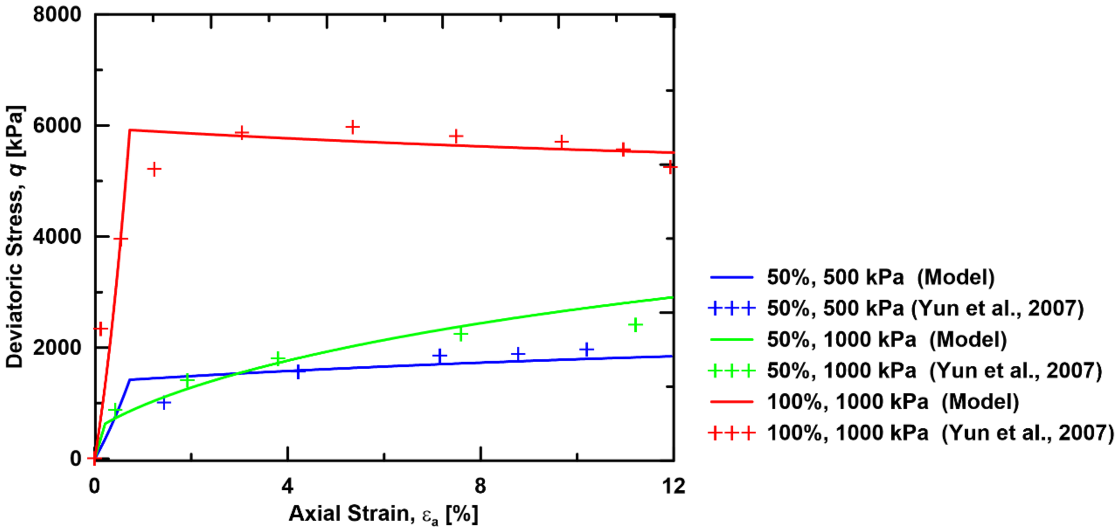

Figure 6. 50 Deviatoric stress against axial strain for GH bearing clayey sediments from numerical results and from Yun et al. (2007)

However, the post-peak strain-softening behaviour was not reproduced by the model.

As discussed earlier, the mechanical behaviour of sandy sediments is not only affected by the presence and morphology of GH but also by the GH content. Thus, experimental results from Hyodo et al. (2013) at different GH content have been compared to numerical results from the model Figure 6. 48 For the case of clean sand, the model perfectly succeeded in reproducing the stress-strain and dilatancy curves. For GH bearing sandy sediments, results are highly satisfactory for the stress-strain curves as well as for the volumetric strain curves. However, the model seems to lose precision as dilatancy of the sediment increases (purple curve in Figure 6. 48.b).

Generally, the model is proved capable of simulating the mechanical behaviour of coarse-grained sandy sediments containing different GH contents and morphology.

6.4.5.3 Clayey sediments

In this part, experimental results, at different mean effective stress and GH content, from Yun et al. (2007) on clayey sediments without and with GH are compared to those simulated by the model (see parameters in Table 6. 12).

Parameters such as M, λ and κ were used recommended by Marto et al., (2014) for the case of Kaolin clay. The effective mean stress and the GH content are given by Yun et al. (2007). The β parameter is set to zero so that the model functions as a classic MCC model. As for the $b\ and\ \beta_h$, they were varied until they represented best the experimental results from Yun et al. (2007). Results for clean clays are shown in Figure 6. 49 where it can be observed that the model perfectly simulates the experimental results at different mean effective stress values. Figure 6. 50 shows results for GH bearing clayey sediments at different GH content as well as different effective mean stress values. Overall, the reproduction of the experimental results is decent and rather satisfactory.

Although the precision of recreating experimental results decreases with increasing GH content, the results are rather satisfactory. One should keep in mind that only one parameter (b) is varying in order to perform these calculations, making the model very easy and simple to use, compared to other models in the literature.

6.5 Conclusion

In this chapter, a literature review on the mechanical behaviour of GH-bearing fine-grained and coarse-grained sediments and on the available numerical models aiming at reproducing that behaviour have been presented. The chapter principally aimed to formulate a new constitutive and simple model for gas hydrate bearing sediments. The following conclusions can be drawn:

For clayey sediments:

- The strength and stiffness of GH-bearing clayey sediments increase with increasing GH content.
- In-situ and experimental data, which does not account for field conditions, seem to be contradictory on whether the presence of GH within the clayey sediment leads to a contractive or dilative behaviour.

For sandy sediments:

- The strength and dilatancy of gas hydrate bearing sediments increase with increasing GH content and are highly affected by GH content morphology.
- The peak deviatoric stress increases with increasing GH content and mean effective pressures.
- The peak deviatoric stress reaches higher values with decreasing void ratio.

Numerical models:

- Models based on the critical state theory are considered amongst the most advanced ones and some of them showed very realistic results when compared to experimental data. However, those models rely on an important number of input parameters that need to be derived from long lasting experiments.

New simple constitutive model:

- A new formulation of the steady state locus in e-p’ space is included in order to consider the dilative/contractive behaviour of sand during shearing.

- In addition to the classic modified Cam Clay parameters, this new model requires :
  - A parameter that accounts for GH morphology (b).
  - A parameter that describes the way the void ratio reaches the locus of the steady state line (β). This parameter is set to zero when simulating the behaviour of GH-bearing clays in so that the model functions as a classic MCC model.
  - A parameter that reflects the impact of GH morphology on the compressibility of GHBS (β_h). This parameter is set to zero when simulating the behaviour of GH-bearing sands considering that the compression indices are not impacted by the presence of hydrate.
- The model is proved capable of simulating the mechanical behaviour of coarse-grained sandy sediments without GH as well as with hydrates of different morphologies and in different quantities.
- The model was observed not capable of reproducing the smooth post-peak strength behaviour (strain softening) often observed in results from experimental data.

Chapter 7. Conclusions and perspectives

Chapitre 7. Conclusions et perspectives

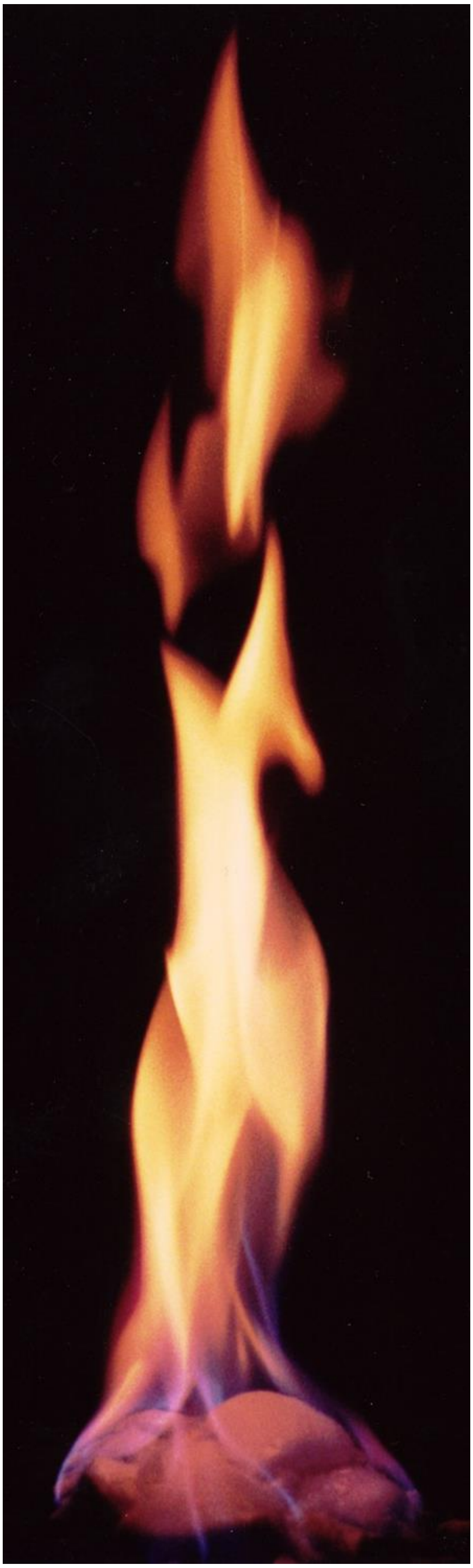

Burning Gas Hydrates (Laura Stern, USGS)

7.1 Introduction

The objective of this thesis was to detect and quantify Gas hydrates (GH) as well as to assess the mechanical behaviour of their host sediment based on in-situ measurements in the deep-water Niger Delta. In this chapter, the main achievements and conclusions of this work are summarized. Perspectives and new scientific questions for future research work are presented at the end of the chapter.

The work structure shown in Figure 7. 1 was followed throughout the PhD work focusing on detecting and quantifying GH and ending by determining their mechanical behaviour under stability conditions. As it can be shown in Figure 7. 1, the contribution of this work is essential to carry out the needed steps to assess the geohazard potential associated with GH.

7.2 What are the methods that allowed the detection of gas hydrates?

The detection of GH within marine sediment was based on the fact that GH are able to alter the physical and mechanical properties of the sediment (Waite et al., 2009; Dai et al., 2012). This was mainly done by using an inter-comparison method between Penfeld CPTu and Penfeld Vp data.

Typically, in a clayey sediment similar to that present in the study area, the compressional velocity vary between 1450 and 1510 m/s. However, the presence of GH can increase these values up to 3600m/s (Sultan et al., 2007). This is mainly because the bulk modulus and shear modulus of hydrates are very high compared to those of water; therefore, this will strongly affect the compressional velocity. This is also accompanied by an increase in the acoustic signal attenuation. Thus, the detection of the presence of GH can be directly linked to simultaneous increase in all in-situ acoustic parameters. However, the presence of free gas affects negatively the shear and bulk moduli and therefore reduces the acoustic velocity. It is noteworthy that in some cases the coexistence of free gas and solid GH have been inferred, especially based on direct observations of GH nodules with a spongy structure.

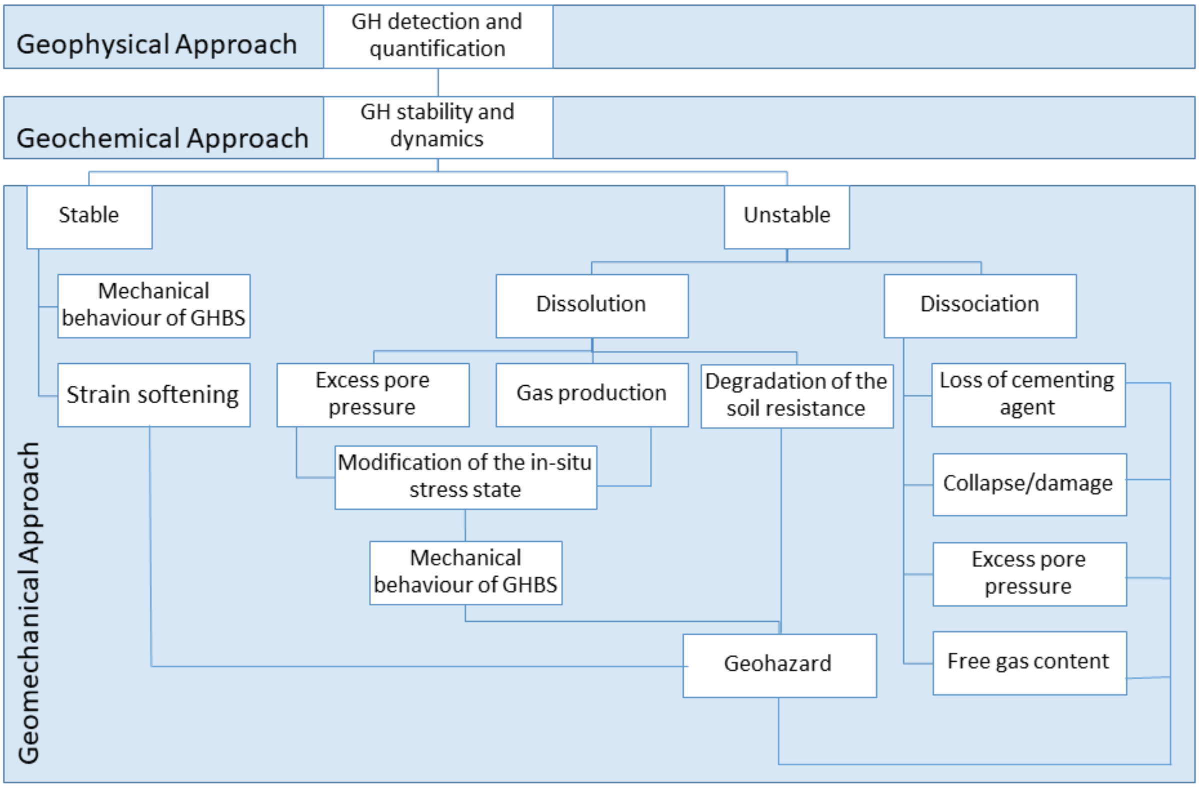

Figure 7. 1 Work structure followed to assess the geohazard associated with GH

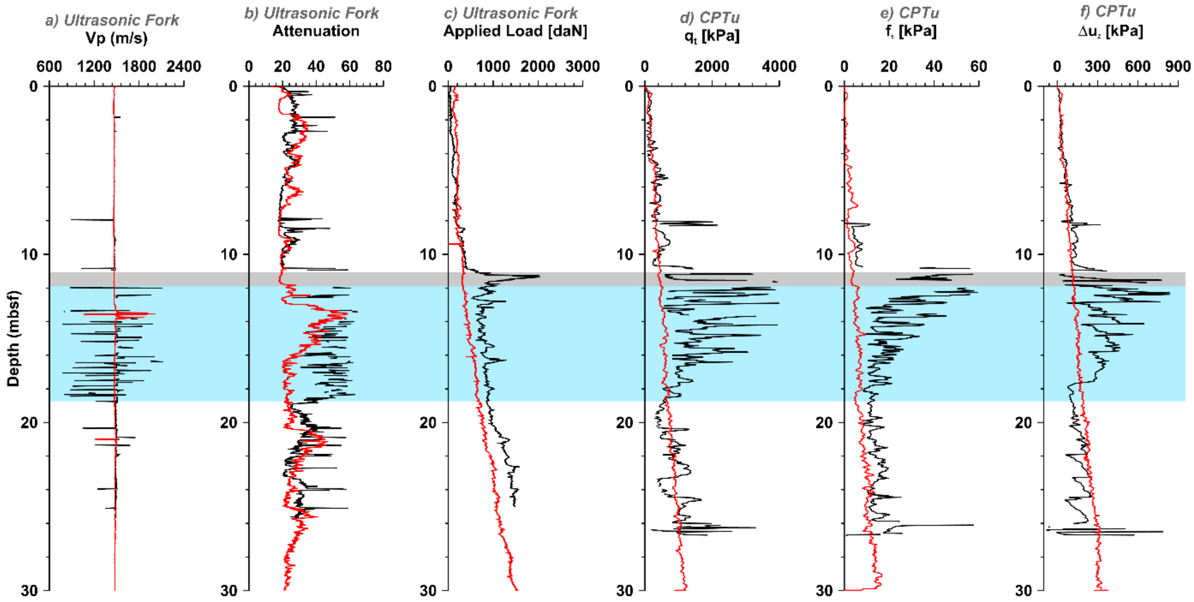

Figure 7. 2 In-situ acoustic data acquired with the ultrasonic fork for site GMPFV10S04 and in-situ geotechnical data acquired from CPTU for site GMPFM05S03: a) Vp, b) attenuation, c) applied load, d) cone tip resistance, e) sleeve friction and f) pore pressure. The grey rectangle indicates the loss of data in the velocity and attenuation profiles and the light blue one represents a layer of GH as detected from the alternative methods reported by Wei et al. (2015)

Figure 7. 3 Natural GH recovered during the Guineco-MeBo oceanographic campaign

The geotechnical data, also acquired with the Penfeld, can give insight into the detection of GH. The simultaneous increase in the cone tip resistance (resistance of the sediment to the penetration of the tip of the piezocone during CPTu), the friction sleeve (friction between the sediment and the sleeve of the piezocone) and the pore water pressure (fluid pressure induced by the penetration of piezocone), indicate the presence of GH (Figure 7. 2).

In some cases, the 30-m long rod of the Penfeld could not completely penetrate into the sediment. This phenomenon is considered as a mechanical refusal and is due to the high resistance of the gas hydrates-bearing sediments (GHBS). Otherwise, it is noteworthy that the device used to perform the in-situ acoustic measurements can measure compressional wave velocities only up to 2200 m/s. Therefore, this could explain the discontinuities in the Vp profiles (grey rectangle in Figure 7. 2), which could be due to the presence of massive hydrate nodules characterised by velocities higher than 3800 m/s. Such presence is confirmed by a significant increase observed on the applied load (to push the acoustic fork in the sediments) profile at around the same depth.

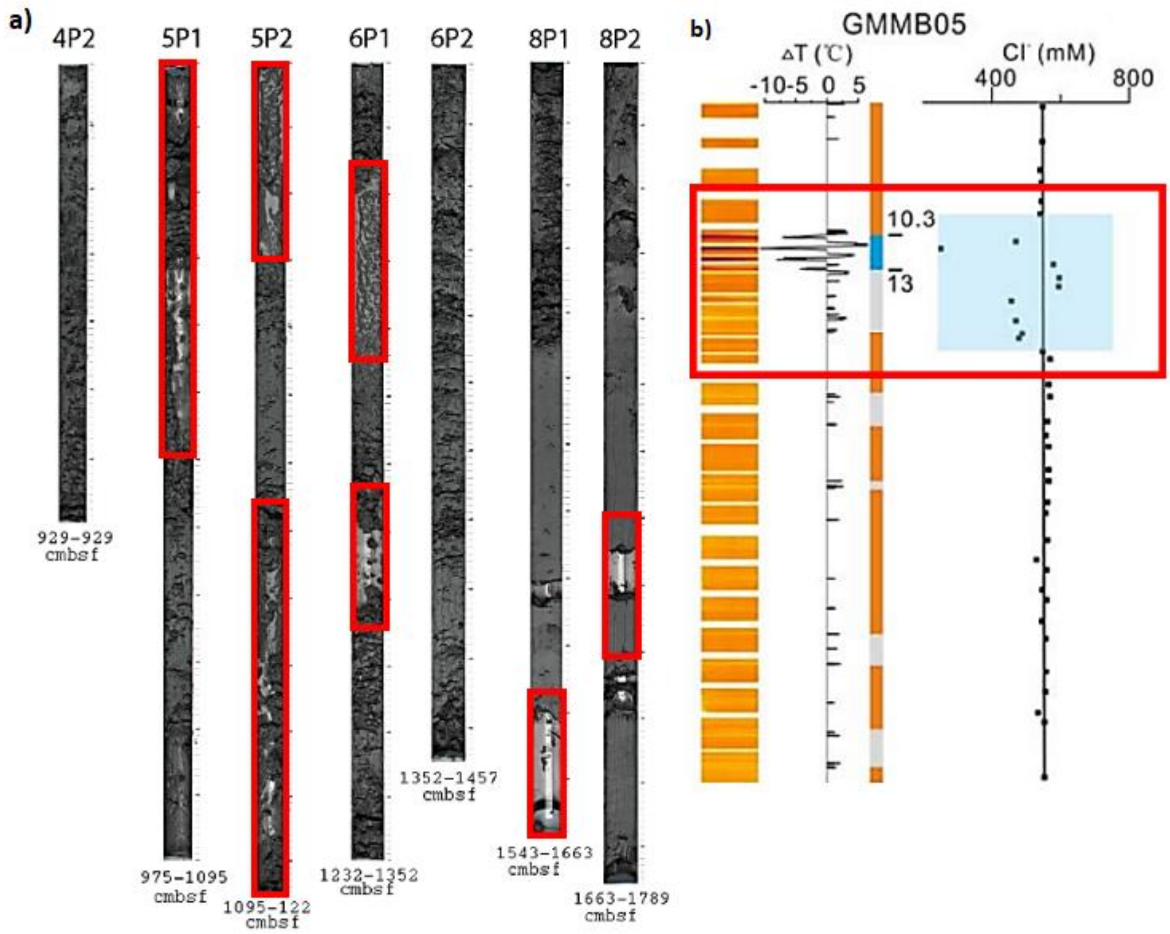

Figure 7. 4 Visual observations of the GMMB05 MeBo core showing fluidised sediments and b) infrared thermal imaging and pore water chloride analysis results showing negative anomalies indicating the previous presence of GH (from Wei et al., 2015)

Detecting the presence of GH was also possible by direct observation of cores recovered during the oceanographic campaigns (Figure 7. 3). Additionally, as upon core recovery gas hydrates dissociated, pore water chloride analysis and infrared imaging were used to detect their presence (Figure 7. 4).

The formation of GH is known to exclude ions dissolved in the surrounding pore water from the clathrate cage. Therefore, upon recovery the dissociation of GH releases freshwater, which is observed as negative anomalies on pore water chloride profiles (Wei et al., 2015). Alternatively, the decomposition of GH is an endothermic process: it requires the absorption of temperature. Therefore, colder temperatures of the recovered cores, compared to reference sediments, is indeed an indicator of the presence of GH. Additionally, seismic profiles throughout the study area showed a marked contrast between the high-amplitude chaotic facies in the central part of the study area and the continuous sub-parallel facies of the surrounding sediments. This allowed confirming the presence of GH. It is noteworthy that results derived from the effective medium theory and those from negative thermal and chloride anomalies were found to yield almost the same GH occurrence zone.

7.3 What are the methods that allowed the quantification of gas hydrates?

Quantification results were derived from the effective medium theory based on Vp anomalies (Helgerud et al., 1999) and from pore-water analysis based on chloride anomalies (Malinverno et al., 2008). Both results were then compared in order to confirm their reliability (Figure 7. 5).

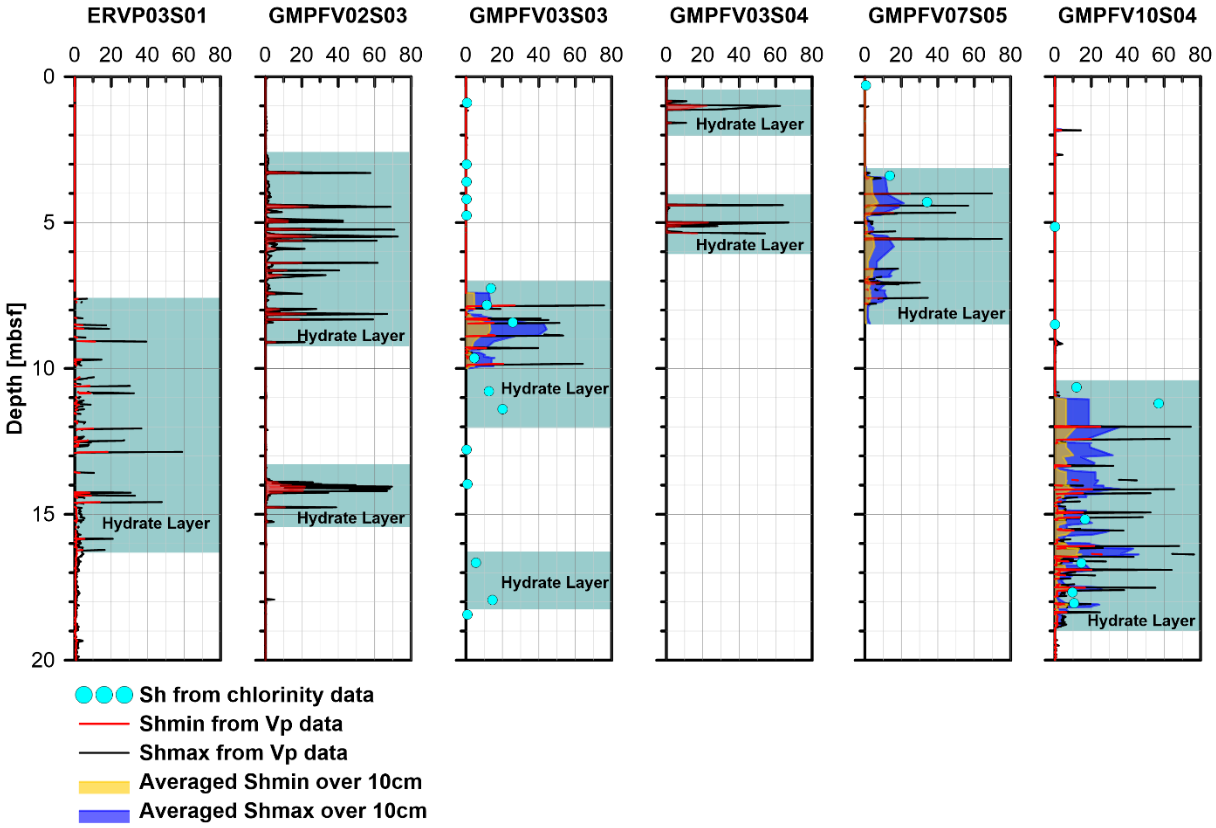

Figure 7. 5 Estimates of GH content for different sites in the study area (from Taleb et al., 2018)

The quantification process first required an accurate definition of the mineralogy profile. This was possible by performing non-destructive tests such as XRD (X-ray diffraction) and XRF (X-ray fluorescence) on the recovered cores. Accordingly, a petro-physical model was developed for reference sites. Interestingly, in-situ attenuation data proved useful in expanding the application of the petro-physical model to sites lacking mineralogical constraints. The detailed method is presented in Chapter 4.

The main conclusions concerning the quantification of GH were:

- The effective medium model allowed estimating a lower and upper bound GH content by assuming that (1) hydrate only affects the pore fluid elastic properties and density (S_{hmax}) and (2) hydrate affects the stiffness of the sediment by contributing to the load-bearing framework (S_{hmin}).
- Comparisons were conducted between results derived from the effective medium theory and those derived from pore-water chloride analysis as well as with studies performed by Ghosh et al. (2010). This showed that S_{hmin} is more adapted to represent GH content in the study area as it yields closer estimates to those obtained from pore water chloride analysis, compared to S_{hmax}.
- A maximum GH content of 26.5% was estimated at a Vp of 2035 m/s using the effective medium model.

7.4 What are the main features of the geomorphology of the study area?

Correlations between seismic profiles and in-situ data as well as visual observations of recovered cores have allowed to define the effect of GH presence and distribution on the geomorphology of the study area. Seismic profiles proved to be means of identifying the presence of GH based on the following remarks:

- High amplitude chaotic facies are an indicator of the presence of GH.
- Low-amplitude subparallel facies represent undisturbed sediments.

Tying these observations with in-situ results have led to the following conclusions:

- The study area accommodates zones where solid GH and free gas coexist as well as zones of free gas pockets.
- Fractures/discontinuities have been identified as preferential pathways in which free gas can migrate and contribute to further GH formations.

Then, 4 meters spaced seismic profiles were used to develop a 3D cube (Figure 7. 6) of the study area. This allowed identifying the GHOZ as well as calculating its occupying volume within the study area:

- With a volume of $2.7 \times 10^6\ m^3$the GHOZ occupies 17% of the total volume of pockmark A for an estimated GH volume of $0.57 \times 10^6\ m^3$.
- The seabed morphology of pockmark A is directly influenced by the distribution of underlying GH accumulations:
    - The highest GH contents (20%-30%) are observed to be in the central part of the pockmark.
    - The lowest GH contents (0%-10%) are mostly observed at the borders of the pockmark.
- The morphology of a given pockmark in the study area might be an indication that can be used to confirm the presence of GH, determine an interval of GH content and identify different GH morphologies.

7.5 What are the main features of the mechanical behaviour of the gas hydrates-bearing sediment from the study area?

Normalised classification charts were used in order to characterise the mechanical properties of GHBS of the study area (Figure 7. 7). Parameters required to use such tables including the normalised cone resistance, the normalised pore pressure and the normalised friction ratio were determined from in-situ geotechnical measurements. Additionally, empirical equations were used to determine specific mechanical parameters of the host sediment. It was therefore possible to observe trends characterising the mechanical behaviour of GHBS as well as the evolution of their mechanical properties with respect to GH content.

In-situ results derived from piezocone data (Figure 7. 7.a) and from pore pressure dissipation measurements have both shown that GH-bearing clayey sediments are characterised by a contractive behaviour upon shearing. It is noteworthy that such behaviour cannot be inferred if only based on classification charts relying on normalised sleeve friction (Figure 7. 7.b).

One might say that a contractive behaviour is the natural response of clayey sediments upon shearing. In other words, the tendency of clayey sediments containing GH to contract is caused by lithology and not by GH presence. However, the aim of this part of the thesis was to show that natural clayey sediment preserve their contractive behaviour in the presence of hydrates.

The main conclusions concerning the mechanical behaviour of GHBS are:

- GH-bearing clayey sediments have a contractive behaviour upon shearing which contrasts with experimental results on sands (Hyodo et al., 2013) and on clays (Yun et al., 2007).
- The resistance of the sediment was observed to increase with increasing GH content. However, GHBS with similar GH contents were sometimes noticed to correlate with different normalised cone resistance values. This suggests that different morphologies of GH are present in the marine sediment.
- The presence of GH was noticed to increase the stiffness and the undrained shear strength while decreasing the compressibility.

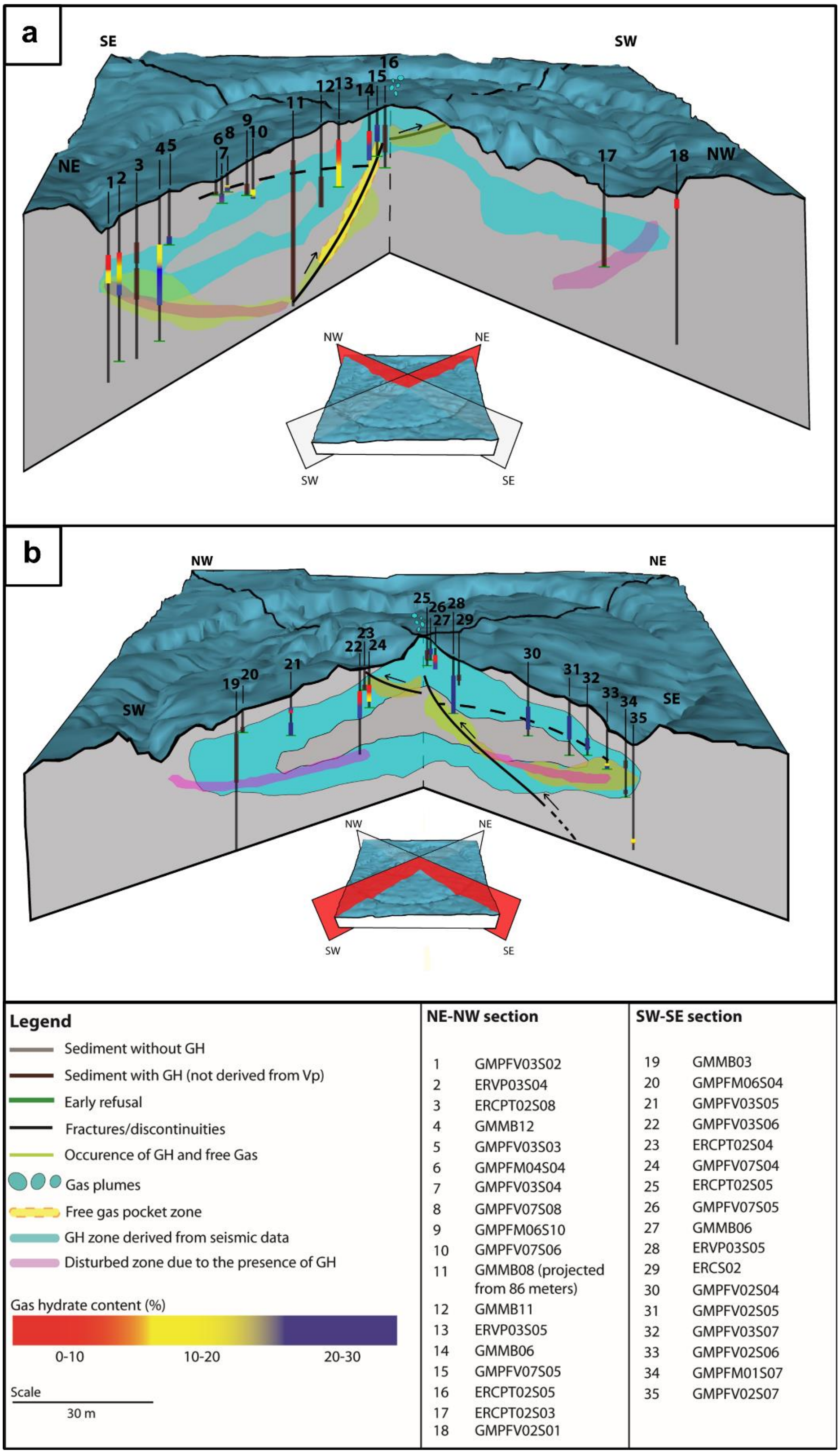

Legend

- Sediment without GH
- Sediment with GH (not derived from Vp)
- Early refusal
- Fractures/discontinuities
- Occurence of GH and free Gas
- ● ● ● Gas plumes
- Free gas pocket zone
- GH zone derived from seismic data
- Disturbed zone due to the presence of GH

Gas hydrate content (%)

0-10 10-20 20-30

Scale

30 m

NE-NW section	
1	GMPFV03S02
2	ERVP03S04
3	ERCPT02S08
4	GMMB12
5	GMPFV03S03
6	GMPFM04S04
7	GMPFV03S04
8	GMPFV07S08
9	GMPFM06S10
10	GMPFV07S06
11	GMMB08 (projected from 86 meters)
12	GMMB11
13	ERVP03S05
14	GMMB06
15	GMPFV07S05
16	ERCPT02S05
17	ERCPT02S03
18	GMPFV02S01

SW-SE section	
19	GMMB03
20	GMPFM06S04
21	GMPFV03S05
22	GMPFV03S06
23	ERCPT02S04
24	GMPFV07S04
25	ERCPT02S05
26	GMPFV07S05
27	GMMB06
28	ERVP03S05
29	ERCS02
30	GMPFV02S04
31	GMPFV02S05
32	GMPFV03S07
33	GMPFV02S06
34	GMPFM01S07
35	GMPFV02S07

Figure 7. 6 a)Perpendicular cross section across the northern part of pockmark A and b) perpendicular cross section across the southern part of pockmark. On each cross section GH contents as estimated from in-situ measurements as well as the GHOZ and fractures/discontinuities as inferred from seismic data are projected.

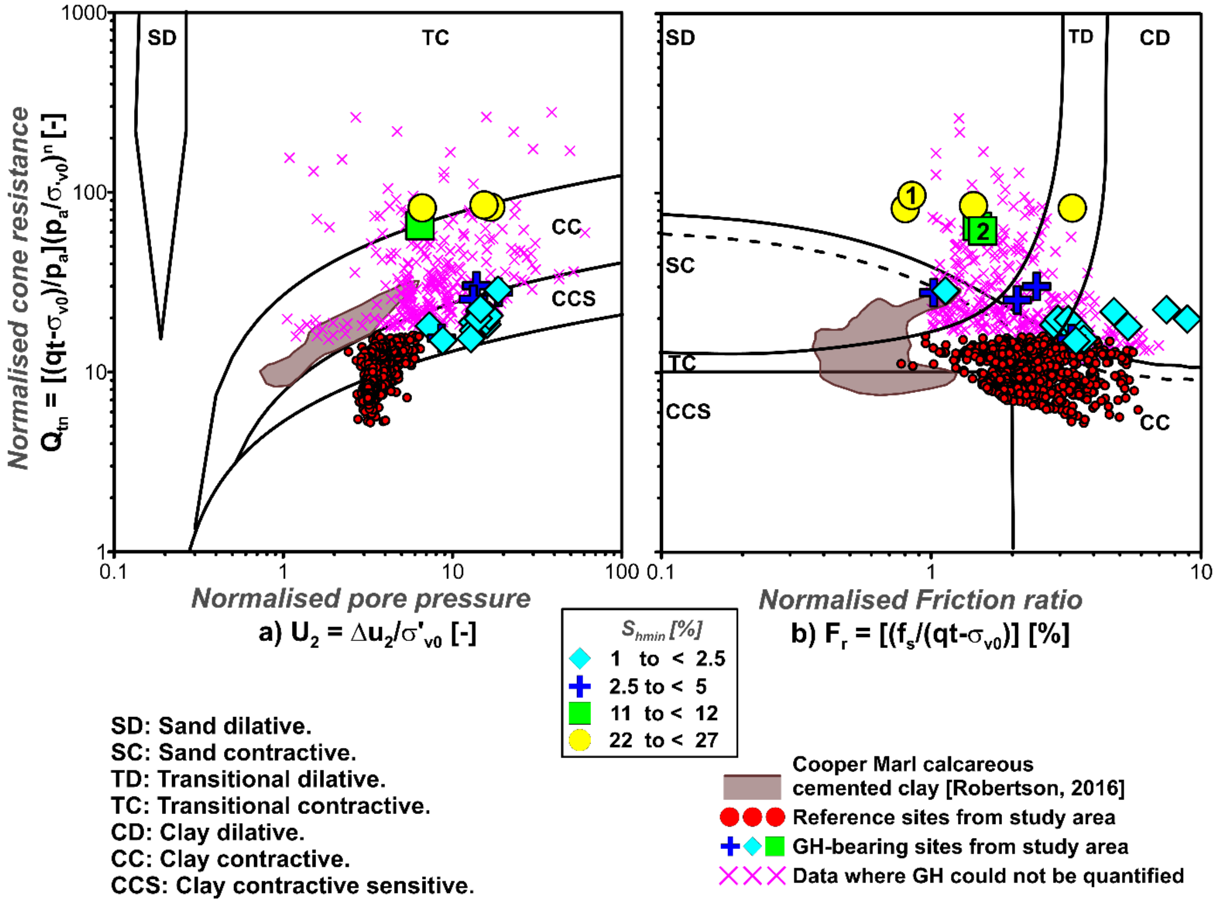

Figure 7. 7 In-situ geotechnical data, for different sites from the study area, plotted in normalised soil classification charts (from Taleb et al., 2018)

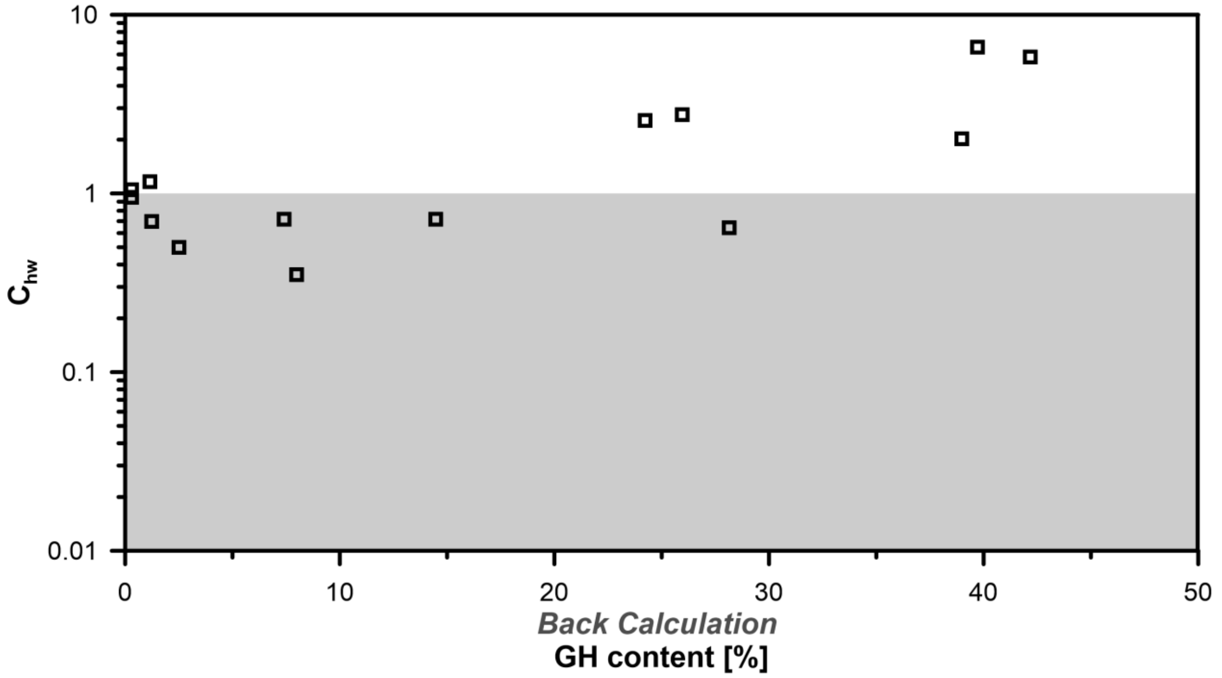

Figure 7. 8 Hydraulic diffusivity as a function of GH content (from Taleb et al., 2018)

7.6 What are the hydraulic properties of the gas hydrates-bearing sediments from the study area?

The hydraulic properties of the GHBS from the study area were determined based on pore pressure dissipation measurements performed by the Ifremer piezometer. The hydraulic diffusivity was then derived and plotted as a function of GH content. While according to experimental results (Katagiri et al., 2017), gas hydrates were found to impede the water or gas fluxes and cause a decrease in the permeability, the following was observed concerning the hydraulic properties of GHBS from the study area:

- For GH content lower than 10%, the hydraulic diffusivity was observed to decrease as expected with respect to experimental results.
- However, for higher GH content values, the hydraulic diffusivity is observed to increase. This was explained by the following points:
    - In natural environments, high hydraulic diffusivities may be linked to the presence of fractures and fluid flow paths.
    - The decrease in compressibility of the sediment due to the presence of GH might be at the origin of the hydraulic diffusivity increase.

7.7 Why is it important to formulate a simple model in order to simulate the mechanical response of gas hydrates-bearing sediments?

A new simple constitutive model, which is able to reproduce the mechanical behaviour and response of GHBS has been developed within the framework of the PhD (personal communication with Sultan).

The main purpose of this part was to develop a model that requires a minimum amount of parameters (only one extra parameter in addition to classical mechanical constitutive models). The new model considers the contractancy/dilatancy upon shearing of the GHBS through a modified expression of the steady state line and by proposing a new “equivalent skeleton void ratio”.

In order to validate the performance of the model for GH-bearing clayey sediments, a large database is required. However, due to the lack of data concerning such sediments, the numerical results were first validated for the case of sandy sediments. Alternatively, an extension of the model able to simulate the behaviour of GH-bearing clayey sediments is proposed.

The main conclusions concerning this part were:

- The fact that only one extra parameter related to the morphology of GH is required is at one advantageous and challenging
    - The model might not be able to precisely reproduce experimental results of GHBS mechanical properties as other introduced models; however,
    - Compared to models available in the literature, the proposed model is easier to apply. This is because, In addition to the classic modified Cam Clay parameters, it requires a parameter (b) that accounts for GH morphology, β that describes the way the void ratio reaches the locus of the steady state line and β_h that is an optional parameter reflecting the impact of GH morphology on the compressibility of GHBS.
- The model was proved capable of simulating the mechanical behaviour of coarse-grained sediments without GH as well as sediments containing different GH contents and morphologies.
- The model was able to reproduce the deviator stress-axial strain response of clays without GH and with different GH contents; however, it did not succeed in reproducing the volumetric strain-axial strain response in the case of dilative behaviour.
- The model lacked precision in reproducing the strain softening caused by the presence of GH.

7.8 Limitations and possible improvements

Like any other work, this work faced some limitations and challenges. Therefore, in this part some of these limitations and trials to improve them are proposed.

7.8.1 Limitations concerning the quantification of gas hydrates

This paragraph will mainly deal with limitations concerning the quantification of GH using the effective medium modelling:

- One might say that using the Helgerud et al. (1999) effective medium modelling is not satisfactory in the case of clayey sediments. However, Ghosh et al. (2010) compared different gas hydrates estimation methods, such as the grain displacing model and the Helgerud effective medium model, to the pressure core method, which is the most direct and reliable one. It was found that the case, where GH are assumed to contribute to the stiffness of their host sediment, gave an overestimation of 7-11% with respect to pressure coring. Although the grain-displacing model is the most reliable method for gas hydrate-bearing clayey sediments, it was not used in this work due to lack of information about the fractures orientation within the sediment. Alternatively, the fact that acoustic-derived results were compared to those derived from the pore water chloride analysis represents a reliable argument to determine which model may yield the most representative results in the study area. Additionally, it is reasonable to consider that the macro-scale hydrates observed in the clayey sediment of the study area contribute to bearing the load they are subjected to.
- The model will always interpret high velocities as an indicator for the presence of GH. It is therefore necessary to compare the measured velocity with other available methods. Alternatively, based on the difference between the measured velocity and the calculated one that oscillates in the range of $\pm 17\ m/s$, estimates of GH content were only provided when the calculated Vp exceeds the measured one by at least $17\ m/s$.
- Another challenge facing the quantification of GH is the fact that the acoustic fork of the Penfeld can detect compressional wave velocities only up to 2200 m/s. However, based on experimental results from Helgerud et al. (2009), in the presence of massive GH, Vp can reach values as high as 3000 m/s. Such massive hydrates were observed in recovered cores at depths correlating with the presence of discontinuities on the in-situ acoustic profiles (grey rectangle in Figure 7. 2). Therefore, in such cases the quantification of GH was not possible.
- The presence of free gas might affect the quantification process. While the presence of GH increases the compressional wave velocity, the presence of free gas decreases it. The coexistence of free gas and solid hydrates have been proved multiple times throughout the manuscript (principally in chapter 4 and chapter 5). This can induce uncertainties regarding the results of the effective medium modelling approach or any other inverse approach which has to solve equations with solid gas hydrates and free gas as two independent variables. Therefore, the quantification of GH can be affected (underestimated) by the decrease in compressional wave velocity induced by the presence of free gas.
- At last, it is noteworthy that during core recovery (using calypso or MeBo) the stability conditions for GH are disturbed. This is problematic since sometimes direct observation of the cores are needed to confirm the presence or absence of GH and their morphology. The dissociation of GH, within the core results in a muddy and fluidised sediment (Figure 7. 4.a). Such problem might be overcome by using pressure coring as shown by Santamarina et al. (2015).

7.8.2 Limitations concerning the characterisation of the mechanical behaviour of gas hydrate-bearing sediments using in-situ measurements

The use of normalised soil classification charts based on correlations between in-situ acoustic and geotechnical data faced limitations such as:

- Positioning limitations inherent to the deep-water depths in the study area might have affected the correlations between neighbouring in-situ acoustic and geotechnical measurements. In some cases, peaks on the velocity and cone tip resistance profiles did not necessarily occur at the same depth. This required depth correlations between both types of data in order to accurately characterise the mechanical behaviour of GH-bearing clays.
- The lack of experimental results leaves some uncertainties concerning the mechanical behaviour of GHBS. Indeed, further investigations can be useful in order to validate the results of this thesis, particularly those concerning different morphologies of GH.

7.8.3 Limitations concerning the derivation of the hydraulic properties of gas hydrate-bearing sediments using in-situ measurements

- The most controversial observation regarding the hydraulic properties of GHBS is the increasing trend of the hydraulic diffusivity for GH contents exceeding 10%. This could be due to the presence of natural and/or artificial fractures. While natural fractures might be due to GH presence, artificial ones might have been caused by the penetration of the piezometer. Therefore, the induction of new fractures or the development of existing ones might have superimposed a secondary porosity to that which actually controls the in-situ hydraulic diffusivity.

7.8.4 Limitations concerning the new mechanical constitutive model

The fact that the model needs only one extra parameter, accounting for GH morphology, to simulate the main features of mechanical behaviour of GHBS presents several limitations:

- Numerical results are not as precise as those of other models relying on a more extensive list of parameters.
- The model is not able to reproduce the smooth strength transition between elastic and elasto-plastic behaviour.
- With increasing GH content, the model fails to capture the dilatancy of the sediment in the volumetric strain – axial strain space.

The lack of experimental data on the mechanical behaviour of clayey GHBS makes the adaptation of the model to clayey sediment challenging.

Therefore, performing experimental studies emulating the in-situ conditions of the study area will contribute to improve the model performance.

7.9 Perspectives

In this work, the effect of GH content and distribution on the mechanical and hydraulic properties of their host clayey sediment was highlighted. However, some of the strong conclusions might be considered premature at this stage. Further investigations supported by experimental data are required in order to substantiate the effect of various GH content and morphologies on the properties of their host sediment.

A step towards validating the observations and conclusions of this PhD work is to compare in-situ results with experimental ones. Such validation is very useful for several reasons:

- Such information will give more insight on the morphology/distribution of GH and their effect on the surrounding clayey sediment.
- Additionally, this will allow refining classic empirical relationships used to derive geotechnical parameters from in-situ mechanical measurements.

- This will ultimately allow improving the numerical model proposed to capture the main features of mechanical behaviour of GH-bearing clayey sediments.

The geotechnical laboratory at Ifremer is equipped with a triaxial cell that allows the study of the mechanical properties of the sediment in question. The machine is equipped with a confining pressure and pore pressure regulation systems, a triaxial press, a confining cell and a gas injection system. This machine can be eventually used to perform triaxial tests on synthetic GHBS made from clays recovered from the study area.

Another approach to characterise GH is through pressure coring, which allows the recovery of GH under in-situ temperature and pressure conditions. Several datasets are available in the literature where pressure coring was used as means to study the mechanical behaviour of GH (see for instance Santamarina et al., 2015). Therefore, it would be interesting to compare the in-situ results of this thesis with those obtained from pressure coring.

Alternatively, this work has shown that CPTu measurements are efficient means of collecting large amount of data, particularly in gas hydrate-bearing sediments. Such technique (1) has been proved a promising and less expensive alternative to costly pressure coring operations and (2) deserves to be adopted by more research studies.

While it is very important to study GH in their in-situ conditions, it is also required to complete this work by characterising the geohazard that might result from GH decomposition (dissolution or dissociation). GH decomposition alters the mechanical properties and behaviour of their host sediments by reducing the strength and resistance of the sediment. Additionally, the presence of gas in sediments reduces its shear strength (Sultan et al., 2012). Understanding these mechanisms helps estimating and preventing the potential geohazard of GH such as slope instabilities. Therefore, it would be interesting to propose a numerical model able to simulate the behaviour of both sediments containing GH and sediments containing free gas. This will allow accounting for the behaviour of a GHBS following the decomposition of GH, which results in free gas and fresh water. Ultimately, this can be one step of many needed in order to give insight into gas production from GH-rich environments.

7.1 Introduction

L'objectif de cette thèse était de détecter et de quantifier les hydrates de gaz (GH) et d'évaluer le comportement mécanique des sédiments qui les contiennent (GHBS) à partir de mesures in-situ dans le delta profond du Niger. Ce chapitre résume les principaux résultats et conclusions associés à ce travail. Les perspectives et les nouvelles questions scientifiques pour les futurs travaux de recherche sont présentées à la fin de ce chapitre. L'approche développée au cours de ce travail de thèse a suivi l'articulation présentée en Figure 7. 1 pour caractériser les potentiels aléas géologiques liés aux hydrates de gaz lorsque ceux-ci sont en conditions de stabilité. Elle est axée sur la détection et la quantification des GH et sur la détermination de leurs comportements mécaniques.

7.2 Quelles sont les méthodes qui ont permis la détection des hydrates de gaz?

Le fait que les hydrates de gaz modifient les propriétés physiques et mécaniques des sédiments est à la base de toutes les méthodes de détections couramment utilisées. (Waite et al., 2009; Dai et al., 2012). Cela a été illustré en utilisant une méthode d'inter-comparaison entre les données Penfeld CPTu et Penfeld Vp. Typiquement, dans un sédiment argileux similaire à celui présent dans la zone d'étude, la vitesse des ondes de compression (Vp) varie entre 1450 et 1510 m/s. Cependant, la présence de GH fait augmenter ces valeurs jusqu'à 3600 m/s (Sultan et al., 2007). Ceci est principalement lié au fait que les modules de compressibilité et de cisaillement des GH sont très élevés comparés à ceux de l'eau ou du gaz. Il a pu être observé in situ que cela s'accompagne également d'une augmentation de l'atténuation du signal acoustique. Ainsi, la détection de la présence de GH peut être directement liée à une augmentation simultanée de tous les paramètres acoustiques in-situ. Au contraire, il est reconnu qu'en présence de gaz libre caractérisé par des modules de compressibilité et de cisaillement plus faibles que ceux de l'eau, la vitesse Vp tend à diminuer de manière significative. Il est important de souligner que dans certains cas, la coexistence de gaz libre et de GH suspectée d'après les mesures acoustiques in situ a pu être confirmée par l'observation de nodules d'hydrates d'aspect spongieux.

En complément de l'approche acoustique, les données géotechniques, également acquises avec le Penfeld, ont permis de détecter la présence de GH. L'augmentation simultanée de la résistance au cône (résistance du sédiment à la pénétration de la pointe du piézocône), du frottement latéral (frottement entre le sédiment et le manchon du piézocône) et de la pression de fluides interstitiels (pression induite par la pénétration du piézocône), indiquent la présence des GH (Figure 7. 2). Dans certains cas, la tige de 30 m du Penfeld n'a pas pu pénétrer complètement dans le sédiment. Ce phénomène est considéré comme un refus mécanique souvent dû à la résistance élevée des GHBS. Il est à noter que le dispositif utilisé pour effectuer les mesures acoustiques in-situ permet seulement de mesurer les vitesses des ondes de compression jusqu'à 2200 m/s. Cela pourrait donc expliquer les discontinuités dans les profils Vp (rectangle gris de la Figure 7. 2), pouvant être causés par présence de nodules d'hydrate massifs dont les Vp pourraient être supérieures à 3800 m/s. Cette présence est également confirmée par une augmentation significative du profil d'effort injecteur (force requise pour foncer la fourche acoustique dans les sédiments) à profondeur sensiblement identique. La détection des GH a été également possible grâce à l'étude des carottes sédimentaires récupérées au cours des campagnes océanographiques (Figure 7. 3). Outre les observations directes des hydrates de gaz les conséquences physico-chimiques de leur dissociation ont permis de les détecter par analyse de la chlorinité des fluides interstitiels et par imagerie infrarouge (Figure 7. 4). La première approche est basée sur le fait que la formation des GH exclut les ions dissous dans l'eau interstitielle de la cage en clathrate. Par conséquent, la dissociation des GH lors de leurs prélèvements libère de l'eau douce, qu'on observe sous forme d'anomalies négatives sur les profils de chlorinité (Wei et al., 2015). Alternativement, la décomposition des GH est un processus endothermique, c'est à dire qu'elle nécessite une absorption de température. Par conséquent, les chutes locales de températures mesurées le long des carottes sont des indices de la présence des GH. Les profils sismiques acquis sur l'ensemble de la zone d'étude montrent également un contraste bien marqué entre les faciès chaotiques de forte amplitude de la partie centrale de la zone d'étude et les faciès bien stratifiés et continus des sédiments environnants. Cela a encore une fois permis de confirmer la présence des GH. Il est notable que les différentes méthodes de détection mises en œuvre sur la zone d'étude ont donné des indications concordantes concernant la distribution des hydrates dans les sédiments.

7.3 Quelles sont les méthodes qui ont permis la quantification des hydrates de gaz?

La première approche de quantification des GH mise en œuvre dans cette thèse est dérivée de la théorie du milieu effectif appliquée aux anomalies positives de Vp (Helgerud et al., 1999). La seconde approche est dérivée de la géochimie des eaux interstitielles appliquée aux anomalies de chlorinité (Malinverno et al., 2008). Les résultats obtenus par ces deux approches ont ensuite été comparés pour attester de leur fiabilité (Figure 7. 5). L'approche de quantification géophysique a premièrement nécessité une détermination précise du profil minéralogique des sédiments. Cela a été possible en effectuant analyses avec la méthode XRD (diffraction des rayons X) et XRF (fluorescence des rayons X) sur les carottes sédimentaires récupérés. Suite à ces essais, un modèle pétro-physique a été développé pour les sites de référence. Les données d'atténuation in-situ se sont révélées utiles pour élargir l'application du modèle aux sites où les profils minéralogiques n'ont pu être directement déterminés. La méthode complète est détaillée dans le chapitre 4.

Les principales conclusions sur la quantification des GH sont les suivantes:

- Le modèle de milieu effectif permet d'estimer une teneur en GH par une limite inférieure et supérieure en supposant que (1) l'hydrate affecte uniquement les propriétés élastiques du fluide interstitiel (S_{hmax}) et (2) l'hydrate affecte la rigidité du sédiment en contribuant à sa structure (S_{hmin}).
- Des comparaisons ont été effectuées entre les résultats dérivés de la théorie du milieu effectif et ceux dérivés de l'analyse de chlorinité dans les pores ainsi que des études effectuées par Ghosh et al. (2010). Cela a montré que $\mathrm{S_{hmin}}$ est plus adapté pour représenter le contenu en GH dans la zone d'étude car il fournit des estimations plus proches que $\mathrm{S_{hmax}}$ de celles obtenues avec la méthode d'anomalies négatives de chlorinité.
- Une teneur en GH maximale de 26,5% a pu être estimée pour une vitesse Vp de 2035 m/s en utilisant le modèle des milieux effectifs (S_{hmin}).

7.4 Quelles sont les principales caractéristiques de la géomorphologie de la zone d'étude?

Les corrélations entre les profils sismiques et les données in-situ issues de l'analyse des carottes ont permis de définir l'effet de la présence et de la distribution des GH sur la géomorphologie de la zone d'étude. Les profils sismiques se sont révélés être un bon moyen pour identifier la présence des GH sur la base des principes suivants:

- Les faciès chaotiques de forte amplitude sont un indicateur de la présence des GH.

Les faciès parallèles et stratifiés de faible amplitude représentent des sédiments non perturbés.

En liant ces observations aux résultats in-situ les conclusions suivantes ont pu être tirées:

- La zone d'étude comprend des zones de coexistence entre des GH et du gaz libre ainsi que des zones ne contenant que des poches de gaz libre.

- Les fractures et discontinuités ont été identifiées comme des voies formant des passages dans lesquelles le gaz libre peut migrer et contribuer à de nouvelles formations de GH.

En complément, des profils sismiques, espacés de 4m, ont été utilisés pour former un cube représentant la zone d'étude en 3D (Figure 7. 6). Cela a permis la délinéation à grande échelle de la zone d'occurrence des GH et de calculer son volume d'occupation. Les points principaux qui en sont ressortis sont les suivants :

- Avec un volume de $2.7 \times 10^6\ m^3$la GHOZ occupe 17% du volume total du Pockmark A pour un volume de GH estimé à $0.57 \times 10^6\ m^3$.
- La morphologie du pockmark A est directement influencée par la distribution des formations de GH sous-jacents:
    - Les teneurs en GH les plus élevées (20% à 30%) se trouvent dans la partie centrale du pockmark.
    - Les teneurs en GH les plus faibles (0% à 10%) sont principalement observées en bordures du pockmark.
- La morphologie d'un pockmark dans la zone d'étude peut servir d'indicateur pouvant confirmer la présence de GH mais aussi déterminer un intervalle de contenu en GH et conjointement identifier différentes morphologies de GH.

7.5 *Quelles sont les principales caractéristiques du comportement mécanique des sédiments contenant des hydrates de gaz de la zone d'étude?*

Des abaques de classification ont été utilisés pour caractériser les traits de comportement mécanique des GHBS à partir des mesures CPTu normalisées incluant : la résistance de pointe, la pression interstitielle et le frottement latéral. De plus, des équations empiriques ont été utilisées pour déterminer certaines propriétés mécaniques des GHBS. En croisant ces résultats avec ceux obtenus à partir de mesures acoustiques il a donc été possible d'observer les tendances caractérisant le comportement mécanique des GHBS ainsi que l'évolution de leurs propriétés mécaniques en fonction de leur saturation en GH.

Les résultats dérivés des CPTu (Figure 7. 7.a) et des mesures de dissipation de pressions interstitielles ont tous les deux montré que les GHBS sont caractérisés par un comportement contractant lors du cisaillement. Il est à noter que la concordance de ces résultats met en avant le fait que les tableaux de classification utilisant de manière alternative les valeurs de frottement latéral normalisées ne sont pas adaptés à la mise en évidence de cette spécificité du comportement des GHBS (Figure 7. 7.b). En d'autres termes, les mesures CPTu de frottement ne permettent pas de faire ressortir le fait que le comportement naturellement contractant des argiles est généralement exacerbé en présence d'hydrates.

Les principales conclusions concernant le comportement mécanique du GHBS sont les suivantes:

- Les GHBS argileux ont un comportement contractant lors du cisaillement qui contraste avec les résultats expérimentaux obtenus sur les sables (Hyodo et al., 2013) et avec du TetraHydroFuran (THF) sur les argiles (Yun et al., 2007).
- La résistance des sédiments augmente avec la saturation en GH. Cependant, dans certains cas, des GHBS ayant la même saturation en GH se caractérisent par différentes valeurs de résistance normalisée. Ceci suggère qu'il existe différentes morphologies de GH dans les sédiments marins et que celles-ci conditionnent fortement la réponse mécanique des sédiments.
- La présence de GH fait augmenter la rigidité tout en diminuant la compressibilité du sédiment dans des proportions qui paraissent fonction à la fois de la teneur en hydrate mais aussi de leur distribution et morphologies.

7.6 Quelles sont les propriétés hydrauliques des sédiments contenant des hydrates de gaz de la zone d'étude?

Les propriétés hydrauliques des GHBS de la zone d'étude ont été déterminées par des mesures de dissipation de pression interstitielle effectuées à l'aide du piézomètre d'Ifremer. La diffusivité hydraulique a ensuite été calculée et représenté graphiquement en fonction de la teneur en GH. Bien que les résultats expérimentaux (Katagiri et al., 2017) montrent que les GH empêche les flux d'eau ou de gaz et entraîne une diminution de la perméabilité des différences importantes ont pu être déterminées à partir des mesures in situ:

- Pour une teneur en GH inférieure à 10%, la diffusivité hydraulique diminue de manière comparable aux résultats expérimentaux sur sédiments sableux.
- Cependant, pour des teneurs en GH supérieures à 10%, on observe une augmentation de la diffusivité hydraulique. Cela peut s'expliquer de deux manières:
    - Des diffusivités hydrauliques élevées peuvent être associées à la présence de fractures et de conduits favorisant l'écoulement des fluides.
    - L'augmentation de la diffusivité hydraulique est peut-être due aux effets des GH sur la diminution de la compressibilité des sédiments.

7.7 Est-il possible de formuler un modèle simple pour simuler la réponse mécanique des sédiments contenant des hydrates de gaz?

Un nouveau modèle constitutif simple, visant à reproduire le comportement mécanique des GHBS a été développé dans le cadre de cette thèse (communication personnelle avec Sultan). L'objectif principal était d'élaborer un modèle demandant un minimum de paramètres (un seul paramètre supplémentaire en plus de ceux des modèles constitutifs classiques). Ce nouveau modèle prend en compte la contractance/dilatance lors du cisaillement des GHBS par une expression modifiée de la ligne d'état stable et en proposant un nouvel “indice des vides equivalent ”.

Afin de valider le modèle pour les GHBS argileux, une base de données volumineuse est nécessaire. Cependant, faute de données disponibles pour de tels sédiments, les résultats numériques ont d'abord été validés avec des sédiments sableux. Alternativement, une extension du modèle permettant de simuler le comportement de GHBS argileux est proposé.

Les principales conclusions concernant ces modèles sont les suivantes:

- Le fait qu'un seul paramètre supplémentaire représentant la morphologie des GH soit nécessaire est à la fois un avantage mais aussi un défi:
    - Le modèle n’est pas toujours en mesure de reproduire avec autant de précision que d’autres modèles publiés les résultats expérimentaux des propriétés mécaniques du GHBS
    - Comparé aux modèles disponibles dans la littérature, le modèle proposé est plus simple d’utilisation. En effet, outre les paramètres classiques de Cam Clay, il nécessite un paramètre b correspondant à la morphologie des GH, β décrivant la manière dont l’indice de vide atteint la ligne d’état stable et β_h un paramètre facultatif qui reflète l'impact de la morphologie des GH sur la compressibilité des GHBS.
- Le modèle a été capable de simuler le comportement mécanique des sédiments sableux sans GH et avec des GH de saturation et morphologies différentes.
- Le modèle a été capable de reproduire le comportement des argiles sans GH et avec différentes saturations en GH; cependant, il n'a pas réussi à recréer le comportement dilatant de GHBS argileux.
- Le modèle manquait de précision pour reproduire le radoucissement à grande déformation provoqué par la présence de GH.

7.8 Limitations et améliorations

Cette partie vise donc à exposer certaines de ces limitations et d'y proposer des améliorations.

7.8.1 Limitations concernant la quantification des hydrates de gaz

Ce paragraphe traite principalement des limitations concernant la quantification des GH par la modélisation des milieux effectifs:

- Le modèle de milieux effectifs utilisé a été développé par Helgerud et al. (1999) pour quantifié la présence d'hydrates dans les pores ou au contact des particules constituantes des sables et non pas directement pour du sédiment argileux. Bien que les interactions entre hydrates et particules solides différent dans ces deux types de sédiment les comparaisons réalisées par Ghosh et al. (2010) ont révélé que les estimations de teneur en hydrate obtenus par l'approche développé par Helgerud et al. (1999) considérant que les hydrates contribuent à la rigidité des GHBS n'excédaient que de 7 à 11% celles faites par dégazage de carottes sous-pression. Ce constat a motivé l'utilisation de l'approche d'Helgerud et al., (1999) dans ce travail en gardant à l'esprit le fait qu'un modèle considérant que les hydrates déplacent les particules d'argiles (« grain displacing ») demeurait le plus juste comme l'on souligné Ghosh et al. (2010). En effet, l'utilisation d'un modèle "grain displacing" n'a pu être envisagée en raison du manque de données d'entrée concernant l'orientation des fractures dans le sédiment. Alternativement, le fait que les résultats de l'estimation de la quantité d'hydrate par approche géophysique aient été comparés à ceux dérivés de l'analyse de la chlorinité permet de considérer que l'utilisation d'un modèle des milieux effectif considérant que les hydrates contribuent à la rigidité du sédiment est capable de donner les résultats les plus représentatifs dans la zone d'étude. De plus, il est raisonnable de penser que la charge supportée par les GHBS de la zone d'étude est répartie entre le sédiment et ses GH.
- Notons que ce modèle interprète toujours les vitesses élevées comme un indicateur de la présence des GH. Cependant, dans certains cas, il a été observé que les concrétions de carbonates augmentent aussi de manière significative la célérité mesurée. Il est donc indispensable de comparer la célérité mesurée avec d'autres mesures disponibles issues de diverses méthodes. Alternativement, la différence entre la vitesse calculée par le modèle et celle mesurée par la fourche acoustique du Penfeld a montré des oscillations ne dépassant pas $\pm 17\ m\ /s$. Par conséquent, les quantifications des GH avec le modèle n'ont été réalisées que lorsque la Vp calculée dépassait la valeur de vitesse mesurée d'au moins $17\ m/s$.
- Une autre limitation à la quantification des GH est liée au fait que le Penfeld ne peut mesurer des vitesses de compression que jusqu'à 2200 m/s. Cependant, d'après les résultats expérimentaux de Helgerud et al. (2009), en présence de GH massifs la vitesse Vp peut atteindre $3\ 000\ \mathrm{m/s}$. De tels hydrates massifs ont pu être observés dans la zone d'étude grâce aux carottes sédimentaires récupérées. Ils sont souvent interprétés par des discontinuités sur les profils des données in-situ (rectangle gris de la figure 7. 2). Ainsi, dans de tels cas, la quantification des GH n'a pas été possible.
- La présence de gaz libre peut aussi affecter le processus de quantification des GH. Contrairement au fait que la présence de GH augmente la vitesse de compression, la présence de gaz libre la diminue. La coexistence de gaz libres et d'hydrates a été prouvée à plusieurs reprises dans ce travail (principalement dans les chapitres 4 et 5). Cela peut induire des incertitudes sur les résultats de quantification car avec l'approche des milieux effectifs utilisée comme avec toute autre approche inverse des équations doivent être résolues avec

deux variables indépendantes qui sont la quantité de gaz libre et d'hydrate de gaz. Par conséquent, la quantité de GH dans les zones où ceux-ci coexistent avec du gaz libre peut être sous-estimée en raison de la diminution de vitesse causée par la présence de gaz libre.

- Enfin, il est important d'ajouter que lors de la récupération des carottes sédimentaires (en utilisant le carottier Calypso ou la foreuse MeBo), les conditions de stabilité des GH sont perturbées. Ceci est problématique car il faut parfois une observation directe des carottes pour confirmer la présence ou l'absence des GH ainsi que leur morphologie. La dissociation des GH, au sein des carottes, rend le sédiment vaseux et fluidisé (comme le montre la figure 7. 4.a). Pour parer à cet inconvénient seuls des carottages sous pression peuvent être envisagés, comme le montrent Santamarina et al. (2015).

7.8.2 Limitations concernant la caractérisation du comportement mécanique des sédiments contenant des hydrates de gaz à partir des mesures in-situ

L'analyse d'abaques normalisés de classification des sols croisant données acoustiques et géotechniques in-situ a pu être affectée par les limitations suivantes :

- Les mesures acoustiques corrélées aux mesures géotechniques in-situ n'ont pas été acquises exactement sur le même point de la zone d'étude. En effet, les données acoustiques ont été couplées au point de données géotechniques le plus proche géographiquement. Par conséquent, dans certains cas, les pics des profils de vitesse et des profils de résistance de pointe du Penfeld ne se produisent pas tout à fait à la même profondeur. Cela a nécessité de réaliser des corrélations « pic à pic » entre ces deux types de données pour pouvoir caractériser avec précision le comportement mécanique GHBS argileux.
- L'absence de résultats expérimentaux laisse encore quelques incertitudes sur le comportement mécanique des GHBS. En effet, des investigations ultérieures peuvent être utiles pour valider les résultats de cette thèse, en particulier ceux concernant l'influence de différentes morphologies de GH sur la réponse mécanique des sédiments.

7.8.3 Limitations concernant la définition des propriétés hydrauliques des sédiments contenant des hydrates de gaz à partir des mesures in-situ

- L'observation la plus controversé concernant les propriétés hydrauliques des GHBS est l'accroissement de la diffusivité hydraulique pour des saturations en GH dans le sédiment supérieures à 10%. Cela peut être lié à la présence de fractures naturelles ou artificielles. Alors que les fractures naturelles seraient causées par la circulation de fluides ayant permis la formation de GH, les fractures artificielles pourraient avoir été induites par la pénétration de la lance du piézomètre dans le sédiment. Quel qu'en soit leur origine, ces fractures pourraient être la cause de l'augmentation de la diffusivité hydraulique observée.

7.8.4 Limitations concernant le nouveau modèle mécanique constitutif

Le fait que le nouveau modèle de comportement des GHBS ne propose qu'un seul paramètre lié à la morphologie des GH peut avoir plusieurs inconvénients:

- Les résultats numériques ne sont pas aussi précis que ceux obtenus avec certains modèles requérant plus de paramètres.
- Le modèle ne permet pas de reproduire la transition entre élasticité et élasto-plasticité (i.e. Strain softening) observé expérimentalement pour un sédiment normalement consolidé saturé en eau.
- Le modèle n'est pas capable de reproduire l'évolution du comportement dilatant du sédiment avec l'augmentation de la saturation en GH.

Le manque de données expérimentales concernant le comportement mécanique des GHBS argileux complique l'adaptation du modèle à ce type de sédiments.

Effectuer des études expérimentales permettra, sans aucun doute, d’améliorer la performance du modèle.

7.9 Perspectives

Au cours de ce travail, les effets de la saturation en GH ainsi que leur distribution et morphologie sur les propriétés mécaniques et hydrauliques des GHBS argileux ont été caractérisés et évalués. Cependant, certaines conclusions méritent d’être approfondies. De nouvelles recherches basées sur des données expérimentales sont encore nécessaires pour justifier les effets de la morphologie et de la teneur en GH sur les propriétés des sédiments.

La validation des observations et des conclusions de ce travail de thèse bénéficieraient de comparaisons entre mesures réalisées in situ et en conditions contrôlées de laboratoire pour les raisons suivantes:

- Ces informations permettraient de mieux caractériser la morphologie/distribution des GH et leurs effets sur les sédiments argileux environnants.
- En outre, cela permettrait d'affiner les relations empiriques classiquement utilisées pour dériver les paramètres géotechniques à partir de mesures mécaniques in-situ (CPTu).
- Cela permettrait également d'améliorer le modèle numérique proposé en affinant la caractérisation des principaux traits du comportement mécanique des GHBS argileux.

Le laboratoire géotechnique d’'Ifremer est équipé d'une cellule triaxiale permettant d'étudier les propriétés mécaniques du sédiment. La machine est équipée d'un système de régulation de la pression de confinement et de la pression interstitielle, d'une presse triaxiale, d'une cellule de confinement et d'un système d'injection de gaz. Cette machine peut être utilisée pour effectuer des essais triaxiaux sur des sédiments synthétiques fabriqués à partir d'argiles naturelles récupérées dans la zone d'étude.

Une autre approche consisterait à caractériser les GHBS après les avoir récupéré par carottage sous pression. Cela permettrait de préserver les conditions de température et de pression in situ. Des données ayant utilisées cette méthode de carottage sous pression sont disponible dans la littérature (voir par exemple Santamarina et al., 2015). Par conséquent, il serait intéressant de comparer les résultats in-situ de cette thèse avec ceux obtenus à l’aide de ce procédé.

Alternativement, ces travaux ont montré que les mesures issues de CPTu sont un moyen d’acquérir efficacement une grande quantité de données. Cette technique (1) s’est révélée être une alternative prometteuse et moins coûteuse que les opérations de carottage sous pression et (2) a le mérite d’être couramment utilisée en ingénierie géotechnique marine.

Bien qu'il demeure important d'étudier les conséquences mécaniques de la présence de GH dans leur zone de stabilité, il est également nécessaire de compléter ce travail en caractérisant les aléas géologiques pouvant résulter de leur décomposition (dissolution ou dissociation). La décomposition des GH altère les propriétés mécaniques des GHBS en réduisant leur résistance. De plus, la présence de gaz dans les sédiments réduit leur résistance au cisaillement (Sultan et al., 2012). La compréhension de ces mécanismes est donc cruciale à la caractérisation et à la prévention des aléas géologiques potentiels comme les instabilités de pente. Par conséquent, il serait intéressant de proposer un modèle numérique capable de simuler à la fois le comportement des sédiments contenant des GH et des sédiments contenant du gaz libre. Cela constitue l’une des nombreuses étapes indispensables au développement de processus de production de gaz à partir d’accumulations de GH.

References

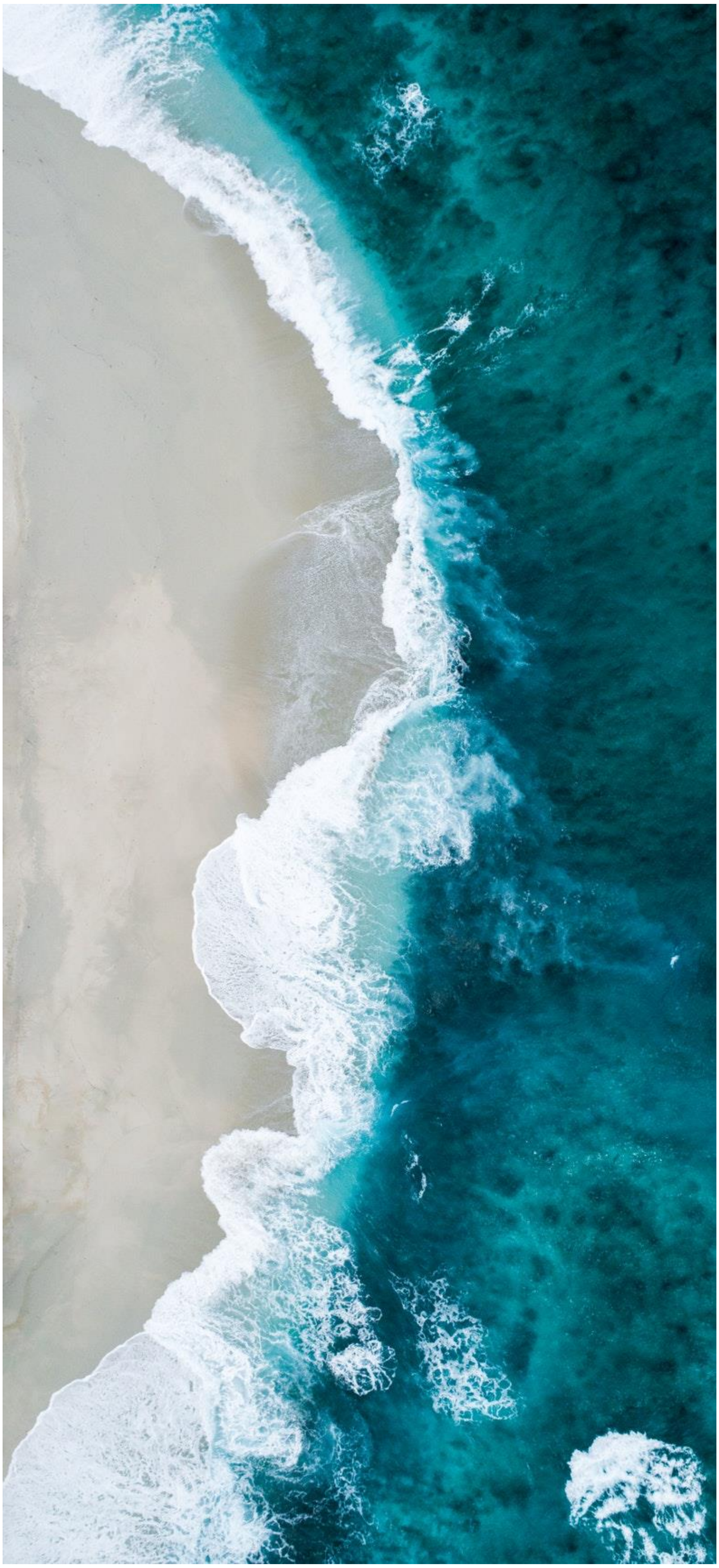

https://unsplash.com/wallpapers/nature/

A

Abid, K., Spagnoli, G., Teodoriu, C., & Falcone, G. (2015). Review of pressure coring systems for offshore gas hydrates research. *Underwater Technology*, *33*(1), 19-30.

B

Bai, Y., & Bai, Q. (2018). *Subsea engineering handbook*. Gulf Professional Publishing. Pages 409-434

Been, K., & Jefferies, M. G. (1985). A state parameter for sands. *Géotechnique*, *35*(2), 99-112.

Berndt, C., Bünz, S., Clayton, T., Mienert, J., & Saunders, M. (2004). Seismic character of bottom simulating reflectors: examples from the mid-Norwegian margin. *Marine and Petroleum Geology*, *21*(6), 723-733.

Berner, U., & Faber, E. (1996). Empirical carbon isotope/maturity relationships for gases from algal kerogens and terrigenous organic matter, based on dry, open-system pyrolysis. *Organic Geochemistry*, *24*(10-11), 947-955.

Bohrmann, G., & Torres, M. E. (2006). Gas hydrates in marine sediments. In *Marine Geochemistry* (pp. 481-512). Springer, Berlin, Heidelberg.

Bonnefoy, O., Gruy, F., & Herri, J. M. (2005). Van der Waals interactions in systems involving gas hydrates. *Fluid Phase Equilibria*, *231*(2), 176-187.

Boswell, R., & Collett, T. (2006). The gas hydrates resource pyramid. *Natural Gas & Oil*, *304*, 285-4541.

Boswell, R., & Collett, T. S. (2011). Current perspectives on gas hydrate resources. *Energy & environmental science*, *4*(4), 1206-1215.

Bourillet, J. F., Damy, G., Dussud, L., Sultan, N., Woerther, P., & Migeon, S. (2007, January). Behaviour of a piston corer from accelerometers and new insights on quality of the recovery. In *OFFSHORE SITE INVESTIGATION AND GEOTECHNICS, Confronting New Challenges and Sharing Knowledge*. Society of Underwater Technology.

Bourry, C., Chazallon, B., Charlou, J. L., Donval, J. P., Ruffine, L., Henry, P., ... & Moreau, M. (2009). Free gas and gas hydrates from the Sea of Marmara, Turkey: Chemical and structural characterization. *Chemical Geology*, *264*(1-4), 197-206.

Buffett, B. A. (2000). Clathrate hydrates. *Annual Review of Earth and Planetary Sciences*, *28*(1), 477-507.

Bugge, T., Befring, S., Belderson, R. H., Eidvin, T., Jansen, E., Kenyon, N. H., ... & Sejrup, H. P. (1987). A giant three-stage submarine slide off Norway. *Geo-marine letters*, *7*(4), 191-198.

Burns, S. E., & Mayne, P. W. (1999wei). Monotonic and dilatory pore-pressure decay during piezocone tests in clay. *Canadian Geotechnical Journal*, *35*(6), 1063-1073.

C

Casagrande, A. (1936). The determination of pre-consolidation load and its practical significance. In Proc. Int. Conf. Soil Mech. Found. Eng. Cambridge, Mass., 1936 (Vol. 3, p. 60).

Castro, G. (1969). Liquefaction of sand. PhD thesis, Division of Engineering and Applied Physics, Harvard University.

Chand, S., Rise, L., Ottesen, D., Dolan, M. F. J., Bellec, V., & Bøe, R. (2009). Pockmark-like depressions near the Goliat hydrocarbon field, Barents Sea: morphology and genesis. *Marine and Petroleum Geology*, *26*(7), 1035-1042.

Chaouachi, M., Falenty, A., Sell, K., Enzmann, F., Kersten, M., Haberthür, D., & Kuhs, W. F. (2015). Microstructural evolution of gas hydrates in sedimentary matrices observed with synchrotron X-ray computed tomographic microscopy. *Geochemistry, Geophysics, Geosystems*, *16*(6), 1711-1722.

Chen, Y., Gao, Y., Chen, L., Wang, X., Liu, K., & Sun, B. (2019). Experimental investigation of the behavior of methane gas hydrates during depressurization-assisted CO2 replacement. *Journal of Natural Gas Science and Engineering*, *61*, 284-292.

Chong, Z. R., Yang, S. H. B., Babu, P., Linga, P., & Li, X. S. (2016). Review of natural gas hydrates as an energy resource: Prospects and challenges. *Applied energy*, *162*, 1633-1652.

Clayton, C., Kingston, E., Priest, J., Schultheiss, P., NGHP, E., & Scientific Party, N. (2008). Testing of pressurised cores containing gas hydrate from deep ocean sediments.

Cohen, H. A., & McClay, K. (1996). Sedimentation and shale tectonics of the northwestern Niger Delta front. *Marine and Petroleum Geology*, *13*(3), 313-328.

Collett, T. S., & Ladd, J. (2000). 19. Detection of gas hydrate with downhole logs and assessment of gas hydrate concentrations (saturations) and gas volumes on the Blake Ridge with electrically resistivity log data. *Proceedings of the Ocean Drilling Program, Scientific Results, Texas A&M University, College Station, TX, USA*, *164*.

Collett, T., Bahk, J. J., Baker, R., Boswell, R., Divins, D., Frye, M., ... & Morell, M. (2014). Methane Hydrates in Nature Current Knowledge and Challenges. *Journal of chemical & engineering data*, *60*(2), 319-329.

Collett, T. S. (2002). Energy resource potential of natural gas hydrates. *AAPG bulletin*, *86*(11), 1971-1992.

Colliat, J. L., Dendani, H., Puech, A., & Nauroy, J. F. (2011). Gulf of Guinea deepwater sediments: Geotechnical properties, design issues and installation experiences. In *Proceedings of the 2nd International Symposium on Frontiers in Offshore Geotechnics (ISFOG), Perth, Australia* (pp. 59-86).

Croudace, I. W., & Rothwell, R. G. (Eds.). (2015). Micro-XRF Studies of *Sediment Cores: Applications of a non-destructive tool for the environmental sciences* (Vol. 17). Springer.

Cunningham, R., & Lindholm, R. M. (2000). AAPG Memoir 73, Chapter 8: Seismic Evidence for Widespread Gas Hydrate Formation, Offshore West Africa.

D

Damuth, J. E. (1994). Neogene gravity tectonics and depositional processes on the deep Niger Delta continental margin. *Marine and Petroleum Geology*, *11*(3), 320-346.

Dai, S., Kim, J., Xu, Y., Waite, W. F., Jang, J., Yoneda, J., ... & Kumar, P. (2018). Permeability anisotropy and relative permeability in sediments from the National Gas Hydrate Program Expedition 02, offshore India. *Marine and Petroleum Geology*.

Dai, S., Santamarina, J. C., Waite, W. F., & Kneafsey, T. J. (2012). Hydrate morphology: Physical properties of sands with patchy hydrate saturation. *Journal of Geophysical Research: Solid Earth*, *117*(B11).

Dai, S., & Seol, Y. (2014). Water permeability in hydrate-bearing sediments: A pore-scale study. *Geophysical Research Letters*, *41*(12), 4176-4184.

Davy, H. (1811). On a combination of oxymuriatic gas and oxygene gas. *Philosophical Transactions of the Royal society of London*, *101*, 155-162.

De Gennaro, V., Puech, A., Delage, P., (2005). On the compressibility of deep water sediments of the Gulf of Guinea. *Proc. Int. Symp. On frontiers in Offshore Geotechnics, Perth, Autralia*.

Delage, P. (2010). A microstructure approach to the sensitivity and compressibility of some Eastern Canada sensitive clays. *Géotechnique*, *60*(5), 353.

Delli, M. L., & Grozic, J. L. (2014). Experimental determination of permeability of porous media in the presence of gas hydrates. *Journal of petroleum science and engineering*, *120*, 1-9.

Demirbas, A., Rehan, M., Al-Sasi, B. O., & Nizami, A. S. (2016). Evaluation of natural gas hydrates as a future methane source. *Petroleum Science and Technology*, *34*(13), 1204-1210.

Durham, W. B., Kirby, S. H., Stern, L. A., & Zhang, W. (2003). The strength and rheology of methane clathrate hydrate. *Journal of Geophysical Research: Solid Earth*, *108*(B4).

E

Ebinuma, T., Kamata, Y., Minagawa, H., Ohmura, R., Nagao, J., & Narita, H. (2005, June). Mechanical properties of sandy sediment containing methane hydrate. In *Proceedings of Fifth International Conference on Gas Hydrates, Pap* (Vol. 3037, pp. 958-961).

Etiope, G., Feyzullayev, A., Milkov, A. V., Waseda, A., Mizobe, K. C. H. S., & Sun, C. H. (2009). Evidence of subsurface anaerobic biodegradation of hydrocarbons and potential secondary methanogenesis in terrestrial mud volcanoes. *Marine and Petroleum Geology*, *26*(9), 1692-1703.

F

Fábián, B., Picaud, S., Jedlovszky, P., Guilbert-Lepoutre, A., & Mousis, O. (2018). Ammonia clathrate hydrate as seen from grand canonical Monte Carlo simulations. *ACS Earth and Space Chemistry*, *2*(5), 521-531.

Faraday, M. (1823). XVII. On the condensation of several gases into liquids. *Philosophical transactions of the Royal Society of London*, (113), 189-198.

Freij-Ayoub, R., Tan, C., Clennell, B., Tohidi, B., & Yang, J. (2007). A wellbore stability model for hydrate bearing sediments. *Journal of Petroleum Science and Engineering*, *57*(1-2), 209-220.

Freudenthal, T., & Wefer, G. (2007). Scientific drilling with the sea floor drill rig MeBo. *Scientific Drilling*, *5*, 63-66.

Freudenthal, T., & Wefer, G. (2013). Drilling cores on the sea floor with the remote-controlled sea floor drilling rig MeBo. *Geoscientific Instrumentation, Methods and Data Systems*, *2*(2), 329-337.

G

Gai, X., & Sánchez, M. (2017). A Geomechanical model for gas hydrate bearing sediments. *Gas*, *1*, 2.

Gabitto, J. F., & Tsouris, C. (2010). Physical properties of gas hydrates: A review. *Journal of Thermodynamics*, *2010*.

de Garidel-Thoron, T., Beaufort, L., Bassinot, F., & Henry, P. (2004). Evidence for large methane releases to the atmosphere from deep-sea gas-hydrate dissociation during the last glacial episode. *Proceedings of the National Academy of Sciences*, *101*(25), 9187-9192.

George, R. A., & Cauquil, E. (2007, January). AUV ultrahigh-resolution 3D seismic technique for detailed subsurface investigations. In *Offshore Technology Conference*. Offshore Technology Conference.

Ghosh, R., Sain, K., & Ojha, M. (2010). Effective medium modeling of gas hydrate-filled fractures using the sonic log in the Krishna-Godavari basin, offshore eastern India. *Journal of Geophysical Research: Solid Earth*, *115*(B6).

Ghiassian, H., & Grozic, J. L. (2013). Strength behavior of methane hydrate bearing sand in undrained triaxial testing. *Marine and petroleum geology*, *43*, 310-319.

Grozic, J. L., & Ghiassian, H. (2010, September). Undrained shear strength of methane hydrate-bearing sand; preliminary laboratory results. In *Proc., 63rd Canadian Geotechnical Conf* (pp. 459-466).

Geuss M. (2017, May). Japan, China have extracted methane hydrate from the seafloor. Ars technical.

H

Hachikubo, A., Khlystov, O., Krylov, A., Sakagami, H., Minami, H., Nunokawa, Y., ... & Kida, M. (2010). Molecular and isotopic characteristics of gas hydrate-bound hydrocarbons in southern and central Lake Baikal. *Geo-Marine Letters*, *30*(3-4), 321-329.

Heggland, R. O. A. R. (2003, May). Vertical hydrocarbon migration at the Nigerian continental slope: Applications of seismic mapping techniques. In *AAPG Annual Meeting, Salt Lake City, May* (pp. 11-14).

Hammerschmidt, E. G. (1934). Formation of gas hydrates in natural gas transmission lines. *Industrial & Engineering Chemistry*, *26*(8), 851-855.

Hampton, M. A., Lee, H. J., & Locat, J. (1996). Submarine landslides. *Reviews of geophysics*, *34*(1), 33-59.

Handa, Y. P., & Stupin, D. Y. (1992). Thermodynamic properties and dissociation characteristics of methane and propane hydrates in 70-. ANG.-radius silica gel pores. *The Journal of Physical Chemistry*, *96*(21), 8599-8603.

Hattab, M., & Favre, J. L. (2010). Analysis of the experimental compressibility of deep water marine sediments from the Gulf of Guinea. *Marine and Petroleum Geology*, *27*(2), 486-499.

Hattab, M., Hammad, T., Fleureau, J. M., & Hicher, P. Y. (2013). Behaviour of a sensitive marine sediment: microstructural investigation.

Helgerud, M. B., Dvorkin, J., Nur, A., Sakai, A., & Collett, T. (1999). Elastic-wave velocity in marine sediments with gas hydrates: Effective medium modeling. *Geophysical Research Letters*, *26*(13), 2021-2024.

Helgerud, M. B., Waite, W. F., Kirby, S. H., & Nur, A. (2009). Elastic wave speeds and moduli in polycrystalline ice Ih, sI methane hydrate, and sII methane-ethane hydrate. *Journal of Geophysical Research: Solid Earth*, *114*(B2).

Henriet, J. P., Mienert, J., & Mienert, J. (Eds.). (1998). Gas hydrates: relevance to world margin stability and climate change. Geological Society of London.

Holland, M., Schultheiss, P., Roberts, J., & Druce, M. (2008, July). Observed gas hydrate morphologies in marine sediments. In *6th International Conference on Gas Hydrates, Chevron, Vancouver, BC, Canada* (pp. 6-10).

Hovland, M., Gallagher, J. W., Clennell, M. B., & Lekvam, K. (1997). Gas hydrate and free gas volumes in marine sediments: Example from the Niger Delta front. *Marine and Petroleum Geology*, *14*(3), 245-255.hatt

Hovland, M., & Svensen, H. (2006). Submarine pingoes: Indicators of shallow gas hydrates in a pockmark at Nyegga, Norwegian Sea. *Marine Geology*, *228*(1-4), 15-23.

Husebø, J., Ersland, G., Graue, A., & Kvamme, B. (2009). Effects of salinity on hydrate stability and implications for storage of CO2 in natural gas hydrate reservoirs. *Energy Procedia*, *1*(1), 3731-3738.

Hyndman, R. D., Yuan, T., & Moran, K. (1999). The concentration of deep sea gas hydrates from downhole electrical resistivity logs and laboratory data. *Earth and Planetary Science Letters*, *172*(1-2), 167-177.

Hyodo, M., Nakata, Y., Yoshimoto, N., & Orense, R. (2005, January). Shear behavior of methane hydrate-bearing sand. In *The Seventeenth International Offshore and Polar Engineering Conference*. International Society of Offshore and Polar Engineers.

Hyodo, M., Wu, Y., Nakashima, K., Kajiyama, S., & Nakata, Y. (2017). Influence of Fines Content on the Mechanical Behavior of Methane Hydrate-Bearing Sediments. Journal of geophysical research: solid earth, 122(10), 7511-7524.

Hyodo, M., Yoneda, J., Yoshimoto, N., & Nakata, Y. (2013). Mechanical and dissociation properties of methane hydrate-bearing sand in deep seabed. *Soils and foundations*, *53*(2), 299-314.

I

IEA greenhouse gas programme (IEAGHG), July 2009, Natural gas and methane hydrates.

J

Jacobi, R. D. (1976). Sediment slides on the northwestern continental margin of Africa. *Marine Geology*, *22*(3), 157-173.

Jang, J., & Santamarina, J. C. (2016). Hydrate bearing clayey sediments: Formation and gas production concepts. *Marine and Petroleum Geology*, *77*, 235-246.

Jansen, E., Befring, S., Bugge, T., Eidvin, T., Holtedahl, H., & Sejrup, H. P. (1987). Large submarine slides on the Norwegian continental margin: sediments, transport and timing. *Marine Geology*, *78*(1-2), 77-107.

Johnson, A., Patil, S., & Dandekar, A. (2011). Experimental investigation of gas-water relative permeability for gas-hydrate-bearing sediments from the Mount Elbert Gas Hydrate Stratigraphic Test Well, Alaska North Slope. *Marine and petroleum geology*, *28*(2), 419-426.

K

Kajiyama, S., Wu, Y., Hyodo, M., Nakata, Y., Nakashima, K., & Yoshimoto, N. (2017). Experimental investigation on the mechanical properties of methane hydrate-bearing sand formed with rounded particles. *Journal of natural gas science and engineering*, *45*, 96-107.

Kang, D. H., Yun, T. S., Kim, K. Y., & Jang, J. (2016). Effect of hydrate nucleation mechanisms and capillarity on permeability reduction in granular media. *Geophysical Research Letters*, *43*(17), 9018-9025.

Katagiri, J., Konno, Y., Yoneda, J., & Tenma, N. (2017). Pore-scale modeling of flow in particle packs containing grain-coating and pore-filling hydrates: Verification of a Kozeny–Carman-based permeability reduction model. *Journal of Natural Gas Science and Engineering*, *45*, 537-551.

Katsuki, D., Ohmura, R., Ebinuma, T., & Narita, H. (2006). Formation, growth and ageing of clathrate hydrate crystals in a porous medium. *Philosophical magazine*, *86*(12), 1753-1761.

Ker, S., Le Gonidec, Y., & Gibert, D. (2012). Multiscale seismic attributes: source-corrected wavelet response and application to high-resolution seismic data. *Geophysical Journal International*, *190*(3), 1746-1760.

Ker, S., Marsset, B., Garziglia, S., Le Gonidec, Y., Gibert, D., Voisset, M., & Adamy, J. (2010). High-resolution seismic imaging in deep sea from a joint deep-towed/OBH reflection experiment: application to a Mass Transport Complex offshore Nigeria. *Geophysical Journal International*, *182*(3), 1524-1542.

Khlystov, O., De Batist, M., Shoji, H., Hachikubo, A., Nishio, S., Naudts, L., ... & Kalmychkov, G. (2013). Gas hydrate of Lake Baikal: Discovery and varieties. *Journal of Asian Earth Sciences*, *62*, 162-166.

Kida, M., Khlystov, O., Zemskaya, T., Takahashi, N., Minami, H., Sakagami, H., ... & Poort, J. (2006). Coexistence of structure I and II gas hydrates in Lake Baikal suggesting gas sources from microbial and thermogenic origin. *Geophysical Research Letters*, *33*(24).

Kim, J., Dai, S., Jang, J., Waite, W. F., Collett, T. S., & Kumar, P. (2018). Compressibility and particle crushing of Krishna-Godavari Basin sediments from offshore India: Implications for gas production from deep-water gas hydrate deposits. *Marine and Petroleum Geology*.

Kim, H. S., Cho, G. C., Lee, J. Y., & Kim, S. J. (2013). Geotechnical and geophysical properties of deep marine fine-grained sediments recovered during the second Ulleung Basin Gas Hydrate expedition, East Sea, Korea. *Marine and Petroleum Geology*, *47*, 56-65.

Kimoto, S., Oka, F., & Fushita, T. (2010). A chemo–thermo–mechanically coupled analysis of ground deformation induced by gas hydrate dissociation. *International Journal of Mechanical Sciences*, *52*(2), 365-376.

Kingston, E., Clayton, C., & Priest, J. (2008). Gas hydrate growth morphologies and their effect on the stiffness and damping of a hydrate bearing sand.

Klapp, S. A., Klein, H., & Kuhs, W. F. (2007). First determination of gas hydrate crystallite size distributions using high-energy synchrotron radiation. *Geophysical research letters*, *34*(13).

Klar, A., Soga, K., & Ng, M. Y. A. (2010). Coupled deformation–flow analysis for methane hydrate extraction. *Geotechnique*, *60*(10), 765-776.

Kleinberg, R. L., Flaum, C., Griffin, D. D., Brewer, P. G., Malby, G. E., Peltzer, E. T., & Yesinowski, J. P. (2003). Deep sea NMR: Methane hydrate growth habit in porous media and its relationship to hydraulic permeability, deposit accumulation, and submarine slope stability. *Journal of Geophysical Research: Solid Earth*, *108*(B10).

Kneafsey, T. J., Tomutsa, L., Moridis, G. J., Seol, Y., Freifeld, B. M., Taylor, C. E., & Gupta, A. (2010). Methane hydrate formation and dissociation in a partially saturated core-scale sand sample. *Journal of Petroleum Science and Engineering*, *56*(1-3), 108-126.

Krage, C. P., Broussard, N. S., & DeJong, J. T. (2014). Estimating rigidity index (IR) based on CPT measurements. In *Third International Symposium on Cone Penetration Testing, Las Vegas, Nevada, USA* (pp. 727-735).

Koh, C. A. (2002). Towards a fundamental understanding of natural gas hydrates. *Chemical Society Reviews*, *31*(3), 157-167.

Kono, H. O., Narasimhan, S., Song, F., & Smith, D. H. (2002). Synthesis of methane gas hydrate in porous sediments and its dissociation by depressurizing. *Powder Technology*, *122*(2-3), 239-246.

Kulenkampff, J., & Spangenberg, E. (2005). Physical properties of cores from the JAPEX/JNOC/GSC et al. Mallik 5L-38 gas hydrate production research well under simulated in situ conditions using the Field Laboratory Experimental Core Analysis System (FLECAS). *Bulletin-Geological Survey of Canada*, *585*, 87.

Kvenvolden, K. A. (1988). Methane hydrate—a major reservoir of carbon in the shallow geosphere?. *Chemical geology*, *71*(1-3), 41-51.

Kvenvolden, K. A. (1988). Methane hydrates and global climate. *Global biogeochemical cycles*, *2*(3), 221-229.

Kvenvolden, K. A. (1993). Gas hydrates as a potential energy resource-a review of their methane content. *United States Geological Survey, Professional Paper; (United States)*, *1570*.

Kvenvolden, K. A. (1995). A review of the geochemistry of methane in natural gas hydrate. *Organic geochemistry*, *23*(11-12), 997-1008.

Kvenvolden, K. A. (1999). Potential effects of gas hydrate on human welfare. *Proceedings of the National Academy of Sciences*, *96*(7), 3420-3426.

Kvenvolden, K. A., & Lorenson, T. D. (2001). The global occurrence of natural gas hydrate. *Natural Gas Hydrates: Occurrence, Distribution, and Detection: Occurrence, Distribution, and Detection*, *124*, 3-18.

Kumar, A., Maini, B., Bishnoi, P. R., Clarke, M., Zatsepina, O., & Srinivasan, S. (2010). Experimental determination of permeability in the presence of hydrates and its effect on the dissociation characteristics of gas hydrates in porous media. *Journal of Petroleum Science and Engineering*, *70*(1-2), 114-122.

Kumar, D., Sen, M. K., & Bangs, N. L. (2007). Gas hydrate concentration and characteristics within Hydrate Ridge inferred from multicomponent seismic reflection data. *Journal of Geophysical Research: Solid Earth*, *112*(B12).

Kwon, T. H., Cho, G. C., & Santamarina, J. C. (2008). Gas hydrate dissociation in sediments: Pressure-temperature evolution. *Geochemistry, Geophysics, Geosystems*, *9*(3).

L

Le, T. X., Aimedieu, P., Bornert, M., Chabot, B., Rodts, S., & Tang, A. M. (2019). Effect of temperature cycle on mechanical properties of methane hydrate-bearing sediment. *Soils and Foundations*.

Lee, J. Y., Santamarina, J. C., & Ruppel, C. (2010). Volume change associated with formation and dissociation of hydrate in sediment. *Geochemistry, Geophysics, Geosystems*, *11*(3).

Lee, J. Y., Yun, T. S., Santamarina, J. C., & Ruppel, C. (2007). Observations related to tetrahydrofuran and methane hydrates for laboratory studies of hydrate-bearing sediments. *Geochemistry, Geophysics, Geosystems*, *8*(6).

Lei, L. (2017). *Gas hydrate in fine-grained sediments—laboratory studies and coupled processes analyses* (Doctoral dissertation, Georgia Institute of Technology).

Lei, L., & Santamarina, J. C. (2018). Laboratory strategies for hydrate formation in fine-grained sediments. *Journal of Geophysical Research: Solid Earth*, *123*(4), 2583-2596.

Lerche, I., & Bagirov, E. (1998). Guide to gas hydrate stability in various geological settings. *Marine and Petroleum Geology*, *15*(5), 427-437.

Li, Y. H., Song, Y. C., Yu, F., Liu, W. G., & Zhao, J. F. (2011). Experimental study on mechanical properties of gas hydrate-bearing sediments using kaolin clay. *China ocean engineering*, *25*(1), 113.

Li, Y., Wu, Q., Wu, P., & Liu, W. (2019). Mechanical Properties of Methane Hydrate Interbedded with Clayey Sediments. *Journal of Energy and Natural Resources*, *7*(1), 24.

Liang, H., Song, Y., Chen, Y., & Liu, Y. (2011). The measurement of permeability of porous media with methane hydrate. *Petroleum Science and Technology*, *29*(1), 79-87.

Lijith, K. P., Malagar, B. R., & Singh, D. N. (2019). A comprehensive review on the geomechanical properties of gas hydrate bearing sediments. *Marine and Petroleum Geology*.

Lin, J. S., Seol, Y., & Choi, J. H. (2015). An SMP critical state model for methane hydrate-bearing sands. *International Journal for Numerical and Analytical Methods in Geomechanics*, *39*(9), 969-987.

Liu, W., Zhao, J., Luo, Y., Song, Y., Li, Y., Yang, M., ... & Wang, D. (2013). Experimental measurements of mechanical properties of carbon dioxide hydrate-bearing sediments. *Marine and Petroleum Geology*, *46*, 201-209.

Liu, T., & Liu, X. (2018). Identifying the morphologies of gas hydrate distribution using P-wave velocity and density: a test from the GMGS2 expedition in the South China Sea. *Journal of Geophysics and Engineering*, *15*(3), 1008-1022.

Loveday, J. S., & Nelmes, R. J. (2008). High-pressure gas hydrates. *Physical Chemistry Chemical Physics*, *10*(7), 937-950.

Low, H. E., Lunne, T., Andersen, K. H., Sjursen, M. A., Li, X., & Randolph, M. F. (2010). Estimation of intact and remoulded undrained shear strengths from penetration tests in soft clays. *Géotechnique*, *60*(11), 843-859.

Lu, N., & Likos, W. J. (2013). Origin of cohesion and its dependence on saturation for granular media. In *Poromechanics V: Proceedings of the Fifth Biot Conference on Poromechanics* (pp. 1669-1675).

Lu, H., Seo, Y. T., Lee, J. W., Moudrakovski, I., Ripmeester, J. A., Chapman, N. R., ... & Pohlman, J. (2007). Complex gas hydrate from the Cascadia margin. *Nature*, *445*(7125), 303.

Lunine, J. I., & Stevenson, D. J. (1987). Clathrate and ammonia hydrates at high pressure: Application to the origin of methane on Titan. *Icarus*, *70*(1), 61-77.

Lunne, T., Robertson, P. K., & Powell, J. J. M. (1997). Cone penetration testing. *Geotechnical Practice*, *20*, 23-35.

M

Malinverno, A., Kastner, M., Torres, M. E., & Wortmann, U. G. (2008). Gas hydrate occurrence from pore water chlorinity and downhole logs in a transect across the northern Cascadia margin (Integrated Ocean Drilling Program Expedition 311). *Journal of Geophysical Research: Solid Earth*, *113*(B8).

Manzari, M. T., & Dafalias, Y. F. (1997). A critical state two-surface plasticity model for sands. *Geotechnique*, *47*(2), 255-272.

Marsset, T., Marsset, B., Ker, S., Thomas, Y., & Le Gall, Y. (2010). High and very high resolution deep-towed seismic system: Performance and examples from deep water Geohazard studies. *Deep Sea Research Part I: Oceanographic Research Papers*, *57*(4), 628-637.

Marsset, T., Ruffine, L., Gay, A., Ker, S., & Cauquil, E. (2018). Types of fluid-related features controlled by sedimentary cycles and fault network in deepwater Nigeria. *Marine and Petroleum Geology*, *89*, 330-349.

Marto, A., Tan, C. S., Makhtar, A. M., & Kung Leong, T. (2014). Critical state of sand matrix soils. *The Scientific World Journal*, *2014*.

Masui, A., Haneda, H., Ogata, Y., & Aoki, K. (2005, June). The effect of saturation degree of methane hydrate on the shear strength of synthetic methane hydrate sediments. In *Proceedings of the 5th International Conference on Gas Hydrates, Trondheim, Norway* (Vol. 2037, pp. 657-663).

Masui, A., Haneda, H., Ogata, Y., & Aoki, K. (2007, January). Mechanical properties of sandy sediment containing marine gas hydrates in deep sea offshore Japan. In *Seventh ISOPE Ocean Mining Symposium*. International Society of Offshore and Polar Engineers.

Masui, A., Miyazaki, K., Haneda, H., Ogata, Y., & Aoki, K. (2008, July). Mechanical characteristics of natural and artificial gas hydrate bearing sediments. In *Proceedings of the 6th International Conference on Gas Hydrates* (pp. 6-10). Vancouver, Canada: ICGH.

Matveeva, T. V., Mazurenko, L. L., Soloviev, V. A., Klerkx, J., Kaulio, V. V., & Prasolov, E. M. (2003). Gas hydrate accumulation in the subsurface sediments of Lake Baikal (Eastern Siberia). *Geo-Marine Letters*, *23*(3-4), 289-299.

Mayoufi, N., Dalmazzone, D., Fürst, W., Delahaye, A., & Fournaison, L. (2009). CO2 enclathration in hydrates of peralkyl-(ammonium/phosphonium) salts: stability conditions and dissociation enthalpies. *Journal of Chemical & Engineering Data*, *55*(3), 1271-1275.

Mazzini, A., Ivanov, M. K., Parnell, J., Stadnitskaia, A., Cronin, B. T., Poludetkina, E., ... & van Weering, T. (2004). Methane-related authigenic carbonates from the Black Sea: geochemical characterisation and relation to seeping fluids. *Marine Geology*, *212*(1-4), 153-181.

McCusker, L. B., Von Dreele, R. B., Cox, D. E., Louër, D., & Scardi, P. (1999). Rietveld refinement guidelines. *Journal of Applied Crystallography*, *32*(1), 36-50.

Mienert, J., Vanneste, M., Bünz, S., Andreassen, K., Haflidason, H., & Sejrup, H. P. (2005). Ocean warming and gas hydrate stability on the mid-Norwegian margin at the Storegga Slide. *Marine and Petroleum Geology*, *22*(1-2), 233-244.

Milkov, A. V. (2004). Global estimates of hydrate-bound gas in marine sediments: how much is really out there? *Earth-Science Reviews*, *66*(3-4), 183-197.

Milkov, A. V. (2005). Molecular and stable isotope compositions of natural gas hydrates: A revised global dataset and basic interpretations in the context of geological settings. *Organic Geochemistry*, *36*(5), 681-702.

Milkov, A. V., & Sassen, R. (2003). Preliminary assessment of resources and economic potential of individual gas hydrate accumulations in the Gulf of Mexico continental slope. *Marine and Petroleum Geology*, *20*(2), 111-128.

Mingjun, Y., Yongchen, S., Yu, L., Yongjun, C. H. E. N., & Qingping, L. I. (2010). Influence of pore size, salinity and gas composition upon the hydrate formation conditions. *Chinese Journal of Chemical Engineering*, *18*(2), 292-296.

Miyazaki, K., Masui, A., Tenma, N., Ogata, Y., Aoki, K., Yamaguchi, T., & Sakamoto, Y. (2010). Study on mechanical behavior for methane hydrate sediment based on constant strain-rate test and unloading-reloading test under triaxial compression. *International Journal of Offshore and Polar Engineering*, *20*(01).

Miyazaki, K., Masui, A., Sakamoto, Y., Aoki, K., Tenma, N., & Yamaguchi, T. (2011). Triaxial compressive properties of artificial methane-hydrate-bearing sediment. *Journal of geophysical research: solid earth*, *116*(B6).

Moridis, G. J. (2002, January). Numerical studies of gas production from methane hydrates. In *SPE Gas Technology Symposium*. Society of Petroleum Engineers.

N

Ning, F., Yu, Y., Kjelstrup, S., Vlugt, T. J., & Glavatskiy, K. (2012). Mechanical properties of clathrate hydrates: status and perspectives. *Energy & Environmental Science*, *5*(5), 6779-6795.

O

Østergaard, K. K., Anderson, R., Llamedo, M., & Tohidi, B. (2002). Hydrate phase equilibria in porous media: effect of pore size and salinity. *Terra Nova*, *14*(5), 307-312.

P

Pinkert, S. (2017). The lack of true cohesion in hydrate-bearing sands. *Granular Matter*, *19*(3), 57.

Pohlman, J. W., Canuel, E. A., Chapman, N. R., Spence, G. D., Whiticar, M. J., & Coffin, R. B. (2005). The origin of thermogenic gas hydrates on the northern Cascadia Margin as inferred from isotopic (13C/12C and D/H) and molecular composition of hydrate and vent gas. *Organic Geochemistry*, *36*(5), 703-716.

Priest, J. A., Clayton, C. R., & Rees, E. V. (2014). Potential impact of gas hydrate and its dissociation on the strength of host sediment in the Krishna–Godavari Basin. *Marine and petroleum geology*, *58*, 187-198.

Priest, J. A., Rees, E. V., & Clayton, C. R. (2009). Influence of gas hydrate morphology on the seismic velocities of sands. *Journal of geophysical research: solid earth*, *114*(B11).

Puech, A., Colliat, J. L., Nauroy, J. F., & Meunier, J. (2005, September). Some geotechnical specificities of Gulf of Guinea deepwater sediments. In *Proceedings of the International Symposium on Frontiers in Offshore Geotechnics, Perth, Australia*.

R

Rahman, M. M., Lo, S. R., & Gnanendran, C. T. (2008). On equivalent granular void ratio and steady state behaviour of loose sand with fines. *Canadian Geotechnical Journal*, *45*(10), 1439-1456.

Ramsey, N. (2010). Some issues related to application of the CPT. In *2nd International Symposium on Cone Penetration Testing, CPT* (Vol. 10).

Rastogi, B. Deka, IL Budhiraja, Girish C. Agarwal, A. (1999). Possibility of large deposits of gas hydrates in deeper waters of India. *Marine Georesources and Geotechnology*, *17*(1), 49-63.

Reijers, T. J. A., Petters, S. W., & Nwajide, C. S. (1997). The Niger delta basin. In *Sedimentary basins of the world* (Vol. 3, pp. 151-172). Elsevier.

Riboulot, V., Ker, S., Sultan, N., Thomas, Y., Marsset, B., Scalabrin, C., ... & Ion, G. (2018). Freshwater lake to salt-water sea causing widespread hydrate dissociation in the Black Sea. *Nature communications*, *9*(1), 117.

Riboulot, V., Sultan, N., Imbert, P., & Ker, S. (2016). Initiation of gas-hydrate pockmark in deep-water Nigeria: Geo-mechanical analysis and modelling. *Earth and Planetary Science Letters*, *434*, 252-263.

Robertson, P. K. (2009). Interpretation of cone penetration tests—a unified approach. *Canadian geotechnical journal*, *46*(11), 1337-1355.

Robertson, P. K. (2016). Cone penetration test (CPT)-based soil behaviour type (SBT) classification system—an update. Canadian Geotechnical Journal, 53(12), 1910-1927.

Roscoe, K.H. and Burland, J.B. On the generalized stress-strain behaviour of "Wet" clay. In: Heyman, J., and Leckie, F.A., editors. Engineering Plasticity. Cambridge University Press, 1968. p. 535-610.

Ruffine, L. (2015). Exploring methane-hydrate formation and dissociation in geologic materials through laboratory experiments: Kinetic behavior and morphology. *Fuel*, *141*, 173-184.

Ruffine, L., Donval, J. P., Croguennec, C., Burnard, P., Lu, H., Germain, Y., ... & Madre, D. (2017). Multiple gas reservoirs are responsible for the gas emissions along the Marmara fault network. *Deep Sea Research Part II: Topical Studies in Oceanography*, *153*, 48-60.

Ruppel, C. (2007). Tapping methane hydrates for unconventional natural gas. *Elements*, *3*(3), 193-199.

Ruppel, C. D., & Kessler, J. D. (2017). The interaction of climate change and methane hydrates. *Reviews of Geophysics*, *55*(1), 126-168.

S

Sahling, Heiko, Gerhard Bohrmann, Volkhard Spiess, Jörg Bialas, Monika Breitzke, Michael Ivanov, Sabine Kasten, Sebastian Krastel, and Ralph Schneider. "Pockmarks in the Northern Congo Fan area, SW Africa: Complex seafloor features shaped by fluid flow." *Marine Geology* 249, no. 3-4 (2008): 206-225.

Sánchez, M., Gai, X., & Santamarina, J. C. (2017). A constitutive mechanical model for gas hydrate bearing sediments incorporating inelastic mechanisms. *Computers and Geotechnics*, *84*, 28-46.

Santamarina, J. C., Dai, S., Terzariol, M., Jang, J., Waite, W. F., Winters, W. J., et al. (2015). Hydro-bio-geomechanical properties of hydrate-bearing sediments from Nankai Trough. *Marine and Petroleum Geology*, *66*, 434-450.

Sauter, E. J., Muyakshin, S. I., Charlou, J. L., Schlüter, M., Boetius, A., Jerosch, K., ... & Klages, M. (2006). Methane discharge from a deep-sea submarine mud volcano into the upper water column by gas hydrate-coated methane bubbles. *Earth and Planetary Science Letters*, *243*(3-4), 354-365.

Schneider, J. A., Randolph, M. F., Mayne, P. W., & Ramsey, N. R. (2008). Analysis of factors influencing soil classification using normalized piezocone tip resistance and pore pressure parameters. *Journal of geotechnical and geoenvironmental engineering*, *134*(11), 1569-1586.

Shankar, U., Gupta, D. K., Bhowmick, D., & Sain, K. (2013). Gas hydrate and free gas saturations using rock physics modelling at site NGHP-01-05 and 07 in the Krishna–Godavari Basin, eastern Indian margin. *Journal of Petroleum Science and Engineering*, *106*, 62-70.

Shipley, T. H., & Didyk, B. M. (1982). Occurrence of methane hydrates offshore southern Mexico (DSDP). *Unknown Journal*, 547-555.

Skinner, L. C., & McCave, I. N. (2003). Analysis and modelling of gravity-and piston coring based on soil mechanics. *Marine Geology*, *199*(1-2), 181-204.

Sloan, E. D. (2003). Fundamental principles and applications of natural gas hydrates. *Nature*, *426*(6964), 353.

Sloan Jr, E. D., & Koh, C. A. (2007). *Clathrate hydrates of natural gases*. CRC press.

Smith, W. E., Priest, J. A., & Hayley, J. L. (2018). Influence of vertical cylindrical tetrahydrofuran hydrate veins on fine-grained soil behaviour. *Canadian Geotechnical Journal*, *55*(12), 1691-1701.

Soga, K., Lee, S. L., Ng, M. Y. A., & Klar, A. (2006). Characterisation and engineering properties of methane hydrate soils. *Characterisation and engineering properties of natural soils*, *4*, 2591-1642.

Spangenberg, E. (2001). Modeling of the influence of gas hydrate content on the electrical properties of porous sediments. *Journal of Geophysical Research: Solid Earth*, *106*(B4), 6535-6548.

Stackelberg, M. V., & Müller, H. R. (1951). On the structure of gas hydrates. *The Journal of Chemical Physics*, *19*(10), 1319-1320.

Stern, L. A., Kirby, S. H., & Durham, W. B. (1996). Peculiarities of methane clathrate hydrate formation and solid-state deformation, including possible superheating of water ice. *Science*, *273*(5283), 1843-1848.

Strauch, B., Schicks, J. M., Spangenberg, E., Seyberth, K., Heeschen, K. U., & Priegnitz, M. (2015, December). Determination of the Physical Properties of Sediments Depending on Hydrate Saturation Using a" Quick Look" Method. In *AGU Fall Meeting Abstracts*.

Sultan, N., De Gennaro, V., & Puech, A. (2012). Mechanical behaviour of gas-charged marine plastic sediments. *Géotechnique*, *62*(9), 751.

Sultan, N., Bohrmann, G., Ruffine, L., Pape, T., Riboulot, V., Colliat, J. L., et al. (2014). Pockmark formation and evolution in deep water Nigeria: Rapid hydrate growth versus slow hydrate dissolution. *Journal of Geophysical Research: Solid Earth*, *119*(4), 2679-2694.

Sultan, N., Cochonat, P., Foucher, J. P., & Mienert, J. (2004). Effect of gas hydrates melting on seafloor slope instability. *Marine geology*, *213*(1-4), 379-401.

Sultan, N., & Garziglia, S. (2011, July). Geomechanical constitutive modelling of gas-hydrate-bearing sediments. In *Proceedings of the 7th International Conference on Gas Hydrates (ICGH 2011), Edinburgh, Scotland, United Kingdom, July* (pp. 17-21).

Sultan, N., & Lafuerza, S. (2013). In situ equilibrium pore-water pressures derived from partial piezoprobe dissipation tests in marine sediments. *Canadian Geotechnical Journal*, *50*(12), 1294-1305.

Sultan, N., Marsset, B., Ker, S., Marsset, T., Voisset, M., Vernant, A. M., et al. (2010). Hydrate dissolution as a potential mechanism for pockmark formation in the Niger delta. *Journal of Geophysical Research: Solid Earth*, *115*(B8).

Sultan, N., Voisset, M., Marsset, T., Vernant, A. M., Cauquil, E., Colliat, J. L., & Curinier, V. (2007). Detection of free gas and gas hydrate based on 3D seismic data and cone penetration testing: An example from the Nigerian Continental Slope. *Marine Geology*, *240*(1-4), 235-255.

Song, Y., Zhu, Y., Liu, W., Zhao, J., Li, Y., Chen, Y., ... & Ji, C. (2013). Experimental research on the mechanical properties of methane hydrate-bearing sediments during hydrate dissociation. *Marine and Petroleum Geology*, *51*, 70-78.

T

Taleb, F., Garziglia, S., & Sultan, N. (2018). Hydromechanical Properties of Gas Hydrate-Bearing Fine Sediments From In Situ Testing. *Journal of Geophysical Research: Solid Earth*, *123*(11), 9615-9634.

Tang, L. G., Xiao, R., Huang, C., Feng, Z. P., & Fan, S. S. (2005). Experimental investigation of production behavior of gas hydrate under thermal stimulation in unconsolidated sediment. *Energy & Fuels*, *19*(6), 2402-2407.

Teh, C. I., & Houlsby, G. T. (1991). Analytical study of the cone penetration test in clay. *Geotechnique*, *41*(1), 17-34.

Thevanayagam, S., Shenthan, T., Mohan, S., & Liang, J. (2002). Undrained fragility of clean sands, silty sands, and sandy silts. *Journal of geotechnical and geoenvironmental engineering*, *128*(10), 849-859.

Thomas, F., Rebours, B., Nauroy, J. F., & Meunier, J. (2005). Mineralogical characteristics of the Gulf of Guinea deep water sediments. In *Proc. 1st Int. Symp. on Frontiers in Offshore Geotechnics (ISFOG 2005), Perth* (pp. 1055-1061).

Tohidi, B., Anderson, R., Clennell, M. B., Burgass, R. W., & Biderkab, A. B. (2001). Visual observation of gas-hydrate formation and dissociation in synthetic porous media by means of glass micromodels. *Geology*, *29*(9), 867-870.

Torres, M. E., Wallmann, K., Tréhu, A. M., Bohrmann, G., Borowski, W. S., & Tomaru, H. (2004). Gas hydrate growth, methane transport, and chloride enrichment at the southern summit of Hydrate Ridge, Cascadia margin off Oregon. *Earth and Planetary Science Letters*, *226*(1-2), 225-241.

U

Uchida, T., Ebinuma, T., & Ishizaki, T. (1999). Dissociation condition measurements of methane hydrate in confined small pores of porous glass. *The Journal of Physical Chemistry B*, *103*(18), 3659-3662.

Uchida, T., Ebinuma, T., Takeya, S., Nagao, J., & Narita, H. (2002). Effects of pore sizes on dissociation temperatures and pressures of methane, carbon dioxide, and propane hydrates in porous media. *The journal of physical chemistry B*, *106*(4), 820-826.

Uchida, S., Soga, K., & Yamamoto, K. (2012). Critical state soil constitutive model for methane hydrate soil. *Journal of Geophysical Research: Solid Earth*, *117*(B3).

Ussler III, W., & Paull, C. K. (2001). Ion exclusion associated with marine gas hydrate deposits. *Washington DC American Geophysical Union Geophysical Monograph Series*, *124*, 41-51.

V

Vaular, E. N., Barth, T., & Haflidason, H. (2010). The geochemical characteristics of the hydrate-bound gases from the Nyegga pockmark field, Norwegian Sea. *Organic Geochemistry*, *41*(5), 437-444.

Verdugo, R., & Ishihara, K. (1996). The steady state of sandy soils. *Soils and foundations*, *36*(2), 81-91.

W

Waite, W. F., Santamarina, J. C., Cortes, D. D., Dugan, B., Espinoza, D. N., Germaine, J. et al. (2009). Physical properties of hydrate-bearing sediments. *Reviews of geophysics*, *47*(4).

Wang, L., Liu, W., Li, Y., Wu, P., & Shen, S. (2019). Mechanical Behaviors of Methane Hydrate-Bearing Sediments Using Montmorillonite Clay. *Energy Procedia*, *158*, 5281-5286.

Wei, J., Pape, T., Sultan, N., Colliat, J. L., Himmler, T., Ruffine, L., et al. (2015). Gas hydrate distributions in sediments of pockmarks from the Nigerian margin–Results and interpretation from shallow drilling. *Marine and Petroleum Geology*, *59*, 359-370.

Wei, X., & Yang, J. (2018). A critical state constitutive model for clean and silty sand. *Acta Geotechnica*, *14*(2), 329-345.

Whiticar, M. J. (1996). Stable isotope geochemistry of coals, humic kerogens and related natural gases. *International Journal of Coal Geology*, *32*(1-4), 191-215.

Whiticar, M. J. (1999). Carbon and hydrogen isotope systematics of bacterial formation and oxidation of methane. *Chemical Geology*, *161*(1-3), 291-314.

Whiticar, M. J., Faber, E., & Schoell, M. (1986). Biogenic methane formation in marine and freshwater environments: CO2 reduction vs. acetate fermentation—isotope evidence. *Geochimica et Cosmochimica Acta*, *50*(5), 693-709.

Wiener, R. W., Mann, M. G., Angelich, M. T., & Molyneux, J. B. (2010). Mobile shale in the Niger Delta: Characteristics, structure, and evolution.

Winters, W. J. (2002). Sediment properties associated with gas hydrate formation. In *Proc. 4th Int. Conf. Gas Hydrate, 2002*.

Winters, W. J., Pecher, I. A., Waite, W. F., & Mason, D. H. (2004). Physical properties and rock physics models of sediment containing natural and laboratory-formed methane gas hydrate. *American Mineralogist*, *89*(8-9), 1221-1227.

Winters, W. J., Waite, W. F., Mason, D. H., Gilbert, L. Y., & Pecher, I. A. (2007). Methane gas hydrate effect on sediment acoustic and strength properties. *Journal of Petroleum Science and Engineering*, *56*(1-3), 127-135.

Winters, W. J., Wilcox-Cline, R. W., Long, P., Dewri, S. K., Kumar, P., Stern, L., & Kerr, L. (2014). Comparison of the physical and geotechnical properties of gas-hydrate-bearing sediments from offshore India and other gas-hydrate-reservoir systems. *Marine and petroleum geology*, *58*, 139-167.

Wyllie, M. R. J., Gregory, A. R., & Gardner, L. W. (1956). Elastic wave velocities in heterogeneous and porous media. *Geophysics*, *21*(1), 41-70.

X

Xu, W., & Germanovich, L. N. (2006). Excess pore pressure resulting from methane hydrate dissociation in marine sediments: A theoretical approach. *Journal of Geophysical Research: Solid Earth*, *111*(B1).

Xu, W., & Ruppel, C. (1999). Predicting the occurrence, distribution, and evolution of methane gas hydrate in porous marine sediments. *Journal of Geophysical Research: Solid Earth*, *104*(B3), 5081-5095.

Y

Yang, M., Zheng, J. N., Gao, Y., Ma, Z., Lv, X., & Song, Y. (2019). Dissociation characteristics of methane hydrates in South China Sea sediments by depressurization. *Applied energy*, *243*, 266-273.

Yatsu, M. (June, 2018). Will 'flammable ice' be a critical factor in Asia's security? The Japan times

Yin, Z., Chong, Z. R., Tan, H. K., & Linga, P. (2015). Review of gas hydrate dissociation kinetic models for energy recovery. *Journal of Natural Gas Science and Engineering*, *35*, 1362-1387.

Yin, Z. Y., Karstunen, M., Chang, C. S., Koskinen, M., & Lojander, M. (2011). Modeling time-dependent behavior of soft sensitive clay. *Journal of geotechnical and geoenvironmental engineering*, *137*(11), 1103-1113.

Yoneda, J., Masui, A., Konno, Y., Jin, Y., Egawa, K., Kida, M., ... & Tenma, N. (2015). Mechanical properties of hydrate-bearing turbidite reservoir in the first gas production test site of the Eastern Nankai Trough. *Marine and Petroleum Geology*, *66*, 471-486.

Yoneda, J., Masui, A., Konno, Y., Jin, Y., Kida, M., Katagiri, J., ... & Tenma, N. (2017). Pressure-core-based reservoir characterization for geomechanics: Insights from gas hydrate drilling during 2012–2013 at the eastern Nankai Trough. *Marine and Petroleum Geology*, *86*, 1-16.

Appendices

Sintef, hydrate management

A part of this work has been presented/published in several seminars and journals:

Taleb Farah, *Garziglia Sébastien, Sultan Nabil.* ***Hydro-mechanical properties of gas hydrate-bearing fine sediments from in-situ testing***. *Journal of Geophysical Research: Solid Earth.* *https://doi.org/10.1029/2018JB015824*

Taleb Farah, *Garziglia Sébastien, Sultan Nabil.* ***In situ characterisation of gas hydrate-bearing clayey sediments in the Gulf of Guinea***. *Cone Penetration Testing 2018: Proceedings of the 4th International Symposium on Cone Penetration Testing (CPT'18), 21-22 June, 2018, Delft, The Netherlands. Hicks, Pisanò & Peuchen (Eds). 2018. ISBN 978-1-138-58449-5. Chap.84, pp.599-604. https://archimer.ifremer.fr/doc/00466/57748/*

Taleb Farah, *Morgane Lemaire, Garziglia Sébastien, Tania Marsset, Sultan Nabil.* ***Seafloor depressions on the Nigerian margin: seabed morphology and sub-seabed hydrate distribution***. *Paper under revision. Marine and Petroleum Geology.*

Taleb Farah, *Garziglia Sébastien, Sultan Nabil. (2018, December*). ***Investigation of the hydro mechanical behaviour of gas-hydrate bearing clayey sediments from the Gulf of Guinea using in-situ geotechnical measurements***. *In AGU Fall Meeting Abstracts.*

Taleb Farah, *Garziglia Sébastien, Sultan Nabil. (2018, November*). ***Investigation of the hydro mechanical behaviour of gas-hydrate bearing clayey sediments from the Gulf of Guinea***. *In GDR Abstracts.*

ADVANCING EARTH AND SPACE SCIENCE

JGR

Journal of Geophysical Research: Solid Earth

RESEARCH ARTICLE
10.1029/2018JB015824

Special Section:
Gas Hydrate in Porous Media: Linking Laboratory and Field Scale Phenomena

Key Points:
- Unlike hydrate-bearing sands, the behavior of hydrate-bearing clays proved contractive upon shearing according to in situ data
- Hydromechanical properties of hydrate-bearing clays depend on hydrate content and superimposed influence of their distribution/morphology
- For gas hydrate contents higher than 20%, the hydraulic diffusivity increases with hydrate concentration

Correspondence to:
F. Taleb,
farah.taleb@ifremer.fr

Citation:
Taleb, F., Garziglia, S., & Sultan, N. (2018). Hydromechanical properties of gas hydrate-bearing fine sediments from in situ testing. *Journal of Geophysical Research: Solid Earth*, *123*, 9615–9634. https://doi.org/10.1029/2018JB015824

Received 23 MAR 2018
Accepted 6 NOV 2018
Accepted article online 10 NOV 2018
Published online 28 NOV 2018

Hydromechanical Properties of Gas Hydrate-Bearing Fine Sediments From In Situ Testing

F. Taleb[1], **S. Garziglia**[1], **and N. Sultan**[1]

[1]Département REM, Unité des Géosciences Marines, IFREMER, Plouzané, France

Abstract The hydromechanical properties of gas hydrate-bearing sediment are key in assessing offshore geohazards and the resource potential of gas hydrates. For sandy materials, such properties were proved highly dependent on hydrate content (S_h) as well as on their distribution and morphology. Owing to difficulties in testing gas hydrate-bearing clayey sediments, the impact of hydrates on the behavior of such materials remains poorly understood. Hence, to provide insight into the characterization of clayey sediments containing hydrate, this study relies on a unique database of in situ acoustic, piezocone, and pore pressure dissipation measurements collected in a high gas flux system offshore Nigeria. Compressional wave velocity measurements were used as means of both detecting and quantifying gas hydrate in marine sediments. The analysis of piezocone data in normalized soil classification charts suggested that contrary to hydrate-bearing sands, the behavior of gas hydrate-bearing clays tends to be contractive. Correlations of acoustic and geotechnical data have shown that the stiffness and strength tend to increase with increasing S_h. However, several sediment intervals sharing the same S_h have revealed different features of mechanical behavior; suggesting that stiffness and strength of gas hydrate-bearing clays are influenced by the distribution/morphology of gas hydrate. Pore pressure dissipation data confirmed the contractive behavior of gas hydrate-bearing clays and showed that at low hydrate content, the hydraulic diffusivity (C_h) decreases when S_h increases. However, for S_h exceeding 20%, it was shown that an increase of C_h with S_h could be linked to the presence of fractures in the hydrate-sediment system.

1. Introduction

Over the last decades, increasing world's energy demand amidst of climate change concerns have encouraged the search for alternative and cleaner energy resources. Gas hydrate (GH) are considered as the largest untapped stock of natural gas in the world (Boswell & Collett, 2011) and are characterized by their widespread occurrence mainly in permafrost regions and continental margins (Kvenvolden, 1993). Due to the estimated staggering amounts of GH and their potential as a future energy resource but furthermore as a geotechnical hazard for various offshore operations and hydrocarbon recovery projects (Kayen & Lee, 1991) and their possible contribution to current and future climate change scenarios (Yun et al., 2007), GH have stimulated international academic and industrial interest.

The formation of GH within the sediment significantly alters the physical and mechanical properties of their host sediment. Such properties are also proved dependent on the hydrate content within the sediment as well as on their morphology/distribution (Dai et al., 2012). Thus, the quantification and characterization of GH within the marine environment have become significantly important in order to either contain their potential geotechnical threat or understand their effect on the hydromechanical properties of the host sediment under stability conditions (Ning et al., 2012).

GH can occur in a variety of sediments such as fine-grained clays and coarse-grained sands. Due to their high permeability and high GH content, coarse-grained sediments are often preferred for potential exploitation activities. However, fine-grained sediments contain over 90% of global GH accumulations (Boswell & Collett, 2006), yet not much research have been carried out concerning the hydromechanical behavior of such sediments.

The formation of GH within the sediment is mainly governed by the changing physical properties of the latter such as grain size, porosity, and permeability (Waite et al., 2009). This directly affects the morphology of the hydrate within the host sediment. Sands and coarse silts are characterized by disseminated pore-filling hydrate (Waite et al., 2009). The grain-displacing morphology is mostly observed in clay-rich sediments where GH form in fractures due to capillary tension forces (Jang & Santamarina, 2016). In this case, they force the clay aggregates to move apart and hence introduce veins or cracks within the sediment. However, Ghosh et al. (2010) suggested that in clayey sediments, GH could be present as pore-filling, grain-displacing, or a combination of both morphologies. This imposes a complexity when it comes to GH quantification in such sediments, since it requires knowledge of the orientation of the GH-bearing discontinuities.

The metastable nature of GH and the challenges they present in terms of identifying their presence via the recovery of natural samples have largely increased the reliance on pressure coring to prevent sediment disturbance (Santamarina et al., 2012). However, as presented by Sultan et al. (2007, 2010, 2014) in situ testing may be a promising alternative to costly pressure coring and testing operations. As reported in much literature, in situ testing is an efficient and cost-effective technique of collecting large amounts of data mainly in materials that are difficult to sample (Lunne et al., 1997; Robertson, 2009). This is particularly efficient in the case of GH-bearing fine-grained sediments, which remain challenging to preserve or synthesize prior to laboratory testing. Hence, to provide insight into the characterization of these geomaterials, this study relies on in situ acoustic, piezocone, and pore pressure dissipation measurements in the Gulf of Guinea.

Numerous oceanographic campaigns have been carried out along the West African margin due to the ongoing development of oil and gas projects. The Gulf of Guinea is one area where the presence of dense accumulations of shallow GH have been reported by several authors (Cunningham & Lindholm, 2000; Hovland et al., 1997; Sultan et al., 2010; Wei et al., 2015). Visual observations within the study area have revealed the presence of different GH morphologies varying from groups of thin veins to massive nodules in clay sediments (Sultan et al., 2007, 2010). In certain cases, solid GH and free gas were observed to coexist due to the presence of free gas voids within hydrate nodules; hence, resulting in a material with a spongy texture (Sultan et al., 2014).

The present work aims to understand the effect of the concentration and distribution/morphology of GH on the hydromechanical properties of their host clayey sediment. This relies on the quantification and characterization of GH using different in situ acoustic and geotechnical methods. The investigation was carried out by correlating these parameters and comparing sites without GH to GH-bearing sites. Different soil classification charts were used to illustrate the behavior of hydrate-bearing clays. Finally, different hydromechanical parameters of GHs bearing fine-grained sediments were derived using empirical relations.

2. Study Area

The study area is located in the deep water Niger Delta at a water depth ranging from 1,100 to 1,250 m. Numerous studies (Sultan et al., 2010, 2014) have shown that this area is characterized by several quasi-circular pockmarks (Figure 1) that are ten to a few hundred meters wide. The evolution and morphologies of these pockmarks have been directly linked to different habits of formation, nucleation, and dissolution of GH (Sultan et al., 2014). Wei et al. (2015) have investigated the distribution of GH in the sediment of the study area by applying infrared thermal imaging and pore water chloride analyses on MeBo cores, which allowed defining hydrate occurrence zones. These zones were shown to accommodate shallow GH accumulations (Sultan et al., 2007) as well as the coexistence of free gas and solid GHs. Based on the latter findings and on seismic data showing evidence of faulting (Sultan et al., 2016), the investigated area has been identified as a high gas flux system.

3. Tools and Methods

The data used in this paper were acquired during the Guineco-MeBo (2011) and ERIG3D (2008) oceanographic campaigns on the French R/V *Pourquoi pas?*. Both campaigns aimed to determine the distribution of GH from geophysical, geotechnical, and geochemical data. Different laboratory and in situ measurements were carried out to assess the physicochemical properties of the sediment at a number of sites outside and within pockmarks as shown in Figure 1 and Table 1.

3.1. In Situ Measurements and Coring

3.1.1. Piezocone (Penfeld)

In situ acoustic and geotechnical measurements were carried out using the Penfeld seabed rig developed by Ifremer. It is provided with a rod that can push two types of probes down to 30 m below seabed with a thrust of 40 kN at a standard rate of 2 cm/s (Sultan et al., 2007).

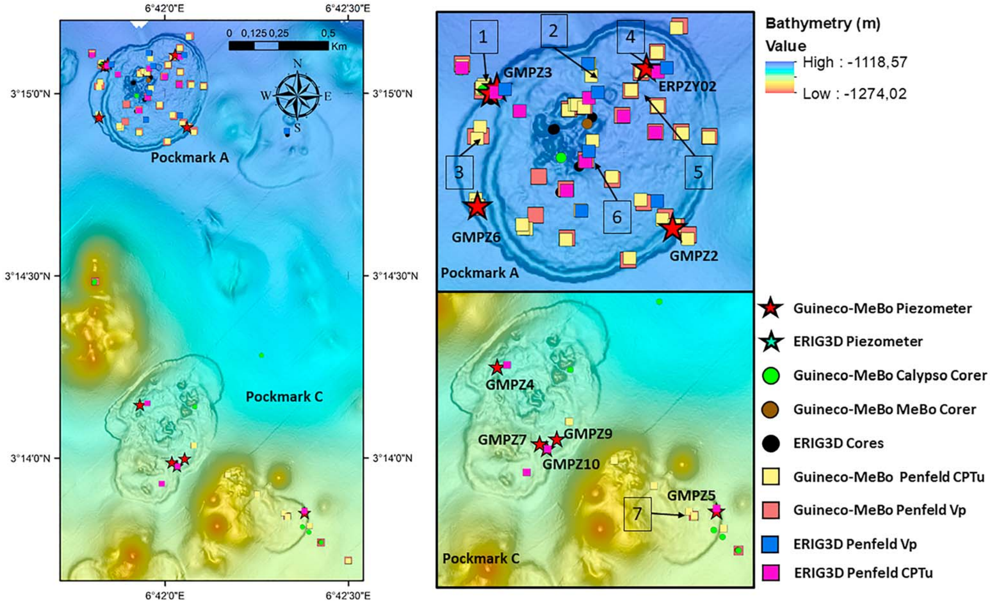

Figure 1. Bathymetry of the study area showing the investigated sites: 1: GMPFV02S02, GMPFM06S01, GMPZ3, GMMB01, and GMCS05; 2: ERVP03S01 and GMPFM12S03; 3: GMPFV02S03 and GMPFM01S03; 4: GMPFV03S03, ERCPT02S08, ERPZY02 and GMMB12; 5: GMPFV03S04 and GMPFM04S04; 6: GMPFV07S05, ERCPT02S05, and GMMB06; and 7: GMPFV10S04, GMPFM05S03, and GMMB05.

The piezocone probe can be used to carry out Cone Penetration Testing with pore pressure measurement (CPTu); thus, providing continuous vertical readings of cone tip resistance (q_t), sleeve friction (f_s), and penetration pore pressure (Δu_2). The latter is measured with a differential pore pressure sensor located immediately behind the cone (u_2 position). The piezocone is equipped with pressure-compensated sensors to provide accurate measurements irrespective of the water depth.

The ultrasonic fork can alternatively be used to measure every 2 cm the velocity of compressional waves (Vp) up to 2,200 m/s. Acoustic measurements are carried out by producing a 1-MHz compressional wave from one branch of the fork and recording its travel time to the opposite branch located 7 cm apart. The amplitude ratio between the input and received signals provides attenuation. As an additional parameter recorded during acoustic measurements, the so-called *applied load*' corresponds to the force required to push the ultrasonic fork in the sediment.

In this paper, seven Penfeld Vp (1: GMPFV02S02, 2: ERVP03S01, 3: GMPFV02S03, 4: GMPFV03S03, 5: GMPFV03S04, 6: GMPFV07S05, and 7: GMPfV10S04) and seven Penfeld CPTu (1: GMPFM06S01, 2: GMPFM12S03, 3: GMPFM01S03, 4: ERCPT02S08, 5: GMPFM04S04, 6: ERCPT02S05, and 7: GMPFM05S03) were investigated, as seen in Figure 1 and Table 1.

Table 1
Investigated Sites Within the Study Area

Investigated site	Depth (m)	Length (m)	Nearby CPTu	Nearby piezocone	Nearby Calypso or MeBo core	Site
GMPFV02S02	1,140	30	GMPFM06S01	GMPZ3	GMCS05	1
ERVP03S01	1,140	30	GMPFM12S03	—	—	2
GMPFV02S03	1,144	30	GMPFM01S03	—	—	3
GMPFV03S03	1,142	10.3	ERCPT02S08	ERPZY02	GMMB12	4
GMPFV03S04	1,140	5.7	GMPFM04S04	—	—	5
GMPFV07S05	1,146	8.5	ERCPT02S05	—	GMMB06	6
GMPFV10S04	1,195	26	GMPFM05S03	—	GMMB05	7

Note. Site 1 cluster was used to characterize sediment from the reference site without gas hydrate while sites 2, 3,4,5,6 and 7 clusters represent areas where the presence of gas hydrate was suspected or proved.

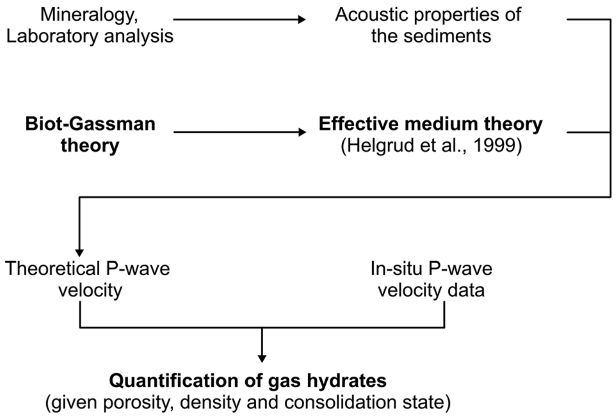

Figure 2. Adopted method to apply the effective medium theory (Helgerud et al., 1999).

3.1.2. Piezometer

The Ifremer piezometer is a free-fall device that allows pore pressure measurements. It is equipped with a 60-mm-diameter sediment-piercing lance whose length can be adapted to the type and the stiffness of the penetrated sediment. For example, a 12-m-length lance is used for soft sediments. Pore pressures are measured at up to 10 ports with a minimum spacing of 70 cm using differential pressure transducers. They measure pressure relative to hydrostatic pressure with an accuracy of 0.4 kPa. The lance is also equipped with temperature sensors having an accuracy of 0.05 °C.

The piezometer can be used in two modes: long- and short-term measurements. In the former, equilibrium pore pressure can be reached after several days; whereas in the latter the equilibrium pore pressure is evaluated following the technique proposed by Sultan and Lafuerza (2013).

In this paper 10 piezometer sites will be investigated (GMPZ2, 3, 4, 5, 6, 7, and 10 and ERPZY02), with only two next to a Penfeld Vp site (1: GMPZ3 and 4: ERPZY02).

3.1.3. Coring and Drilling

Core sediments used in this paper are obtained from a Calypso coring system. It is equipped with a Kullenberg type piston that minimizes the variations of the internal pressure during the coring process. Hence, the sediment is less disturbed when recovered to the surface. The Calypso Corer allows the recovery of up to 35 m of marine sediment.

The seafloor drill rig MeBo (Freudenthal & Wefer, 2007; Freudenthal & Wefer, 2013) was also used to recover longer sedimentary cores.

In this work, one Calypso core (1: GMCS05) and four MeBo cores (1: GMMB01, 4: GMMB12, 6: GMMB06, and 7: GMMB05) have allowed the investigation of the study area (Figure 1 and Table 1).

3.2. Laboratory Testing

3.2.1. MSCL and XRD

The Multi-Sensor Core Logger (MSCL) from Geotech was used onboard in order to measure the *P* wave velocity, the Gamma density, and the magnetic susceptibility on 1-m-long whole core sections. This was done at 1-cm step for all cores without hydrate and at 2-cm step for cores containing hydrate. In this work, the density profile from Calypso core GMCS05 (site 1 in Figure 1) was taken as representative of the study area.

The X-ray diffraction (XRD) method was used to characterize the mineralogical composition of sediment sampled with a 10-cm spacing on core GMCS05. By correlating X-ray diffraction results with those obtained with an Avaatech X-ray fluorescence core scanner, the clay, calcite, and quartz fractions in sediment from core GMCS05 were determined with a finer spacing of 2 cm. (Figure 2).

3.3. GH Quantification

3.3.1. From Pore Water Chloride Analysis

The formation of GH is known to exclude ions dissolved in pore water from the clathrate cage, hence, increasing the salinity of the surrounding pore water (Paul & Ussler, 2001). Therefore, the dissociation of GH upon core recovery releases fresh water, causing negative anomalies on pore water chloride profiles (Wei et al., 2015).

As reported by Wei et al., (2015), pore water was extracted using Rhizon samplers on 12 MeBo cores collected in the study area. Chloride concentrations were subsequently determined using ion chromatography (Wei et al., 2015). This led Wei et al., (2015) to determine a baseline pore water chlorinity in the absence of GH of 550 mM. This was done by measuring chloride concentrations in bottom waters and in reference sediments.

This value served as an input parameter in the estimation of the GH content S_h from chloride anomalies following the method presented by Malinverno et al. (2008):

Table 2
Elastic and Density Properties of Selected Sediment Components (After Helgerud et al., 1999)

Constituent m	*K* (GPa)	*G* (GPa)	ρ (g/cm^3)
Clay	20.9	6.85	2.58
Calcite	76.8	32	2.71
Quartz	36.6	45	2.65
Gas hydrate	7.9	3.3	0.90
Water	2.4–2.6	0	1.032
Methane gas	0.10–0.12	0	0.23

Note. *K* is the bulk modulus, *G* the shear modulus, and ρ the density.

$$S_h = \frac{\beta(C_{\mathrm{cb}} - C_c)}{C_c + \beta(C_{\mathrm{cb}} - C_c)} \tag{1}$$

where β is a coefficient that accounts for the density change from GH to water and equals 1.257, C_{cb} is the baseline pore water chlorinity prior to dissociation, and C_c is the chlorinity measured in the core after dissociation.

3.3.2. From In Situ Vp Measurements and Rock Physics Characterization

The effective medium model developed by Helgerud et al. (1999) was used to estimate GH content within the marine sediment from in situ Vp measurements. The principle of this model is to relate the stiffness of the dry frame to porosity, mineralogy, and effective stress. As key input parameters to the model, the sediment mineralogy, porosity, and its evolution with effective stress were determined from analyses of core GMCS05 taken as representative of the study area. The elastic properties and densities used in the calculation were similar to those used by Helgerud et al. (1999) as shown in Table 2.

Differences between calculated and measured *P* wave velocities (Figure 2) were used to obtain an upper- and lower-bound estimate of GH content within the sediment by assuming that: (a) hydrate alters only the pore fluid elastic properties (S_{hmax}); (b) hydrate contributes stiffness to the sediment by becoming part of the load-bearing framework (S_{hmin}).

It is noteworthy that considering one case or the other has implications on the derivation of the lithostatic stress as explained by Helgerud et al. (1999). However, when calculating the effective stress as the difference between the lithostatic stress and the pore fluid pressure, hydrostatic conditions were always assumed for the latter.

3.4. Derivation of Geotechnical Properties From Piezocone Results

Piezocone readings including q_t, f_s, and Δu_2 were, first, used to classify sediments based on their behavior characteristics and, second, to derive their geotechnical properties. The classification process relied on the method suggested by Robertson (2016) using the following equations:

The normalized friction ratio

$$F_r = 100\times\frac{f_s}{q_t - \sigma_{v0}}\ [\%] \tag{2}$$

The normalized pore pressure

$$U_2 = \frac{\Delta u_2}{\sigma'_{v0}}\ [-] \tag{3}$$

A revised value of normalized cone resistance

$$Q_{\mathrm{tn}} = \left(\frac{q_t - \sigma_{v0}}{p_a}\right)\left(\frac{p_a}{\sigma'_{v0}}\right)^n\ [-] \tag{4}$$

Where p_a is the atmospheric reference pressure (i.e., 100 kPa) and n a stress exponent defined as

$$n = 0.381(I_c) + 0.05\left(\frac{\sigma'_{v0}}{p_a}\right) - 0.15 \tag{5}$$

Where I_c is a soil behavior type index defined as

$$I_c = \left[\left(3.47 - \log\left[\frac{q_t - \sigma_{v0}}{\sigma'_{v0}}\right]\right)2 + (\log F_r + 1.22)2\right]^{0.5} \tag{6}$$

For sediments without GH, the values of total and vertical effective stresses (σ_{v0} and σ'_{v0}, respectively) were calculated from the unit weight profile obtained on core GMCS05. For GH-bearing sediment, the values were obtained from back calculations of GH content using the effective medium model developed by Helgerud et al., (1999; see section 3.3.2).

The geotechnical properties were empirically derived from piezocone results following the unified interpretation approach presented by Robertson (2009). Since the reliability and applicability of empirical correlations vary according to precedent and local experience, the properties derived from piezocone sounding in GH-bearing sediments must be treated with caution due to the lack of statistical study on this soil type.

Compression indices were estimated from piezocone results using the following equation:

$$\lambda = \frac{\left[(1+e_0)\sigma'_{v0}\right]}{\left[\alpha_M(q_t-\sigma_{v0})\right]} \tag{7}$$

Where α_M is the constrained modulus cone factor. Based on correlations between piezocone data and results of oedometer tests reported by Sultan et al. (2007), a site-specific value of $\alpha_M = 1$ and a value of void ratio, $e_0 = 6.15$ (at $\sigma'_{v0} = 1$ kPa) were used to calculate compression indices for both hydrate-free and hydrate-bearing sediments.

Values of shear modulus at small strain (G_0) were estimated using

$$G_0 = 0.0188\left[10^{(0.55I_c+1.68)}(q_t-\sigma_{v0})\right] \tag{8}$$

where I_c is the soil behavior type index previously defined (equation (8)). Following Krage et al. (2014) values of G_0 were converted into values of shear modulus at 50% mobilized strength (G_{50}) by assuming that (G_{50}/G_0) = 0.26 for both hydrate-free and hydrate-bearing sediments.

Values of peak undrained shear strength (Su) were derived from:

$$Su = \frac{(q_t-\sigma_{v0})}{N_{kt}} \tag{9}$$

where N_{kt} is a cone factor typically varying from 10 to 20. Following the works of Low et al. (2010) on soft clays, a N_{kt} value of 13.6 was used to calculate Su in hydrate-free sediments. A lower-bound estimate of the Su of GH-bearing sediments was calculated using a similar N_{kt}. Calculations were additionally performed using a N_{kt} value of 10 to provide an upper bound estimate.

Based on the assumption that values of sleeve friction (f_s) correspond to the remolded shear strength of the sediment, values of sensitivity were estimated using

$$St = \frac{Su}{f_s} \tag{10}$$

3.5. Derivation of Hydraulic Properties From Piezometer Results

The Ifremer piezometer was used to carry out pore pressure measurements at several selected locations and depths where the presence of GH was suspected and/or proved (GMPZ2, 4, 6, 7, and 10 and ERPZY02) as well as at two reference sites (GMPZ3 and 5). The measured pore water pressure (u) corresponds to an excess pore pressure (Δu) generated by the rod insertion and an in situ equilibrium pore pressure (u_{eq}), which is assumed constant during the dissipation of the measured maximum excess pore pressure ($u = \Delta u + u_{\text{eq}}$). The time for 50% dissipation of the measured maximum excess pore pressure (t_{50}) was determined using a graphical method in which u_{eq} was either reached from the dissipation test or calculated using the Sultan and Lafuerza (2013) numerical algorithm and after determining Δu_{100}, Δu_0, and Δu_{50} (see ASTM Standard D2435, 1996). It was then possible to derive the hydraulic diffusivity C_h (or the horizontal coefficient of consolidation) of the medium normalized by the square root of the rigidity index (I_r) using the following equation (Teh & Houlsby, 1991):

$$\frac{C_h}{\sqrt{I_r}} = \frac{C_p\, r^2}{t_{50}} \tag{11}$$

Where C_p is a factor related to the location of the sensor and r is the radius of the rod.

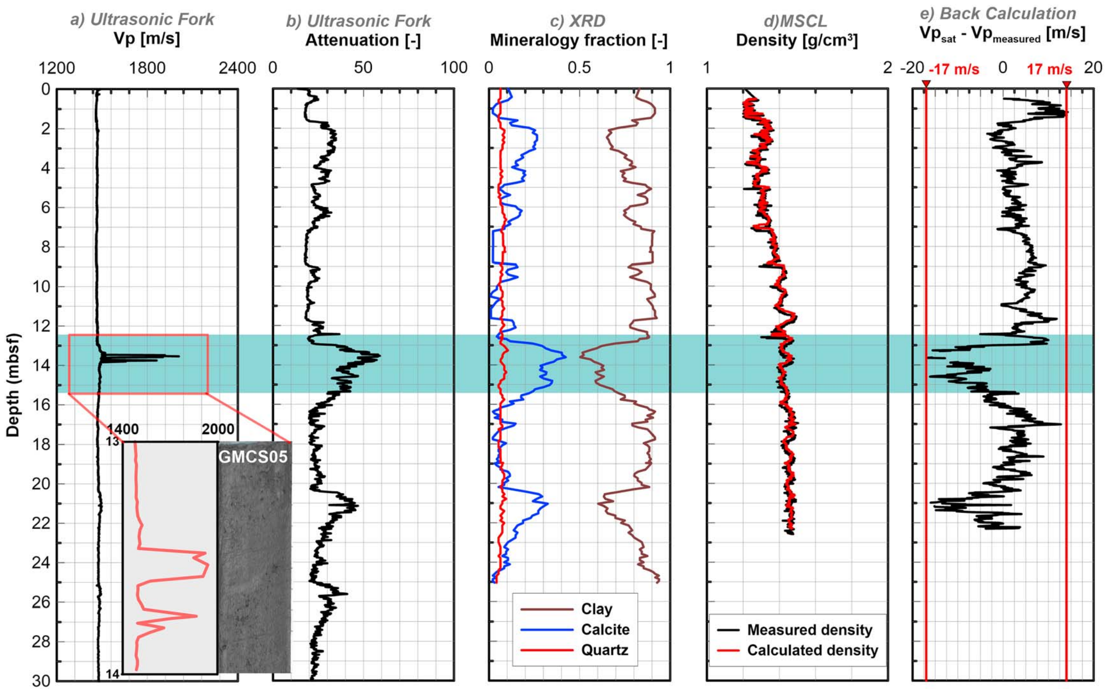

Figure 3. (a) *P* wave velocity and (b) signal attenuation for site GMPFV02S02, (c) mineral fraction and (d) vertical effective stress derived from Multi-Sensor Core Logger (MSCL) density data (core GMCS05) and model calculation (e) difference between calculated velocity and measured velocity. XRD = X-ray diffraction.

4. Results

4.1. Characterization of Sediment Without GH—Reference Site

Sites GMPFV02S02 and GMPFM06S01 (site 1 in Figure 1) were considered as Penfeld Vp and CPTu reference sites, respectively, since they are located outside of the pockmarks. Reference sites are characterized by compressional wave velocities varying between 1,450 m/s and 1,510 m/s. However at site GMPFV02S02, velocity and attenuation peaks of 2,015 m/s and 59, respectively, can be identified at 13.6 mbsf (Figures 3a and 3b). Additionally, while the quartz fraction profile is nearly constant along the core, the calcite and clay fractions vary from 0.5 to 0.9 and from 0.01 to 0.42, respectively (Figure 3c). It is noteworthy that there is great resemblance between the calcite, Vp, and signal attenuation profiles. Therefore, Vp peaks were linked to the presence of calcium carbonate (mainly foraminifera) within the sediment. This is further confirmed by visual observations of core GMCS05, which do not reveal any fractures or cracks as would be expected if GH were present at this site. The calculated vertical effective stress $\left(\sigma'_{v0}\right)$ profile (Figure 3d) was determined with the model presented in section 3.3.2 assuming hydrostatic pressure and based on laboratory predefined compressibility and void ratio data. It can be observed that the measured σ'_{v0} and the calculated σ'_{v0} profiles yield almost the same results, confirming the reliability of the used model. Figure 3e shows that the difference between the velocity calculated by the model and the measured velocity tend to oscillate in the range ±17 m/s This served to set the detection threshold of GH in sediments. That is to say that, in this study, estimates of GH contents are only provided when the difference between the calculated Vp and measured Vp is greater than 17 m/s.

As shown in Figure 4, piezocone data for reference site GMPFM06S01 (site 1 in Figure 1) are characterized by a linear increase with depth of the corrected cone tip resistance (q_t), sleeve friction (f_s), and pore water pressure (Δu_2) up to 1,000, 12, and 320 kPa, respectively, at 30 mbsf.

By adopting the *P* wave velocity intercomparison method and considering sites GMPFV02S02 and GMPFM06S01 as a reference, the distinct features between GH-bearing sediments and sediments without hydrate were identified and discussed.

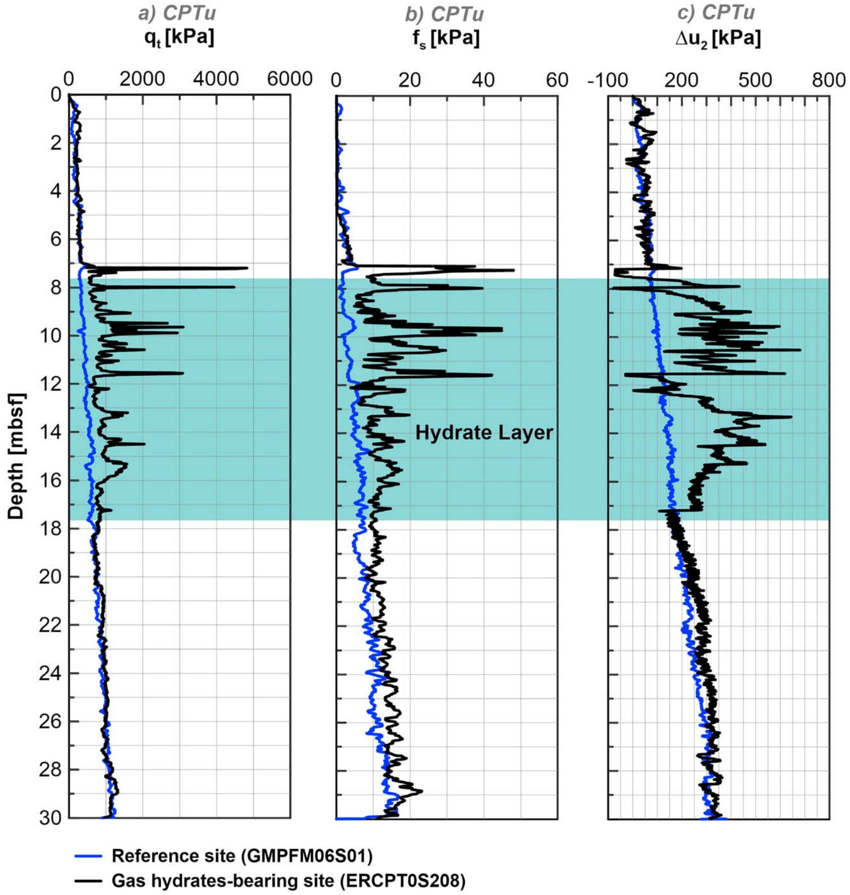

Figure 4. GH-bearing site ERCPT02S08 (site 4 in Figure 1): (a) Corrected cone tip resistance, (b) sleeve friction, and (c) pore water pressure. The light blue rectangle shows the GH occurrence zone identified by Wei et al. (2015) from chloride anomalies and infrared images. Cone Penetration Testing with pore pressure measurement.

4.2. GH Characterization and Quantification

Figure 4 presents the corrected cone tip resistance (q_t), the sleeve friction (f_s), and the pore water pressure (Δu_2) from the Penfeld CPTu for site ERCPT02S08 (site 4 in Figure 1). At 7.23 mbsf q_t was found to be almost 10 times higher than that of the reference site GMPFM06S01 at the same depth. Wei et al. (2015) identified the top of the GH occurrence zone at almost the same depth (see light blue rectangle in Figure 4).

The simultaneous and strong increase in these parameters (q_t, f_s, and Δu_2)confirms the presence of GH within the marine sediment. Additionally the q_t profile suggests the presence of two distinct GH layers: (1) from 7 to 11.5 mbsf with $q_t$ranging between 3,153 and 4,913 kPa and (2) from 12.5 to 17.5 mbsf with q_t ranging between 1,062 and 2,004 kPa. It is also noteworthy that at depths 7.23 and 8 mbsf, high f_s and q_t values correlate with negative Δu_2 values.

GHs were quantified at all sites where Vp data were available and after definition of the mineralogy profile of the sediment in question. Hydrate quantification results obtained from the numerical model using the effective medium theory were compared with those obtained from chloride anomalies using equation (1).

Figure 5 presents the *P* wave velocity (V_p), the signal attenuation and the applied load profiles obtained from the Penfeld Vp, and the back calculation for GH content for the GMPFV03S03 (site 4 in Figure 1) and the corrected cone tip resistance (q_t) obtained from Penfeld CPTu for the ERCPT02S08 (site 4 on Figure 1). Strong and positive variations of these parameters along the depth confirm the presence of GH. However, negative anomalies in the Vp profile is an indicator for the presence of free gas within the sediment. Therefore, it is possible to define areas where free gas and solid GH layers form alternatively or even coexist. CPTu = Cone Penetration Testing with pore pressure measurement.

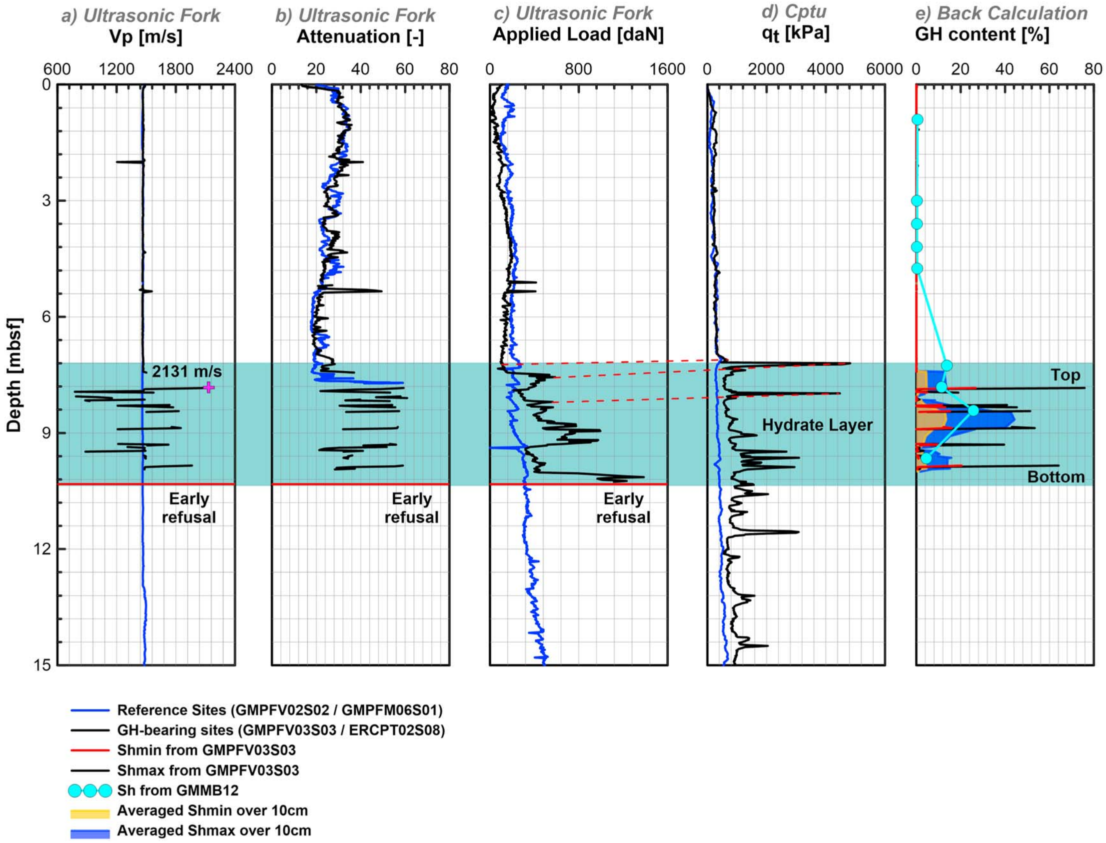

Figure 5. (a) *P* wave velocity, (b) signal attenuation, (c) applied load for GH-bearing site GMPFV03S03, (d) corrected cone tip resistance for GH-bearing site ERCPT02S08, and (e) back calculation of GH content.

While missing data is observed in the *P* wave velocity and attenuation profiles between 7.45 and 7.84 mbsf for the GMPFV03S03, the applied load profile suggests that GHs were reached at 7.45 mbsf (Figure 5). This was confirmed by the pore water chloride data that shows that the GH content reaches 14% at around 7.26 mbsf. This is followed by sudden increases of 2,131 m/s in Vp and 60 in the signal attenuation at 7.85 mbsf, which highlights the effect of the presence of GH within the marine sediment.

Using the effective medium theory, the GH content in the sediment was estimated and then averaged over 10 cm, allowing the comparison with estimates of GH content derived from chloride anomalies. Maximum GH content were estimated to occur at 7.85 mbsf: 27% for S_{hmin}, 76% for S_{hmax}, 6% for averaged S_{hmin} and 14.5% for averaged S_{hmax}. At this same depth, a GH content of 11.5% was estimated by the pore water chloride data, which almost equals the average value of averaged S_{hmin} and averaged S_{hmax}. Based on Vp anomalies, the top of the GH occurrence zone was assumed to start at 7.85 mbsf.

Quantification results derived from the effective medium theory and from the pore water chloride analysis for all investigated sites are presented in Figure 6. GH clearly exhibit a heterogeneous vertical distribution within the GH occurrence zones without showing any systematic pattern. By comparing both GH quantification methods for sites GMPFV03S03 (site 4 in Figure 1) and GMPFV10S04 (site 7 in Figure 1), it can be observed that averaged S_{hmax} and S_{hmin}values oscillate around values of S_h derived from the chlorinity data. On the other hand, for site GMPFV07S05 S_{hmax} values are closer to those derived from chlorinity data compared to S_{hmin} values. By contrast, nonaveraged values of S_{hmax} are much higher than those estimated from chlorinity data. Additionally, studies performed by Ghosh et al. (2010), showed that for GH-bearing clayey sediments S_{hmin} yields estimates closer to that obtained from the pressure core depressurization method compared to S_{hmax}. Hence, in the next chapters only S_{hmin} (called in the following s_h) values will be considered and discussed.

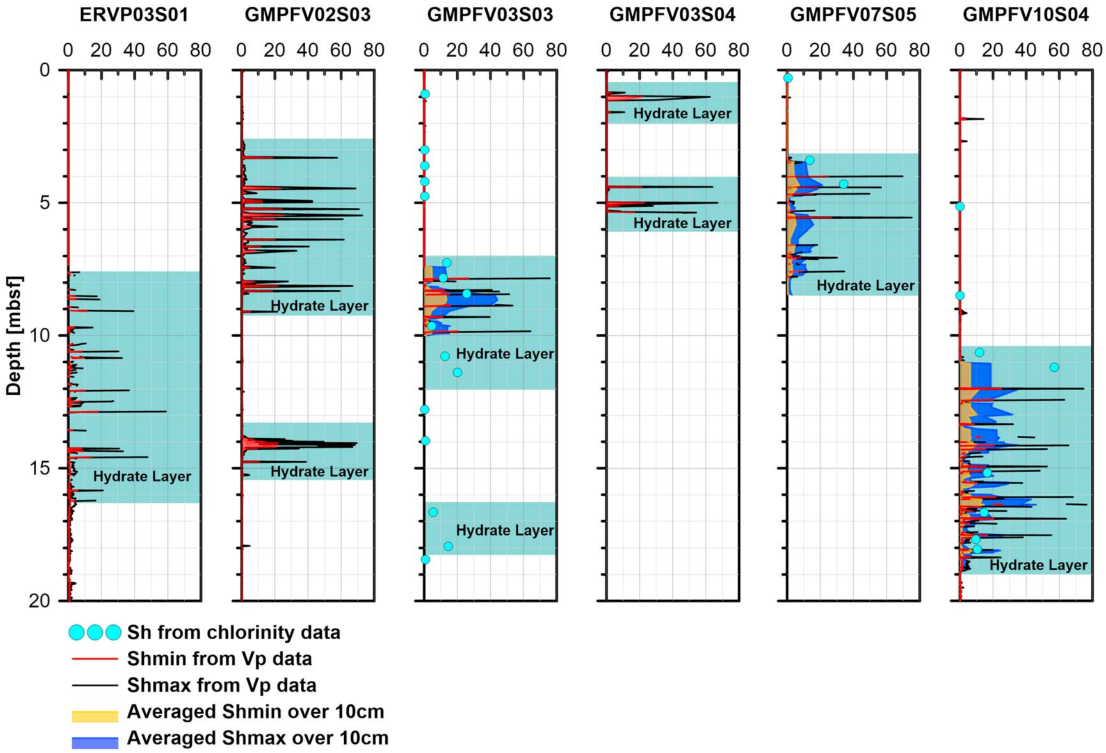

Figure 6. Estimates of gas hydrate content for all the six investigated sites: ERVP03S01 (site 2 in Figure 1), GMPFV02S03 (site 3 in Figure 1), GMPFV03S03 (site 4 in Figure 1), GMPFV03S04 (site 4 in Figure 1), GMPFV07S05 (site 6 in Figure 1), and GMPFV10S04 (site 7 in Figure 1).

4.3. Soil Behavior Classification Charts Using CPTu and Vp Data

To further highlight features of GH-bearing sediments, normalized CPTu data were plotted in Robertson (2016) updated classification charts. Figure 7 shows the data from GH-bearing sites (GMPFM12S03, GPFM04S04, GMPFM01S03, GMPFM05S03, ERCPT02S05, and ERCPT02S08) plotted as symbols whose shape represent GH content (S_h%) within the sediment. The diagrams charts also show the piezocone data where the GH content could not have been estimated. This is mainly due to missing Vp data (values higher than 2,200 m/s), which is a key parameter in the effective medium model. Correlations between in situ acoustic and geotechnical measurements were necessary in order to highlight the mechanical behavior of GH-bearing clayey sediment. This step was achieved by first identifying peaks and common patterns on the applied load and q_t profiles as it was thought to have the most physical meaning. As illustrated in Figure 5, correlations were made by relating depths of significant peaks in both profiles. This method was adopted for all other investigated sites. Due to difficulties in constantly correlating peaks, only 25 data points were considered in this work as unambiguous.

Based on the $Q_{tn} - \mathrm{U}_2$ chart, sediment from reference sites exhibits U_2 values varying between 3 and 5.5 and Q_{tn} values not exceeding 16. Sediment containing GH is characterized by large Q_{tn} values up to 84 and correlating with U_2 values varying between 6 and 25. Most of the data from these sites plot in the contractive zone of the chart with 82% of the data in the clay contractive sensitive region and 18% in the clay contractive (CC) region. Points having the highest GH content plot at the limit of the CC region and tend toward a transitional contractive behavior. However, points where GH could not be quantified show a more pronounced trend toward a transitional contractive behavior with high Q_{tn} and U_2 values up to 280 and 70, respectively. No points were detected in the sand dilative region where the pore pressure remains zero during the piezocone penetration and corresponds to the drained region on the original classification chart presented by Schneider et al. (2008). This indicates that the piezocone penetration occurred fully undrained in GH-bearing sediments.On the other hand, the $Q_{\mathrm{tn}} - \mathrm{F}_{\mathrm{r}}$ chart shows a range of F_r values (0.7 to 8.8) that is almost the same for GH-bearing sites and sites without hydrate. It also suggests a tendency toward a dilative behavior for GH-bearing sediment, with almost 79% of the data plotting between the sand dilative, the transitional dilative

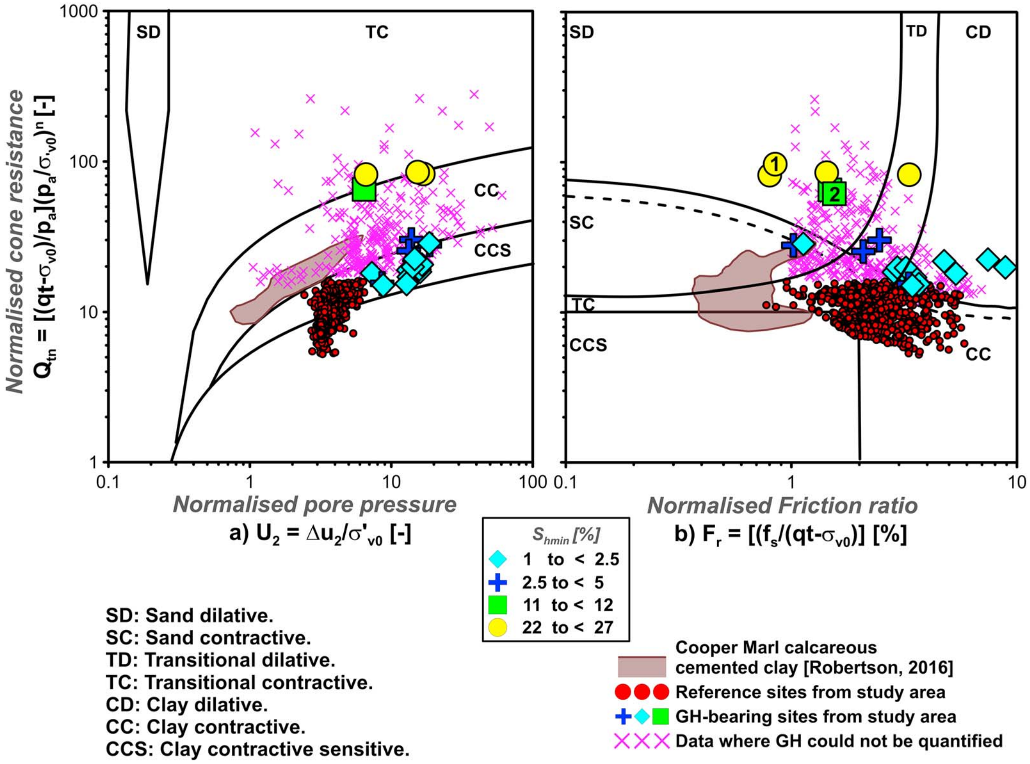

Figure 7. Piezocone data from reference sites (without GH), GH-bearing sites, and calcareous cemented clay (after Robertson, 2016) plotted in: (a) $Q_{\text{tn}} - U_2$ chart and (b) $Q_{\text{tn}} - Fr$ chart (Robertson, 2016). Data from GH-bearing sites are represented by pink crosses where the GH content could not have been estimated and by different symbols and colors referring to estimates of GH content (i.e., S_{hmin}, see legend).

and the clay dilative regions. However, some points that were classified as CC in the $Q_{tn} - \text{U}_2$ chart are also classified as contractive in the $Q_{tn} - \text{F}_\text{r}$ chart. It is noteworthy that two of these points show a behavior that correlates with the upper limit of Cooper Marl cemented clays on the $Q_{\text{tn}} - F_r$ chart, as proposed by Robertson (2016).

4.4. Mechanical Properties of GH-Bearing Sediment

In line with previous observation regarding changes in corrected cone tip resistance(q_t), sleeve friction (f_s), and pore water pressure (Δu_2) in the GH occurrence zone identified by Wei et al. (2015), Figure 8 reveals that the presence of GH has a noticeable effect on the compressibility, stiffness, and strength properties of their host clayey sediments. For instance, the compression indices (λ), the shear moduli at 50% mobilized strength (G_{50}), and the undrained shear strengths (Su) in the GH-bearing sediment do not follow the linear trends exhibited by the reference sediment. The compression indices (λ) are constantly lower in the GH occurrence zone with values 20 to 40 times lower than those estimated at equivalent depths at the reference site (GMPFM06S01). Away from those spikes, λ values are about 3 to 4 times lower in the GH-bearing sediment.

Increases in stiffness seem less significant with G_{50} values being 1.25 to 7 times higher in GH-bearing sediments compared to sediments without GH (Figure 8).

The increases in undrained shear strength mimic the increases in stiffness, though GH-bearing sediments are up to 25 times stronger than reference sediments where spikes are observed and 2 to 3 times stronger away from the spikes (Figure 8). The fact that the stiffness and strength of GH-bearing sediments vary simultaneously explains why their rigidity indices ($I_r = G_{50}/S_u$) do not remarkably differ from those of sediments without hydrate (Figure 8). By contrast, with the noticeable changes in compressibility, stiffness, and strength, the sensitivity does not appear to be affected by the presence of hydrate (Figure 8).

Plots of geotechnical properties derived from piezocone data against GH content shown in Figure 9 suggest that the compressibility of GH-bearing clayey sediment follows two distinct trends. The first trend may be

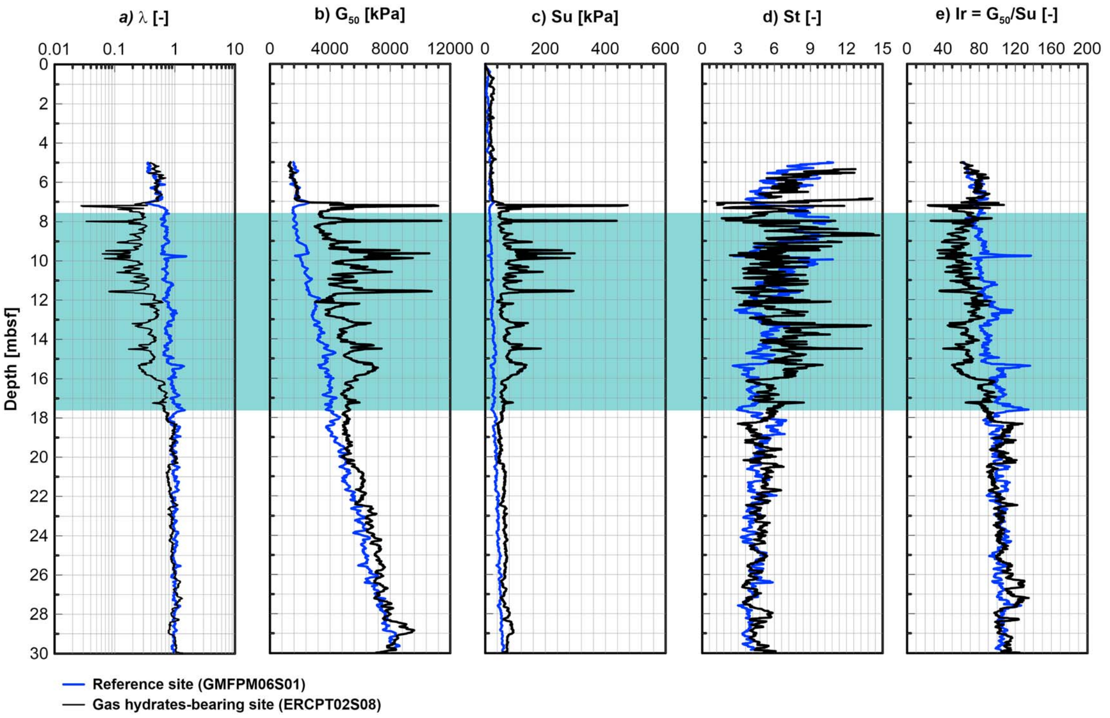

Figure 8. Depth profiles of geotechnical properties derived from piezocone data from the reference site GMPFM06-01 (blue), and the GH-bearing site ERCPT02-08 (black): a. compression index, λ; shear modulus at 50% mobilized strength, G_{50}, undrained shear strength, Su; sensitivity, St; rigidity index, I_r. The light blue rectangle shows the GH occurrence zone identified by Wei et al., (2015) from chloride anomalies and infrared images.

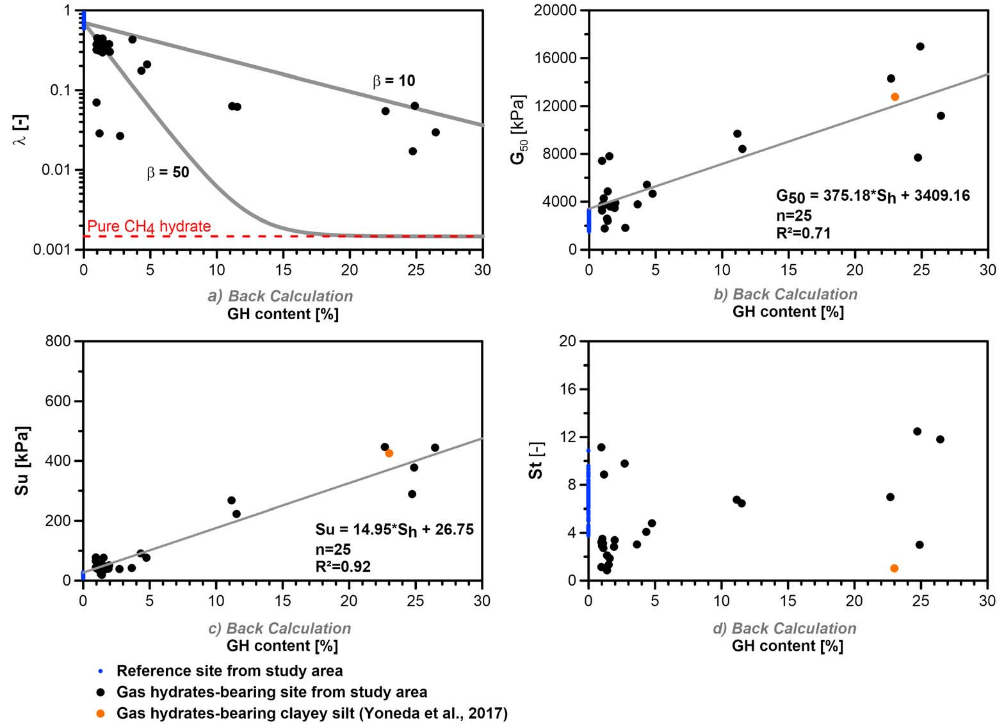

Figure 9. Plots of geotechnical properties derived from piezocone data against hydrate content, S_h estimated from nearby acoustic soundings: (a) compression index, λ; (b) shear modulus at 50% mobilized strength, G_{50}; (c) undrained shear strength, Su, (d) sensitivity, St. hydrate-free sediments are plotted for reference as blue dots. The orange dots in (b–d) are determined from the results of triaxial compression tests on natural, never depressurized gas hydrate (GH)-bearing clayey silt samples from the eastern Nankai trough as reported by Yoneda et al. (2017).

defined by values of compression indices decreasing from 0.47 to 0.026 for values of S_h increasing from 0.94% to 2.76%. The second one outlines a softer decrease in compressibility with GH content with λ reaching 0.06 to 0.017 for S_h values ranging from 22.7% to 26.5%. Values of shear moduli at 50% mobilized strength (G_{50}) appear to follow a more linearly increasing trend with S_h despite some scatter at low and high S_h (Figure 9). With a regression coefficient $R2$ of 0.92, values of undrained shear strength follow a linear increase with increasing S_h. By contrast, no clear trend can be observed when plotting values of sensitivity against S_h. Sensitivities around 7 are indeed associated with S_h ranging from 0.94% to 22.7%.

4.5. Hydraulic Properties of GH-Bearing Sediment

Figure 10 shows the initial excess pore pressure pulse (U_{ini}) and dissipation generated by the piezometer penetration during a maximum time-period of 64 hr from different depths at sites GMPZ2, 3, 4, 6, 7, and 10 (for location see Figure 1). Data in Figure 10 were arbitrarily subdivided into two classes: (1) High initial excess pore pressure pulse ($U_{\text{ini}} > 150$ kPa) and (2) low initial excess pore pressure pulse ($U_{\text{ini}} < 150$ kPa).

Following Burns and Mayne (1999), sediments with a dilative behavior are characterized by Δu curves increasing with time to a certain maximum and then decreasing to in situ equilibrium pore water pressure. In this study, Δu curves are observed to decrease in a monotonic way with time, which is indicative of a contractive behavior as described by Burns and Mayne (1999).

Figure 11 shows $\frac{C_h}{\sqrt{I_r}}$ and U_{ini} as a function of the corrected tip resistance q_t obtained from CPTu testing carried out near the piezometer sites. The clear increase of U_{ini} with q_t for the two reference sites as well as for sites with GH confirms the dependency of U_{ini} on the mechanical properties of the sediments. In effect, U_{ini} is the result of a mean normal octahedral stress (Δu_n) caused by the displacement of the sediment and fluid by the penetrating rod and the shear stress generated at the sediment-rod interface $(\Delta_{u_{\text{shear}}})$ (Burns & Mayne, 1998).

The $\frac{C_h}{\sqrt{I_r}}$ values obtained from the two reference sites indicate a decrease of this normalized parameter with the increase of qt (Figure 11). However, $\frac{C_h}{\sqrt{I_r}}$ values for GH-bearing sediments did not show any tendency to increase with q_t. Such result is unusual since the $\frac{C_h}{\sqrt{I_r}}$ values are expected to be proportional to the permeability of the medium and therefore to decrease with the increase of GH content and the increase of q_t.

Figure 12 shows $\frac{C_h}{\sqrt{I_r}}$ as a function of GH content S_h derived from the chloride data and in situ Vp measurements. It can be observed that $\frac{C_h}{\sqrt{I_r}}$ decreases to a minimum value for S_h equal to 10% and then increases again. However, considering the small change of the rigidity index I_r with S_h (Figure 8), it is obvious that the tendency of hydraulic diffusivity to decrease with increasing GH content is not confirmed by the present in situ pore pressure measurements.

5. Discussion

5.1. Quantification and Characterization of GH

In this study, the presence of GH within fine-grained marine sediment have been characterized based on in situ geotechnical and acoustic measurements. The presence of GH was linked to positive Vp anomalies that correlate with an increase in all of the CPTu parameters. However, negative Vp anomalies were indicators of the presence of free gas. The effective medium theory developed by Helgerud et al. (1999) was used to obtain an upper- and lower-bound estimate of GH content within the sediment based on compressional wave velocity anomalies.

Comparisons of velocity-derived estimates were made with those derived from pore water chloride anomalies to evaluate which of the upper- or lower-bound GH content might be more reliable to use in the study area. It was found that S_{hmin} values are fairly close to those derived from pore water chloride analyses. These observations are in line with studies performed by Ghosh et al. (2010), in which it was shown that S_{hmin} yields closer estimates to that of the pressure core depressurization method compared to S_{hmax}. Hence, for this paper S_{hmin} was used to carry out the investigation of the effect of GH content on the mechanical and hydraulic properties of the host sediment. In general, no systematic vertical pattern was noticed on the GH profiles (Figure 6).

Wei et al. (2015) discussed GH distribution in the study area based on cold temperatures obtained from infrared imaging. Therefore, negative thermal anomalies derived from MeBo cores by Wei et al. (2015) were compared to GH occurrence zones determined using the effective medium theory. Both methods showed close results by exhibiting almost the same GH occurrence zone; therefore, confirming the relation between Vp anomalies and the presence of hydrates.

Using the effective medium theory, a maximum GH content of 26.5% (S_{hmin}) was estimated to correlate with a Vp of 2,035 m/s. Because of the limitation of the ultrasonic fork, which can only measure Vp up to 2,200 m/s, higher GH content could not have been estimated.

The estimation of GH content might have been also affected by the coexistence of free gas and solid GH in the study area as reported by Sultan et al. (2007, 2010). This phenomenon is mainly caused by the fact that the study area is characterized by a high gas flux system; hence, in some cases free gas can be isolated within the pores of GHs where no water is available for the formation of solid hydrates; resulting in a GH containing voids and having a spongy texture. It is indeed thought that GH content might have been locally underestimated when the presence of free gas could have counteracted the effect of hydrates in increasing Vp.

Soil classification charts were used to define a general trend that illustrates the behavior of GH-bearing clayey sediments by correlating in situ acoustic data with geotechnical properties. While the highest GH content correlates with the highest U_2 and Q_{tn} values, the rest of the data do not bear a proportional relationship with hydrate content. However, GH-bearing sediments are clearly characterized by slightly increasing U_2 values that correlate with large Q_{tn} values (compared to reference sites), which reflect a contractive behavior. These observations are in contrast with results from laboratory triaxial experiments performed on GH-bearing sandy sediments, where the behavior was found to be significantly dilative at high GH content (Hyodo et al., 2013). Interestingly, Liu et al. (2018), showed that upon shearing the dilatancy of GH-bearing sands is higher compared to that of GH-bearing silts. Moreover, data from sites where GH content could not have been estimated show a general trend of increasing Q_{tn} values toward the upper limit of the charts. This confirms that GH contribute to the increase of the stiffness and strength of their host sediment. However, the fact that no clear trend of increasing $U_2$with increasing Q_{tn} can be discerned tends to suggest that the sensitivity of GH-bearing sediments does not increase proportionally to their stiffness and strength. This suspicion is supported by the analysis of the $Q_{\mathrm{tn}} - \mathrm{F_r}$ chart, which reveals that high values of Q_{tn} correlate with values of F_r varying over a wide range. The combination of $Q_{\mathrm{tn}} - U_2$ and $Q_{\mathrm{tn}} - \mathrm{F_r}$ charts also reveals that data from GH-bearing sites tend to plot in different regions.

While, the $Q_{\mathrm{tn}} - \mathrm{F_r}$ chart suggests a dilative behavior for most of the data, the $Q_{\mathrm{tn}} - U_2$ chart reflects a contractive behavior. Robertson (2016) suggested that such a difference is representative of the influence of the increasing microstructure in in situ soils. Here the difference between both classification charts can be explained by the increasing GH content within the sediment. By contrast, for some data points, the behavior is classified as contractive in both charts.

These findings can be explained with reference to different GH concentrations and morphologies accommodated by clayey sediments. Visual observations of recovered cores in the study area show GH morphologies varying from groups of millimeter-thick veins to massive nodules (Sultan et al., 2010). Correlations of these observations with the acoustic and geotechnical data show high GH concentrations (up to 27%) plotting in the dilative region of the $Q_{\mathrm{tn}} - \mathrm{F_r}$ chart, which could be related to the presence of nodule type hydrate. However, low GH concentrations (1% to 5%) plotting in or at the limit of the contractive region of the $Q_{\mathrm{tn}} - \mathrm{F_r}$ chart could be an indicator of the presence of a group of hydrate veins.

Alternatively, Ramsey (2010) discussed that the presence of massive inclusion (i.e., GH nodules in this study) within the sediment might influence piezocone response. This can eventually lead to local suctions that prevent the proper functioning of the pore pressure sensor, therefore, producing sharp drops in pore water pressure data correlating with spikes in the f_s profile. Such a response has been observed twice during this analysis (symbols 1 and 2 on Figure 7) for GH content of 26.5% and 11.5%, respectively. During the penetration, Δu_2 did not reduce below -70 kPa confirming that it did not drastically affect the reliability of the measuring method.

5.2. Mechanical Properties of GH-Bearing Sediment

The derivation of geotechnical properties from piezocone data allowed estimating the extents to which the presence of GH tend to decrease the compressibility of clayey sediments while increasing their stiffness and strength (Figures 8 and 9). Keeping in mind that empirical correlations primarily defined for *ideal soils* have been used to derive these properties and that there are difficulties inherent to the estimation of GH content, the trends that emerged are cautiously discussed here. A common feature to the compression index, shear modulus, and undrained shear strength is to show a wide scatter with S_h ranging from 0.94% to 3%. In the lack of laboratory results to substantiate these observations, one may suspect that the morphology and orientation of grain-displacing hydrate readily take over from S_h as the primary control of the compressibility, stiffness, and strength. Following Ghosh et al. (2010) one may also infer that the orientation of grain-displacing hydrate affects the estimation of GH content (S_h) using an effective medium theory approach.

Values of compression indices can be compared to the model proposed by Sultan et al., (2010) to capture the evolution of compressibility with S_h. According to this empirical model, compression indices of GH-bearing sediments (λ_h) are expected to asymptotically decrease from a value typical of purely water-saturated sediments in the study area ($\lambda_0 = 0.7$) toward that of pure hydrate ($\lambda_1 = 0.00147$) according to the following equation:

$$\lambda_h = \lambda_0 \left[1 - \left(1 - \left(\frac{\lambda_1}{\lambda_0} \right) \right) \left(1 - \exp\left(-\beta . \frac{S_h}{100} \right) \right) \right] \tag{12}$$

Where the coefficient β is expected to reflect the distribution and morphology of GH within the sediment.

As shown in Figure 9, a β value of 10 appears to provide an upper limit for the compression indices of GH-bearing sediments. It would predict that the compressibility of the host sediments approaches that of pure methane hydrate for S_h= 100%. A β value of 50 would provide a lower limit for the compression indices of most of the GH-bearing sediments. The fact that it implies that the compressibility of GH-bearing sediments approaches that of pure methane hydrate for S_h = 18% can hardly be reconciled with the data showing that when S_h is in the range 25–27%, compression indices remain 1 order of magnitude higher than that of pure GH. This raises the possibility that a single β value cannot capture the change in compressibility with S_h as the morphology of GH is itself evolving with S_h. Thus, the identification of robust trends from laboratory testing of natural, fine-grained GH-bearing sediments is required to expand upon this empirical suspicion.

Despite some scatter in the plots of Figure 9b, the overall distribution suggests that the stiffness and strength of GH-bearing clayey sediments tend to increase linearly with S_h. The fact that S_u data appear less scattered than the G_{50} data may be ascribed to the fact that the latter have been calculated using the soil behavior type index (I_c), whose calculation may be affected by a lack of accuracy of sleeve friction measurements, f_s (see section 3.4). An additional note of caution has to do with the fact that density was assumed to be constant when calculating G_{50}. One may however note that the unique natural GH-bearing fine-grained sediments subjected to triaxial compression by Yoneda et al. (2017) has G_{50} and S_u values falling close to the linear trends that emerged from the present study. As for compression indices, it can be expected that the stiffness and strength is influenced by the distribution and morphology of GH such that S_h alone cannot wholly capture the natural variability of these properties.

Sensitivity values are discussed separately from the previous properties as they appear to be the most scattered when plotted against S_h. Such a scatter might be attributed to a lack of accuracy of sleeve friction measurements. However, the plots in the $Q_{\text{tn}} - \text{U}_2$ chart in Figure 7a, which do not rely on sleeve friction measurements, also suggest that sensitivity bears little relationship to S_h. Indeed, values of Q_{tn} ranging from 11 to 80 are observed to display similar U_2 values for S_h ranging from less than 2.5% to more than 22%, while sensitive sediments are expected to display trends of increasing Q_{tn} with increasing U_2 (Robertson, 2016).

In line with previous interpretations, this tend to support the view that the distribution and morphology of GH have a strong influence on sensitivity.

5.3. Hydraulic Properties of GH-Bearing Sediment

The water permeability of GH-bearing sediments is a constraint for reservoir engineering studies but, moreover, a key parameter to evaluate the excess pore pressure generated by hydrate decomposition in natural environment.

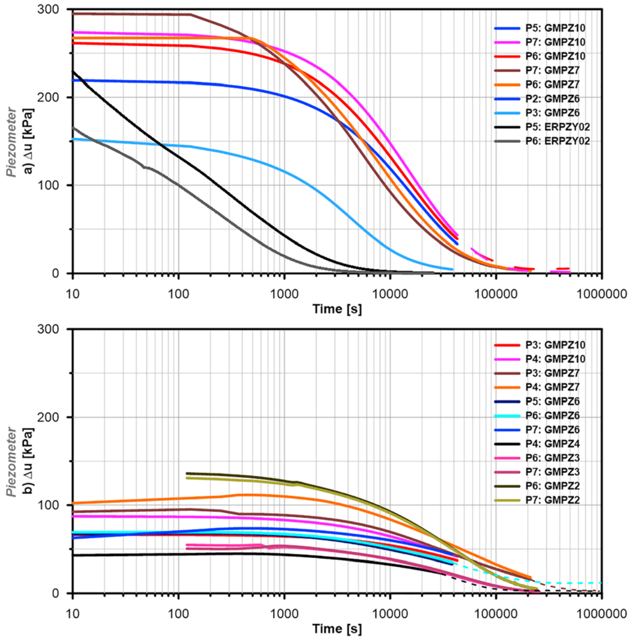

Figure 10. Pore pressure dissipation curves from different depths at different sites (GMPZ2, 3, 4, 6, 7, and 10) where the presence of GH was suspected and/or proved. Panels (a) and (b) show data where the initial excess pore pressure pulse (U_{ini}) values are higher and lower than 150 kPa. When the excess pore pressure was not equilibrated at the end of the deployment, the extrapolation of the excess pore pressure was carried out using the numerical algorithm developed by Sultan and Lafuerza (2013; dashed lines).

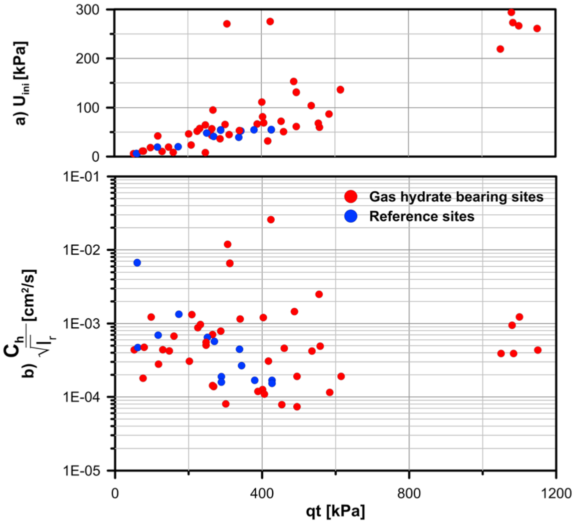

Figure 11. (a) U_{ini} and (b) $\frac{C_h}{\sqrt{I_r}}$ as a function of q_t showing a strong dependence of the initial excess pore pressure pulse on the corrected tip resistance. The $\frac{C_h}{\sqrt{I_r}}$ values do not show any clear tendency.

The evolution of the octahedral stress (Δu) with time is a means to predict if the investigated soil is contractive or dilative. Pore pressure dissipation curves from different piezometer sites have indeed showed a monotonic change with time. This trend is representative of a contractive behavior as proposed by Burns and Mayne (1999); thus confirming what has been observed in section 5.1 for GH-bearing clayey sediments.

The rare available data from literature are often obtained from laboratory experimental tests carried out on reconstructed GH-bearing sand samples. Those laboratory data show a clear tendency of the permeability to decrease with increasing GH content (see, for instance, Katagiri et al., 2017, and references therein). On the other hand, different authors show that the water permeability versus porosity of the hydrate-sediment system depends on the way GH accommodates the pore spaces (grain coating or pore filling). Several theoretical models were developed in the recent years in order to define the link between GH content and relative permeability (Katagiri et al., 2017; Kleinberg et al., 2003; Moridis, 2002, among others).

Kleinberg et al. (2003) have summarized existing expressions for the relative permeability k_{hw} in hydrate-bearing sediment. For pore-filling hydrate, a simple relative permeability to water can be expressed by the following expression:

$$k_{\text{hw}} = \frac{k}{k_0} = \frac{(1-S_h)^{m+2}}{\left(1+\sqrt{S_h}\right)^2} \tag{13}$$

where k_0 is the reference permeability of the saturated sediment, k is the permeability of the system for a given hydrate saturation, and m is the saturation exponent decreasing from 0.4 for S_h = 10% to 0.1 in a fully hydrate saturated system. For grain-coating hydrate, a simple expression of the relative permeability to water is given by

$$k_{\text{hw}} = \frac{k}{k_0} = (1-S_h)^{m+1} \tag{14}$$

where $m = 1.5$ for $S_h < 80\ \%$.

Before discussing changes in relative permeability to water, attention is paid to the changes in relative hydraulic diffusivity with GH content from in situ measurements:

$$C_{\text{hw}} = \frac{C_h}{C_{h0}} \tag{15}$$

where C_h is the hydraulic diffusivity of the system for a given hydrate content and C_{h0} is the reference hydraulic diffusivity of the saturated sediment.

The C_{hw} values shown in Figure 13a are derived from piezometer data in Figure 12 and the rigidity indices (I_r) obtained from CPTu data using the Robertson (2009) method (Figure 8). The plots in Figure 13a confirm the decreasing trend of C_{hw} with increasing S_h up to 15%. However, a clear increase of C_{hw} with S_h can be observed for S_h values higher than 20%. Such results were unexpected and were initially considered as erroneous data, compromising the used in situ method to determine the hydraulic properties of GH-bearing sediments. However, published experimental data and models often consider the sediment hydrate medium as a

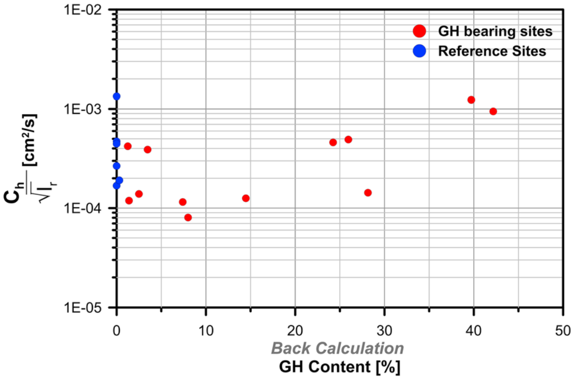

Figure 12. $\frac{C_h}{\sqrt{I_r}}$ as a function of GH content (S_h). $\frac{C_h}{\sqrt{I_r}}$ decreases to a minimum value for S_h equal 10% and then increases again.

continuous system without discontinuities and fractures. In natural environments, the presence of fractures at different scales may imply high hydraulic diffusivities and fluid flows paths through GH-bearing areas. The coexistence of free gas and GH as well as gas plumes in the water column above hydrate occurrence zones is a clear evidence of the presence of these discontinuities (Riboulot et al., 2018; Sauter et al., 2006; Torres et al., 2004). The impact of those discontinuities on the evolution of the hydraulic diffusivity with the GH content seems essential to account for accurate prediction of fluid flow through hydrate-sediment systems. The use of in situ pore pressure measurements and the pore pressure decay with time to derive the hydraulic diffusivity of the medium looks, at first sight, as a reliable method to access the in situ hydraulic properties of sediment-hydrate fracture mediums. Therefore, our data importantly suggest that, in the study area, fractures occurring for S_h values higher than 20% may drastically increase the hydraulic diffusivity of the GH-bearing sediments. Unfortunately, this strong conclusion is premature, since alternative explanation related either to the piezometer installation or to the important decrease of the compressibility could also be at the origin of the increase in C_{hw} with S_h. The free-fall method used for piezometer installation with a rod diameter of 0.06 m and the stiffness of the GH-bearing sediments could enhance fracture propagation or even initiation. The expected consequence would be an increase in hydraulic diffusivity. Although, fractures generated by piezometer penetrations are more likely to occur at the tip of the piezometer and not all over its shaft (Santamarina et al., 2015), at this stage, it is not possible to firmly conclude about their origin. However, it is obvious that the general thought about the decrease of the hydraulic diffusivity with increasing hydrate content cannot be systematically applied in natural sediment-hydrate systems.

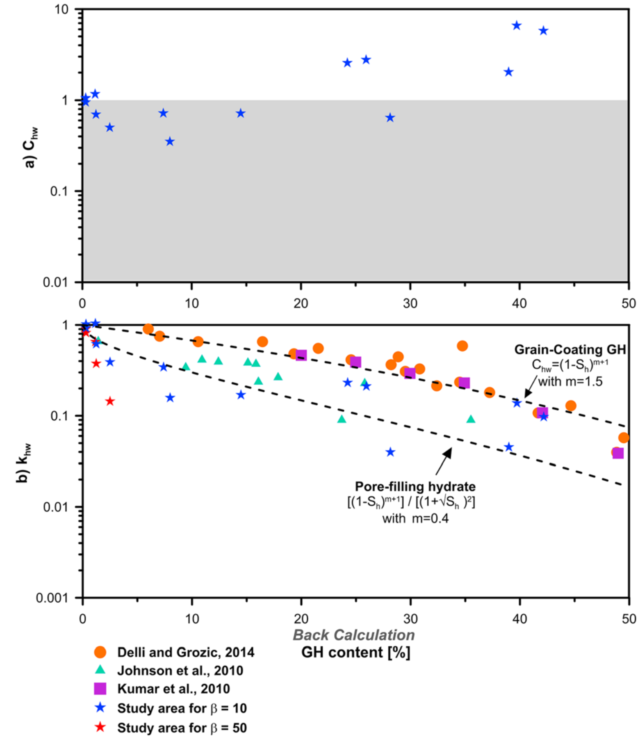

Figure 13. (a) Relative hydraulic diffusivity (C_{hw}) as a function of hydrate content (S_h) showing a decrease tendency with the increase of S_h to 15%. A clear increase of C_{hw} with S_h can be observed for S_h values higher than 20%. (b) Relative permeability data for β values of 10 and 50.

To further the discussion, it is important to mention that the hydraulic diffusivity is equal to the relative permeability to water divided by the storage parameter:

$$k_{\mathrm{hw}} = \frac{k}{k_0} = \frac{C_h.St_h}{C_{h0}.St_0} = C_{\mathrm{hw}}.\frac{\gamma_w.m_{\mathrm{vh}}}{\gamma_w.m_{v0}} = C_{\mathrm{hw}}.\frac{\lambda_h}{\lambda_0}$$
$$= C_{\mathrm{hw}}\left[1-\left(1-\left(\frac{\lambda_1}{\lambda_0}\right)\right)\left(1-\exp\left(-\beta.\frac{S_h}{100}\right)\right)\right] \quad (16)$$

Where St_0 and St_h are storage factors, γ_w is the water unit weight, and m_{v0} and m_{vh} are the volume compressibility coefficients of water-saturated and hydrate-bearing sediments, respectively. As shown in Table 3 and Figure 13, values of relative permeability to water (k_{hw}) can be calculated using equation (16), assuming upper and lower β values of 10 and 50 as explained in section 5.2. However, since for $S_h > 5\%$ no data plot near the limit curve obtained using a $\beta = 50$ (Figure 9a), k_{hw} values were calculated using $\beta = 50$ only for values of $S_h < 5\%$.

Figure 13b shows that overall the calculated k_{hw} data decrease with increasing S_h. This trend reflects the fact that the compressibility of GH-bearing sediments decreases more rapidly than the hydraulic diffusivity does with increasing S_h. The k_{hw} values obtained with β values of 10 generally plot between the two limit curves defined by equations (13) and (14) while showing a decreasing trend with increasing S_h. While these equations were developed for coarse-grained sediments, they appear here to have the potential to serve as lower and upper bounds for describing the evolution of permeability as a function of hydrate content in clayey sediments also. On the other hand, for $\beta = 50$, k_{hw} data plot completely outside of the grain-coating and pore-filling hydrate limits

Table 3
Hydraulic Properties From Different Depths at Different Sites (GMPZ2, 3, 4, 6, 7, and 10) Where the Presence of Gas Hydrate Was Suspected and/or Proved

Site	Depth (mbsf)	t_{50} (s)	S_h (%)	C_h(m^2/s)	C_{hw}	k_{hw} for $\beta = 10$	$k_{hw}$for $\beta = 50$
GMPZ2	7.08	23686	0.3	2.23E−07	0.951	0.923	0.819
GMPZ2	7.11	23686	0.3	2.46E−07	1.049	1.018	0.904
GMPZ3	7.11	28347	1.16	2.72E−07	1.161	1.034	0.651
GMPZ4	6.17	31550	28.15	1.51E−07	0.642	0.040	
GMPZ4	6.97	9806	24.2375	5.99E−07	2.555	0.231	
GMPZ4	7.005	9183	25.95	6.47E−07	2.761	0.211	
GMPZ6	6.98	10715	1.24	1.64E−07	0.698	0.616	
GMPZ7	6.23	32546	2.5	1.17E−07	0.500	0.390	
GMPZ7	7.78	35944	14.475	1.68E−07	0.716	0.169	
GMPZ7	10.13	3668	39.725	1.55E−06	6.591	0.138	
GMPZ7	10.165	4766	42.175	1.36E−06	5.787	0.097	
GMPZ10	6.93	56169	8	8.22E−08	0.350	0.158	
GMPZ10	8.48	39219	7.4	1.68E−07	0.718	0.343	
GMPZ10	10.03	11574	38.9875	4.75E−07	2.025	0.045	

(equations (13) and (14)) while decreasing with a slope 14 times steeper than that of the k_{hw} obtained with $\beta = 10$. This implies that the trends defined by equations (13) and (14) are clearly not adapted to represent the evolution of k_{hw} calculated with β values of 50. This highlights the need for developing new models that can account for the evolution of the morphology of GH with that of S_h.

6. Conclusion

The main objective of this work was to study the effect of GH concentration and morphology on the mechanical and hydraulic properties of their host clayey sediment. This was achieved by using a unique database containing multiple in situ acoustic, geotechnical, coring, and drilling data. This investigation allowed capturing the behavior of clayey sediment with GH content varying between 1% and 26.5% in a high gas flux system in the Gulf of Guinea. This analysis led to the following key observations:

1. Positive Vp anomalies correlating with simultaneous increase of all geotechnical parameters (q_t, f_s, and Δu_2) are indicative of the presence of GH.
2. Using the effective medium theory, a maximum GH content of 26.5% was estimated to correlate with a Vp of 2,035 m/s.
3. Comparisons of results derived from the effective medium theory with those derived from negative thermal anomalies yielded almost the same GH occurrence zone.
4. GH-bearing clayey sediments generally show a contractive behavior, which was confirmed by the analysis of pore pressure dissipation data recorded by piezometers. Such a behavior contrasts sharply with the dilative behavior of GH-bearing sandy sediments
5. Results have shown that the normalized piezocone resistance (Q_{tn}) increases with the GH content. High Q_{tn} values were found to correlate with the same range of U_2 values. This suggests that the morphology and the distribution of GH has an important effect on the mechanical properties of the host sediment.
6. The use of different soil behavior classification charts, while carefully analyzing all used parameters, might be a means to identify different GH morphologies based on zones in which the piezocone data plot.
7. The presence of GH has a noticeable effect on the compressibility, stiffness, and strength properties of their host clayey sediments. It tends to increase the stiffness G_{50} and undrained shear strength (S_u) while decreasing the compressibility. While no clear trend was observed between the sensitivity and GH content, S_u and G_{50} appear to follow a linear increase with GH content.
8. Oscillations around the linear trend are thought to reflect the superimposed influence of the distribution and morphology of GH on the stiffness and strength.
9. Pore pressure dissipation data were used to derive the relative hydraulic diffusivity (C_{hw}) as a function of hydrate content (S_h). At low hydrate content, C_{hw} was observed to decrease with increasing S_h. For S_h

values higher than 20, C_{hw} values rising above 1 were linked either to the presence of fractures in the hydrate-sediment system or to the important decrease of compressibility with increasing GH content. This observation leads to the conclusion that the pore pressure diffusion within GH systems could be much faster than previously thought for high hydrate content.

Further investigations supported by experimental data would be helpful in substantiating the influence of various morphologies and amount of GH on the mechanical and hydraulic properties of the clayey host sediment.

Acknowledgments

Data used in the present paper are covered by a confidentiality agreement between Total, Ifremer, and Marum that restrict access; interested readers can contact the authors for more information. Sandrine Cheron from Ifremer is thanked for her assistance in performing mineralogical analyses. The authors would like to express their great appreciation to the French National Research Agency for funding the present study, which is part of the project HYDRE "Mechanical behavior of gas-hydrate-bearing sediments" – ANR-15-CE06-0008.

References

ASTM Standard D2435 (1996). Standard TEST method for one-dimensional consolidation properties of the soil, ASTM International, West Conshohocken, PA 19428, www.astm.org.

Boswell, R., & Collett, T. (2006). The gas hydrate resource pyramid. *Natural Gas & Oil*, *304*, 285–4541.

Boswell, R., & Collett, T. S. (2011). Current perspectives on gas hydrate resources. *Energy & Environmental Science*, *4*(4), 1206–1215. https://doi.org/10.1039/C0EE00203H

Burns, S., & Mayne, P. (1999). Pore pressure dissipation behaviour surrounding driven piles and cone penetrometers. *Transportation Research Record: Journal of the Transportation Research Board*, *1675*, 17–23. https://doi.org/10.3141/1675-03

Burns, S. E., & Mayne, P. W. (1998). Monotonic and dilatory pore-pressure decay during piezocone tests in clay. *Canadian Geotechnical Journal*, *35*(6), 1063–1073. https://doi.org/10.1139/t98-062

Cunningham, R., & Lindholm, R. M. (2000). AAPG memoir 73, Chapter 8: Seismic evidence for widespread gas hydrate formation, offshore West Africa.

Dai, S., Santamarina, J. C., Waite, W. F., & Kneafsey, T. J. (2012). Hydrate morphology: Physical properties of sands with patchy hydrate saturation. *Journal of Geophysical Research*, *117*, B11205. https://doi.org/10.1029/2012JB009667

Freudenthal, T., & Wefer, G. (2007). Scientific drilling with the sea floor drill rig MeBo. *Scientific Drilling*, *5*, 63–66. https://doi.org/10.5194/sd-5-63-2007

Freudenthal, T., & Wefer, G. (2013). Drilling cores on the sea floor with the remote-controlled sea floor drilling rig MeBo. *Geoscientific Instrumentation, Methods and Data Systems*, *2*(2), 329–337. https://doi.org/10.5194/gi-2-329-2013

Ghosh, R., Sain, K., & Ojha, M. (2010). Effective medium modeling of gas hydrate-filled fractures using the sonic log in the Krishna-Godavari basin, offshore eastern India. *Journal of Geophysical Research*, *115*, B06101. https://doi.org/10.1029/2009JB006711

Helgerud, M. B., Dvorkin, J., Nur, A., Sakai, A., & Collett, T. (1999). Elastic-wave velocity in marine sediments with gas hydrate: Effective medium modeling. *Geophysical Research Letters*, *26*(13), 2021–2024. https://doi.org/10.1029/1999GL900421

Hovland, M., Gallagher, J. W., Clennell, M. B., & Lekvam, K. (1997). Gas hydrate and free gas volumes in marine sediments: Example from the Niger Delta front. *Marine and Petroleum Geology*, *14*(3), 245–255. https://doi.org/10.1016/S0264-8172(97)00012-3

Hyodo, M., Yoneda, J., Yoshimoto, N., & Nakata, Y. (2013). Mechanical and dissociation properties of methane hydrate-bearing sand in deep seabed. *Soils and Foundations*, *53*(2), 299–314. https://doi.org/10.1016/j.sandf.2013.02.010

Jang, J., & Santamarina, J. C. (2016). Hydrate bearing clayey sediments: Formation and gas production concepts. *Marine and Petroleum Geology*, *77*, 235–246. https://doi.org/10.1016/j.marpetgeo.2016.06.013

Katagiri, J., Konno, Y., Yoneda, J., & Tenma, N. (2017). Pore-scale modeling of flow in particle packs containing grain-coating and pore-filling hydrate: Verification of a Kozeny–Carman-based permeability reduction model. *Journal of Natural Gas Science and Engineering*, *45*, 537–551. https://doi.org/10.1016/j.jngse.2017.06.019

Kayen, R. E., & Lee, H. J. (1991). Pleistocene slope instability of gas hydrate-laden sediment on the Beaufort Sea margin. *Marine Georesources & Geotechnology*, *10*(1–2), 125–141. https://doi.org/10.1080/10641199109379886

Kleinberg, R. L., Flaum, C., Griffin, D. D., Brewer, P. G., Malby, G. E., Peltzer, E. T., & Yesinowski, J. P. (2003). Deep sea NMR: Methane hydrate growth habit in porous media and its relationship to hydraulic permeability, deposit accumulation, and submarine slope stability. *Journal of Geophysical Research*, *108*(B10), 2508. https://doi.org/10.1029/2003JB002389

Krage, C. P., Broussard, N. S., & DeJong, J. T. (2014). Estimating rigidity index (IR) based on CPT measurements. In *Third international symposium on cone penetration testing, Las Vegas, Nevada, USA* (pp. 727–735). Las Vegas, NV.

Kvenvolden, K. A. (1993). Gas hydrate as a potential energy resource—A review of their methane content. United States Geological Survey, *Professional Paper; (United States)*, *1570*.

Liu, Z., Dai, S., Ning, F., Peng, L., Wei, H., & Wei, C. (2018). Strength estimation for hydrate-bearing sediments from direct shear tests of hydrate-bearing sand and silt. *Geophysical Research Letters*, *45*, 715–723. https://doi.org/10.1002/2017GL076374

Low, H. E., Lunne, T., Andersen, K. H., Sjursen, M. A., Li, X., & Randolph, M. F. (2010). Estimation of intact and remoulded undrained shear strengths from penetration tests in soft clays. *Géotechnique*, *60*(11), 843–859. https://doi.org/10.1680/geot.9.P.017

Lunne, T., Robertson, P. K., & Powell, J. J. M. (1997). Cone penetration testing. *Geotechnical Practice*, *20*, 23–35.

Malinverno, A., Kastner, M., Torres, M. E., & Wortmann, U. G. (2008). Gas hydrate occurrence from pore water chlorinity and downhole logs in a transect across the northern Cascadia margin (Integrated Ocean drilling program expedition 311). *Journal of Geophysical Research*, *113*, B08103. https://doi.org/10.1029/2008JB005702

Moridis, G. J. (2002). Numerical studies of gas production from methane hydrate. In *SPE Gas Technology Symposium*. Calgary Alberta, Canada: Society of Petroleum Engineers.

Ning, F., Yu, Y., Kjelstrup, S., Vlugt, T. J., & Glavatskiy, K. (2012). Mechanical properties of clathrate hydrates: Status and perspectives. *Energy & Environmental Science*, *5*(5), 6779–6795. https://doi.org/10.1039/c2ee03435b

Paul, C. K., & Ussler, I. W. (2001). History and significance of gas sampling during DSDP and ODP. *Natural Gas Hydrates: Occurrence, Distribution and Detection. American Geophysical Union*, *124*, 53–66. https://doi.org/10.1029/GM124

Ramsey, N. (2010). Some issues related to application of the CPT. In *2nd International Symposium on Cone Penetration Testing, CPT* (Vol. 10). Huntington Beach, CA.

Riboulot, V., Ker, S., Sultan, N., Thomas, Y., Marsset, B., Scalabrin, C., Ruffine, L., et al. (2018). Freshwater lake to salt-water sea causing widespread hydrate dissociation in the Black Sea. *Nature Communications*, *9*(1), 117. https://doi.org/10.1038/s41467-017-02271-z

Robertson, P. K. (2009). Interpretation of cone penetration tests—A unified approach. *Canadian Geotechnical Journal*, *46*(11), 1337–1355. https://doi.org/10.1139/T09-065

Robertson, P. K. (2016). Cone penetration test (CPT)-based soil behaviour type (SBT) classification system—An update. *Canadian Geotechnical Journal*, *53*(12), 1910–1927. https://doi.org/10.1139/cgj-2016-0044

Santamarina, J. C., Dai, S., Jang, J., & Terzariol, M. (2012). Pressure core characterization tools for hydrate-bearing sediments. *Scientific Drilling*, *14*, 44–48. https://doi.org/10.5194/sd-14-44-2012

Santamarina, J. C., Dai, S., Terzariol, M., Jang, J., Waite, W. F., Winters, W. J., Nagao, J., et al. (2015). Hydro-bio-geomechanical properties of hydrate-bearing sediments from Nankai trough. *Marine and Petroleum Geology*, *66*, 434–450. https://doi.org/10.1016/j.marpetgeo.2015.02.033

Sauter, E. J., Muyakshin, S. I., Charlou, J. L., Schlüter, M., Boetius, A., Jerosch, K., Damm, E., et al. (2006). Methane discharge from a deep-sea submarine mud volcano into the upper water column by gas hydrate-coated methane bubbles. *Earth and Planetary Science Letters*, *243*(3–4), 354–365. https://doi.org/10.1016/j.epsl.2006.01.041

Schneider, J. A., Randolph, M. F., Mayne, P. W., & Ramsey, N. R. (2008). Analysis of factors influencing soil classification using normalized piezocone tip resistance and pore pressure parameters. *Journal of Geotechnical and Geoenvironmental Engineering*, *134*(11), 1569–1586. https://doi.org/10.1061/(ASCE)1090-0241(2008)134:11(1569)

Sultan, N., Bohrmann, G., Ruffine, L., Pape, T., Riboulot, V., Colliat, J. L., de Prunelé, A., et al. (2014). Pockmark formation and evolution in deep water Nigeria: Rapid hydrate growth versus slow hydrate dissolution. *Journal of Geophysical Research: Solid Earth*, *119*, 2679–2694. https://doi.org/10.1002/2013JB010546

Sultan, N., Garziglia, S., & Ruffine, L. (2016). New insights into the transport processes controlling the sulfate-methane-transition-zone near methane vents. *Scientific Reports*, *6*(1), 26701. https://doi.org/10.1038/srep26701

Sultan, N., & Lafuerza, S. (2013). In situ equilibrium pore-water pressures derived from partial piezoprobe dissipation tests in marine sediments. *Canadian Geotechnical Journal*, *50*(12), 1294–1305. https://doi.org/10.1139/cgj-2013-0062

Sultan, N., Marsset, B., Ker, S., Marsset, T., Voisset, M., Vernant, A. M., Bayon, G., et al. (2010). Hydrate dissolution as a potential mechanism for pockmark formation in the Niger delta. *Journal of Geophysical Research*, *115*, B08101. https://doi.org/10.1029/2010JB007453

Sultan, N., Voisset, M., Marsset, T., Vernant, A. M., Cauquil, E., Colliat, J. L., & Curinier, V. (2007). Detection of free gas and gas hydrate based on 3D seismic data and cone penetration testing: An example from the Nigerian continental slope. *Marine Geology*, *240*(1–4), 235–255. https://doi.org/10.1016/j.margeo.2007.02.012

Teh, C. I., & Houlsby, G. T. (1991). Analytical study of the cone penetration test in clay. *Geotechnique*, *41*(1), 17–34. https://doi.org/10.1680/geot.1991.41.1.17

Torres, M. E., Wallmann, K., Tréhu, A. M., Bohrmann, G., Borowski, W. S., & Tomaru, H. (2004). Gas hydrate growth, methane transport, and chloride enrichment at the southern summit of hydrate ridge, Cascadia margin off Oregon. *Earth and Planetary Science Letters*, *226*(1–2), 225–241. https://doi.org/10.1016/j.epsl.2004.07.029

Waite, W. F., Santamarina, J. C., Cortes, D. D., Dugan, B., Espinoza, D. N., Germaine, J., Jang, J., et al. (2009). Physical properties of hydrate-bearing sediments. *Reviews of Geophysics*, *47*, RG4003. https://doi.org/10.1029/2008RG000279

Wei, J., Pape, T., Sultan, N., Colliat, J. L., Himmler, T., Ruffine, L., de Prunelé, A., et al. (2015). Gas hydrate distributions in sediments of pockmarks from the Nigerian margin–results and interpretation from shallow drilling. *Marine and Petroleum Geology*, *59*, 359–370. https://doi.org/10.1016/j.marpetgeo.2014.09.013

Yoneda, J., Masui, A., Konno, Y., Jin, Y., Kida, M., Katagiri, J., Nagao, J., et al. (2017). Pressure-core-based reservoir characterization for geomechanics: Insights from gas hydrate drilling during 2012–2013 at the eastern Nankai trough. *Marine and Petroleum Geology*, *86*, 1–16. https://doi.org/10.1016/j.marpetgeo.2017.05.024

Yun, T. S., Santamarina, J. C., & Ruppel, C. (2007). Mechanical properties of sand, silt, and clay containing tetrahydrofuran hydrate. *Journal of Geophysical Research*, *112*, B04106. https://doi.org/10.1029/2006JB004484

UNIVERSITE BRETAGNE LOIRE / SCIENCES DE LA MER ET DU LITTORAL

UBO
Université de Bretagne Occidentale

Titre : Etude du comportement mécanique de sédiments argileux contenant des hydrates de gaz à partir de mesures in-situ

Mots clés : Hydrate de gaz, propriétés mécaniques, milieu argileux, mesures in-situ, Golf de Guinée

Résumé : Les hydrates de gaz (GH) sont composés de molécules de gaz, souvent du méthane, piégées dans des cages d'eau. Ils se trouvent principalement dans les sédiments des marges continentales et du pergélisol, où les conditions de stabilité (haute pression et basse température) nécessaires à leur présence sont réunies. Les GH sont considérés comme une source d'énergie mais aussi un facteur aggravant des aléas sous-marins et une source de gaz à effet de serre. Il est indispensable de comprendre les conséquences de la présence de ces composés métastables sur les propriétés géo-mécaniques des sédiments qui les contiennent (GHBS). Ifremer a mené plusieurs campagnes océanographiques visant à évaluer ce type d'aléas géologique dans le Golfe de Guinée, où un système à flux de gaz élevé avait pu être observé. La base de données est composée d'un ensemble de mesures in-situ acoustiques, géotechniques et de mesures de dissipation de pression interstitielle, ainsi que de carottes sédimentaires et de profils sismiques.

Dans le but de comprendre l'effet de la saturation en GH et de leur morphologie et distribution sur les propriétés mécaniques des GHBS, ce travail de thèse a exploité l'ensemble de ces données. Cette étude a révélé que les GHBS argileux ont un comportement contractant lors du cisaillement qui s'oppose au comportement dilatant des sédiments sableux. En outre, différentes morphologies des GH ont été associées aux différents traits de comportement mécanique des GHBS. Pour des saturations en GH élevées (>10%), la diffusivité hydraulique des GHBS a tendance à augmenter avec l'accroissement de la concentration de ces hydrates. Ce phénomène est lié à la présence de fractures ou à la diminution de la compressibilité du sédiment. Un nouveau modèle constitutif basé sur le principe d' « indices des vides equivalents » a été utilisé pour simuler le comportement mécanique des GHBS. Les résultats ont montré qu'un seul paramètre lié à la présence et la morphologie des GH est nécessaire au modèle pour reproduire correctement le comportement mécanique des GHBS.

Title: Study of the mechanical behaviour of hydrate-bearing clayey sediments based on in situ measurements

Keywords : Gas hydrates, mechanical properties, clayey sediments, in-situ measurements, Gulf of Guinea

Abstract: Gas hydrates (GH) are composed of gas molecules, often methane, trapped in a lattice of hydrogen-bonded water molecule. They are found in sediments of continental margins and permafrost, lakes and inland seas, where their stability conditions (high pressure and low temperature) are met. GH are considered as a potential energy resource but furthermore as a potential submarine geohazard and source of greenhouse gases. It is essential to understand the consequences of the presence of these metastable components on the geo-mechanical properties of their host sediment (GHBS). Ifremer has conducted several oceanographic campaigns aiming to assess such geohazard in an area of the deep-water Niger Delta, characterised by hydrates which formed in high gas flux environments in clayey sediment. The database is composed of in-situ acoustic, geotechnical, pore-pressure dissipation measurements, as well as cores and seismic profiles.

The PhD work exploited the dataset with the aim of understanding the effect of GH content, morphology and distrubution on the mechanical and hydraulic properties of the GHBS. This rare field study revealed that marine GH-bearing clays have a contractive behaviour upon shearing, which contrasts with the dilative behaviour of sandy GHBS often discussed in litterature. Alternatively, different morphologies of GH have been linked with different features of the mechanical behaviour of GHBS. For high GH saturtion (> 10%), the hydraulic diffusivity of the GHBS was observed to increase with increasing GH content, which was linked to fractures or decrease in compressibility. A new simple constitutive model based on "equivalent skeleton void ratio" was used in order to simulate the mechanical behaviour of GHBS. Preliminary results show that only one additional parameter related to the morphology of hydrate is necessary to correctly simulate the mechanical behaviour of GHBS.